Structural Immunology of Humoral and Cellular Recognition of a MUC1 Breast Cancer Antigen

Jeffrey Scott Grinstead

A dissertation submitted in partial fulfillment of the requirements for the degree of

Doctor of Philosophy

University of Washington

2003

Program Authorized to Offer Degree: School of Pharmacy-Medicinal Chemistry

UMI Number: 3102656

Copyright 2003 by
Grinstead, Jeffrey Scott

All rights reserved.

UMI Microform 3102656
Copyright 2003 by ProQuest Information and Learning Company.
All rights reserved. This microform edition is protected against
unauthorized copying under Title 17, United States Code.

ProQuest Information and Learning Company
300 North Zeeb Road
P.O. Box 1346
Ann Arbor, MI 48106-1346

©Copyright 2003

Jeffrey Scott Grinstead

In presenting this dissertation in partial fulfillment of the requirements for the Doctoral degree at the University of Washington, I agree that the Library shall make its copies freely available for inspection. I further agree that extensive copying of the dissertation is allowable only for scholarly purposes, consistent with "fair use" as prescribed in the U.S. Copyright Law. Requests for copying or reproduction of this dissertation may be referred to ProQuest Information and Learning, 300 North Zeeb Road, Ann Arbor, MI 48106-1346, to whom the author has granted "the right to reproduce and sell (a) copies of the manuscript in microform and/or (b) printed copies of the manuscript made from microform."

Signature 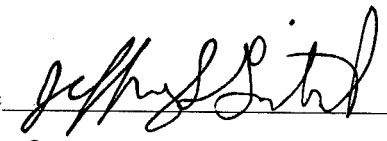

Date 08-13-03

University of Washington
Graduate School

This is to certify that I have examined this copy of a doctoral dissertation by

Jeffrey Scott Grinstead

and have found that it is complete and satisfactory in all respects,
and that any and all revisions required by the final
examining committee have been made.

Chair of Supervisory Committee:

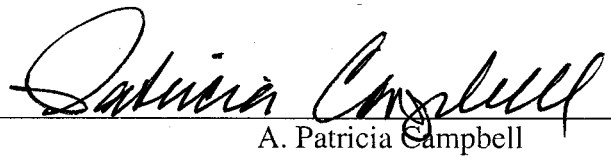

A. Patricia Campbell

Reading Committee:

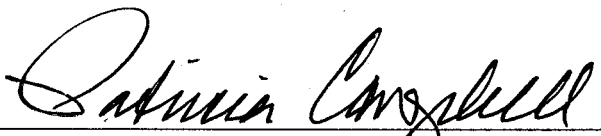

A. Patricia Campbell

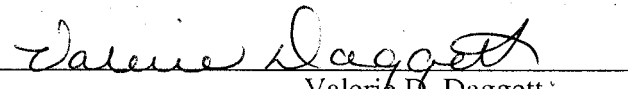

Valerie D. Daggett

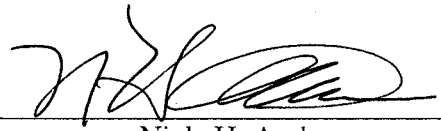

Niels H. Andersen

Date: 8/19/03

University of Washington

Abstract

Structural Immunology of Humoral and Cellular Recognition of a MUC1 Breast Cancer Antigen

Jeffrey Scott Grinstead

Chair of the Supervisory Committee: Assistant Professor A. Patricia Campbell

Department of Medicinal Chemistry

MUC1 mucins have recently been the target of breast cancer vaccine trials. MUC1 peptide vaccine studies in mice have resulted in rejection of solid tumor and protection from further tumor challenge. These results represent the desired immune response in humans, but clinical trials have not shown MUC1 peptide-based vaccines to be effective. Clinical trials using tumor-associated MUC1 carbohydrate vaccines have produced immune responses with limited efficacy, and leave much room for improvement.

Both immunological and biophysical evidence suggests that a combination of MUC1 peptide and carbohydrate moieties in a glycopeptide vaccine could be more effective at inducing an effective anti-tumor immune response in humans. The results presented in this thesis describe intermolecular interactions of MUC1 peptides and glycopeptides with the tumor-associated antibody B27.29. The identification of both peptide and carbohydrate interactions with B27.29 points to a mechanism for immune recognition of the tumor-associated MUC1 mucin, and suggests that a MUC1 glycopeptide vaccine might better represent the tumor-associated antigen. Further experiments are presented that give methodology for determining how MUC1 peptides or glycopeptides might stimulate a cellular immune response, as well. These results are discussed within the framework of developing a next-generation MUC1 glycopeptide vaccine that might be able to effectively treat and/or prevent recurrence of breast cancer.

Table of Contents

List of Figures

List of Tables

Acknowledgements

I thank Patricia for being an excellent mentor during my studies, and I thank my family for their love and support. Most of all I thank my wife Amy, who inspires me to excellence every day.

Dedication

For my mother, Amelia and my grandmother, Jody. You are the motivation for this research.

Chapter 1: Introduction

The MUC1 Tumor Antigen:

Mucin (MUC) proteins are large transmembrane glycoproteins that are expressed on the ductal surface of epithelial cells. Mucin proteins are expressed on all epithelial tissues, and serve to screen the cell surface from extracellular pathogens, retain moisture, and to lubricate the extracellular tract (Patton *et al.*, 1995). Many different classes of mucin have been discovered, each with some tissue specificity and sequence similarity (Bhavanandan, 1991).

The extracellular region of the mucin consists of a variable number of tandem repeats of the 20-amino acid sequence GVTSA**PDTRPAP**GSTAPPAH, in the case of the MUC1 mucin. The VNTR region of the protein is repeated from 20 to over 100 times to produce a very large, extended glycopeptide chain protruding from the surface of the cell (Figure 1.1). MUC1 is extensively O-glycosylated at the five threonine and serine sites with large, branched sugars (Carlstedt & Davies, 1997; Koganty *et al.*, 1997; Rudd & Dwek, 1997; Van den Steen *et al.*, 1998).

Recently, mucins have been targeted for vaccine or immunotherapy development in cancers of the breast, colon, pancreas, lung, and ovary because of the differences between their normal and tumor-associated forms (Apostolopoulos *et al.*, 1999a; Apostolopoulos *et al.*, 1999b; Miles & Taylor-Papadimitriou, 1999; Taylor-Papadimitriou *et al.*, 1999) (see also Figure 1.1). MUC1 is overexpressed in 90% of all breast carcinomas (Zotter *et al.*, 1988), and in the tumor-associated state MUC1 becomes an autoantigen as a result of incomplete glycosylation and sparse distribution of

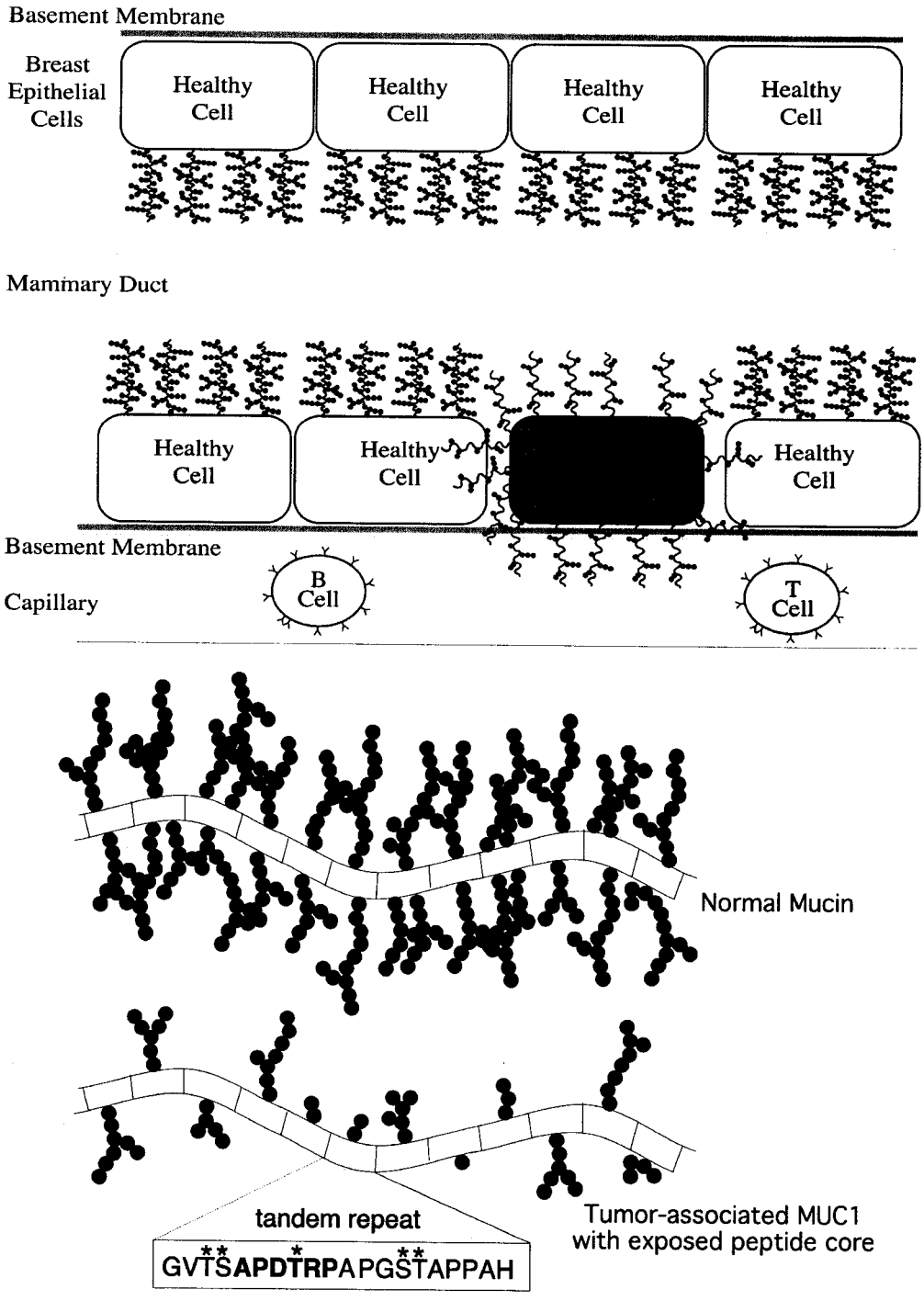

Figure 1.1: Tumor-associated MUC1 mucin undergoes several key changes affecting its immunogenicity. The top panel illustrates how a MUC1 mucin loses its apical distribution and becomes exposed to the immune system. The bottom panel depicts the differences in glycosylation state between normal and tumor-associated MUC1. The MUC1 repeat sequence is shown, with the five possible sites of O-glycosylation starred.

remaining carbohydrate structures (Hanisch, 2001). The reduced glycosylation is believed to result in the exposure of a highly immunogenic core peptide sequence (PDTRPAP in bold above) (Girling *et al.*, 1989). The MUC1 sequence PDTRPAP has been identified as the immunodominant B-cell epitope from monoclonal antibody studies in mice (Bashford *et al.*, 1993; Burchell *et al.*, 1989; Denton *et al.*, 1993; Kotera *et al.*, 1994; Xing *et al.*, 1992). This PDTRPAP core peptide sequence is also believed to be immunodominant in humans. Breast cancer patients with MUC1-expressing tumors develop limited humoral and cellular immune responses against the tumor (Finn *et al.*, 1995; Nakamura *et al.*, 1998; Petrarca *et al.*, 1999), with the elicited antibodies and T cells cross-reactive to the PDTRPAP core peptide sequence (Ding *et al.*, 1993; Jerome *et al.*, 1991; Musselli *et al.*, 2002).

Abnormal glycosylation is also believed to result in exposure of the normally cryptic core Tn (GalNAc), STn (sialyl α2-6 GalNAc) and TF (Gal β1-3 GalNAc) carbohydrates (Brockhausen *et al.*, 1998; Itzkowitz *et al.*, 1989). All three carbohydrate epitopes are strongly expressed on human carcinoma cells (Cao *et al.*, 1999; Cao *et al.*, 1997; Itzkowitz et al., 1989; Springer, 1995; Springer, 1997), and may be associated with cancer progression and metastasis (David *et al.*, 1992; Kishikawa *et al.*, 1999; Terasawa *et al.*, 1996). Like the exposed MUC1 sequence, these carbohydrates are also known to induce an immune response, and both MUC1 peptides and MUC1-associated carbohydrate groups have been the subjects of clinical research to develop a cancer vaccine or immunotherapy (Mitchell, 2002).

Vaccine Trials:

Over the past decade, many different clinical trials have been undertaken to assess the ability of MUC1-based vaccines to generate anti-MUC1 immune responses effective at destroying the solid MUC1-expressing tumor (Figure 1.2 shows an overview of cell

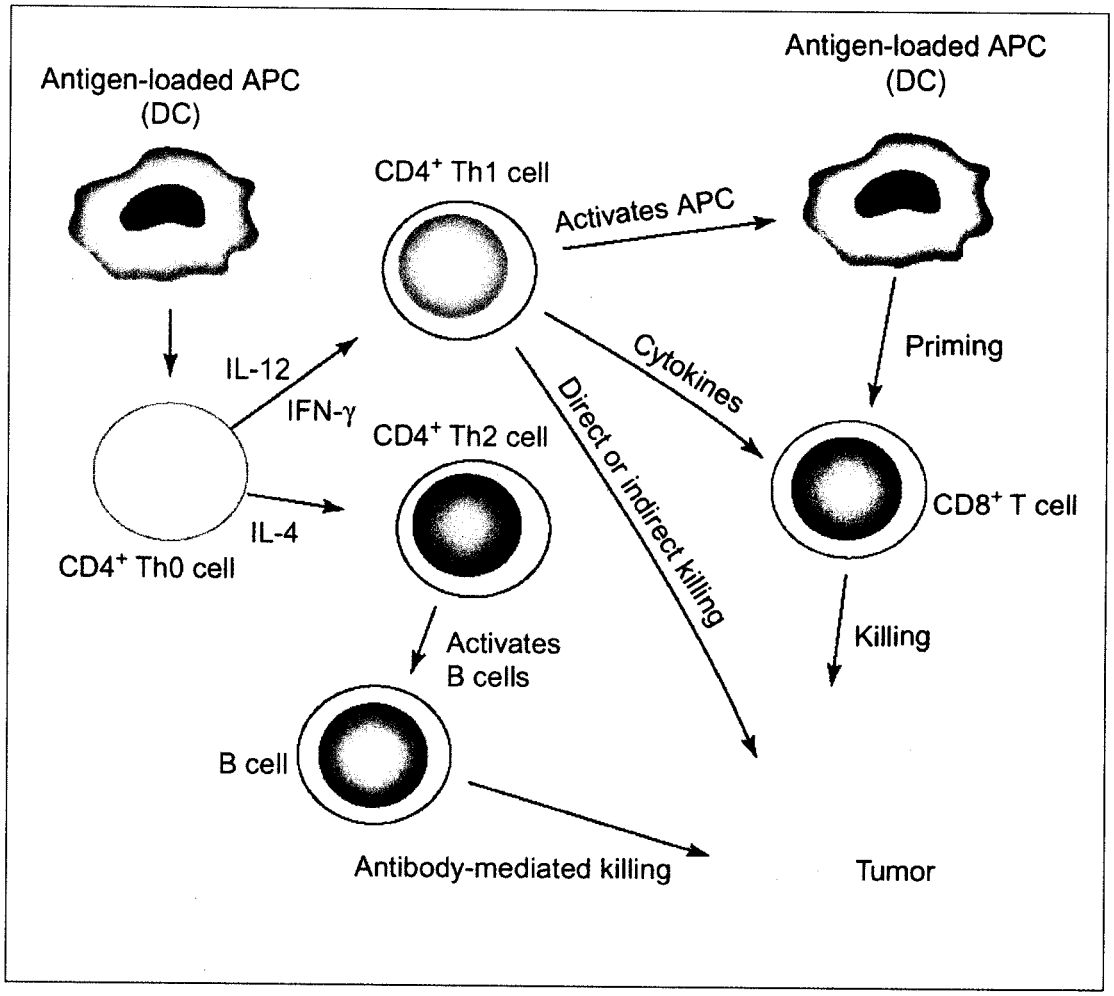

Figure 1.2: Overview of immune response to tumor cells. Antigen presenting cells (APC) such as dendritic cells and B cells activate both CD4+ helper T cells (Th) and CD8+ cytotoxic T cells (CTL). B cells recognize MUC1 mucin on the tumor cell surface and secrete antibodies specific for this antigen. CD8+ T cells recognize the MUC1 antigen on the tumor cell and are able to lyse the tumor cell directly. The Th cells play a major role in regulating the other immune system cells, while CD8+ CTL and antibody-mediated cell killing are the primary direct cytotoxic mechanisms of the immune system.

types involved in immune responses to the MUC1 tumor). Early MUC1 synthetic peptide vaccines utilized multiple repeats of the 20-amino acid sequence. Conjugated and administered with the proper adjuvant, these peptides have generated B cell and T cell immune responses in animal models (Apostolopoulos *et al.*, 2000; Apostolopoulos *et al.*, 1996; Barratt-Boyes *et al.*, 1999; Lofthouse *et al.*, 1997; Vaughan *et al.*, 1999). Most encouraging were the immunization results with MUC1-transgenic mice where MHC Class 1 restricted CD8+ cytotoxic T-cells were produced that eradicated the MUC1 tumors and provided protection against further MUC1 tumor challenge (Apostolopoulos et al., 2000; Apostolopoulos et al., 1996; Lofthouse et al., 1997). Unfortunately, the strong cellular immune responses observed in animals do not translate well to humans. Phase I & II trials of a 5-repeat MUC1 peptide-GST fusion protein conjugated to oxidized mannan produced only weak T-cell proliferative responses in adenocarcinoma patients, demonstrating instead a high antibody titre indicative of a predominantly humoral immune response (Apostolopoulos et al., 1996; Goydos *et al.*, 1996; Karanikas *et al.*, 1997). Several other recent clinical trials have explored the use of MUC1 peptides coupled to different haptens, keyhole limpet hemocyanin, glutathione S-transferase, and oxidized mannan (Apostolopoulos et al., 1999a). All of these clinical trials have demonstrated predominantly humoral immune responses, and none have been able to shrink the solid tumor. Boosting MUC1-specific cellular immunity in adenocarcinoma patients may be key to successful development of a MUC1-based cancer vaccine, but this still represents a major hurdle in MUC1 vaccine design.

Progress is being made in the field of immunology to develop methods to better stimulate cellular immunity to a particular antigen. Undoubtedly this type of research will improve the efficacy of vaccines or immunotherapy for many diseases. Recently, dendritic cells have been recognized to be highly efficient at antigen processing and

presentation to T cells, and several vaccination trials have attempted to boost the immune response to cancer by utilizing peptide- or DNA-pulsed dendritic cells as vaccine vectors. Dendritic cells pulsed with either MUC1 peptides or cDNA have been able to generate limited $CD8^+$ T cell responses to solid breast tumors (Brossart *et al.*, 2000; Pecher *et al.*, 2002), although these responses did not result in tumor rejection. Indeed, none of the MUC1 vaccine candidates described above have been shown to be effective at tumor rejection, although the reasons for this are not absolutely clear (Denda-Nagai & Irimura, 2000; Doehn & Jocham, 2000; Foon, 2001; Morse, 2000; Morse, 2001).

Elucidation of this specific immune mechanism necessary for tumor rejection would advance the field of cancer vaccine design. However, one fundamental problem with present MUC1-based cancer vaccine candidates is that they may not accurately reflect the tumor-associated state of the MUC1 antigen. MUC1 peptide vaccine candidates lacking the MUC1 tumor-associated carbohydrates probably do not best represent the structure, dynamics, peptide epitope exposure, or even glycosylation state of the tumor-associated mucin. For example, vaccination with a MUC1 peptide is unlikely to generate an immune response to the heavily glycosylated region of the extracellular domain of MUC1 on the surface of healthy epithelial cells. While this situation should limit the possibility of an autoimmune response against healthy epithelial tissues, it is also unlikely to lead to a strong tumor-specific immune response against the partially glycosylated tumor-associated MUC1 protein. Therefore, even if the mechanisms necessary for a strong immune response could be triggered, this response would probably lack the specificity required to recognize the MUC1-expressing tumor.

Several lines of evidence suggest that an important element for boosting MUC1 specific immunity in adenocarcinoma patients may be the inclusion of MUC1 tumor-associated carbohydrates at select sites in the MUC1 peptide vaccine. Exposure of these

tumor-associated core carbohydrate epitopes through the use of O-glycosylation inhibitors has been shown to lead to lysis of MUC1 transfected targets in a Class I MHC-restricted manner (Bohm *et al.*, 1997). In addition, immunization trials using MUC1 carbohydrate epitopes can elicit both a tumor-shrinking immune response against the MUC1-expressing tumor and a protective effect against further tumor challenge (Fung *et al.*, 1990; Henningsson *et al.*, 1987). One of these vaccines uses the cancer-associated MUC1 core STn carbohydrate coupled to the keyhole limpet hemocyanin (KLH) adjuvant and is presently in Phase III clinical trials (Mitchell, 2002). These results suggest that preferential killing of MUC1 expressing tumors may be due to T-cell recognition of an internal carbohydrate epitope accessible only on the underglycosylated MUC1. Furthermore, natural MUC1 antibodies from breast cancer patients have been shown to react more strongly with GalNAc-glycosylated peptides than with the naked peptide sequence (von Mensdorff-Pouilly *et al.*, 2000), which suggests that a MUC1 glycopeptide more closely approximates the mucin epitope as it exists on the partially glycosylated tumor cell surface.

Structural Hypothesis for MUC1 Immune Recognition:

Redesign of a next-generation MUC1 glycopeptide vaccine requires a better characterization of the tumor-associated MUC1 antigen. Figure 1.3 describes schematically our structural hypothesis for MUC1 immune recognition. MUC1 can be recognized by the immune system in three different ways. First, B cells can secrete antibodies (see the IgG molecule in Figure 1.3) that are specific for MUC1. These antibodies should be capable of recognizing the tumor-associated MUC1 glycoprotein on the tumor cell surface. This recognition event is likely modulated by the glycosylation state of the MUC1 peptide sequence, the number of MUC1 tandem repeats, and MUC1

peptide structure and dynamics. Second, T cell recognition of the tumor-associated MUC1 sequence can and usually involves Class I MHC presentation of the MUC1 tumor antigen. In this case, the glycosylation state of the peptide can be envisioned to affect T cell recognition and activation if the glycopeptide is presented by the MHC. As the MUC1 peptides or glycopeptides are bound to Class I MHC in the restricted case, the native peptide structure and dynamics of the unrestricted antigen is probably irrelevant. Finally, it has been demonstrated in the literature that T cells recognize tumor-associated

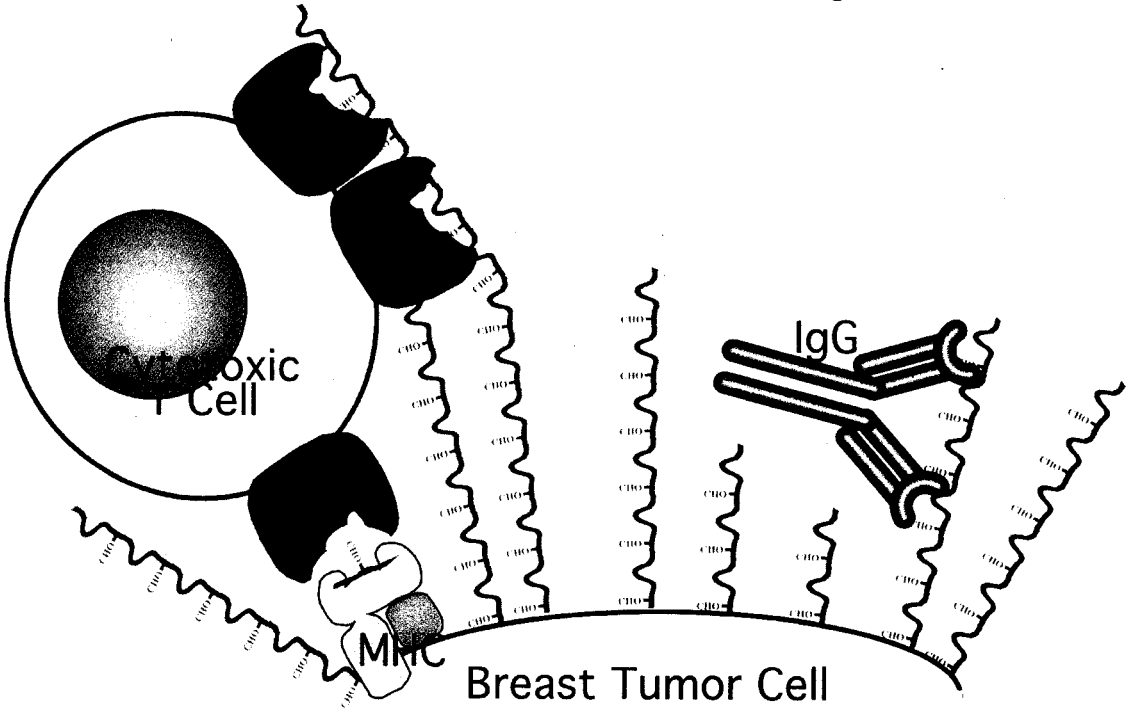

Figure 1.3: Structural hypothesis for humoral and cellular immune recognition of tumor-associated MUC1. Humoral immune recognition of MUC1 involves antibodies secreted by B cells. Antibodies bind directly to the extracellular portion of the MUC1 glycoprotein, and recognition of the antigen should be dependent upon MUC1 structure, dynamics, and glycosylation state. Cellular immune recognition of MUC1 is mediated primarily by CD8+ cytotoxic T cells. T cells recognize MUC1 in two ways: Class I MHC-restricted recognition of the peptide-MHC complex, or direct multivalent binding to the extracellular portion of the MUC1 glycoprotein.

MUC1 in a MHC-unrestricted manner. In this case, the native structure and dynamics, as well as the glycosylation state of the tumor-associated MUC1 sequence could be envisioned to play a significant role in T cell receptor binding. The number of MUC1 repeats is probably also important, because crosslinking of T cell receptors with a multivalent antigen is known to better activate the T cell. Therefore, a detailed understanding of immune recognition of the MUC1 tumor antigen requires an exploration of the role of multiple repeats, glycosylation state, and native MUC1 structure and dynamics in B cell/T cell recognition.

Humoral Immune Recognition of the MUC1 Antigen:

Exposure of the immunogenic MUC1 B cell epitope sequence (PDTRPAP) is a primary requirement for humoral immune recognition of the MUC1 antigen. Synthetic MUC1 peptides have been used extensively to study both antibody binding and MUC1 peptide structure. Spectroscopic techniques such as NMR and CD have identified native β-turn secondary structure and poly-proline type II helix (PPII) in unglycosylated MUC1 (Fontenot, 1993; Fontenot *et al.*, 1993; Fontenot *et al.*, 1995; Grinstead *et al.*, 2002; Liu *et al.*, 1995; Schuman *et al.*, 2003). Since the β-turn is a common structural motif in antigenic regions of proteins (Koebnik *et al.*, 2000) and is commonly found in NMR and crystal structures of antibody-antigen complexes (Derrick *et al.*, 1999; Stanfield *et al.*, 1999; Tugarinov *et al.*, 1999; Zvi *et al.*, 2000), the presence of a β-turn within the MUC1 B-cell epitope may explain the immunodominance of this region. Indeed, it has been suggested that β-turn structure is important in humoral immune recognition of the MUC1 sequence (Fontenot, 1993). At the time of our initial studies on this system, no structural studies of MUC1 peptides bound to tumor-associated antibodies had been performed.

Furthermore, no research has attempted to correlate MUC1 β-turn structure to the partially-glycosylated MUC1 protein as it exists on the tumor cell surface.

In addition to previous structural studies showing β-turn structure within the PDTRPAP B-cell epitope, other structural studies of single versus multiple repeat MUC1 peptides have shown significant PPII helix structure, and β-turn structure that adopts more 'native-like structure' with increasing repeat number (Fontenot, 1993). If increases in repeat number lead to more ordered immunogenic structure in the tumor-associated MUC1 sequence, then this might explain why longer peptides are more immunogenic. In this regard, a study of 56 MUC1-specific antibodies showed that 47 out of the 56 antibodies bound with higher affinity to a 5-repeat MUC1 sequence than a one-repeat sequence (Price *et al.*, 1998). However, there remains the question as to whether the observed differences in antibody binding are due to differences in length-dependent MUC1 structure or dynamics, or only due to increased avidity from multivalent binding.

In addition to β-turn structure and repeat number, the glycosylation state of tumor-associated MUC1 is a major factor in humoral immunity, because the glycosylation state of the MUC1 sequence directly regulates the exposure of the peptide core to antibodies and modifies the structure and dynamics of the exposed MUC1 sequence. There are five potential O-glycosylation sites in each tandem repeat of the MUC1 sequence (GVTSAPDTRPAPGSTAPPAH). Identifying which of these sites remains glycosylated in the tumor-associated state is important for MUC1 vaccine design, as the vaccine should approximate as closely as possible the glycosylation state and peptide backbone exposure of the intact tumor. *In vitro* glycosylation studies using human tumor cell extracts (Nishimori *et al.*, 1994a; Nishimori *et al.*, 1994b) and three different recombinant GalNAc transferases identified from human tumor cell lines (Wandall *et al.*, 1997) have demonstrated glycosylation at three separate sites (GVTSA

and GSTAP), but not at the threonine within the PDTRPAP B cell epitope sequence. These findings are significant because they suggest that reduced glycosylation of MUC1 permits antibodies access to this region of the peptide sequence. However, recent *in vivo* studies have demonstrated that all five sites on the MUC1 tandem repeat are glycosylation targets (Muller *et al.*, 1999; Muller *et al.*, 1997), although there is no evidence to suggest that all sites are actually glycosylated. Ultimately, we do not know where or what types of carbohydrates exist on the tumor-associated MUC1 sequence. In fact, there is most likely not a single, uniformly presented glycoform of the tumor-associated MUC1 antigen. The glycosylation state is probably highly heterogeneous (Cao et al., 1999; Cao et al., 1997).

In summary, prior research performed by other groups has raised the following questions as to how the humoral immune system recognizes the MUC1 tumor-associated antigen. 1) What is the role of the β-turn in humoral recognition of the tumor-associated MUC1 antigen? 2) What are the effects of repeat number on MUC1 structure and dynamics and humoral recognition of the MUC1 antigen? 3) What are the effects of glycosylation of the MUC1 B cell epitope on native MUC1 structure and dynamics and therefore on humoral recognition and immunogenicity?

Cellular Immune Recognition of the MUC1 Antigen:

T cells recognize antigenic peptides that are presented bound to MHC molecules on the surface of a target cell. Class I MHC binds 8- to 10-residue peptides along a platform of eight antiparallel β-strands that are bound on the sides by two α-helices that make a conserved network of hydrogen bonds to the main chain of the bound peptide (Madden, 1995). Detailed structural studies have identified six different pockets in the

peptide binding groove of the human Class I MHC molecule HLA-A*0201 (Madden *et al.*, 1993). Two main pockets bind the sidechains of the N- and C-terminal residues for canonical high-affinity antigens. The remaining pockets provide secondary binding interactions that modulate bound peptide affinity.

Two T cell epitopes (SAPDTRPA and STAPPAHGV) have been identified in the MUC1 sequence. These sequences do not contain the canonical primary sidechains required for high-affinity binding to Class I MHC. Without these sidechains, MUC1 peptides bind MHC with low affinity. However, these peptides are still weakly immunogenic, so methods for improving their immunogenicity are being explored in depth (Berzofsky *et al.*, 2001). Higher affinity for Class I MHC has been correlated with greater immunogenicity (Sette *et al.*, 2002). Therefore, if the basis for low-affinity binding to MHC could be characterized, it might be possible to improve affinity for MHC without altering T cell specificity for the antigen. For example, in the only published crystal structure of a MUC1 peptide in complex with Class I MHC, several of the peptide sidechains do not fill the MHC binding pockets completely (Apostolopoulos *et al.*, 2002) (see Figure 1.4). It may be possible to mutate the sidechains of the MUC1 peptide residues that fill pockets in the MHC to increase affinity for the MHC without altering the orientation of upper peptide face that interacts with the T cell receptor. The increased affinity of this molecule for MHC may then better stimulate T cells to recognize the MUC1 antigen.

Since MUC1 glycosylation plays an important role in the humoral immune response to MUC1 antigenic peptides, it is not surprising that carbohydrate-specific T cell responses have been generated from immunization of mice with MUC1 glycopeptides (Gad *et al.*, 2003; Vlad *et al.*, 2002). Around 0.5% of peptides presented

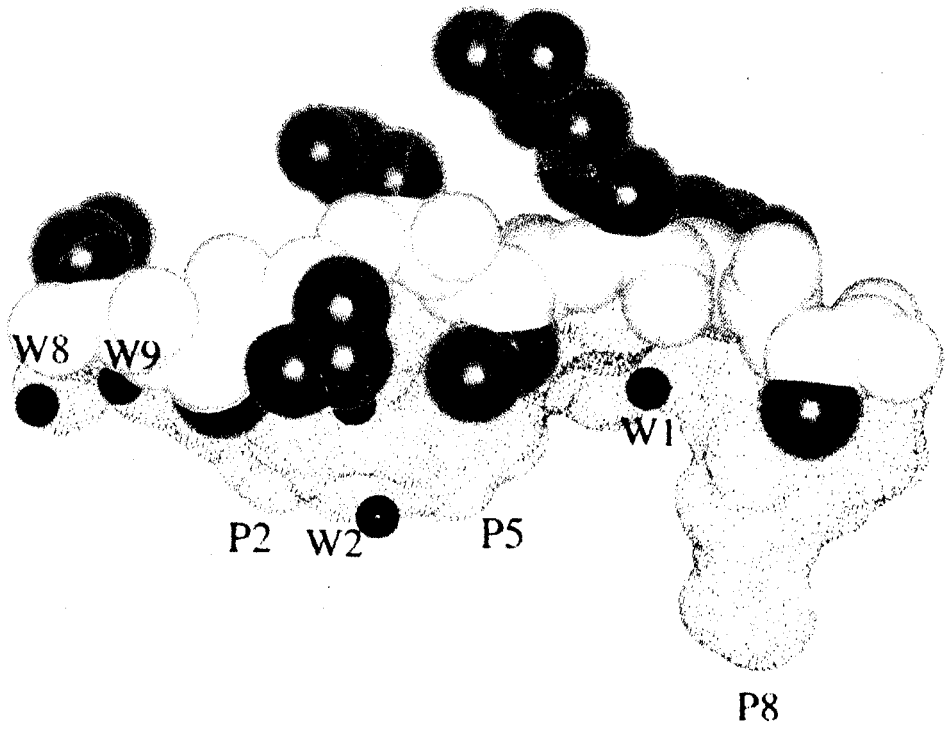

Figure 1.4: 1.6 Å crystal structure of murine Class I MHC H-2K^b in complex with MUC1 peptide SAPDTRPA (Apostolopoulos et al., 2002). Occupancy of H-2K^b pockets (dotted surface) by MUC1 peptide sidechains (in red) is shown. Small secondary anchors at positions P2, P5 and P8, coupled with the absence of 'rescuing' water and a large cavity at the side of the C pocket are hypothesized to contribute to the low affinity of the peptide for MHC.

by Class I MHC on normal cell surfaces are glycosylated with a N-acetyl glucosamine (GlcNAc) (Haurum *et al.*, 1999), and both CD8+ and CD4+ T cells are capable of binding to peptides with mono-and disaccharide modifications (Abdel-Motal *et al.*, 1996; Deck *et al.*, 1999). While glycopeptide presentation to T cells clearly plays an important role in immunity (Rudd *et al.*, 2001), the cellular mechanism for glycopeptide production and loading onto Class I MHC is not known. Furthermore, the structural mechanisms whereby T cell receptors recognize MUC1 carbohydrate are also unknown. The crystal structure of a glycopeptide-MHC complex is shown in Figure 1.5, which demonstrates that the carbohydrate moiety of the peptide is available to make substantial stabilizing interactions with a T cell receptor (modeled above the glycopeptide). No crystal structure

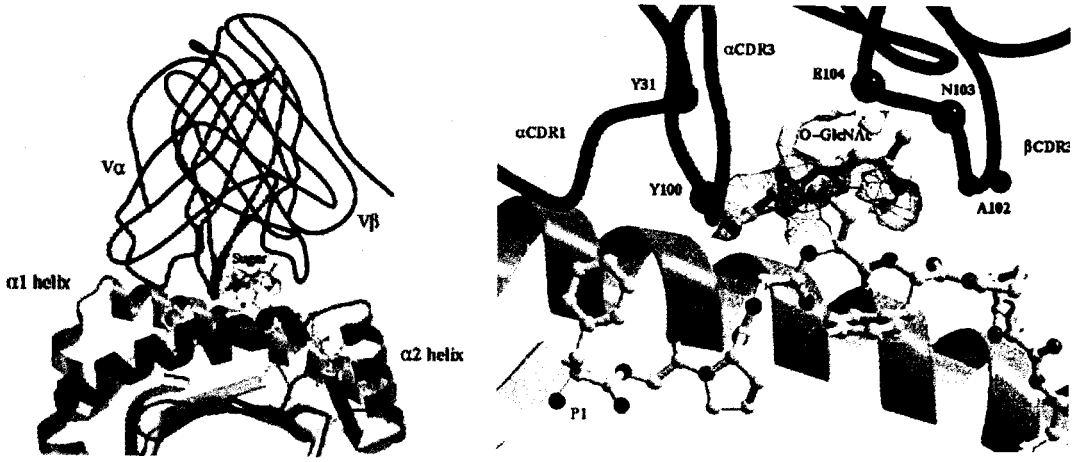

Figure 1.5: 2.85 Å crystal structure of murine Class I MHC H-2D^b in complex with an O-GlcNAc substituted peptide, FAPS(O-GlcNAc)NYPAL (Glithero *et al.*, 1999). The carbohydrate (in yellow) is solvent exposed and available for direct recognition by the αβTCR. The modeled MHC-glycopeptide-TCR complex (left and right) shows that a single saccharide residue can be accommodated in the standard TCR-MHC geometry. H-2D^b CTL clones raised against the glycopeptide were shown to require the carbohydrate moiety for recognition.

of a MUC1 glycopeptide-MHC complex has been solved, and structural information about this type of complex would be very useful, as it might resolve the role of carbohydrate in cellular recognition and immunogenicity.

In addition to Class I MHC-restricted T cell responses to the MUC1 antigen, several groups have characterized MHC-unrestricted T cell responses (Finn et al., 1995; Rudd et al., 2001). The structural basis for T cell responses directly to the MUC1 antigen is not known, but is thought to involve the interactions of multiple T cell receptors with the multiple repeat MUC1 antigen. The increased stability afforded by the multivalent binding may overcome the inherently weak affinities of T cell receptors for antigens free in solution (not presented by MHC). Since MHC-unrestricted T cell immune responses appear to be well established in the literature, a characterization of the structural and dynamic properties of MUC1 peptides and glycopeptides free in solution could provide

fundamental insight into the role of MUC1 structure and dynamics (as well as how repeat number or multivalency may play into these attributes) in cellular recognition and immunogenicity.

NMR Approach to the Study of MUC1 Immune Recognition:

In the absence of a clear picture of MUC1 mucin in its tumor-associated state, the design of a peptide or glycopeptide vaccine that mimics that unknown state is a difficult undertaking. In order to circumnavigate this difficulty, we utilize an approach that does not rely on *a priori* knowledge of peptide conformation or glycosylation state of the tumor-associated MUC1 mucin. Our approach uses an anti-MUC1 antibody, Mab B27.29, as a 'reverse-template' for MUC1 vaccine design, which allows exploration of the humoral immune response to MUC1 tumor antigen. Mab B27.29 was raised directly against MUC1-expressing tumors, so should bind most tightly to a MUC1 peptide or glycopeptide that best approximates the structure, dynamics, and glycosylation state of the tumor-associated MUC1 mucin. Therefore, Mab B27.29 is an immunologically relevant reverse-template of the structure, dynamics, and chemistry of the tumor-associated MUC1 mucin. In brief, this approach identifies the immunologically relevant peptide conformation and glycosylation states of the tumor-associated MUC1 mucin by probing the structure and dynamics of MUC1 peptide - Mab B27.29 binding. Solution state NMR is used as the probe in these systems, because it allows both structure and dynamics information to be obtained for the bound state, even if that bound state is dynamic and conformationally heterogeneous. Figure 1.6A outlines the experimental approach to studying MUC1 humoral immunogenicity. Our approach uses ^{15}N and ^{13}C HSQC experiments to map the boundaries of the B27.29 epitope, and NMR relaxation experiments to characterize immobilization of MUC1 residues upon antibody binding.

Our approach to exploration of the cellular immune response to the MUC1 tumor antigen involves refolding of human Class I MHC HLA-A*0201 with various antigenic peptides, and then using NMR spectroscopy to characterize the structure and dynamics of the bound peptides. Figure 1.6B outlines the experimental approach to study of MUC1 peptides in a stable complex with refolded human Class I MHC HLA-A*0201. Through analysis of differential linewidth of resonances and other strategies, we can infer which peptide sidechains might point out of the MHC binding groove for potential interactions with the T cell receptor, and which peptide sidechains point down into the MHC peptide binding groove to stabilize the peptide-MHC complex. Multiple peptides can be studied in this manner, and hopefully the structural and dynamic basis for low-affinity tumor-associated antigenic peptide binding can be established. The same approach could also be used to characterize glycopeptides bound to HLA-A*0201, and to determine how MUC1-associated carbohydrate substituents might be positioned to interact with either MHC or TCR. In addition, the effects of carbohydrate location and type on MUC1 glycopeptide-MHC complex stability could be easily assayed using our refolding protocol. This would allow simple screening of MUC1 glycoforms and analogs for Class I MHC binding, without using more complicated NMR methodologies.

Overview of Chapters:

In Chapter 2, we use heteronuclear NMR methods to characterize the differences between 1-repeat and 2-repeat MUC1 peptides. These peptides exhibit identical structural features and very similar dynamics in solution, and point to the effects of avidity from multivalent binding as being important for humoral recognition of MUC1 peptides.

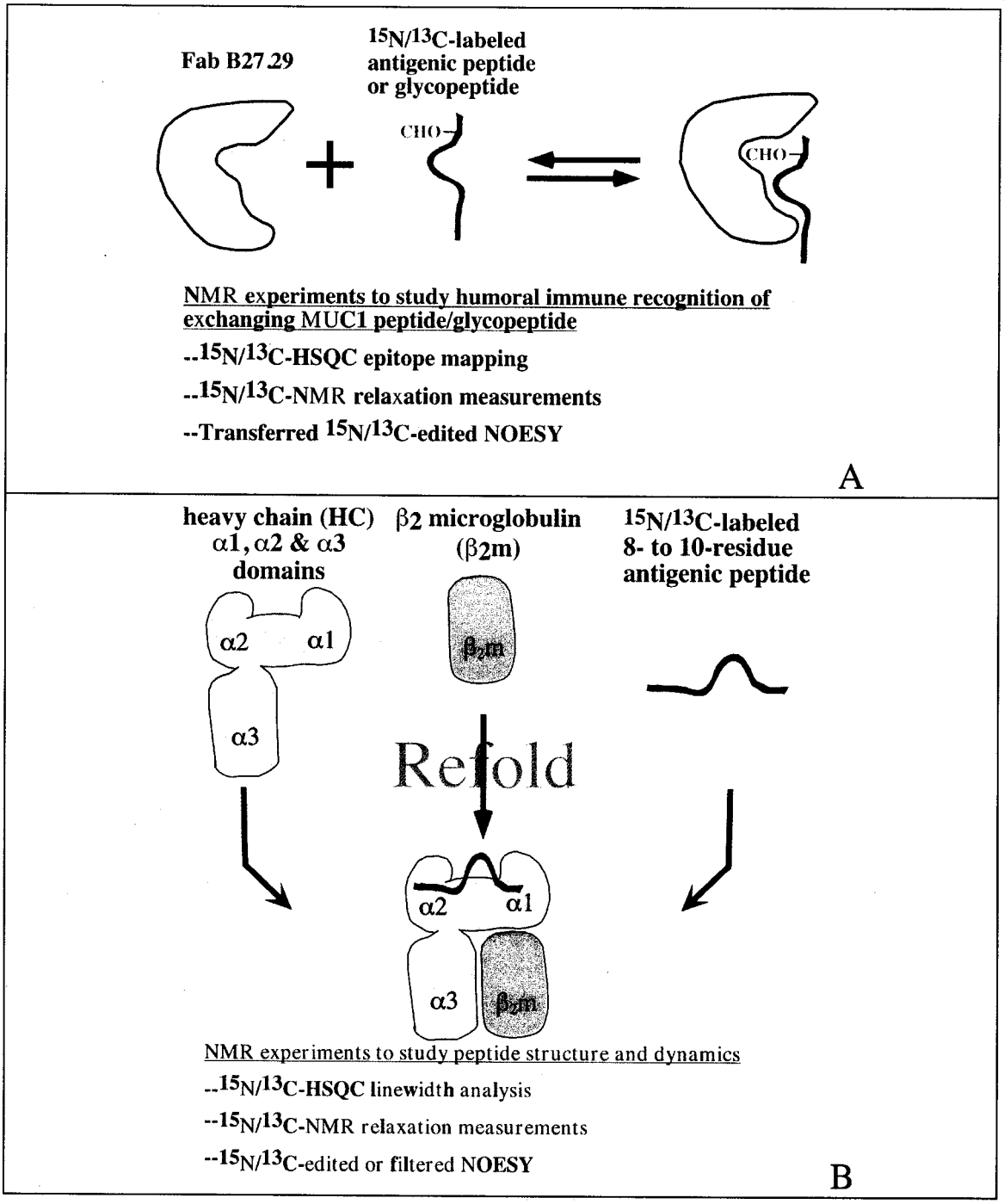

Figure 1.6: Experimental approach to the study of MUC1 immunogenicity. Panel A shows the proposed protocol for study of the MUC1 peptide or glycopeptide interactions with Fab B27.29. Panel B shows the protocol for study of antigenic peptides or glycopeptides refolded with human Class I MHC HLA-A*0201.

In Chapter 3, we use NMR methods to probe the structural and dynamic consequences of glycosylation at serine and threonine residues upstream of the PDTRPAP core epitope region of MUC1 synthetic peptides. We correlate these structural and dynamic effects of glycosylation to the recognition of a monoclonal antibody, B27.29, raised against the intact tumor-associated MUC1 mucin. Four peptides were studied: a MUC1 16mer peptide of the sequence (Gly1-Val2-Thr3-Ser4-Ala5-Pro6-Asp7-Thr8-Arg9-Pro10-Ala11-Pro12-Gly13-Ser14-Thr15-Ala16), two singly Tn-glycosylated versions of this peptide at either Thr3 or Ser4, and a doubly Tn-glycosylated version at both Thr3 and Ser4. Included in the study are two-dimensional ^{1}H NMR TRNOESY studies of the binding of the doubly-glycosylated MUC1 16mer to the Fab fragment of B27.29. These studies allowed a mapping of the MUC1 B-cell epitope, and an assessment of the contribution of the PDTRP core peptide epitope versus the Tn core carbohydrate epitope to antibody B27.29 recognition. The results of these studies are discussed within the framework of developing a glycosylated second-generation MUC1 glycopeptide vaccine.

In Chapter 4, we extend our NMR-based approach to examine the role of peptide structure and dynamics in Fab B27.29 recognition of the same 16 residue MUC1 peptide (GVTSAPDTRPAPGSTA), as well as of a 40 residue MUC1 peptide, $(VTSAPDTRPAPGSTAPPAHG)_2$, that represents two repeats of the MUC1 sequence.

Included in this present study are two-dimensional isotope-edited NMR experiments, as well as heteronuclear NMR relaxation measurements, monitoring the binding of the isotopically-labeled MUC1 peptides to the unlabeled Fab fragment of B27.29. These experiments allowed a precise mapping of the boundary of the B27.29 epitope, based on a determination of the immobilized portion of the peptide as it is bound within the B27.29 antibody combining site. The results of these studies are discussed

within the framework of developing a second-generation MUC1 peptide vaccine that better represents the peptide portion of the tumor-associated MUC1 mucin, as it is recognized by B27.29.

In Chapter 5 we present a refolding protocol to produce the ternary HLA-A*0201 complex (HC/β_2m/peptide) for study by NMR spectroscopy. Combined with a novel approach to producing recombinant, uniformly isotope-labeled MUC1 peptides, this procedure will allow study of the basis for low-affinity binding of MUC1 antigenic peptides to Class I MHC HLA-A*0201. In addition, the system also should allow study of MUC1 glycopeptide-MHC complexes.

In summary, the above chapters have characterized several features affecting the humoral and cellular immune responses to the tumor-associated MUC1 antigen. Our conclusions are as follows: that the β-turn region appears to be recognizing the cancer-associated antibody B27.29, that repeat number does not affect the structure or dynamics of the MUC1 sequence, and that site-specific glycosylation of the MUC1 sequence upstream from the β-turn structure interacts with B27.29. In addition, we have established a protocol for study of Class I MHC HLA-A*0201-MUC1 peptide complex using NMR spectroscopy. Implications for next-generation vaccine design are discussed in Chapter 6 (Conclusion and Future Directions).

Notes to Chapter 1

Abdel-Motal, U. M., Berg, L., Rosen, A., Bengtsson, M., Thorpe, C. J., Kihlberg, J., Dahmen, J., Magnusson, G., Karlsson, K. A. & Jondal, M. (1996). Immunization with glycosylated Kb-binding peptides generates carbohydrate-specific, unrestricted cytotoxic T cells. *Eur J Immunol* **26**(3), 544-51.

Apostolopoulos, V., McKenzie, I. F. & Pietersz, G. A. (2000). Generation of MUC1 cytotoxic T-cells in mice and epitope mapping. *Methods Mol Biol* **125**, 455-62.

Apostolopoulos, V., Pietersz, G. A. & McKenzie, I. F. (1999a). MUC1 and breast cancer. *Curr Opin Mol Ther* **1**(1), 98-103.

Apostolopoulos, V., Pietersz, G. A. & McKenzie, I. F. C. (1996). Cell-Mediated Immune Response to MUC1 Fusion Protein Coupled to Mannan. *Vaccine* **14**(9), 930-938.

Apostolopoulos, V., Sandrin, M. S. & McKenzie, I. F. C. (1999b). Carbohydrate/Peptide mimics: effect on MUC1 Cancer Immunotherapy. *J Mol Med* **77**, 427-436.

Apostolopoulos, V., Yu, M., Corper, A. L., Teyton, L., Pietersz, G. A., McKenzie, I. F., Wilson, I. A. & Plebanski, M. (2002). Crystal structure of a non-canonical low-affinity peptide complexed with MHC class I: a new approach for vaccine design. *J Mol Biol* **318**(5), 1293-305.

Barratt-Boyes, S. M., Vlad, A. & Finn, O. J. (1999). Immunization of chimpanzees with tumor antigen MUC1 mucin tandem repeat peptide elicits both helper and cytotoxic T-cell responses. *Clin Cancer Res* **5**(7), 1918-24.

Bashford, J. L., Robins, R. A. & Price, M. R. (1993). Development of an anti-idiotypic antibody reactive with an antibody defining the epitope RPAP in the MUC-1 epithelial mucin core. *Int J Cancer* **54**(5), 778-83.

Berzofsky, J. A., Ahlers, J. D. & Belyakov, I. M. (2001). Strategies for designing and optimizing new generation vaccines. *Nat Rev Immunol* **1**(3), 209-19.

Bhavanandan, V. P. (1991). Cancer-associated mucins and mucin-type glycoproteins. *Glycobiology* **1**(5), 493-503.

Bohm, C. M., Mulder, M. C., Zennadi, R., Notter, M., Schmitt-Graff, A., Finn, O. J., Taylor-Papadimitriou, J., Stein, H., Clausen, H., Riecken, E. O. & Hanski, O. (1997). Carbohydrate Recognition on MUC-1 Expressing Targets Enhances Cytoxicity of a T Cell Subpopulation,. *Scand J Immunol* **46**, 27-34.

Brockhausen, I., Yang, J., Dickinson, N., Ogata, S. & Itzkowitz, S. H. (1998). Enzymatic basis for sialyl-Tn expression in human colon cancer cells. *Glycoconj J* **15**(6), 595-603.

Brossart, P., Wirths, S., Stuhler, G., Reichardt, V. L., Kanz, L. & Brugger, W. (2000). Induction of cytotoxic T-lymphocyte responses in vivo after vaccinations with peptide-pulsed dendritic cells. *Blood* **96**(9), 3102-8.

Burchell, J., Taylor-Papadimitriou, J., Boshell, M., Gendler, S. & Duhig, T. (1989). *Int J Cancer* **44**, 691-696.

Cao, Y., Karsten, U., Otto, G. & Bannasch, P. (1999). Expression of MUC1, Thomsen-Friedenreich antigen, Tn, sialosyl-Tn, and alpha2,6-linked sialic acid in hepatocellular carcinomas and preneoplastic hepatocellular lesions. *Virchows Arch* **434**(6), 503-9.

Cao, Y., Schlag, P. M. & Karsten, U. (1997). Immunodetection of epithelial mucin (MUC1, MUC3) and mucin-associated glycotopes (TF, Tn, and sialosyl-Tn) in benign and malignant lesions of colonic epithelium: apolar localization corresponds to malignant transformation. *Virchows Arch* **431**(3), 159-66.

Carlstedt, I. & Davies, J. R. (1997). Glycoconjugates facing the outside world. *Biochem Soc Trans* **25**(1), 214-9.

David, L., Nesland, J. M., Clausen, H., Carneiro, F. & Sobrinho-Simoes, M. (1992). Simple mucin-type carbohydrate antigens (Tn, sialosyl-Tn and T) in gastric mucosa, carcinomas and metastases. *APMIS Suppl* **27**, 162-72.

Deck, M. B., Sjolin, P., Unanue, E. R. & Kihlberg, J. (1999). MHC-restricted, glycopeptide-specific T cells show specificity for both carbohydrate and peptide residues. *J Immunol* **162**(8), 4740-4.

Denda-Nagai, K. & Irimura, T. (2000). MUC1 in carcinoma-host interactions. *Glycoconj J* **17**(7-9), 649-58.

Denton, G., Sekowski, M. & Price, M. R. (1993). Induction of antibody responses to breast carcinoma associated mucins using synthetic peptide constructs as immunogens. *Cancer Lett* **70**(3), 143-50.

Derrick, J. P., Maiden, M. C. & Feavers, I. M. (1999). Crystal structure of an Fab fragment in complex with a meningococcal serosubtype antigen and a protein G domain. *J Mol Biol* **293**(1), 81-91.

Ding, L., Lalani, E. N., Reddish, M., Koganty, R., Wong, T., Samuel, J., Yacyshyn, M. B., Meikle, A., Fung, P. Y. & Taylor-Papadimitriou, J. (1993). Immunogenicity of synthetic peptides related to the core peptide sequence encoded by the human MUC1 mucin gene: effect of immunization on the growth of murine mammary adenocarcinoma cells transfected with the human MUC1 gene. *Cancer Immunol Immunother* **36**(1), 9-17.

Doehn, C. & Jocham, D. (2000). Technology evaluation: TG-1031, Transgene SA. *Curr Opin Mol Ther* **2**(1), 106-11.

Finn, O. J., Jerome, K. R., Henderson, R. A., Pecher, G., Domenech, N., Magarian-Blander, J. & Barratt-Boyes, S. M. (1995). MUC-1 epithelial tumor mucin-based immunity and cancer vaccines. *Immunol Rev* **145**, 61-89.

Fontenot, J. D. (1993). Biophysical Characterization of One, Two, and Three-Tandem Repeats of Human Mucin (MUC-1) Protein Core. *Cancer Research* **53**, 5386-5394.

Fontenot, J. D., Finn, O. J., Dales, N., Andrews, P. C. & Montelaro, R. C. (1993). Synthesis of large multideterminant peptide immunogens using a poly-proline beta-turn helix motif. *Pept Res* **6**(6), 330-6.

Fontenot, J. D., Mariappan, S. V., Catasti, P., Domenech, N., Finn, O. J. & Gupta, G. (1995). Structure of a tumor associated antigen containing a tandemly repeated immunodominant epitope. *J Biomol Struct Dyn* **13**(2), 245-60.

Foon, K. A. (2001). Immunotherapy for colorectal cancer. *Curr Oncol Rep* **3**(2), 116-26.

Fung, P. Y., Madej, M., Koganty, R. R. & Longenecker, B. M. (1990). Active specific immunotherapy of a murine mammary adenocarcinoma using a synthetic tumor-associated glycoconjugate. *Cancer Res* **50**(14), 4308-14.

Gad, M., Jensen, T., Gagne, R., Komba, S., Daugaard, S., Kroman, N., Meldal, M., Werdelin, O., Vlad, A. M., Muller, S., Cudic, M., Paulsen, H., Otvos, L., Jr., Hanisch, F. G. & Finn, O. J. (2003). MUC1-derived glycopeptide libraries with improved MHC anchors are strong antigens and prime mouse T cells for proliferative responses to lysates of human breast cancer tissue. *Eur J Immunol* **33**(6), 1624-32.

Girling, A., Bartkova, J., Burchell, J., Gendler, S., Gillett, C. & Taylor-Papadimitriou, J. (1989). A core protein epitope of the polymorphic epithelial mucin detected by the monoclonal antibody SM-3 is selectively exposed in a range of primary carcinomas. *Int J Cancer* **43**(6), 1072-6.

Glithero, A., Tormo, J., Haurum, J. S., Arsequell, G., Valencia, G., Edwards, J., Springer, S., Townsend, A., Pao, Y. L., Wormald, M., Dwek, R. A., Jones, E. Y. & Elliott, T. (1999). Crystal structures of two H-2Db/glycopeptide complexes suggest a molecular basis for CTL cross-reactivity. *Immunity* **10**(1), 63-74.

Goydos, J. S., Elder, E., Whiteside, T. L., Finn, O. J. & Lotze, M. T. (1996). A phase I trial of a synthetic mucin peptide vaccine. Induction of specific immune reactivity in patients with adenocarcinoma. *J Surg Res* **63**(1), 298-304.

Grinstead, J. S., Koganty, R. R., Krantz, M. J., Longenecker, B. M. & Campbell, A. P. (2002). Effect of glycosylation on MUC1 humoral immune recognition: NMR studies of MUC1 glycopeptide-antibody interactions. *Biochemistry* **41**(31), 9946-61.

Hanisch, F. G. (2001). O-glycosylation of the mucin type. *Biol Chem* **382**(2), 143-9.

Haurum, J. S., Hoier, I. B., Arsequell, G., Neisig, A., Valencia, G., Zeuthen, J., Neefjes, J. & Elliott, T. (1999). Presentation of cytosolic glycosylated peptides by human class I major histocompatibility complex molecules in vivo. *J Exp Med* **190**(1), 145-50.

Henningsson, C. M., Selvaraj, S., MacLean, G. D., Suresh, M. R., Noujaim, A. A. & Longenecker, B. M. (1987). T cell recognition of a tumor-associated glycoprotein

and its synthetic carbohydrate epitopes: stimulation of anticancer T cell immunity in vivo. *Cancer Immunol Immunother* **25**(3), 231-41.

Itzkowitz, S. H., Yuan, M., Montgomery, C. K., Kjeldsen, T., Takahashi, H. K., Bigbee, W. L. & Kim, Y. S. (1989). Expression of Tn, sialosyl-Tn, and T antigens in human colon cancer. *Cancer Res* **49**(1), 197-204.

Jerome, K. R., Barnd, D. L., Bendt, K. M., Boyer, C. M., Taylor-Papadimitriou, J., McKenzie, I. F., Bast, R. C., Jr. & Finn, O. J. (1991). Cytotoxic T-lymphocytes derived from patients with breast adenocarcinoma recognize an epitope present on the protein core of a mucin molecule preferentially expressed by malignant cells. *Cancer Res* **51**(11), 2908-16.

Karanikas, V., Hwang, L. A., Pearson, J., Ong, C. S., Apostolopoulos, V., Vaughan, H., Xing, P. X., Jamieson, G., Pietersz, G., Tait, B., Broadbent, R., Thynne, G. & McKenzie, I. F. (1997). Antibody and T cell responses of patients with adenocarcinoma immunized with mannan-MUC1 fusion protein. *J Clin Invest* **100**(11), 2783-92.

Kishikawa, T., Ghazizadeh, M., Sasaki, Y. & Springer, G. F. (1999). Specific role of T and Tn tumor-associated antigens in adhesion between a human breast carcinoma cell line and a normal human breast epithelial cell line. *Jpn J Cancer Res* **90**(3), 326-32.

Koebnik, R., Locher, K. P. & Van Gelder, P. (2000). Structure and function of bacterial outer membrane proteins: barrels in a nutshell. *Mol Microbiol* **37**(2), 239-53.

Koganty, R. R., Reddish, M. A. & Longenecker, B. M. (1997). Glycopeptides in the Immunotherapy of Cancer. In *Glycopeptides and Related Compounds: Synthesis, Analysis and Application* (C.D., L. D. G. a. W., ed.), pp. 707-743. Dekker, New York.

Kotera, Y., Fontenot, J. D., Pecher, G., Metzgar, R. S. & Finn, O. J. (1994). Humoral immunity against a tandem repeat epitope of human mucin MUC-1 in sera from breast, pancreatic, and colon cancer patients. *Cancer Res* **54**(11), 2856-60.

Liu, X., Sejbal, J., Kotovych, G., Koganty, R. R., Reddish, M. A., Jackson, L., Gandhi, S. S., Mendonca, A. J. & Longenecker, B. M. (1995). Structurally defined synthetic cancer vaccines: analysis of structure, glycosylation and recognition of cancer associated mucin, MUC-1 derived peptides. *Glycoconj J* **12**(5), 607-17.

Lofthouse, S. A., Apostolopoulos, V., Pietersz, G. A., Li, W. & McKenzie, I. F. (1997). Induction of T1 (cytotoxic lymphocyte) and/or T2 (antibody) responses to a mucin-1 tumour antigen. *Vaccine* **15**(14), 1586-93.

Madden, D. R. (1995). The three-dimensional structure of peptide-MHC complexes. *Annu Rev Immunol* **13**, 587-622.

Madden, D. R., Garboczi, D. N. & Wiley, D. C. (1993). The antigenic identity of peptide-MHC complexes: a comparison of the conformations of five viral peptides presented by HLA-A2. *Cell* **75**(4), 693-708.

Miles, D. W. & Taylor-Papadimitriou, J. (1999). Therapeutic aspects of polymorphic epithelial mucin in adenocarcinoma. *Pharmacol Ther* **82**(1), 97-106.

Mitchell, M. S. (2002). Cancer vaccines, a critical review--Part II. *Curr Opin Investig Drugs* **3**(1), 150-8.

Morse, M. A. (2000). Technology evaluation: Theratope, Biomira Inc. *Curr Opin Mol Ther* **2**(4), 453-8.

Morse, M. A. (2001). Technology evaluation: BLP-25, Biomira Inc. *Curr Opin Mol Ther* **3**(1), 102-5.

Muller, S., Alving, K., Peter-Katalinic, J., Zachara, N., Gooley, A. A. & Hanisch, F. G. (1999). High density O-glycosylation on tandem repeat peptide from secretory MUC1 of T47D breast cancer cells. *J Biol Chem* **274**(26), 18165-72.

Muller, S., Goletz, S., Packer, N., Gooley, A., Lawson, A. M. & Hanisch, F. G. (1997). Localization of O-glycosylation sites on glycopeptide fragments from lactation-associated MUC1. All putative sites within the tandem repeat are glycosylation targets in vivo. *J Biol Chem* **272**(40), 24780-93.

Musselli, C., Ragupathi, G., Gilewski, T., Panageas, K. S., Spinat, Y. & Livingston, P. O. (2002). Reevaluation of the cellular immune response in breast cancer patients vaccinated with MUC1. *Int J Cancer* **97**(5), 660-7.

Nakamura, H., Hinoda, Y., Nakagawa, N., Makiguchi, Y., Itoh, F., Endo, T. & Imai, K. (1998). Detection of circulating anti-MUC1 mucin core protein antibodies in patients with colorectal cancer. *J Gastroenterol* **33**(3), 354-61.

Nishimori, I., Johnson, N. R., Sanderson, S. D., Perini, F., Mountjoy, K., Cerny, R. L., Gross, M. L. & Hollingsworth, M. A. (1994a). Influence of acceptor substrate primary amino acid sequence on the activity of human UDP-N-acetylgalactosamine:polypeptide N-acetylgalactosaminyltransferase. Studies with the MUC1 tandem repeat. *J Biol Chem* **269**(23), 16123-30.

Nishimori, I., Perini, F., Mountjoy, K. P., Sanderson, S. D., Johnson, N., Cerny, R. L., Gross, M. L., Fontenot, J. D. & Hollingsworth, M. A. (1994b). N-acetylgalactosamine glycosylation of MUC1 tandem repeat peptides by pancreatic tumor cell extracts. *Cancer Res* **54**(14), 3738-44.

Patton, S., Gendler, S. J. & Spicer, A. P. (1995). The epithelial mucin, MUC1, of milk, mammary gland and other tissues. *Biochim Biophys Acta* **1241**(3), 407-23.

Pecher, G., Haring, A., Kaiser, L. & Thiel, E. (2002). Mucin gene (MUC1) transfected dendritic cells as vaccine: results of a phase I/II clinical trial. *Cancer Immunol Immunother* **51**(11-12), 669-73.

Petrarca, C., Casalino, B., von Mensdorff-Pouilly, S., Rughetti, A., Rahimi, H., Scambia, G., Hilgers, J., Frati, L. & Nuti, M. (1999). Isolation of MUC1-primed B lymphocytes from tumour-draining lymph nodes by immunomagnetic beads. *Cancer Immunol Immunother* **47**(5), 272-7.

Price, M. R., Rye, P. D., Petrakou, E., Murray, A., Brady, K., Imai, S., Haga, S., Kiyozuka, Y., Schol, D., Meulenbroek, M. F., Snijdewint, F. G., von Mensdorff-

Pouilly, S., Verstraeten, R. A., Kenemans, P., Blockzjil, A., Nilsson, K., Nilsson, O., Reddish, M., Suresh, M. R., Koganty, R. R., Fortier, S., Baronic, L., Berg, A., Longenecker, M. B., Hilgers, J. & et al. (1998). Summary report on the ISOBM TD-4 Workshop: analysis of 56 monoclonal antibodies against the MUC1 mucin. San Diego, Calif., November 17-23, 1996. *Tumour Biol* **19 Suppl 1**, 1-20.

Rudd, P. M. & Dwek, R. A. (1997). Glycosylation: heterogeneity and the 3D structure of proteins. *Crit Rev Biochem Mol Biol* **32**(1), 1-100.

Rudd, P. M., Elliott, T., Cresswell, P., Wilson, I. A. & Dwek, R. A. (2001). Glycosylation and the immune system. *Science* **291**(5512), 2370-6.

Schuman, J., Campbell, A. P., Koganty, R. R. & Longenecker, B. M. (2003). Probing the conformational and dynamical effects of O-glycosylation within the immunodominant region of a MUC1 peptide tumor antigen. *J Pept Res* **61**(3), 91-108.

Sette, A., Newman, M., Livingston, B., McKinney, D., Sidney, J., Ishioka, G., Tangri, S., Alexander, J., Fikes, J. & Chesnut, R. (2002). Optimizing vaccine design for cellular processing, MHC binding and TCR recognition. *Tissue Antigens* **59**(6), 443-51.

Springer, G. F. (1995). T and Tn pancarcinoma markers: autoantigenic adhesion molecules in pathogenesis, prebiopsy carcinoma-detection, and long-term breast carcinoma immunotherapy. *Crit Rev Oncog* **6**(1), 57-85.

Springer, G. F. (1997). Immunoreactive T and Tn epitopes in cancer diagnosis, prognosis, and immunotherapy. *J Mol Med* **75**(8), 594-602.

Stanfield, R., Cabezas, E., Satterthwait, A., Stura, E., Profy, A. & Wilson, I. (1999). Dual conformations for the HIV-1 gp120 V3 loop in complexes with different neutralizing fabs. *Structure Fold Des* **7**(2), 131-42.

Taylor-Papadimitriou, J., Burchell, J., Miles, D. W. & Dalziel, M. (1999). MUC1 and cancer. *Biochim Biophys Acta* **1455**(2-3), 301-13.

Terasawa, K., Furumoto, H., Kamada, M. & Aono, T. (1996). Expression of Tn and sialyl-Tn antigens in the neoplastic transformation of uterine cervical epithelial cells. *Cancer Res* **56**(9), 2229-32.

Tugarinov, V., Zvi, A., Levy, R. & Anglister, J. (1999). A cis proline turn linking two beta-hairpin strands in the solution structure of an antibody-bound HIV-1IIIB V3 peptide. *Nat Struct Biol* **6**(4), 331-5.

Van den Steen, P., Rudd, P. M., Dwek, R. A. & Opdenakker, G. (1998). Concepts and principles of O-linked glycosylation. *Crit Rev Biochem Mol Biol* **33**(3), 151-208.

Vaughan, H. A., Ho, D., Karanikas, V., Ong, C.-S., Hwang, L. A., Pearson, J., McKenzie, I. F. C. & Pietersz, G. A. (1999). Induction of Humoral and Cellular Responses in Cynomolgus Monkeys Immunisied with Mannan-human MUC1 conjugates. *Vaccine* **17**, 2740-2752.

Vlad, A. M., Muller, S., Cudic, M., Paulsen, H., Otvos, L., Jr., Hanisch, F. G. & Finn, O. J. (2002). Complex carbohydrates are not removed during processing of

glycoproteins by dendritic cells: processing of tumor antigen MUC1 glycopeptides for presentation to major histocompatibility complex class II-restricted T cells. *J Exp Med* **196**(11), 1435-46.

von Mensdorff-Pouilly, S., Petrakou, E., Kenemans, P., van Uffelen, K., Verstraeten, A. A., Snijdewint, F. G., van Kamp, G. J., Schol, D. J., Reis, C. A., Price, M. R., Livingston, P. O. & Hilgers, J. (2000). Reactivity of natural and induced human antibodies to MUC1 mucin with MUC1 peptides and n-acetylgalactosamine (GalNAc) peptides. *Int J Cancer* **86**(5), 702-12.

Wandall, H. H., Hassan, H., Mirgorodskaya, E., Kristensen, A. K., Roepstorff, P., Bennett, E. P., Nielsen, P. A., Hollingsworth, M. A., Burchell, J., Taylor-Papadimitriou, J. & Clausen, H. (1997). Substrate specificities of three members of the human UDP-N-acetyl-alpha-D-galactosamine:Polypeptide N-acetylgalactosaminyltransferase family, GalNAc-T1, -T2, and -T3. *J Biol Chem* **272**(38), 23503-14.

Xing, P. X., Prenzoska, J. & McKenzie, I. F. (1992). Epitope mapping of anti-breast and anti-ovarian mucin monoclonal antibodies. *Mol Immunol* **29**(5), 641-50.

Zotter, S., Hageman, P. C., Lossnitzer, A., Mooi, W. J. & Hilgers, J. (1988). *Cancer Rev* **111**, 55-101.

Zvi, A., Tugarinov, V., Faiman, G. A., Horovitz, A. & Anglister, J. (2000). A model of a gp120 V3 peptide in complex with an HIV-neutralizing antibody based on NMR and mutant cycle-derived constraints. *Eur J Biochem* **267**(3), 767-79.

Chapter 2: Effect of Repeat Number on MUC1 Structure and Dynamics

ABSTRACT: MUC1 mucin is large transmembrane glycoprotein with an extracellular domain composed of repeating units of a 20 amino acid sequence. In the cancer-associated state, mucin expression is upregulated and the extracellular region is aberrantly glycosylated. Previous antibody binding studies show higher affinity for a 5-repeat MUC1 peptide over a 1-repeat MUC1. Results in our laboratory have led us to investigate the structural and dynamic consequences of increasing repeat number. Isotopically labeled MUC1 peptides were cloned, expressed, and purified, and the structure and dynamics of the peptides were characterized using ^{15}N and ^{13}C NMR spectroscopy. We find that a type I β-turn is formed within the PDTR B-cell epitope sequence and another β-turn is formed within the sequence APGS. The data show that MUC1 structure, dynamics, and binding affinity for an anti-MUC1 antibody are all insensitive to the number of MUC1 repeats. The results of this study are discussed with regard to vaccine design.

Introduction:

Mucins have been implicated as targets for vaccine development in cancers of the breast, colon, pancreas, lung, and ovary because of the differences between normal and tumor-associated mucin (Apostolopoulos *et al.*, 1999a; Apostolopoulos *et al.*, 1999b; Miles & Taylor-Papadimitriou, 1999; Taylor-Papadimitriou *et al.*, 1999). Mucin 1 (MUC1) is a large transmembrane glycoprotein that is expressed on the ductal surface of epithelial cells. The extracellular region of the protein consists of a variable number of tandem repeats of the 20-amino acid sequence (GVTSA**PDTRPAP**GSTAPPAH)$_n$, extensively O-glycosylated at threonine and serine sites with large, branched sugars

(Carlstedt & Davies, 1997; Koganty *et al.*, 1997; Rudd & Dwek, 1997; Van den Steen *et al.*, 1998). However, in the tumor-associated state MUC1 becomes an autoantigen as a result of incomplete glycosylation and sparse distribution of remaining carbohydrate structures (Hanisch, 2001). The reduced glycosylation is believed to result in the exposure of a highly immunogenic core peptide sequence (PDTRPAP in bold above) (Girling *et al.*, 1989), identified as the immunodominant B-cell epitope from monoclonal antibody studies in mice (Bashford *et al.*, 1993; Burchell *et al.*, 1989; Denton *et al.*, 1993; Kotera *et al.*, 1994; Xing *et al.*, 1992a). This PDTRPAP core peptide sequence is also believed to be immunodominant in humans. Breast cancer patients with MUC1-expressing tumors develop limited humoral and cellular immune responses against the tumor (Finn *et al.*, 1995; Nakamura *et al.*, 1998; Petrarca *et al.*, 1999), with the elicited antibodies and T cells cross-reactive to the PDTRPAP core peptide sequence (Ding *et al.*, 1993; Jerome *et al.*, 1991; Musselli *et al.*, 2002).

Many different clinical trials have been undertaken over the past few years to assess the ability of MUC1-based vaccines to generate strong and cytotoxic anti-MUC1 immune responses against the solid MUC1-expressing tumor. Several of these trials have explored the use of MUC1 peptides coupled to different haptens, keyhole limpet hemocyanin, oxidized mannan, and glutathione S-transferase (Apostolopoulos et al., 1999a). In addition, at least two different vaccine trials have used MUC1-associated antigenic sugars (without peptide) (Mitchell, 2002). Other more recent clinical trials have utilized peptide- or DNA-pulsed dendritic cells as vaccine vectors, attempting to capitalize on the superior immune activation by these antigen presenting cells. Dendritic cells pulsed with either MUC1 peptides or cDNA have been able to generate limited $CD8^+$ T cell responses to solid breast tumors (Brossart *et al.*, 2000; Pecher *et al.*, 2002), although these responses did not result in tumor rejection. Indeed, none of the MUC1 vaccine candidates described above have been shown to be effective at tumor rejection,

although the reasons for this are not absolutely clear (Denda-Nagai & Irimura, 2000; Doehn & Jocham, 2000; Foon, 2001; Morse, 2000; Morse, 2001).

The unusual characteristics of tumor-associated MUC1 suggest a mechanism for recognition by the immune system. Tumor-associated MUC1 is present at over 50-fold greater expression levels on the tumor cell surface relative to normal MUC1 (Gendler & Spicer, 1995). Each molecule of the protein has many copies of the same B cell and T cell epitope sequence exposed on its surface, and should offer a highly immunogenic target. Previous work in our laboratory has focused on the effects of glycosylation of the MUC1 sequence on antibody recognition (Grinstead *et al.*, 2002; Grinstead *et al.*, 2003; Schuman *et al.*, 2003) (see also Chapters 3 and 4). Results from other studies have suggested that the multiple repeat nature of MUC1 also contributes to its immunogenicity. For example, a large cooperative workshop study of 56 anti-MUC1 antibodies showed that 47 of the antibodies had higher affinity for a 5-repeat relative to a 1-repeat MUC1 peptide (Karanikas *et al.*, 1998; Price *et al.*, 1998). Other studies have found multiple repeat MUC1 peptides to be better at binding antibodies from breast cancer sera (Kotera et al., 1994), and another study has characterized length-dependent differences in the structure of MUC1 peptides (Fontenot, 1993). Differences in structure based on the length of MUC1 peptides are not consistent with data from our laboratory. Therefore, the effect of MUC1 repeat number on peptide structure and dynamics is addressed here.

The experiments described below seek to identify the effect of MUC1 repeat number on MUC1 peptide structure and dynamics. Solution state NMR is used as the probe in these systems, because it allows both structure and dynamics information to be obtained for the MUC1 peptides, even if those peptides are dynamic and conformationally heterogeneous. NMR studies probing the structure and dynamics of the 16 and 40 residue MUC1 peptides are significantly facilitated by our ability to generate

isotopically labeled recombinant peptides. This allows for the acquisition of isotope-edited NMR experiments of the MUC1 peptides, offering a significant increase in the information content relative to our previous efforts with simple homonuclear NMR experiments. In addition, isotope labels allow us to perform NMR relaxation experiments to characterize the dynamics of the $^{15}N/^{13}C$-labeled MUC1 peptides. In this study, we have performed ^{13}C- and ^{15}N-based NMR experiments to analyze the solution state conformation and backbone dynamics of two MUC1 peptides: a 16mer corresponding to one repeat of the MUC1 tandem repeat sequence (GVTSAPDTRPAPGSTA), and a 40mer corresponding to two repeats of the MUC1 sequence $(VTSAPDTRPAPGSTAPPAHG)_2$. This study aims to determine the effect of repeat number on MUC1 peptide structure and dynamics, and to correlate those findings with the affinity of known anti-MUC1 antibodies. Results are discussed with regard to the structural/dynamic basis for antibody affinity and consequences for vaccine design.

Materials and Methods:

Cloning of 16mer and 40mer peptides. Two MUC1 sequences derived from the extracellular domain of the MUC1 protein were cloned and expressed for the purposes of this study: (1) a one-repeat 16mer MUC1 sequence (Gly1-Val2-Thr3-Ser4-Ala5-Pro6-Asp7-Thr8-Arg9-Pro10-Ala11-Pro12-Gly13-Ser14-Thr15-Ala16) MUC1 peptide; and (2) a two-repeat 40mer MUC1 sequence (Val1-Thr2-Ser3-Ala4-Pro5-Asp6-Thr7-Arg8-Pro9-Ala10-Pro11-Gly12-Ser13-Thr14-Ala15-Pro16-Pro17-Ala18-His19-Gly20-Val21-Thr22-Ser23-Ala24-Pro25-Asp26-Thr27-Arg28-Pro29-Ala30-Pro31-Gly32-Ser33-Thr34-Ala35-Pro36-Pro37-Ala38-His39-Gly40). These two 16mer and 40mer MUC1 sequences were expressed as $^{15}N,^{13}C$-labeled recombinant peptides in *E. coli* using a methodology previously described (Kuliopulos & Walsh, 1994). Briefly stated, genes

with multiple repeats of MUC1 DNA sequences were constructed from purchased oligonucleotides, purified, and ligated into plasmid DNA vector pET-31b(+). The MUC1 16mer and 40mer DNA-containing plasmids were transformed separately into the competent *E. coli* strain BLR(DE3) for protein expression. Isotopically ^{15}N,^{13}C-labeled peptides were then expressed by growing the transformed bacteria in minimal media containing M9 salts, and with $^{15}NH_4Cl$ and $^{13}C_6$-glucose as the sole sources of nitrogen and carbon, respectively. Isotopically labeled minimal media was inoculated at OD_{600} of 0.1 from an overnight culture, and grown to an OD_{600} of 0.6 - 0.8 before induction of protein expression with 1mM IPTG. Induced cultures were grown overnight before cell harvest by centrifugation.

Harvested cell pellets were lysed by sonication, and the insoluble fraction was collected by centrifugation. The insoluble fraction was washed with Tris buffer, and then solubilized using Tris buffer containing 4 M guanidine hydrochloride. The solubilized fusion protein was purified using nickel column chromatography under denaturing conditions of 4 M guanidine. Purified fusion protein was eluted from the column with a linear gradient of 4 - 500 mM imidazole. Fractions containing protein were dialyzed against water overnight, exchanging with fresh water several times. The water-insoluble fusion protein precipitate was collected by centrifugation.

The expressed fusion protein was designed with methionine residues separating the KSI domain from the inserted MUC1 peptide sequence, between each repeat of the MUC1 peptide sequence, and before the histidine tag. The fusion was digested with an excess of CNBr in 88% formic acid under nitrogen gas overnight at room temperature to cleave at all methionine residues and leave a homoserine lactone at the C-terminus of all fragments. Formic acid was removed by rotary evaporation, and the products were stirred in distilled water. The insoluble KSI domain remained as precipitate, and was

removed by centrifugation. The soluble peptide cleavage products were lyophilized and resuspended in 90% water, 10% acetonitrile for HPLC purification.

MUC1 peptides were purified using reverse-phase HPLC on a prep scale radial compression C18 column (Alltech, USA). MUC1 peptides were eluted with a linear gradient of 10% - 95% acetonitrile. One major peak was observed in most cases, which eluted with the same retention time as a standard synthetic MUC1 peptide. Fractions containing purified MUC1 peptides were collected, and the volatile solvents were removed by rotary evaporation. The aqueous solutions lyophilized to give pure peptide at a yield of 17 mg isotope-labeled peptide per liter of minimal media (50 mg/L for peptide in unlabeled LB medium).

Inhibition ELISA. Inhibition (liquid phase) ELISA was used to determine the 50% inhibition of binding for the recombinant MUC1 16mer and 40mer peptides to a panel of anti-MUC1 peptide antibodies. The inhibition ELISAs were performed as previously described (Xing *et al.*, 1991; Xing *et al.*, 1989). Briefly stated, polyvinyl chloride microtitre 96 well plates were coated with 20μg/ml of peptide Cp1-30 (C-PDTRPAPGSTAPPAHGVTSAPDTRPAPGST)x2 in 0.2M $NaHCO_3$ buffer, pH9.6 for 2 hours at 37°C. Non specific binding was blocked with 2% bovine serum albumin/PBS for 1 hour at 37 °C, and washed 5 times with PBS 0.2% Tween 20. On another plate, titrating 16mer or 40mer peptide (0.001-10μg/ml) was mixed with constant (5μg/ml) anti-peptide monoclonal antibodies (BCP7, epitope VTSA; BCP8, epitope DTR; BCP9, epitope GSTAP; BCP10, epitope RPAP) (Xing *et al.*, 1992b) for 3 hours at room temperature (RT). The mixture was then added onto the pre-coated/blocked plates and left at 4 °C for 16-18 hours. Plates were washed and incubated with horseradish peroxidase-conjugated sheep anti-mouse Ig (Selinus, Australia) for 1 hour at RT and washed again before adding developing buffer [50μl, 0.03% 2,2'-azino-di(3-

ethylbenzthiazoline sulphonate (Amersham, UK), 0.02% H_20_2 (100 Volume, Ajax Chemical) in 0.1M citrate buffer, pH4.0] at RT for 30 min. Plates were read on an EL312e microplate reader at 405 nm. The percentage of inhibition was calculated by comparing the binding of monoclonal antibody with and without inhibitor: % of inhibition = (binding of monoclonal antibody with inhibitor / binding of monoclonal antibody without inhibitor) x 100%.

Fluorescence binding measurements. Fluorescence measurements were used to determine the equilibrium dissociation constants (K_D) for the binding of the recombinant MUC1 16mer and 40mer peptides to Fab B27.29, a generous gift from Biomira Inc. (Edmonton, Alberta, Canada). Fab B27.29 (0.86 μM stock solution) was titrated with small aliquots of peptide to a final concentration greater than 200-fold in excess of Fab concentration. The change in Fab fluorescence intensity was monitored, and the concentration of bound ligand was calculated (percent of maximum fluorescence change). The natural log of the free ligand concentration was plotted against the concentration of the bound ligand, and the curve was fit to equation 1

$$[\text{bound}] = (\text{capacity} * [\text{free ligand}]) / (K_D + [\text{free ligand}]) \quad (1)$$

according to Michaelis-Menton kinetics, where the capacity is the concentration of the Fab, and the K_D is the equilibrium dissociation constant.

Preparation of peptide NMR samples. The ^{15}N,^{13}C-labeled recombinant MUC1 16mer and 40mer peptide NMR samples used for the ^{15}N-edited NMR experiments were 2.0 mM peptide in 90% H_20/10% D_20 PBS buffer, pH 7.15, 0.05% NaN_3, with 1 mM DSS

added as an internal chemical shift reference. These same samples were lyophilized and resuspended in 99.9% D_2O for the ^{13}C-edited {$^1H\alpha$}-$^{13}C\alpha$ NOE experiments.

NMR experiments. All NMR experiments were performed on a Varian Inova 500MHz spectrometer, equipped with three channels, a pulsed-field gradient triple resonance probe with an actively shielded z gradient, and a gradient amplifier unit. ^1H, ^{15}N and ^{13}C NMR resonances were assigned as previously reported (Grinstead et al., 2003). 2D ^1H-^{15}N HSQC spectra were acquired using a spectral width of 1024 Hz and 32 points in t_1 (^{15}N), and 6000 Hz and 1024 points in t_2 (^1HN). 2D ^1H-^{13}C HSQC spectra (Vuister & Bax, 1992) and all ^{13}C relaxation experiments (see below) were acquired using a spectral width of 3750 Hz and 48 points in t_1 (^{13}C), and a spectral width of 6000 Hz and 1024 points in t_2 (^1HC). 3D ^{15}N-edited NOESY-HSQC spectra (Zhang *et al.*, 1994) used a mixing time of 300 ms, and were acquired using the following spectral widths and numbers of complex points: 5000 Hz and 75 points in t_1 (^1H), 1024 Hz and 32 points in t_2 (^{15}N), and 6000 Hz and 1024 points in t_3 (^1HN). 3D HNHA spectra (Vuister & Bax, 1993) were acquired using the following spectral widths and numbers of complex points: 1024 Hz and 32 points in t_1 (^{15}N), 5000 Hz and 75 points in t_2 (^1H), and 6000 Hz and 1024 points in t_3 (^1HN). Broadband decoupling for ^{15}N and ^{13}C was achieved in each of these experiments using WALTZ-16 (Shaka *et al.*, 1983) and GARP (Shaka *et al.*, 1985) decoupling, respectively.

The ^{15}N NMR relaxation experiments of Farrow *et al.* (Farrow *et al.*, 1994) were used to measure ^{15}N T_1, T_2 and {^1H}-^{15}N NOE values for the ^{15}N,^{13}C-labeled recombinant MUC1 16mer and 40mer peptides. All ^{15}N NMR relaxation experiments were acquired using a spectral width of 1024 Hz and 32 points in t_1 (^{15}N), and 6000 Hz and 1024 points in t_2 (^1HN). Relaxation delays of 11.1, 55.5, 555, 832, 1110, 1388 and 1665 ms were used for the ^{15}N T_1 experiments, with duplicate experiments recorded for

the 55.5 ms data point to confirm our error estimates. Relaxation delays of 15.8, 31.7, 63.4, 126.7, 158.4, 174.2 ms were used for the ^{15}N T_2 experiments. The $\{^1H\}$-^{15}N NOE was obtained by recording spectra with and without 3 s of ^1H saturation. In the case of spectra acquired without NOE, a net relaxation delay of 5 s was employed, whereas a delay of 2 s prior to 3 s of ^1H saturation was employed for spectra with NOE. The NOE values were calculated as the ratio of peak intensities in the experiments with and without proton presaturation. ^{15}N T_1 and T_2 experiments were obtained with 32 transients per complex point, whereas $\{^1H\}$-^{15}N NOE experiments were obtained with 64 transients per complex point.

The ^{13}C relaxation experiments of Yamakazi *et al.* (Yamazaki *et al.*, 1994) were used to measure $^{13}C\alpha$ T_1, $T_{1\rho}$ and $\{^1H\alpha\}$-$^{13}C\alpha$ NOE values for the ^{15}N,^{13}C-labeled recombinant MUC1 16mer and 40mer peptides. Relaxation delays of 10, 50, 100, 150, 200, and 300 ms were used for the ^{13}C T_1 experiments, with the 100 ms data set duplicated for confirmation of error estimates. Relaxation delays of 10, 20, 40, 60, 100, 150, 200, and 250 ms were used for the ^{13}C $T_{1\rho}$ experiments, with the 40 ms data set duplicated for confirmation of error estimates. The $\{^1H\alpha\}$-$^{13}C\alpha$ NOE was obtained by recording spectra with and without 3 s of ^1H saturation, as described above. ^{13}C T_1 and T_2 experiments were obtained with 32 transients per complex point, whereas $\{^1H\alpha\}$-$^{13}C\alpha$ NOE experiments were obtained with 64 transients per complex point.

Data processing and analysis. All spectra were processed on a SGI Octane® workstation using NMRPipe/NMRDraw (Delaglio *et al.*, 1995) software and analyzed using ANSIG (Kraulis, 1989). The FIDs in the indirect dimension of ^{15}N- and ^{13}C-edited experiments were doubled using forward linear prediction. $^{15}N/^{13}C$ T_1 and T_2 values were determined using non-linear least-squares fitting of the measured peak heights to a two-parameter exponential decay, also within the NMRPipe package. Uncertainties in the calculated T_1

and T_2 values from the least-squares fitting were determined by the signal-to-noise ratio of individual peaks in each of the T_1 and T_2 experiments (Farrow et al., 1994; Yamazaki et al., 1994). Two groups have recently shown that error estimates from least-squared fitting is unreasonably small, and have used the value of 5% as being more realistic (Volkman *et al.*, 1998; Zhang *et al.*, 1997). Therefore, we have set the error in the calculated T_1 and T_2 to 5% of the values.

Temperature coefficients ($-\Delta\delta/\Delta T$ ppb) for all backbone amide (NH) protons of the ^{15}N,^{13}C-labeled recombinant MUC1 16mer and 40mer peptides were calculated from linear plots of chemical shift versus temperature measured from ^{1}H-^{15}N HSQC spectra acquired at 5, 10, 15, and 20, and 25 °C. $^{3}J_{N\alpha}$ coupling constants were obtained for each residue from the ratio of the intensities of the diagonal peak of residue i to its αH-NH (i,i) cross-peak in the HNHA spectra (Vuister & Bax, 1993).

Reduced Spectral Density Mapping. Reduced spectral density mapping is a convenient method for characterizing the motion of each N-H bond at J(0), $J(\omega_N)$, and $J(\omega_H)$ frequencies (Peng & Wagner, 1992a; Peng & Wagner, 1992b). The spectral densities at these three frequencies can be obtained from relaxation rates R_1 ($1/T_1$) and R_2 ($1/T_2$) and the heteronuclear NOE using equations 2 – 4.

$$J(\omega_H) = [4/(5d^2)]\,(\gamma_N/\gamma_H)\,(NOE - 1)/T_1 \qquad (2)$$

$$J(\omega_N) = [1/T_1 - (7d^2/4)\,J(\omega_H)]/\,[(3d^2/4) + c^2] \qquad (3)$$

$$J(0) = [1/T_2 - (3d^2/8 + c^2/2)J(\omega_N) - (13d^2/8)\,J(\omega_H)]/[(d^2/2) + 2c^2/3] \qquad (4)$$

For the above equations, $d = [\mu_0 h(\gamma_N\gamma_H)/8\pi^2]\langle 1/r^3_{NH}\rangle$ and $c = (\omega_N/(3)^{1/2})(\sigma_{\|} - \sigma_{\perp})$ and ω_N and ω_H are the Larmor frequencies of the ^{15}N and ^{1}H nuclei, respectively.

Results and Discussion:

^{15}N and ^{13}C HSQC spectra. ^{15}N and ^{13}C HSQC spectra of the MUC1 16mer and 40mer peptides are shown in Figure 2.1. The spectra show that most of the 16mer and 40mer

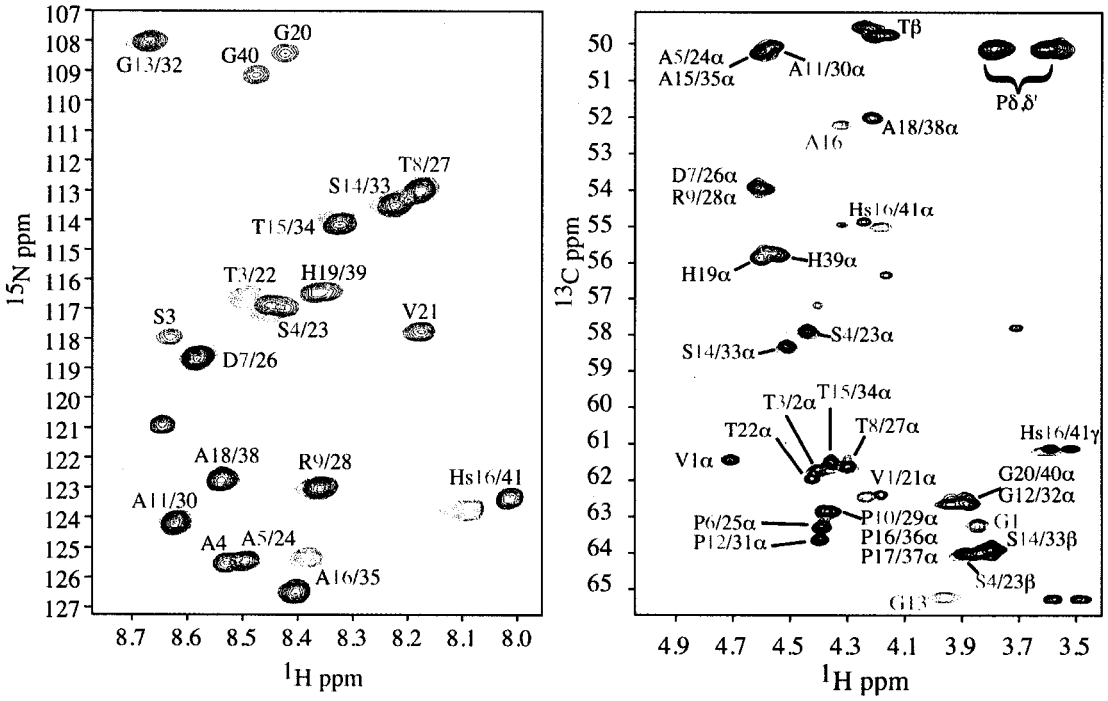

Figure 2.1: 500 MHz ^{1}H-^{15}N (left panel) and ^{1}H-^{13}C (right panel) HSQC spectra of the recombinant, ^{15}N,^{13}C-labeled MUC1 16mer (overlaid in red) and 40mer (black). Experimental conditions were 2 mM peptide in PBS buffer, pH 7.15, 5.0 °C.

resonances overlap. Chemical shift is a sensitive indicator of the structure of a molecule, and the identical chemical shifts for many of the resonances indicate that the two peptides have identical structure for the residues with overlapping resonances (Wishart *et al.*, 1995). Specifically, the resonances that have identical chemical shift include (using the 40mer numbering) P5/25, D6/26, T7/27, R8/28, P9/29, A10/30, P11/31, G12/32, S13/33, and T14/34. This stretch of residues spans the B cell epitope sequence PDTRPAP. The residues at the ends of the 16mer are slightly shifted relative to the corresponding 40mer

residues due to the different starting and ending residues of the 16mer and 40mer. This was expected, since the 16mer sequence ends at a residue (A16) that would be in the center of the 40mer (A15). However, it was surprising that nearly identical chemical shifts were observed for the residues preceding these. For example, the 16mer resonance for T15 was less than 0.02 ppm separated from the corresponding 40mer T14/34 resonance, and the preceding serine resonances overlay exactly. For the N-terminal resonances, P5 is chemical shift degenerate, and A4 of the 40mer is separated from the A5 of the 16mer by 0.05 ppm. These trends indicate that near native MUC1 structure is achieved in 3-4 residues. This is in agreement with other studies of MUC1 glycopeptides in our group that showed nearly identical structure 2-3 residues from the site of glycosylation for a 9 residue peptide (TSAPDTRPA) and the same peptide glycosylated at the central threonine (Schuman et al., 2003). The same trend was seen in a series of 16 residue MUC1 glycopeptides (Grinstead et al., 2002).

We have also measured the ^{13}C and ^{1}H chemical shifts for a synthetic 80mer 4-repeat peptide using natural abundance ^{13}C NMR. The chemical shifts of the 40mer and 80mer MUC1 peptides are degenerate (data not shown). If we assume that the 80 residue peptide represents "native" structure, the observation of chemical shift degeneracy between the 40 and 80 residue peptides indicates that the 40mer has the same structure as the native MUC1 structure. It is not surprising that the 16, 40, and 80 residue peptides all display the same native structure, since the extracellular portion of the MUC1 protein is a tandem repeat of 20 residue peptide units with no global fold, as determined by a lack of long-range NOEs and limited chemical shift dispersion.

Structural characterization of MUC1 16mer and 40mer. Figures 2.2 and 2.3 show strip plots of the ^{15}N-edited NOESY spectra for the 16mer and 40mer acquired at pH 7 and 5

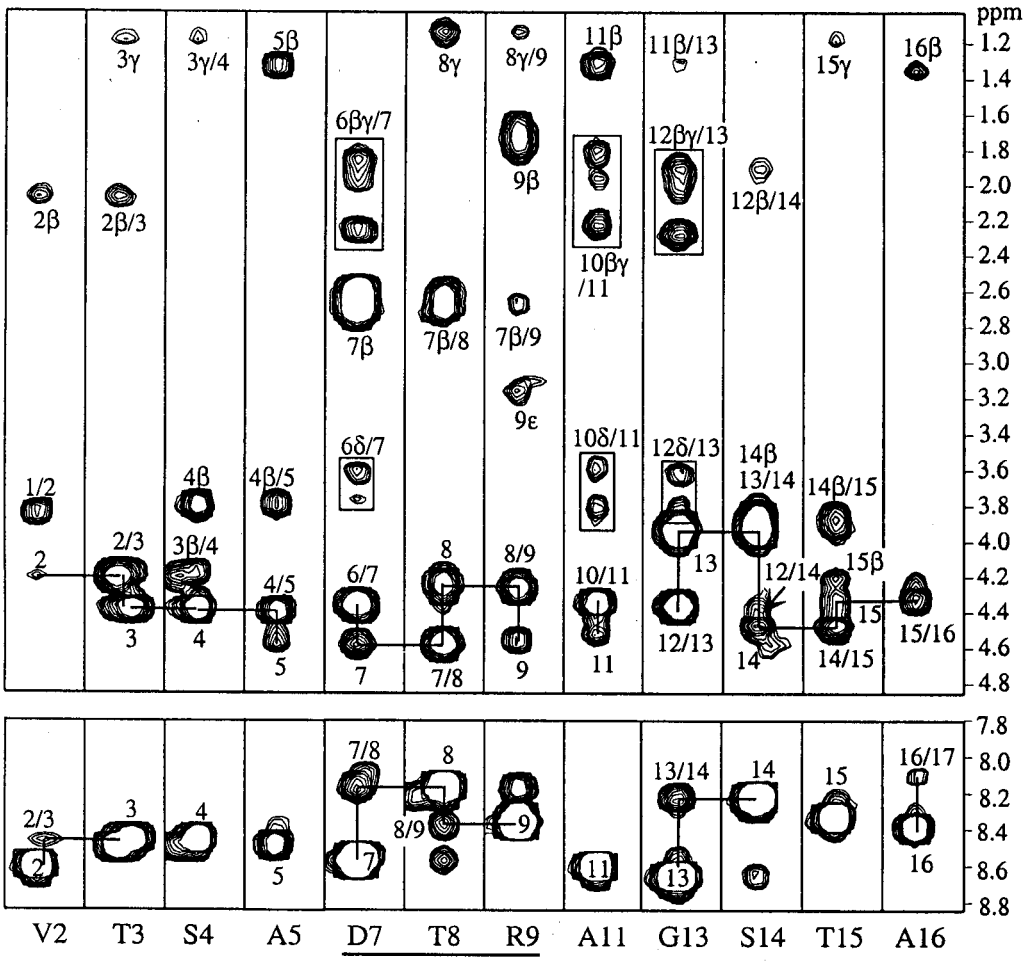

Figure 2.2: Strip plot from the 500 MHz ^{1}H-^{15}N NOESY-HSQC spectrum of the recombinant ^{15}N,^{13}C-labeled MUC1 16mer, showing the amide crosspeaks with amide protons (lower panel) and alpha and sidechain protons (upper panel). Resonances were assigned by connecting interresidue $d_{\alpha N}$ NOEs with intraresidue $d_{\alpha N}$ NOEs, illustrated by horizontal and vertical connecting lines in the upper panel. The three proline residues were assigned by their NOEs to the amide proton of the following residue (in boxes, upper panel). The PDTR β-turn sequence is underlined. Experimental conditions were 2 mM peptide in PBS buffer, pH 7.15 and 5.0 °C.

°C. The crosspeaks connected with horizontal and vertical lines represent $d_{\alpha N}$ and d_{NN} connectivities associated with the backbone amide proton of the residue indicated in the

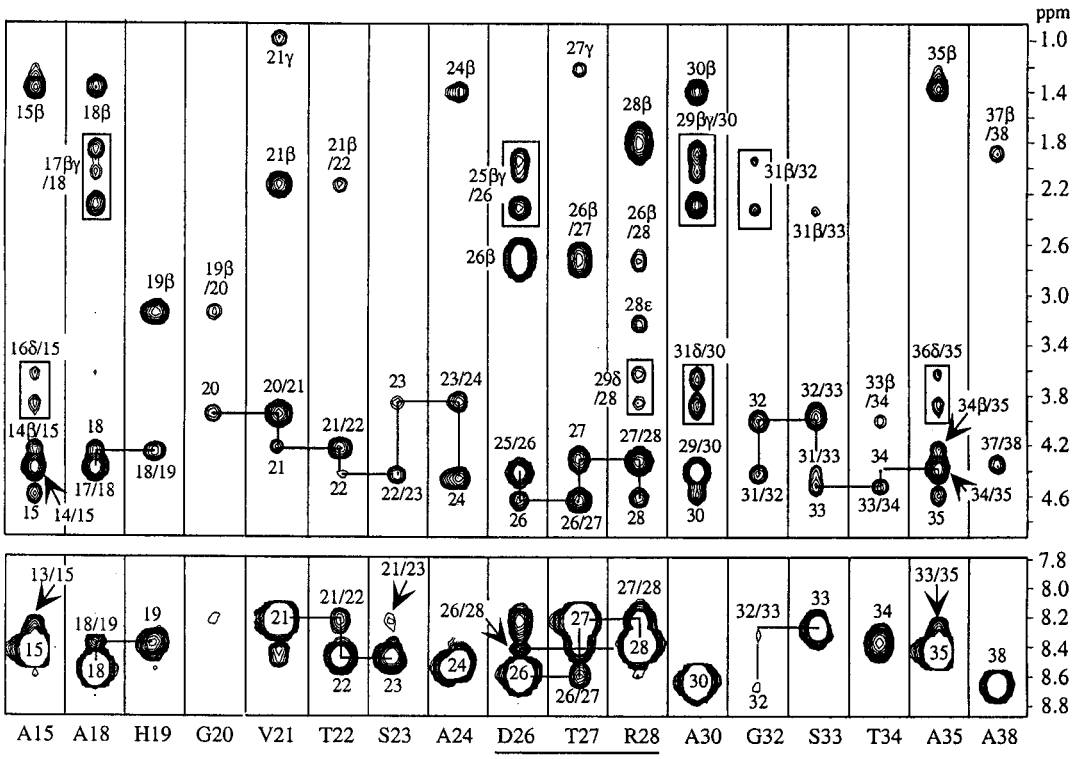

Figure 2.3: Strip plot from the 500 MHz ^{1}H-^{15}N NOESY-HSQC spectrum of the recombinant ^{15}N,^{13}C-labeled MUC1 40mer, showing the amide crosspeaks with amide protons (lower panel) and alpha and sidechain protons (upper panel). Resonances were assigned by connecting interresidue $d_{\alpha N}$ NOEs with intraresidue $d_{\alpha N}$ NOEs, illustrated by horizontal and vertical connecting lines in the upper panel. The three proline residues were assigned by their NOEs to the amide proton of the following residue (in boxes, upper panel). The PDTR β-turn sequence is underlined. For simplicity, only the second repeat of the MUC1 repeat sequence is shown.

sequence. Intra- and inter-residue $d_{\alpha N}$ NOEs allow sequential assignment of all of the resonances from both peptides, except for prolines. Proline connectivities were assigned using the sequential $d_{\beta N}$ and $d_{\gamma N}$ NOEs from the proline sidechain to the amide group of the following residue.

In addition to assignment information, the NOESY experiment gives excellent structural information. β-turn secondary structure is indicated by the presence of strong

$d_{NN}(2,3)$ and $d_{NN}(3,4)$ NOEs, and a medium $d_{\alpha N}$ (2,4) NOE (Wuthrich, 1986). The strip plot of the NOESY HSQC in Figure 2.3 shows the presence of strong $d_{NN}(2,3)$ and $d_{NN}(3,4)$ NOEs between D6/T7 and between T7/R8 in the MUC1 PDTR sequence. Medium $d_{\alpha N}(2.4)$ and weak $d_{\beta N}(2,4)$ NOEs are also observed. The conformation of the $P^5D^6T^7R^8$ turn in the 40mer (where proline is residue 1 in the 4-residue turn) is type I, as determined from the $d_{\alpha N}(2,3)/d_{NN}(2,3)$ ratios (a type I turn has a ratio less than 1, whereas a type II turn has a ratio greater than 1) and by the presence of a medium $d_{\alpha N}(2,4)$ connectivity (Wuthrich, 1986). The 40mer also displays a strong $d_{NN}(3,4)$ connectivity between G12 and S13, a weak $d_{\beta N}(2,4)$ connectivity between P11 and S13, and a weak $d_{\alpha N}(2,4)$ connectivity between P11 and S13. This second cluster of connectivities is diagnostic of another type I β-turn spanning residues APGS in the sequence. This β-turn has not been detected in previous NMR studies using synthetic versions of these peptides, demonstrating the utility of isotope-edited NMR techniques for elucidating localized conformational preferences.

The same NOEs are present in the spectra of both the 16mer and the 40mer, indicating that each of the recombinant MUC1 peptides appears to contain two type I β-turns. In order to quantify the differences in structure between the MUC1 16mer and 40mer peptides, we have measured the intensities of the $d_{\beta N}(2,4)$ NOEs from the first β-turn spanning PDTR. Figure 2.4 shows the homonuclear ^1H-^1H NOESY spectra of the MUC1 16mer and 40mer peptides. Both spectra have the $d_{\beta N}(2,4)$ NOE, and it appears that the 40mer NOE is much stronger. This most likely does not indicate a shorter distance between these protons. The NOE in the 40mer spectrum appears larger for two possible reasons. First, the chemical shifts of the resonances for the aspartic acid β protons from each repeat of the MUC1 sequence are degenerate, resulting in twice the intensity as the NOE in the 16mer for the same concentration of peptide. Second, the 40mer peptide is twice the molecular weight of the 16mer and experiences a substantially

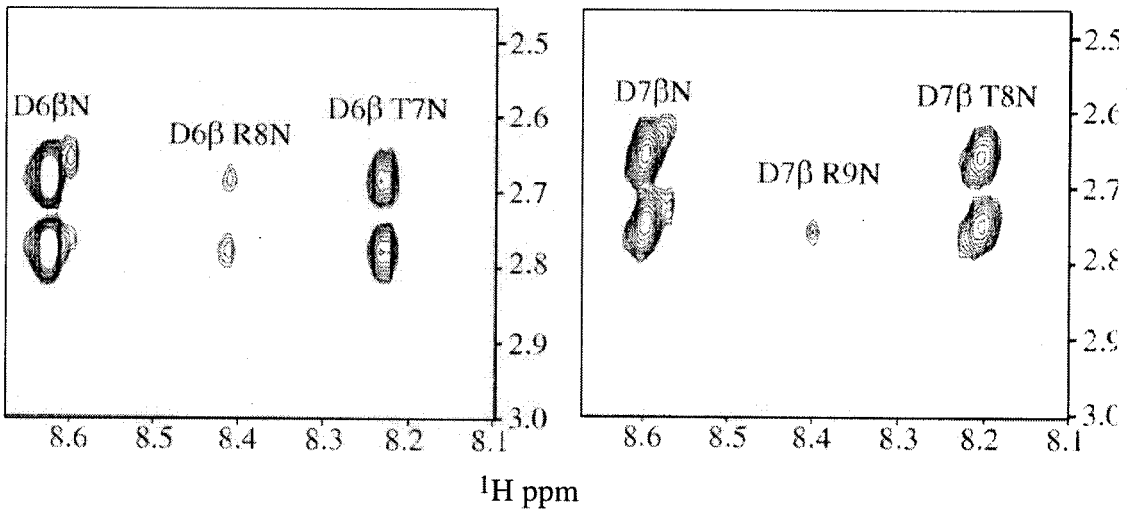

Figure 2.4: The $d_{\beta N}(2,4)$ NOE from the $d_{\beta N}$ region of the 2D ^{1}H-^{1}H NOESY spectra of the recombinant ^{15}N,^{13}C-labeled MUC1 40mer (left panel) and 16mer (right panel). The NOE connects the D6/7 β protons with the amide of R8/9. Experimental conditions were 2 mM peptide in PBS buffer, pH 7.15, 5.0 °C.

longer rotational correlation time in solution. Therefore, the cross-relaxation rate of the 40mer could be much different than the 16mer, resulting in a larger NOE. Both of these possibilities can be accounted for by normalizing the NOEs to an internal reference peak, such as the intra-residue $d_{\beta N}$ NOE for aspartic acid, which should be independent of the peptide backbone conformation. Normalized in this way, the 40mer and 16mer $d_{\beta N}(2,4)$ NOEs have the same intensity. These results suggest that β-turn structure in the MUC1 16mer and 40mer peptides is populated to the same extent.

In addition to the β-turn NOEs mentioned above, we have identified no long-range NOEs in the NOESY spectra of the MUC1 peptides. This observation suggests that there is no globular, folded tertiary structure of the sequence, and this is generally in agreement with the literature. In a previous structural analysis of multiple repeat MUC1 mucins using CD and ^{1}H-NMR, Fontenot and coworkers suggested that the structure of the MUC1 sequence was a poly-proline type II (PPII) helix, as evidenced by a CD absorption at 198nm. PPII helix is defined by trans proline peptide bonds (PP I involves

cis bonds), an absence of sequential d_{NN} connectivities and $J_{\alpha N}$ values of 3.8 Hz, corresponding to a ϕ angle of -78° (Cowan & McGavine, 1955; Dalcol *et al.*, 1996). They also observed a type II β-turn spanning PDTR and an increase in structure with increasing repeat number, as suggested by increasing complexity in the β protons of aspartic acid and histidine residues (Fontenot, 1993). In contrast to these data, our observations of type I β-turns at residues PDTR and APGS refine and improve upon the structural information available for MUC1. Our finding of a lack of a globular MUC1 fold, combined with the likely presence of PPII helix does suggest a model for overall MUC1 structure as an extended string of β-turns on a PPII helix scaffold.

Figure 2.5 shows the consolidated results from our NOESY studies of the MUC1 16mer and 40mer peptides. In addition, this schematic shows coupling constants, temperature coefficients, and deviations from random coil chemical shift. The temperature coefficients, coupling constants, and chemical shift deviations sharply contrast the NOE data. For example, NOEs identify two β-turns in the MUC1 sequence. Stable type I and type II β-turn structures are characterized by a dihedral angle of $\phi 2 = -60^{o}$ for the second residue in the four residue turn (Richardson, 1981; Wilmot & Thornton, 1988). This local conformation should result in a coupling constant of $4 \text{ Hz} \leq {}^{3}J_{N\alpha} \leq 5$ Hz, assuming 100% β-turn population in solution. ${}^{3}J_{\alpha N}$ coupling constants measured for all non-proline residues in the MUC1 16mer and 40mer peptides are greater than 5 Hz, and suggest that neither of the β-turns identified by NOE patterns are 100% populated in solution. This is not surprising, since most small peptides are highly

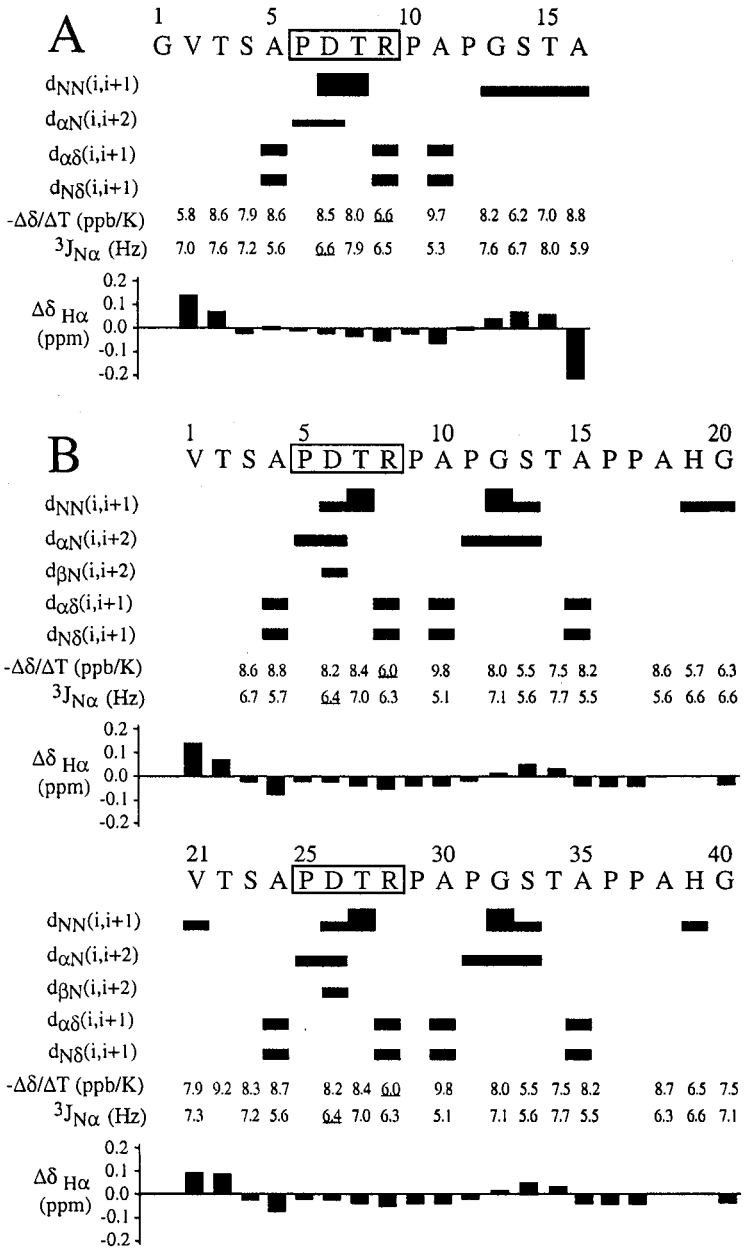

Figure 2.5: Schematic diagram showing the magnitude of d_{NN}, $d_{\alpha N}$, and $d_{\beta N}$ NOEs observed in the ^{1}H-^{15}N NOESY-HSQC spectra of the recombinant ^{15}N,^{13}C-labeled MUC1 16mer (A) and 40mer (B). The diagram also includes coupling constants ($^{3}J_{N\alpha}$), temperature coefficients ($-\Delta\delta/\Delta T$) and chemical shift deviations from random coil values ($\Delta\delta_{\alpha} = \delta_{\alpha}$ obs - δ_{α} coil). Table A3 in Appendix A lists the values of $-\Delta\delta/\Delta T$, $^{3}J_{N\alpha}$, $\Delta\delta_{H\alpha}$ and $\Delta\delta_{C\alpha}$ for both the 16mer and 40mer peptides.

dynamic in solution and may sample many different conformational states. PPII helix is expected to give $^3J_{\alpha N}$ coupling constant values of 3.8 Hz. The observed $^3J_{\alpha N}$ coupling constants do not support high population of this type of structure, either.

Most of the temperature coefficients measured are very close to the average coefficient for the entire peptide, indicating that most of the backbone amide protons are exposed to solvent and under exchange with water. However, the amide protons in position 4 of both of the β-turns have temperature coefficients that are somewhat smaller than the rest of the amides, indicating that these amide protons may participate in stabilizing hydrogen bonds. In a β-turn, the amide proton of the fourth residue is positioned appropriately so as to hydrogen bond with the carbonyl group of the first residue in the turn. Resonances generally shift upfield with increasing temperature. An amide proton that is hydrogen bonded to a carbonyl will conversely be shifted downfield. Upon heating, the hydrogen bond is weakened, resulting in a slight upfield shift. This upfield shift is generally much smaller than if the amide proton is interacting with solvent. Temperature coefficients below 6 ppb/°C can be indicative of hydrogen bonds (Baxter & Williamson, 1997). Prediction of hydrogen bonding using temperature coefficients can be complicated by the overlapping effect of changes in structure upon heating (Andersen *et al.*, 1997). That is to say that the observed temperature dependence of the amide proton is a superposition of the intrinsic temperature coefficient and the temperature dependent chemical shift between the structured and random coil states.

The deviation from random coil chemical shifts measured for the recombinant MUC1 16mer and 40mer are corrected for proline effects and use the random coil values of Wishart *et al.* (Wishart et al., 1995). A deviation from random coil chemical shift (in ppm) of +0.4 for Hα (–1.4 for Cα) or –0.3 for Hα (+1.2 for Cα) are indicative of β-sheet or α-helix, respectively. Because the largest deviations from random coil (except for the peptide termini) are a slight positive deviation (~+0.1 ppm) for the Hα resonances

of the APGS β-turn, it appears that the MUC1 peptides have a conformation near that of random coil. We conclude that the time averaged MUC1 peptide structure is near that of random coil, even though NOEs indicate that for a significant portion of time these residues exist as a β-turn. Once again, identical results were obtained for both the 16mer and 40mer peptides. The combination of coupling constants, temperature coefficients, random coil chemical shift deviations, and NOE patterns indicates that the peptides both exist in equilibrium between β-turn and unfolded states.

MUC1 16mer and 40mer dynamics measurements. ^{15}N and ^{13}C NMR relaxation results for the MUC1 16mer peptide are shown in Figure 2.6. In the top panel, ^{15}N and ^{13}C values parallel each other. Generally, the center of the peptide displays shorter relaxation times than the ends of the peptide, and this is because of increased flexibility at the ends of the peptide. The magnitude of the ^{15}N T_1 and T_2, and the ^{13}C T_1 and $T_{1\rho}$ are representative of a flexible 16-residue peptide. The PDTR β-turn region does not display distinctly shorter relaxation times than the rest of the peptide, suggesting that the turn is not a well-ordered element of secondary structure.

The bottom panel in Figure 2.6 displays the $\{^1H\}$-^{15}N NOE and $\{^1H\alpha\}$-$^{13}C\alpha$ NOE for the 16mer. In this case, the $\{^1H\}$-^{15}N NOE values indicate a dramatic difference between the center of the peptide around the B cell epitope sequence PDTRPAP relative to the rest of the peptide. The ends of the peptide appear to be far

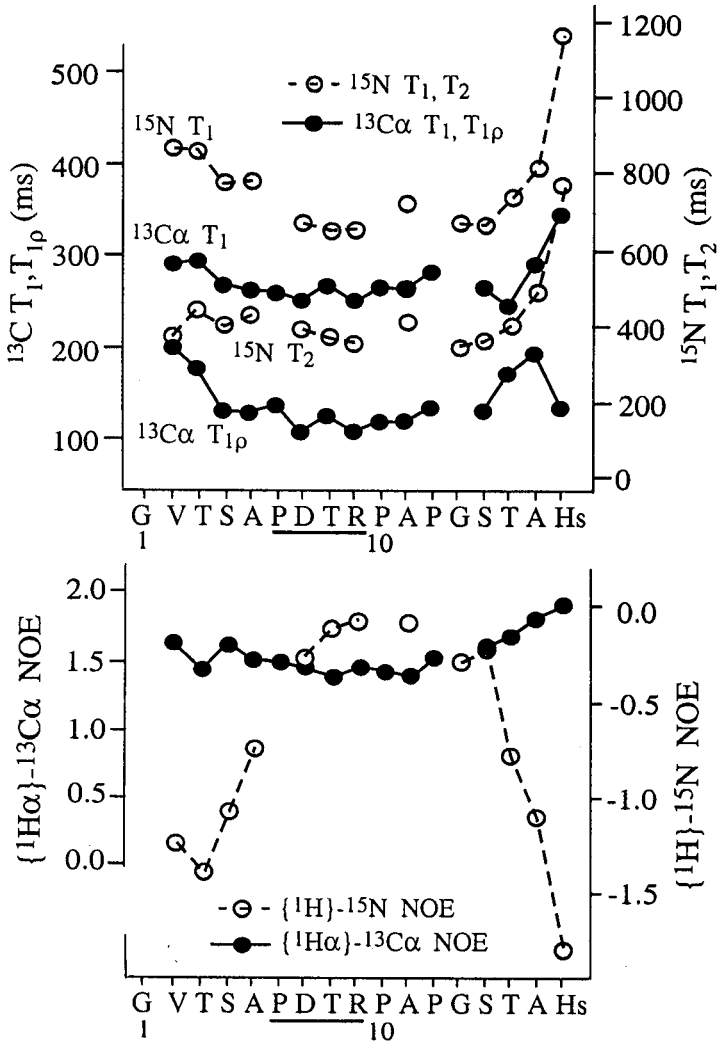

Figure 2.6: ^{15}N T_1, T_2 and $\{^1H\}$-^{15}N NOE, and ^{13}C T_1, $T_{1\rho}$ and $\{^1H\alpha\}$-$^{13}C\alpha$ NOE measured for the ^{15}N,^{13}C-labeled MUC1 16mer. Experimental conditions were 2 mM peptide in PBS buffer, pH 7.15, 5.0 °C. Tables B2, B3, and B4 in Appendix B list the values for the ^{15}N T_1, T_2 and $\{^1H\}$-^{15}N NOE, and ^{13}C T_1, $T_{1\rho}$ and $\{^1H\alpha\}$-$^{13}C\alpha$ NOE.

more disordered than the rest of the peptide. In contrast to the $\{^1H\}$-^{15}N NOE, the $\{^1H\alpha\}$-$^{13}C\alpha$ NOE displays larger values in regions of higher flexibility. The 16mer $\{^1H\alpha\}$-$^{13}C\alpha$ NOE values do not show much difference between the center and ends of the peptide. It should be noted that the magnitudes of both NOE parameters are typical of small, flexible peptides.

Figure 2.7 shows the ^{15}N T_1, T_2, and $\{^1H\}$-^{15}N NOE and ^{13}C T_1, $T_{1\rho}$ and $\{^1H\alpha\}$-$^{13}C\alpha$ NOE values for the MUC1 40mer peptide. The trends for the PDTRPAP region of the sequence are the same as those of the 16mer peptide. The 40mer sequence has two repeats of this sequence, and the residues separating the two repeats shows significantly higher flexibility than the B cell epitope portion of the sequence. These trends indicate that both MUC1 peptides have a significant increase in the order of the β-turn sequences, separated by a sort of 'hinge' region. The absolute value of the 16mer and 40mer relaxation parameters are slightly different due to the longer rotational correlation time of the 40mer. The differences are most likely not indicative of greater order in the longer 40mer.

It can be informative to analyze relaxation parameters in terms of a motional model. The Lipari-Szabo Model Free formalism is typically used to obtain order parameters, a global τ_c, and local internal τ_i. This formalism depends on having fast internal motion of the protein backbone that is distinct and separable from the timescale of global rotation of the molecule. In the case of the small, flexible MUC1 peptides, the relevance of the formalism breaks down because the internal motion of the peptide approaches that of the overall rotational correlation time. This is evidenced in the large deviation from the average relaxation times across the peptide sequences. In a large, well-ordered protein the relaxation parameters tend to have much more uniform values due to a high degree of order achieved by stable secondary and tertiary structure.

Even in flexible systems like MUC1 peptides, spectral density mapping allows analysis of relaxation parameters. In general, the spectral density at J(0) is proportional

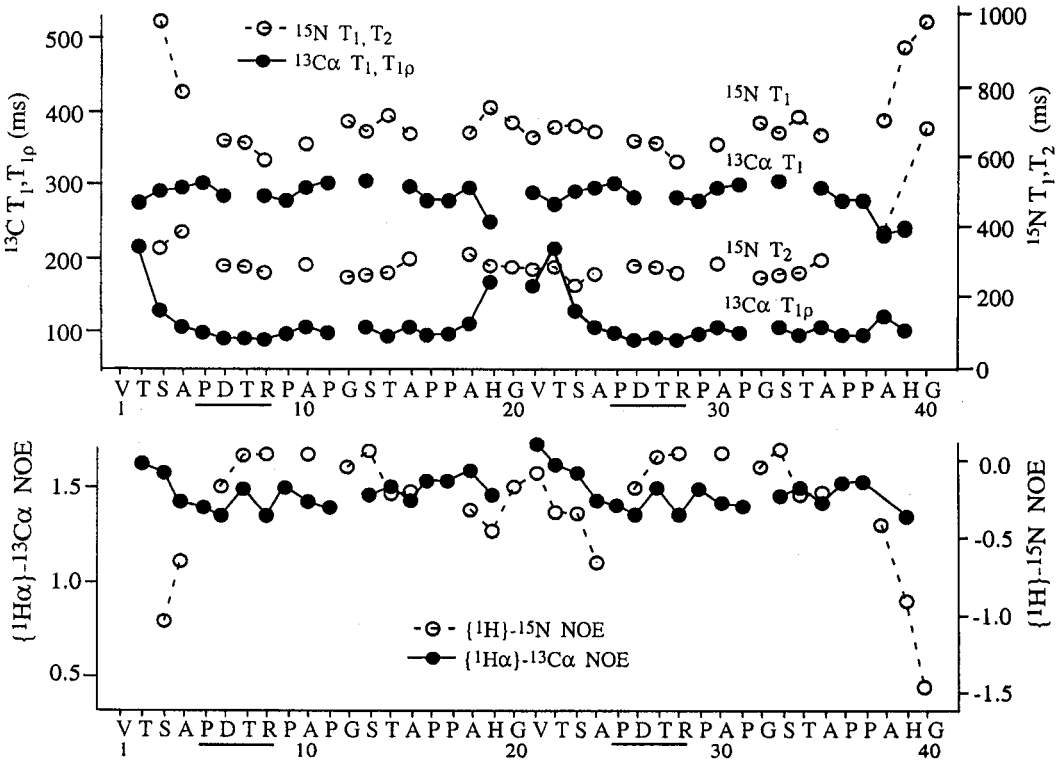

Figure 2.7: ^{15}N T_1, T_2 and $\{^1H\}$-^{15}N NOE, and ^{13}C T_1, $T_{1\rho}$ and $\{^1H\alpha\}$-$^{13}C\alpha$ NOE measured for the ^{15}N,^{13}C-labeled MUC1 40mer. Experimental conditions were 2 mM peptide in PBS buffer, pH 7.15, 5.0 °C. Tables B2, B3, and B4 in Appendix B list the values for the ^{15}N T_1, T_2 and $\{^1H\}$-^{15}N NOE, and ^{13}C T_1, $T_{1\rho}$ and $\{^1H\alpha\}$-$^{13}C\alpha$ NOE.

to the local correlation time of the backbone nitrogen (Peng & Wagner, 1992b). Thus, it is possible to interpret differences in J(0) on the basis of changes in local correlation times. This interpretation is valid only in the absence of conformational exchange phenomena, which can lead to shortening of T_2 times, and therefore larger values of J(0) (Davis & Agard, 1998). Therefore, the contribution of slow exchange motions (μs-ms) to J(0) must also be considered in spectral density analysis.

Using equations 2 – 4 in Materials and Methods, the J(ω) spectral density values, J(0), $J(\omega_N)$ and $J(\omega_H)$, were calculated from the ^{15}N T_1 and T_2 relaxation rates and the steady-state heteronuclear $\{^1H\}$-^{15}N NOE measured for the $^{15}N/^{13}C$-labeled MUC1

16mer and 40mer peptides free in solution (see Tables B2, B3, and B4 in Appendix B). These values are shown in Figure 2.8, which plots the J(0) and $J(\omega_N)$ values only (see Table B5 in Appendix B for the raw data). The peptide J(0) yield average values across the entire sequence of $\langle J(0) \rangle = 0.53$ ns rad^{-1} for the 16mer and $\langle J(0) \rangle = 0.78$ ns rad^{-1} for the 40mer, consistent with the longer global correlation time of the larger two-repeat peptide. In comparison, the average J(0) value for the PDTRPAP epitope sequence is $\langle J(0) \rangle^{epitope} = 0.57$ for the 16mer, and $\langle J(0) \rangle^{epitope} = 0.79$ for the 40mer. Therefore, the epitope sequences are not especially ordered relative to other parts of the sequence.

As previously alluded to, conformational exchange processes on slow timescales can artificially elevate the value of J(0) (Davis & Agard, 1998). However, these slow timescale motions have a negligible effect on the calculated values of the $J(\omega_N)$ and $J(\omega_H)$ spectral densities, as these represent only high frequency motions (Bhattacharya *et al.*, 2002; Peng & Wagner, 1992b; Peng & Wagner, 1995). Figure 2.8 plots the $J(\omega_N)$ values calculated from the relaxation data presented in Tables B2, B3, and B4 in Appendix B. A comparison of the $J(\omega_N)$ and J(0) plots for the 16mer and 40mer reveals similar trends for the two parameters, with slightly larger spectral density values for the 40mer peptide. These plots suggest that slow timescale conformational exchange on the μs-ms timescale does not occur in the MUC1 peptides, and supports our interpretation of increased local correlation time for the 40mer over the 16mer. Because the trends in the spectral density

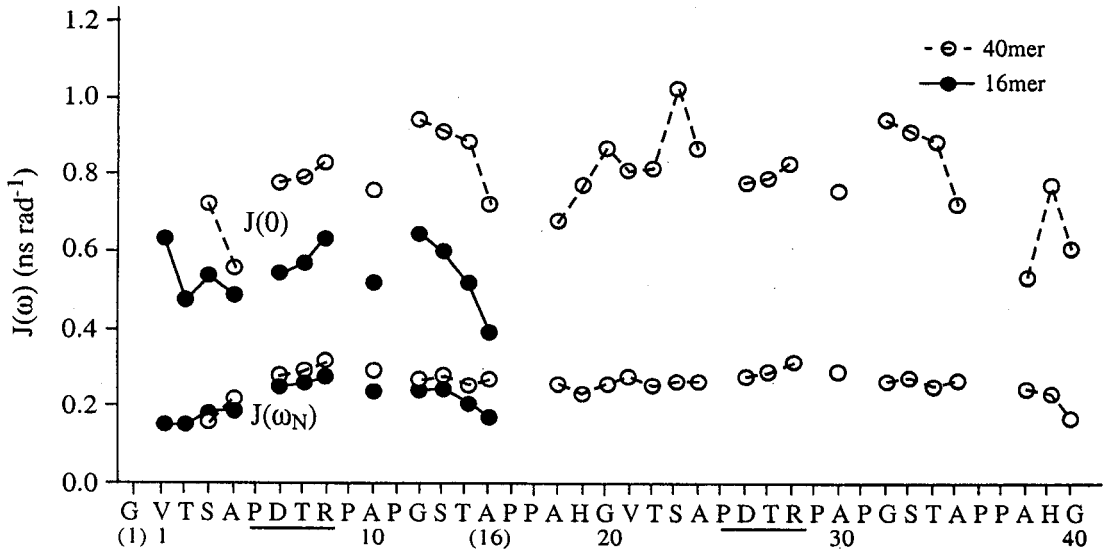

Figure 2.8: Spectral density values J(0) and $J(\omega_N)$, calculated from ^{15}N NMR relaxation data acquired for the ^{15}N,^{13}C-labeled recombinant MUC1 16mer and 40mer peptides. Table B5 in Appendix B lists the values of the J(0), $J(\omega_N)$ and $J(\omega_H)$ for both the 16mer and 40mer peptides.

parameters for the MUC1 peptides parallel each other, and because the 40mer does not have dramatically larger J(0) and $J(\omega_N)$ values, it can therefore be assumed that there is no significant increase in peptide backbone order for the 40mer.

ELISA binding assays. ELISA binding assays were performed to complement existing studies of 5-repeat versus 1-repeat MUC1 peptides binding to anti-MUC1 antibodies. These studies used the MUC1 16mer and 40mer peptides binding to four anti-MUC1 antibodies. The concentration of 50% inhibition for monoclonal antibodies BCP7 (epitope VTSA), BCP8 (epitope DTR), BCP9 (epitope GSTAP), and BCP10 (epitope RPAP) are shown in Table 2.1. BCP7 and BCP10 both bound similarly to the 16mer and 40mer peptides, with 50% inhibition of binding achieved at 0.9 μg/ml for BCP7 and 0.4

Table 2.1: Equilibrium dissociation constants (K_D) measured for the binding of the recombinant MUC1 16mer and 40mer peptides to anti-MUC1 tumor Fab B27.29 (epitope PDTRPAP), compared to 50% inhibition values obtained by competitive ELISA for anti-MUC1 peptide antibodies BCP7 (epitope VTSA), BCP8 (epitope DTR), BCP9 (epitope GSTAP), and BCP10 (epitope RPAP).

Antibody	Binding Affinity 16mer (50% inhibition)	Binding Affinity 40mer (50% inhibition)
B27.29	10.9 μM (K_D)	[illegible]
BCP7	0.9 μg/ml	[illegible]
BCP8	0.3 μg/ml	[illegible]
BCP9	0.2 μg/ml	[illegible]
BCP10	0.4 μg/ml	[illegible]

μg/ml for BCP10. The similar binding of these two antibodies suggests that the two MUC1 peptides adopt identical structures.

Monoclonal antibody BCP9 (epitope GSTAP) bound to the 40mer more tightly than did the 16mer, with 50% inhibition of binding achieved at 0.2 μg/ml for the 16mer and 0.05 μg/ml for the 40mer. The 16mer sequence lacks the full epitope sequence for BCP9, which could offer an explanation for the difference in affinity for the two peptides. BCP8 (epitope DTR) also bound to the 40mer more tightly than to the 16mer. BCP8 bound to the 16mer with 50% inhibition of binding at 0.3 μg/ml, compared to 0.05 μg/ml for the 40mer. It is unclear why the 40mer appears to bind more tightly to BCP8 than does the 16mer.

In summary, these ELISA binding experiments parallel the literature regarding the length-dependent binding of MUC1 peptides to anti-MUC1 antibodies. Some of the antibodies show binding with no length preference, while others do display a length-

dependent binding affinity. In this study, the differences in binding cannot be attributed to increased avidity from multivalent binding. However, since we have not observed any differences in the structures of the two peptides, we cannot tell why BCP8 binds more tightly to the longer MUC1 peptide, but BCP7 and BCP10 do not discriminate based on peptide length.

Fluorescence binding titrations. Since most of the antibodies reported in the literature as being specific for MUC1 were raised against synthetic MUC1 peptides, they may not be relevant to cancer vaccine design. Since we are interested in MUC1 immunogenicity, we really want to test the binding of MUC1 peptides to a cancer-associated antibody. Monoclonal antibody B27.29 was raised against breast tumor cells and is the basis for a screening test administered to breast cancer patients to determine prognosis (Gion *et al.*, 2001). Therefore, the preferences of this antibody should be more useful in vaccine design. Table 2.1 shows the equilibrium dissociation constants for the MUC1 16mer and 40mer peptides binding to the antibody fragment of B27.29 as determined by a fluorescence-monitored binding titration. The MUC1 16mer has a K_D of 10.9 ± 0.4 μM and the 40mer has a K_D of 11.2 ± 0.5 μM. These values show that the binding constants are the same within experimental error.

Conclusions:

The data presented in this study indicate that the MUC1 16mer and 40mer peptides populate the β-turn structure to the same extent, as determined by NOE connectivities, coupling constants, temperature coefficients, and chemical shift deviations from random coil values. The peptides do not form rigid secondary structure, but interconvert between random coil and β-turn structures. This conclusion is supported by

the NMR relaxation measurements, which find that the two peptides demonstrate very similar dynamics distinguished only by the larger size and longer rotational correlation time of the 40mer peptide.

The peptides do not display a uniform length-dependent difference in binding affinity to four anti-MUC1 antibodies tested by ELISA. We also find that the peptides bind with the same affinity for the breast cancer-associated antibody B27.29. Therefore, the two MUC1 peptides used in this study do not appear to have any definite length-dependent differences in binding affinity for anti-MUC1 antibodies. Most of the antibodies reported in the literature have a higher affinity for multiple-repeat MUC1 peptides (Karanikas et al., 1998; Price et al., 1998). Our findings of no differences in β-turn structure or fast ns-ps timescale dynamics between the 16mer and 40mer peptides imply that the increase in antibody binding affinity is simply due to multivalent binding.

Multivalency can be ruled out for the MUC1 16mer and 40mer peptides binding to antibodies. Using molecular modeling (modeling the peptide as extended, with two β-turns spanning PDTR and APGS), Schuman *et al.* (unpublished results), have determined that a two-repeat MUC1 peptide is not long enough to bind to both binding sites on an antibody simultaneously. Specifically, the average distance between the two combining sites of an IgG1 molecule is 110-150 Å, depending on the angle between the two Fab domains. The distance between the end of the first PDTRP epitope and the beginning of the last PDTRP epitope of a 3-repeat MUC1 peptide is 105 Å, not long enough to accomplish multivalent binding to the antibody. Therefore, avidity due to multivalent binding is not possible.

These results have implication for vaccine design, because without length-dependent binding preferences smaller, more cost-effective peptide vaccines can be utilized. Furthermore, these vaccines can also be engineered to improve their oral bioavailability or to position multiple binding epitopes on a stable, semi-flexible linker.

Multivalency plays a major role in many cellular recognition processes, and could be relevant here.

Notes to Chapter 2

Andersen, N. H., Neidigh, J. W., Harris, S. M., Lee, G. M., Liu, Z. & Tong, H. (1997). Extracting Information from the Temperature Gradients of Polypeptide NH Chemical Shifts. 1. The Importance of Conformational Averaging. *J Am Chem Soc* **119**, 8547-8561.

Apostolopoulos, V., Pietersz, G. A. & McKenzie, I. F. (1999a). MUC1 and breast cancer. *Curr Opin Mol Ther* **1**(1), 98-103.

Apostolopoulos, V., Sandrin, M. S. & McKenzie, I. F. C. (1999b). Carbohydrate/Peptide mimics: effect on MUC1 Cancer Immunotherapy. *J Mol Med* **77**, 427-436.

Bashford, J. L., Robins, R. A. & Price, M. R. (1993). Development of an anti-idiotypic antibody reactive with an antibody defining the epitope RPAP in the MUC-1 epithelial mucin core. *Int J Cancer* **54**(5), 778-83.

Baxter, N. J. & Williamson, M. P. (1997). Temperature dependence of 1H chemical shifts in proteins. *J Biomol NMR* **9**(4), 359-69.

Bhattacharya, S., Botuyan, M. V., Hsu, F., Shan, X., Arunkumar, A. I., Arrowsmith, C. H., Edwards, A. M. & Chazin, W. J. (2002). Characterization of binding-induced changes in dynamics suggests a model for sequence-nonspecific binding of ssDNA by replication protein A. *Protein Sci* **11**(10), 2316-25.

Brossart, P., Wirths, S., Stuhler, G., Reichardt, V. L., Kanz, L. & Brugger, W. (2000). Induction of cytotoxic T-lymphocyte responses in vivo after vaccinations with peptide-pulsed dendritic cells. *Blood* **96**(9), 3102-8.

Burchell, J., Taylor-Papadimitriou, J., Boshell, M., Gendler, S. & Duhig, T. (1989). *Int J Cancer* **44**, 691-696.

Cowan, P. M. & McGavine, S. (1955). *Nature* **176**, 501-503.

Dalcol, I., Pons, M., Ludevid, M. D. & Giralt, E. (1996). Convergent Synthesis of Repeating Peptides (Val-X-Leu-Pro-Pro-Pro)(8) Adopting a Polyproline II Conformation. *J Org Chem* **61**(20), 6775-6782.

Davis, J. H. & Agard, D. A. (1998). Relationship between enzyme specificity and the backbone dynamics of free and inhibited alpha-lytic protease. *Biochemistry* **37**(21), 7696-707.

Delaglio, F., Grsesiek, S., Vuister, G. W., Zhu, G., Pfeifer, J. & Bax, A. (1995). NMRPipe: A multidimensional spectral processing system based on UNIX pipes. *J Biomol NMR* **6**, 277 - 293.

Denda-Nagai, K. & Irimura, T. (2000). MUC1 in carcinoma-host interactions. *Glycoconj J* **17**(7-9), 649-58.

Denton, G., Sekowski, M. & Price, M. R. (1993). Induction of antibody responses to breast carcinoma associated mucins using synthetic peptide constructs as immunogens. *Cancer Lett* **70**(3), 143-50.

Ding, L., Lalani, E. N., Reddish, M., Koganty, R., Wong, T., Samuel, J., Yacyshyn, M. B., Meikle, A., Fung, P. Y. & Taylor-Papadimitriou, J. (1993). Immunogenicity of synthetic peptides related to the core peptide sequence encoded by the human MUC1 mucin gene: effect of immunization on the growth of murine mammary adenocarcinoma cells transfected with the human MUC1 gene. *Cancer Immunol Immunother* **36**(1), 9-17.

Doehn, C. & Jocham, D. (2000). Technology evaluation: TG-1031, Transgene SA. *Curr Opin Mol Ther* **2**(1), 106-11.

Farrow, N. A., Muhandiram, R., Singer, A. U., Pascal, S. M., Kay, C. M., Gish, G., Shoelson, S. E., Pawson, T., Forman-Kay, J. D. & Kay, L. E. (1994). Backbone dynamics of a free and phosphopeptide-complexed Src homology 2 domain studied by 15N NMR relaxation. *Biochemistry* **33**(19), 5984-6003.

Finn, O. J., Jerome, K. R., Henderson, R. A., Pecher, G., Domenech, N., Magarian-Blander, J. & Barratt-Boyes, S. M. (1995). MUC-1 epithelial tumor mucin-based immunity and cancer vaccines. *Immunol Rev* **145**, 61-89.

Fontenot, J. D. (1993). Biophysical Characterization of One, Two, and Three-Tandem Repeats of Human Mucin (MUC-1) Protein Core. *Cancer Research* **53**, 5386-5394.

Foon, K. A. (2001). Immunotherapy for colorectal cancer. *Curr Oncol Rep* **3**(2), 116-26.

Gendler, S. J. & Spicer, A. P. (1995). Epithelial mucin genes. *Annu Rev Physiol* **57**, 607-34.

Gion, M., Mione, R., Leon, A. E., Luftner, D., Molina, R., Possinger, K. & Robertson, J. F. (2001). CA27.29: a valuable marker for breast cancer management. A confirmatory multicentric study on 603 cases. *Eur J Cancer* **37**(3), 355-63.

Grinstead, J. S., Koganty, R. R., Krantz, M. J., Longenecker, B. M. & Campbell, A. P. (2002). Effect of glycosylation on MUC1 humoral immune recognition: NMR studies of MUC1 glycopeptide-antibody interactions. *Biochemistry* **41**(31), 9946-61.

Grinstead, J. S., Schuman, J. T. & Campbell, A. P. (2003). Epitope Mapping of Antigenic MUC1 Peptides to Breast Cancer Antibody Fragment B27.29: a Heteronuclear NMR Study. *Biochemistry* **accepted for publication**.

Jerome, K. R., Barnd, D. L., Bendt, K. M., Boyer, C. M., Taylor-Papadimitriou, J., McKenzie, I. F., Bast, R. C., Jr. & Finn, O. J. (1991). Cytotoxic T-lymphocytes derived from patients with breast adenocarcinoma recognize an epitope present on the protein core of a mucin molecule preferentially expressed by malignant cells. *Cancer Res* **51**(11), 2908-16.

Karanikas, V., Patton, K., Jamieson, G., Pietersz, G. & McKenzie, I. (1998). Affinty of Antibodies to MUC1 Antigens. *Tumor Biology* **19**, 71-78.

Kotera, Y., Fontenot, J. D., Pecher, G., Metzgar, R. S. & Finn, O. J. (1994). Humoral immunity against a tandem repeat epitope of human mucin MUC-1 in sera from breast, pancreatic, and colon cancer patients. *Cancer Res* **54**(11), 2856-60.

Kraulis, P. J. (1989). ANSIG. *J Magn Reson* **84**, 627-633.

Kuliopulos, A. & Walsh, C. T. (1994). Production, Purification, and Cleavage of Tandem Repeats of Recombinant Peptides. *J Am Chem Soc* **116**, 4599-4607.

Miles, D. W. & Taylor-Papadimitriou, J. (1999). Therapeutic aspects of polymorphic epithelial mucin in adenocarcinoma. *Pharmacol Ther* **82**(1), 97-106.

Mitchell, M. S. (2002). Cancer vaccines, a critical review--Part II. *Curr Opin Investig Drugs* **3**(1), 150-8.

Morse, M. A. (2000). Technology evaluation: Theratope, Biomira Inc. *Curr Opin Mol Ther* **2**(4), 453-8.

Morse, M. A. (2001). Technology evaluation: BLP-25, Biomira Inc. *Curr Opin Mol Ther* **3**(1), 102-5.

Musselli, C., Ragupathi, G., Gilewski, T., Panageas, K. S., Spinat, Y. & Livingston, P. O. (2002). Reevaluation of the cellular immune response in breast cancer patients vaccinated with MUC1. *Int J Cancer* **97**(5), 660-7.

Nakamura, H., Hinoda, Y., Nakagawa, N., Makiguchi, Y., Itoh, F., Endo, T. & Imai, K. (1998). Detection of circulating anti-MUC1 mucin core protein antibodies in patients with colorectal cancer. *J Gastroenterol* **33**(3), 354-61.

Pecher, G., Haring, A., Kaiser, L. & Thiel, E. (2002). Mucin gene (MUC1) transfected dendritic cells as vaccine: results of a phase I/II clinical trial. *Cancer Immunol Immunother* **51**(11-12), 669-73.

Peng, J. W. & Wagner, G. (1992a). *J Magn Reson* **98**, 308-332.

Peng, J. W. & Wagner, G. (1992b). Mapping of the spectral densities of N-H bond motions in eglin c using heteronuclear relaxation experiments. *Biochemistry* **31**(36), 8571-86.

Peng, J. W. & Wagner, G. (1995). Frequency spectrum of NH bonds in eglin c from spectral density mapping at multiple fields. *Biochemistry* **34**(51), 16733-52.

Petrarca, C., Casalino, B., von Mensdorff-Pouilly, S., Rughetti, A., Rahimi, H., Scambia, G., Hilgers, J., Frati, L. & Nuti, M. (1999). Isolation of MUC1-primed B lymphocytes from tumour-draining lymph nodes by immunomagnetic beads. *Cancer Immunol Immunother* **47**(5), 272-7.

Price, M. R., Rye, P. D., Petrakou, E., Murray, A., Brady, K., Imai, S., Haga, S., Kiyozuka, Y., Schol, D., Meulenbroek, M. F., Snijdewint, F. G., von Mensdorff-Pouilly, S., Verstraeten, R. A., Kenemans, P., Blockzjil, A., Nilsson, K., Nilsson, O., Reddish, M., Suresh, M. R., Koganty, R. R., Fortier, S., Baronic, L., Berg, A., Longenecker, M. B., Hilgers, J. & et al. (1998). Summary report on the ISOBM TD-4 Workshop: analysis of 56 monoclonal antibodies against the MUC1 mucin. San Diego, Calif., November 17-23, 1996. *Tumour Biol* **19 Suppl 1**, 1-20.

Richardson, J. S. (1981). The anatomy and taxonomy of protein structure. *Adv Protein Chem* **34**, 167-339.

Schuman, J., Campbell, A. P., Koganty, R. R. & Longenecker, B. M. (2003). Probing the conformational and dynamical effects of O-glycosylation within the immunodominant region of a MUC1 peptide tumor antigen. *J Pept Res* **61**(3), 91-108.

Shaka, A. J., Barker, P. B. & Freeman, R. (1985). Computer-optimized decoupling scheme for wideband applications and low-level operation. *J Magn Reson* **64**, 547-552.

Shaka, A. J., Keeler, J., Frenkiel, T. & Freeman, R. (1983). *J Magn Reson* **52**, 335-338.

Taylor-Papadimitriou, J., Burchell, J., Miles, D. W. & Dalziel, M. (1999). MUC1 and cancer. *Biochim Biophys Acta* **1455**(2-3), 301-13.

Volkman, B. F., Alam, S. L., Satterlee, J. D. & Markley, J. L. (1998). Solution structure and backbone dynamics of component IV Glycera dibranchiata monomeric hemoglobin-CO. *Biochemistry* **37**(31), 10906-19.

Vuister, G. W. & Bax, A. (1992). Measurement of two-bond JCOH alpha coupling constants in proteins uniformly enriched with 13C. *J Biomol NMR* **2**(4), 401-5.

Vuister, G. W. & Bax, A. (1993). *J Am Chem Soc* **115**, 7772-7777.

Wilmot, C. M. & Thornton, J. M. (1988). Analysis and prediction of the different types of beta-turn in proteins. *J Mol Biol* **203**(1), 221-32.

Wishart, D. S., Bigam, C. G., Holm, A., Hodges, R. S. & Sykes, B. D. (1995). 1H, 13C and 15N random coil NMR chemical shifts of the common amino acids. I. Investigations of nearest-neighbor effects. *J Biomol NMR* **5**(1), 67-81.

Wuthrich, K. (1986). *NMR of proteins and nucleic acids / Kurt Wuthrich*, Wiley,, New York :.

Xing, P. X., Prenzoska, J. & McKenzie, I. F. (1992a). Epitope mapping of anti-breast and anti-ovarian mucin monoclonal antibodies. *Mol Immunol* **29**(5), 641-50.

Xing, P. X., Prenzoska, J., Quelch, K. & McKenzie, I. F. (1992b). Second generation anti-MUC1 peptide monoclonal antibodies. *Cancer Res* **52**(8), 2310-2317.

Xing, P. X., Reynolds, K., Pietersz, G. A. & McKenzie, I. F. (1991). Effect of variations in peptide sequence on anti-human milk fat globule membrane antibody reactions. *Immunology* **72**(2), 304-11.

Xing, P. X., Tjandra, J. J., Stacker, S. A., Teh, J. G., Thompson, C. H., McLaughlin, P. J. & McKenzie, I. F. (1989). Monoclonal antibodies reactive with mucin expressed in breast cancer. *Immunol Cell Biol* **67**(Pt 3), 183-95.

Yamazaki, T., Muhandiram, R. & Kay, L. E. (1994). NMR Experiments for the Measurement of Carbon Relaxation Properties inHighly Enriched, Uniformly 13C, 15N-Labeled Proteins: Application to 13C-alpha Carbons. *J Am Chem Soc* **116**(18), 8266-8278.

Zhang, O., Kay, L. E., Olivier, J. P. & Forman-Kay, J. D. (1994). Backbone 1H and 15N resonance assignments of the N-terminal SH3 domain of drk in folded and unfolded states using enhanced-sensitivity pulsed field gradient NMR techniques. *J Biomol NMR* **4**(6), 845-58.

Zhang, P., Dayie, K. T. & Wagner, G. (1997). Unusual lack of internal mobility and fast overall tumbling in oxidized flavodoxin from Anacystis nidulans. *J Mol Biol* **272**(3), 443-55.

Chapter 3: Effect of Glycosylation on MUC1 Humoral Immune Recognition: NMR Studies of MUC1 Glycopeptide-Antibody Interactions

ABSTRACT: MUC1 mucin is a large transmembrane glycoprotein, of which the extracellular domain is formed by a repeating 20 amino acid sequence, GVTSAPDTRPAPGSTAPPAH. In normal breast epithelial cells, the extracellular domain is densely covered with highly branched complex carbohydrate structures. However, in neoplastic breast tissue, the extracellular domain is under-glycosylated, resulting in the exposure of a highly immunogenic core peptide epitope (PDTRP in bold above) as well as the normally cryptic core Tn (GalNAc), STn (sialyl 2-6 GalNAc) and TF (Gal β1-3 GalNAc) carbohydrates.

In the present study, NMR methods were used to correlate the effects of cryptic glycosylation outside of the PDTRP core epitope region to the recognition and binding of a monoclonal antibody, Mab B27.29, raised against the intact tumor-associated MUC1 mucin. Four peptides were studied: a MUC1 16mer peptide of the sequence (Gly1-Val2-Thr3-Ser4-Ala5-Pro6-Asp7-Thr8-Arg9-Pro10-Ala11-Pro12-Gly13-Ser14-Thr15-Ala16), two singly Tn-glycosylated versions of this peptide at either Thr3 or Ser4, and a doubly Tn-glycosylated version at both Thr3 and Ser4. The results of these studies showed that the B27.29 MUC1 B-cell epitope maps to two separate parts of the glycopeptide, the core peptide epitope spanning the PDTRP sequence, and a second (carbohydrate) epitope comprised of the Tn moieties attached at Thr3 and Ser4. The implications of these results are discussed within the framework of developing a glycosylated second-generation MUC1 glycopeptide vaccine.

Introduction:

Mucins are attracting real interest as potential targets in the development of vaccines for adenocarcinomas expressing Mucin 1 (MUC1), particularly for breast cancer but also for pancreatic, lung, colorectal and ovarian cancers (Apostolopoulos *et al.*, 1999a; Apostolopoulos *et al.*, 1999b; Miles & Taylor-Papadimitriou, 1999; Taylor-Papadimitriou *et al.*, 1999). MUC1 mucin is a large transmembrane glycoprotein, of which the extracellular domain is formed by a repeating 20 amino acid sequence (GVTSA**PDTRP**APGSTAPPAH)$_n$. In normal breast epithelial cells, the extracellular domain is densely covered with highly branched complex carbohydrate structures, attached to the proximal serine and threonine residues within the peptide sequence (Carlstedt & Davies, 1997; Koganty *et al.*, 1997; Rudd & Dwek, 1997; Van den Steen *et al.*, 1998). However, in the tumor-associated state, MUC1 becomes an autoantigen as a result of incomplete glycosylation and sparse distribution of these carbohydrate structures (Hanisch, 2001). This is believed to result in the exposure of a highly immunogenic core peptide sequence (PDTRP in bold above) (Girling *et al.*, 1989) identified as the immunodominant B-cell epitope from monoclonal antibody studies in mice (Bashford *et al.*, 1993; Burchell *et al.*, 1989; Denton *et al.*, 1993; Kotera *et al.*, 1994; Xing *et al.*, 1992a; Xing *et al.*, 1992b). Abnormal glycosylation is also believed to result in the exposure of the normally cryptic core Tn (GalNAc), STn (sialyl α2-6 GalNAc) and TF (Gal β1-3 GalNAc) carbohydrates (Itzkowitz *et al.*, 1989) (Brockhausen *et al.*, 1998). All three carbohydrate epitopes are strongly expressed on human carcinoma cells (Cao *et al.*, 1999; Cao *et al.*, 1997; Itzkowitz et al., 1989; Springer, 1995; Springer, 1997), and

may be associated with cancer progression and metastasis (David *et al.*, 1992; Kishikawa *et al.*, 1999; Terasawa *et al.*, 1996).

There are five potential O-glycosylation sites in each tandem repeat of the MUC1 sequence (GVTSAPDTRPAPGSTAPPAH). Identifying which of these sites remains glycosylated in the tumor-associated state is important for MUC1 vaccine design, as the vaccine should approximate as closely as possible the glycosylation state and peptide backbone exposure of the intact tumor. *In vitro* glycosylation studies using human tumor cell extracts (Nishimori *et al.*, 1994a; Nishimori *et al.*, 1994b) and three different recombinant GalNAc transferases identified from human tumor cell lines (Wandall *et al.*, 1997) have demonstrated glycosylation at three separarate sites (GVTSA and GSTAP), but not at the threonine within the PDTRP core peptide epitope region. These findings are significant insofar as reduced glycosylation of MUC1 is assumed to permit the immune system access to this region of the peptide sequence. However, recent *in vivo* studies have demonstrated that all five sites on the MUC1 tandem repeat are glycosylation targets (Muller *et al.*, 1999; Muller *et al.*, 1997), although there is no evidence to suggest that all sites are actually glycosylated.

In a recent study by this group, NMR methods were used to probe the structural and dynamical consequences of glycosylation at the central threonine within the PDTRP core epitope region of MUC1 synthetic peptides (Schuman *et al.*, 2003). This study showed that a partially-populated type I β-turn was adopted by residues PDTR in the unglycosylated MUC1 sequence, and that attachment of a Tn carbohydrate to the central threonine within this sequence resulted in a destabilization of the β-turn and a shift in the conformational equilibrium of the underlying peptide backbone toward a less dynamic and more extended structure. The existence of a similar β-turn within the PDTRP core peptide epitope of the underglycosylated tumor-associated MUC1 mucin protein might

explain the immunodominance of this region *in vivo*, as the presence of β-turn structure has been correlated with increased immunogenicity in other systems.

In the present study, we use NMR methods to probe the structural and dynamical consequences of glycosylation at serine and threonine residues upstream of the PDTRP core epitope region of MUC1 synthetic peptides, and correlate these effects to the recognition and binding of a monoclonal antibody, Mab B27.29[1], raised against the intact tumor-associated MUC1 mucin. Four peptides were studied: a MUC1 16mer peptide of the sequence (Gly1-Val2-Thr3-Ser4-Ala5-Pro6-Asp7-Thr8-Arg9-Pro10-Ala11-Pro12-Gly13-Ser14-Thr15-Ala16), two singly Tn-glycosylated versions of this peptide at either Thr3 or Ser4, and a doubly Tn-glycosylated version at both Thr3 and Ser4. Included in the study are two-dimensional ^{1}H NMR TRNOESY studies of the binding of the doubly-glycosylated MUC1 16mer to the Fab fragment of B27.29, so as to allow a mapping of the MUC1 B-cell epitope, and an assessment of the contribution of the PDTRP core peptide epitope versus the Tn core carbohydrate epitope to Mab B27.29 recognition and binding. The results of these studies are discussed within the framework of developing a glycosylated second-generation MUC1 glycopeptide vaccine.

Materials and Methods:

MUC1 Peptides and Fab B27.29. MUC1 peptides and glycopeptides were provided by Biomira Inc., Edmonton, Alberta, Canada. These included an unglycosylated 16mer

---

[1] Monoclonal antibody B27.29 was raised against ovarian tumor cell derived mucin and displays specificity for MUC1 expressing tumors of the ovaries and breast (Reddish *et al.*, 1992). Epitope fingerprinting studies identify the B27.29 epitope as PDTRPAP (GVTSA**PDTRPAP**GSTAPPAH) within the immunodominant PDTRP epitope region (Schol *et al.*, 1998). B27.29 is used as a diagnostic antibody for cancer expressing the MUC1 mucin (MacLean *et al.*, 1992).
??

(Gly1-Val2-Thr3-Ser4-Ala5-Pro6-Asp7-Thr8-Arg9-Pro10-Ala11-Pro12-Gly13-Ser14-Thr15-Ala16), two singly-glycosylated versions of this 16mer, one with a Tn carbohydrate α-linked to the β-hydroxyl of Thr3 (Tn3-glycosylated 16mer), the other with the Tn carbohydrate α-linked to the β-hydroxyl of Ser4 (Tn4-glycosylated 16mer), and a doubly-glycosylated version of the 16mer, with Tn carbohydrates α-linked to the β-hydroxyls of both Thr3 and Ser4 (Tn3,Tn4-glycosylated 16mer). The Fab fragment of anti-MUC1 monoclonal antibody B27.29 was prepared by papain digestion of the purified intact IgG, and was also provided in lyophilized form by Biomira Inc.

2D ^1H NMR Spectroscopy of MUC1 Peptides Free in Solution. Peptide NMR samples of the unglycosylated 16mer, Tn3-glycosylated 16mer, Tn4-glycosylated 16mer and Tn3,Tn4-glycosylated 16mer were prepared by dissolving the lyophilized peptides in 450 μl of 90% H_20/10% D_20 PBS buffer to a concentration of 1 mM by mass. DSS was then added as an internal chemical shift reference and the final pH was adjusted to 7.0. ^1H NMR experiments were acquired at 500 MHz on a Varian Inova 500 spectrometer equipped with an actively shielded z-axis gradient and a triple resonance probe. The hypercomplex method (States *et al.*, 1982) was used for acquisition of all 2D data sets. DQFCOSY (Piatini *et al.*, 1982) (Rance *et al.*, 1983) and TOCSY (Bax & Davis, 1985) data sets typically included 6000 Hz spectral widths, 64 transients, 300 increments and 4096 points along F2; whereas NOESY (Jeener *et al.*, 1979; Macura & Ernst, 1980) data sets typically included 6000 Hz spectral widths, 256 transients, 256 increments and 2048 points along F2. TOCSY experiments utilized a spin lock field of 7.12 kHz. NOESY experiments were acquired with a mixing time of 300 ms. All 2D data sets were collected in duplicate at two separate temperatures; 5 °C to retard rapid backbone amide proton exchange, and 25 °C to temperature shift the water peak and allow observation of

carbohydrate resonances between 4.7 and 5.0 ppm. Water suppression was achieved using a gradient-tailored echo pulse sequence incorporating two selective pulses around the 180° pulse of the echo that prevent the water signal from refocusing. In addition, a water selective 90° pulse followed by a gradient was used to diffuse water. 2D data sets were processed on a SGI Octane workstation using NMRPipe/NMRDraw software (Delaglio *et al.*, 1995). Typical processing utilized 90° shifted sine-bell squared window functions and zero filling to 4K X 4K prior to Fourier transformation.

Temperature coefficients ($-\Delta\delta/\Delta T$ ppb) for all backbone amide (NH) protons of the unglycosylated and Tn-glycosylated MUC1 16mers were calculated from linear plots of NH chemical shift versus temperature. The NH chemical shifts were measured from DQFCOSY spectra acquired at 5 and 25 °C and from one dimensional spectra acquired at 5, 10, 15, 20 and 25 °C. $^{3}J_{N\alpha}$ coupling constants were obtained from the backbone NH proton region of the one dimensional spectra acquired at 5 °C, where the individual resonances were curve-fitted using a program written by R. Boyko (University of Alberta; xcrvfit program available at www.pence.ualberta.ca.ftp) which utilizes an iterative fitting procedure. Where overlap of the NH resonances in the one dimensional spectrum precluded analysis, $^{3}J_{N\alpha}$ coupling constants were obtained from the αCH-NH fingerprint region of the 4K x 4K (F2 x F1) DQFCOSY spectrum acquired at 5 °C. The DQFCOSY spectrum was zero filled to 16K in the F2 dimension and processed using 90° shifted sine-bell weighting in the F1 dimension and no weighting in the F2 dimension. Traces were taken in ω2 and then curve-fitted as described above.

Natural Abundance $^{13}C\alpha$ Relaxation Measurements of MUC1 Peptides Free in Solution. 500 MHz $^{13}C\alpha$ T_1 and $^{13}C\alpha$ $T_1\rho$ relaxation times and steady-state $\{^{1}H\alpha\}$-$^{13}C\alpha$ heteronuclear NOE values were measured for the unglycosylated and Tn3,Tn4-

glycosylated 16mers to determine the effect of glycosylation on local backbone motion. NMR samples were prepared by dissolving the peptides in 500 µl of 99.9% D_20 PBS buffer, pH 7.0, to a concentration of 10 mM. The pulse sequences of Yamakazi and co-workers (Yamazaki *et al.*, 1994) were used for these measurements, modified to remove ^{15}N and $^{13}C'$ decoupling. ^{13}C broadband decoupling during acquisition was achieved using GARP, with a field strength of 8.2 kHz. Relaxation delays of 5, 50, 100, 150, 200, 300, 400, 500 and 600 ms were used for the T_1 experiments; and delays of 4.0, 8.0, 12.1, 16.1, 24.1, 40.2, 56.3, and 80.0 ms were used for the $T_1\rho$ experiments. Both the T_1 and $T_1\rho$ experiments used a recycling delay of 1.2 s between transients. The $\{^1H\alpha\}$-$^{13}C\alpha$ NOE was obtained by recording spectra with and without 3 s of ^1H saturation. In the case of spectra acquired without NOE, a net recycling delay of 5 s was employed, whereas a recycling delay of 2 s prior to 3 s of ^1H saturation was employed for spectra with NOE. All T_1, $T_1\rho$ and NOE spectra were recorded at 5 ^oC using spectral widths of 6000 Hz and 2500 Hz for ^1H and ^{13}C, respectively, 105 increments in the ^{13}C dimension and 1024 complex points per FID.

$^{13}C\alpha$ T_1, $T_1\rho$ and NOE data sets were processed on a SGI Octane workstation using NMRPipe/NMRDraw software (Delaglio et al., 1995). The FIDs in the ^{13}C dimension were doubled using forward linear prediction. Typically, spectra were processed in the acquisition and indirect dimensions with 90^o shifted sine-bell squared window functions. For the ^{13}C T_1 and $T_1\rho$ data sets, a Lorentz-to-Gauss transformation was performed. NMRPipe/NMRDraw software was used to pick peaks and fit the measured peak heights to a two-parameter exponential decay function of the form

$$I(t) = I_0\exp(-t/T_{1,1}\rho) \qquad [1]$$

where $I(t)$ is the intensity after a delay of time t and I_0 is the intensity at time t = 0. The uncertainties in the T_1 and $T_1\rho$ values from non-linear least-squares fit were calculated using the assumption that the RMS noise in each spectrum gives a good estimation of the error in the measured intensities of the peaks. This assumption was validated by comparison of two experiments with identical relaxation times, where the standard deviation of the peak heights was shown to approximate $\sqrt{2}$ * RMS noise in each of the spectra.

The steady-state $\{^1H\}$-^{13}C NOE values were determined from the ratios of the average intensities of the peaks with and without ^1H saturation. The standard deviation of the NOE value, σ_{NOE} was determined on the basis of measured background noise levels using the following relationship

$$\sigma_{NOE}/NOE = ((\sigma_{Isat}/I_{sat})^2 + (\sigma_{Iunsat}/I_{unsat})^2)^{1/2} \quad [2]$$

where I_{sat} and I_{unsat} represent the measured intensities of a resonance in the presence and absence of proton saturation, respectively. The standard deviations of these values, estimated from the root-mean-square noise of background regions, are represented by σ_{Isat} and σ_{Iunsat}.

Fluorescence Measurements of MUC1 Peptides Binding to Fab B27.29. Fluorescence measurements were used to determine the equilibrium dissociation constants (K_D) and off-rates (k_{off}) for the binding of the unglycosylated 16mer, Tn3-glycosylated 16mer, Tn4-glycosylated 16mer and Tn3,Tn4-glycosylated 16mer peptides to Fab B27.29. Fab B27.29 (0.86μM stock solution) was titrated with small aliquots of peptide and glycopeptide to final concentrations greater than 200-fold in excess of Fab concentration.

The change in Fab fluorescence intensity was monitored, and the concentration of bound ligand was calculated (percent of maximum fluorescence change). The natural log of the free ligand concentration was plotted against the concentration of the bound ligand, and the curve was fit to the equation

$$[\text{bound}] = (\text{capacity} * [\text{free ligand}]) / (K_D + [\text{free ligand}]) \quad [3]$$

according to Michaelis-Menton kinetics, where the capacity is the concentration of the Fab, and the K_D is the equilibrium dissociation constant.

^{1}H NMR-Monitored Titrations of MUC1 Peptides with Fab B27.29. ^{1}H NMR-monitored titrations of the unglycosylated 16mer and the Tn3,Tn4-glycosylated 16mer with Fab B27.29 were next undertaken. These included forward titrations (peptide NMR sample titrated with Fab) and reverse titrations (Fab NMR sample titrated with peptide), so as to correct for any nonspecific linebroadening of peptide resonances caused by Fab-induced increases in sample viscosity. The forward titrations used the 1 mM peptide NMR samples prepared above in 90% H_20/10% D_20 PBS buffer. Lyophilized Fab was added to these peptide NMR samples in small aliquots of a few milligrams at a time to a final concentration of 400 μM (0.4 molar equivalents Fab/peptide). In the reverse titration, lyophilized Fab was dissolved in 450 μl 90% H_20/10% D_20 PBS buffer, pH 7.0, to a concentration of 200 μM by mass. Peptide was then added in aliquots of 10-20 μL from an 8 mM stock solution to a final concentration of 1.4 mM (0.14 molar equivalents Fab/peptide). All NMR samples contained DSS as an internal chemical shift reference, and the pH was adjusted to within 7.0 ± 0.05 after each aliquot of peptide or Fab added.

One-dimensional ^{1}H NMR data sets were collected at four points in each of the

forward and reverse titrations. In the forward titration, these points represented 0 μM Fab (1 mM free peptide), 100 μM Fab (0.1 molar equivalents Fab/peptide), 200 μM Fab (0.2 molar equivalents Fab/peptide) and 400 μM Fab (0.4 molar equivalents Fab/peptide). In the reverse titration, these points represented 0 μM peptide (200 μM free Fab), 400 μM peptide (0.5 molar equivalents Fab/peptide), 800 μM peptide (0.25 molar equivalents Fab/peptide) and 1.4 mM peptide (0.14 molar equivalents Fab/peptide). NOESY and TRNOESY data sets were acquired at 5 °C and 25 °C for the beginning and end point of the forward titration, and for all four points in the reverse titration. DQFCOSY data sets were acquired at 5, 10, 15, 20 and 25 °C for the beginning and end points of the forward titration. Data acquisition and processing details for these NMR experiments have been described earlier in Experimental Methods, as have the methodologies for calculation of temperature coefficients and $^3J_{N\alpha}$ coupling constants from the DQFCOSY data sets.

Determination of Exchange Timescales for the Binding of the MUC1 Peptides to Fab B27.29. Interpreting ^1H NMR results for systems undergoing chemical exchange (for example, the MUC1 peptides binding to Fab B27.29) requires a determination of exchange timescales with respect to both chemical shift and T_1 relaxation. BIAcore analysis of the binding of a one-repeat unglycosylated MUC1 peptide to Mab B27.29 have measured a K_D = 63 nM (Karanikas *et al.*, 1998). Since most Fab fragments have K_D values 10 - 20 fold higher than their parent IgG (reflecting differences in avidity due to monovalent binding; (Nice *et al.*, 1996), the K_D for the binding of the same one-repeat peptide to Fab B27.29 is expected to be in the range of $0.1 \leq K_D \leq 1$ μM. Our own fluorescence measurements of the MUC1 16mer peptides and glycopeptides binding to Fab B27.29 have produced K_D values in the range of 10 ± 10 μM, in rough agreement with these calculations. Assuming a $K_D \approx 1$ μM and a diffusion-controlled on-rate (k_{on}

= 10^8 $M^{-1}s^{-1}$), k_{off} is then calculated to be ~ 100 s^{-1}, or 100 Hz. Typical differences between free and bound chemical shifts are 100-1000 Hz (Gemmecker, 1999), so a k_{off} = 100 Hz places the MUC1 system into intermediate exchange on the chemical shift timescale. In this regime, resonances do not shift with varying concentration of ligand, but instead experience a loss in signal intensity due to linebroadening (Gemmecker, 1999). This is the behavior exhibited in our NMR titrations of MUC1 peptides and glycopeptides binding to Fab B27.29 (see results).

It is appropriate to note here that the linebroadening observed in the MUC1 peptide-Fab titrations is only partly caused by intermediate exchange chemical shift behavior. Changes in the relaxation properties of MUC1 peptide backbone and sidechain resonances as these regions are bound and partially immobilized within the antibody combining site also contributes to linebroadening effects. Indeed, NMR relaxation measurements of MUC1 peptides in the presence of Fab have demonstrated a strong correlation between Fab-induced linebroadening and Fab-induced decreases in T_1 (Grinstead *et al.*, 2003), indicating decreased mobilities for broadened resonances, and more importantly, fast exchange on the relaxation timescale. The existence of these two exchange regimes for the MUC1 system, intermediate on the chemical shift timescale but fast on the relaxation timescale, allows implementation of TRNOESY experiments (see below) which rely on changes in T_1 to relay information of the bound state.

TRNOESY Studies of the Binding of MUC1 Peptides to Fab B27.29. The transferred nuclear Overhauser effect (TRNOE) is an extension of the nuclear Overhauser effect (NOE) to exchanging systems such as peptide-protein complexes (Campbell & Sykes, 1993). In the presence of chemical exchange, NOEs conveying conformational information of the bound peptide are 'transferred' to the free peptide resonances. Eqn. 4

diagramatically represents a system undergoing chemical exchange, in this case a MUC1 16mer peptide binding to Fab 27.29. Here, P_F and P_B are the free and bound peptide, k_1[Fab] and k_{-1}

$$\text{Fab} + \mathbf{P_F} \underset{k\text{-}1}{\overset{k1[\text{Fab}]}{\rightleftharpoons}} \text{Fab} \bullet \mathbf{P_B} \qquad [4]$$

are the exchange rates, τ_F and τ_B are the correlation times which modulate the interaction between protons in the free and bound peptide, and W_F and W_B are the dipolar cross-relaxation rates between protons in the free and bound peptide (proportional to the measured NOE intensities, NOE_F and NOE_B, at short mixing times):

$$\tau_F \approx 10^{-9}\ s \qquad \tau_B > 10^{-9}\ s$$

$$W_F \propto NOE_F \qquad W_B \propto NOE_B$$

The only necessary condition for the transfer of magnetization is that the exchange rate be faster than the T_1 longitudinal relaxation rate of the bound peptide ($k_{-1} > 1/T_{1B}$), i.e. fast exchange with respect to relaxation. This condition is met in the MUC1 system studied. Under these conditions, the TRNOE is dominated by the bound peptide conformation (even for $P_F > P_B$), since the cross-relaxation rates for the bound peptide are so much faster than they are for the free ($W_B >> W_F$). However, since the MUC1 system is also in intermediate exchange with respect to chemical shift, the measured TRNOE cannot be simply deconvoluted into a populated-weighted average of free and bound NOEs (Campbell & Sykes, 1993). Thus, a qualitative as opposed to a quantitative

approach must be adopted in analyzing the TRNOE results obtained for the MUC1 system.

Results:

Chemical Shifts and Resonance Assignments for the Unglycosylated and Tn-Glycosylated MUC1 16mers. Table A1 in Appendix A presents the ^{1}H NMR assignments for the peptide and carbohydrate resonances of the unglycosylated, Tn3-glycosylated, Tn4-glycosylated and Tn3,Tn4-glycosylated MUC1 16mers in 90% H_20/10% D_20 PBS buffer, pH 7.0, 5 °C. Table A2 in Appendix A presents the ^{13}C NMR assignments for the unglycosylated and Tn3,Tn4-glycosylated 16mers in 99.9% D_20 PBS buffer, pH 7.0, 5 °C, obtained from natural abundance ^{13}C-edited HSQC spectra. With allowances made for different temperature and solvent conditions, assignments are in good agreement with those previously published in 60% CD_3OH/40% H_20, pH 5.5, 10 °C (Liu *et al.*, 1995).

The assignments in Tables A1 and A2 in Appendix A show that glycosylation-induced chemical shift perturbations are localized to residues at or immediately adjacent to the site of carbohydrate attachment. For example, a comparison of the chemical shifts for the unglycosylated 16mer versus the Tn4-glycosylated 16mer shows significant downfield shifts for the NH and Hα resonances of Ser4 (8.49 to 8.71 ppm, and 4.45 to 4.62 ppm, respectively), less significant shifts for the NH of Ala5 (8.53 to 8.65 ppm), and only small perturbations for the Hα and Hβ resonances of Thr3. Even the doubly glycosylated 16mer exhibits no significant ^{1}H or ^{13}C chemical shift perturbations for residues more than two positions removed from the site(s) of carbohydrate attachment. Indeed, the chemical shifts for the backbone and sidechain resonances of residues within the PDTRP peptide epitope region are virtually identical across the series of MUC1

16mer peptides and glycopeptides studied (see Table A1 in Appendix A), suggesting that the chemical and conformational environment of the peptide epitope region is unaffected by upstream glycosylation events at Thr3 and Ser4.

The localized glycosylation-induced chemical shift perturbations observed in Tables 3.1 and 3.2 can be correlated to localized shifts in the conformational equilibrium of the underlying peptide backbone, as assessed from a calculation of the deviation of the $^{1}H\alpha$ proton and $^{13}C\alpha$ carbon chemical shift values from random-coil (Wishart *et al.*, 1991). $\Delta\delta_{H\alpha}$ and $\Delta\delta_{C\alpha}$ values (observe - random coil) were calculated for the unglycosylated and Tn-glycosylated MUC1 16mer peptides, and these values are presented in Table A3 in Appendix A and Figures 3.1A (unglycosylated 16mer), 3.1B (Tn3-glycosylated 16mer), 3.1C (Tn4-glycosylated 16mer) and 3.1D (Tn3,Tn4-glycosylated 16mer). The $\Delta\delta_{H\alpha}$ and $\Delta\delta_{C\alpha}$ values for the unglycosylated 16mer are close to random coil (Wishart *et al.*, 1995) for all residues, except for Gly1 and Val2 at the N-terminus and Ala16 at the C-terminus. In contrast, the $\Delta\delta_{H\alpha}$ and $\Delta\delta_{C\alpha}$ values for glycosylated residues in the Tn-glycosylated 16mers show significant downfield shifts and upfield shifts, respectively.

These values can be explained by either inductive effects of chemical substitution of the sidechain hydroxyl group with an ester linkage to the sugar or by an increase in the population of extended structure for these residues.[2] In addition to the chemical shift values, the coupling constants for the site of glycosylation increases with glycosylation. The coupling constant is to a first-order approximation independent of chemical

---

[2] $^{1}H\alpha$ proton chemical shift deviations measured for all 20 naturally occurring amino acids show a mean α proton shift of - 0.39 ppm (upfield from the random coil value) when the residue is placed in a helical conformation, and a mean α proton shift of + 0.37 ppm when the residue is placed in an extended conformation (Wishart et al., 1991). The shifting tendancies for ^{13}C nuclei are opposite in direction to those found for ^{1}NH and $^{1}H\alpha$ protons, so that the $^{13}C\alpha$ carbons experience a upfield shift from the random coil value when in an extended conformation (Wishart et al., 1991).

??

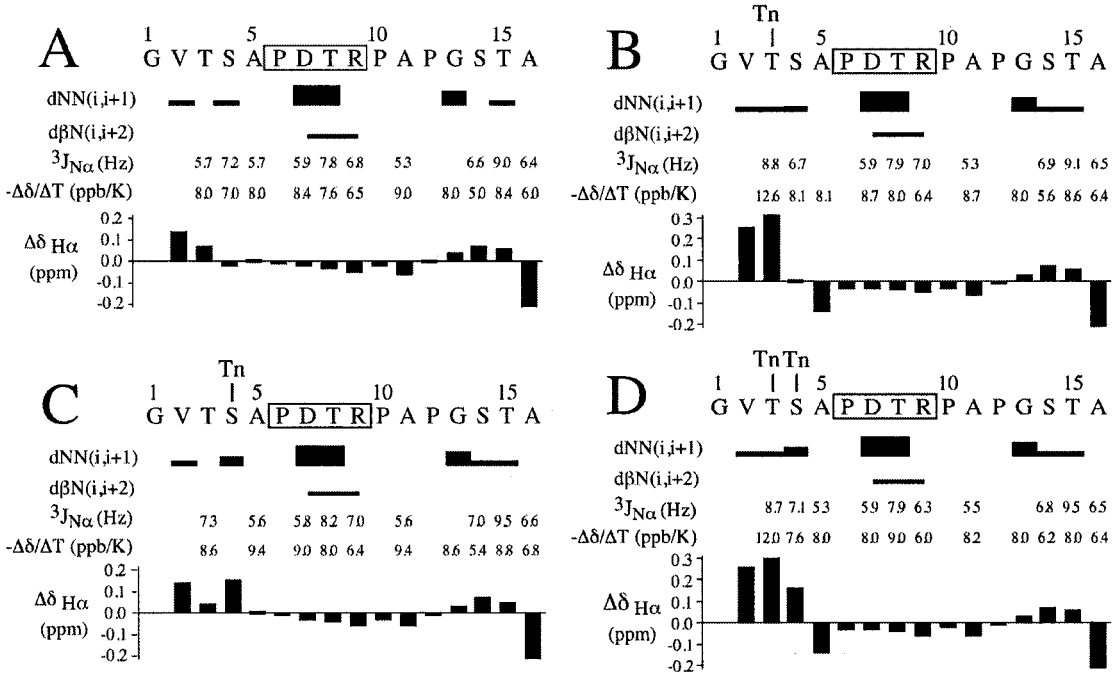

Figure 3.1: Schematic diagram showing the magnitude of dNN, dβN, dαδ and dNδ NOE connectivities observed in the NOESY spectrum of the unglycosylated MUC1 16mer (panel A), Tn3-glycosylated MUC1 16mer (panel B), Tn4-glycosylated MUC1 16mer (panel C), and Tn3,Tn4-glycosylated MUC1 16mer (panel D). The diagram also includes coupling constants ($^3J_{N\alpha}$), temperature coefficients ($-\Delta\delta/\Delta T$) and chemical shift deviations ($\Delta\delta_{H\alpha} = \delta_{H\alpha}obs - \delta_{H\alpha}coil$). The strong sequential dNN(i,i+1) NOEs between Asp7 and Thr8, and Thr8 and Arg9, and the medium dβN(i,i+2) NOE between Asp7 and Arg9 define a type I β-turn spanning Pro6-Asp7-Thr8-Arg9 in each peptide (boxed). The medium dαδ(i,i+1) and dNδ(i,i+1) NOEs linking all X-Pro pairs in the sequence define an 'all-*trans*' configuration (Wuthrich, 1986) for each peptide.

environment and suggests that glycosylation shifts the conformational equilibrium of the underlying peptide backbone toward extended strand. This phenomenon probably arises from limitations placed by the carbohydrate on the ϕ, ψ dihedral space available to the underlying peptide backbone. In line with these steric arguments is the observation that Tn-glycosylation at either Thr3 or Ser4 shifts the degenerate Hβ resonances of Ser4 (3.85 ppm for the unglycosylated 16mer) into nondegenerate positions (3.76 and 3.91 ppm in the Tn4-glycosylated 16mer, for example), which suggests that carbohydrate also

hinders rotation about the $\chi 1$ bond of Ser4. Although chemical induction can have a large effect on chemical shift, the coupling constants for the sites of glycosylation increase from 5.7 Hz for Thr3 in the unglycosylated 16mer to 8.8 Hz for the glycosylated peptide, which suggests that glycosylation results in a more extended conformation at Thr3.

NOESY Connectivities for the Unglycosylated and Tn-Glycosylated MUC1 16mers. The NOEs diagnostic of β-turn secondary structure include dNN(2,3), dNN(3,4) and dαN(2,4) crosspeaks (Wuthrich, 1986), where the numbering indicates the position in the 4-residue turn. Figure 3.1 shows the magnitudes of these β-turn defining NOEs observed in the NOESY spectra of the unglycosylated (Figure 3.1A), Tn3-glycosylated (Figure 3.1B), Tn4-glycosylated (Figure 3.1C), and Tn3,Tn4-glycosylated (Figure 3.1D) 16mer peptides. All peptides display strong sequential dNN(i,i+1) NOEs between Asp7 and Thr8, and between Thr8 and Arg9. These NOEs are diagnostic of a type I β-turn ($\phi 2 = -60^o$, $\psi 2 = -30^o$, $\phi 3 = -90^o$, $\psi 3 = 0^o$) spanning Pro6-Asp7-Thr8-Arg9 within the PDTRP peptide epitope region of each peptide, as such a turn would give rise to equally strong dNN(2,3) and dNN(3,4) NOEs (Chandrasekhar *et al.*, 1991). A type I β-turn conformation for this region in each peptide is further suggested by the medium dβN(2,4) NOEs observed between Asp7 and Arg9, since this distance can approach as closely as 2.9 Å in a type I turn, but only as closely as 3.6 Å in a type II turn[3] (Chandrasekhar et al., 1991). Glycosylation does not appear to affect either the stability or conformation of the type I β-turn, as the relative intensities of the dNN(2,3) and dNN(3,4) NOEs measured in the

[3] Unfortunately, the dαN(2,4) NOE between Asp7 and Arg9 is overlapped with the intraresidue dαN of Arg9 in the NOESY spectrum of each MUC1 16mer peptide (the Hα resonances of Arg7 and Arg9 are degenerate in each case). However this NOE has been observed in the NOESY spectra of both the unglycosylated and Tn3,Tn4-glycosylated 16mer peptides in a methanol/water mixture (Liu et al., 1995).

unglycosylated versus Tn-glycosylated 16mer NOESY spectra are comparable. This suggests that the conformation of the peptide PDTRP epitope region is unaffected by upstream glycosylation events at Thr3 and Ser4.

Our findings of a type I β-turn spanning the PDTR sequences of the unglycosylated and Tn-glycosylated MUC1 16mer peptides are in agreement with the results of three separate biophysical studies of MUC1 peptides: the previously referenced NMR study involving the unglycosylated and Tn3,Tn4-glycosylated 16mer peptides in methanol/water (Liu et al., 1995), an earlier NMR study by another group involving a 20-residue MUC1 peptide (PDTRPAPGSTAPPAHGVTSA) in DMSO (Scanlon *et al.*, 1992), and our own recent NMR studies involving a shorter 9-residue MUC1 peptide (TSAPDTRPA) in water (Schuman et al., 2003). Other studies of MUC1 peptides have found different favored turn conformations for the PDTR sequence. Fontenot and co-workers proposed a type II β-turn conformation ($\phi 2 = -60^o$, $\psi 2 = +120^o$, $\phi 3 = +90^o$, $\psi 3 = 0^o$) on the basis of their NMR/CD studies of three-repeat MUC1 peptides in water (Fontenot, 1993; Fontenot *et al.*, 1993; Fontenot *et al.*, 1995). However, a type II conformation would give rise to a weak dNN(2,3) crosspeak between Asp7 and Thr8, which is not observed in our 16mer peptides. It has also been proposed by Kirnarsky and co-workers on the basis of their NMR structure calculations that the PDTR sequence adopts two overlapping inverse γ-turns in solution, the first spanning Pro-Asp-Thr and second Asp-Thr-Arg (Kirnarsky *et al.*, 2000). However, the strong dNN(i,i+1) connectivities observed for this region of the sequence argue against the existence of two overlapping inverse γ-turns, as this arrangement would give rise to only weak dNN(i,i+1) crosspeaks between Asp7 and Thr8, and Thr8 and Arg9, corresponding to distances of 3.8 Å in each γ-turn[4]. Although it is conceivable that the different experimental

[4] The NOEs characteristic of an inverse γ-turn ($-85^o \leq \phi 2 \leq -70^o$, $+60^o \leq \psi 2 \leq +70^o$) (57, 58) include include a strong dαN(2,3) crosspeak, corresponding to a distance of 2.4 Å, a weak

conditions used in each NMR study might have led to a different favored turn conformation, it is more probable that the PDTR region of the MUC1 epitope is conformationally heterogeneous, sampling different turn conformations (type I β-turn, type II β-turn, inverse γ-turn, etc.) as part of a complex conformational equilibrium. This possibility has been explored in greater detail in our recently published NMR studies of a 9-residue MUC1 peptide and its Tn-glycosylated derivative (Schuman et al., 2003).

Coupling Constants for the Unglycosylated and Tn-Glycosylated MUC1 16mers. Type I and type II β-turns are characterized by a dihedral angle of $\phi 2 = -60^{o}$ for the second residue in the four residue turn (Richardson, 1981; Wilmot & Thornton, 1988). This local conformation is consistent with a coupling constant of 4 Hz $\leq {}^{3}J_{N\alpha} \leq$ 5 Hz, assuming a β-turn which is stably folded (100% populated) in solution. ${}^{3}J_{N\alpha}$ coupling constants were measured for all non-proline and non-glycine residues in the unglycosylated and Tn-glycosylated MUC1 16mer peptides, and these values are presented in Table A3 in Appendix A and Figures 3.1A (unglycosylated 16mer), 3.1B (Tn3-glycosylated 16mer), 3.1C (Tn4-glycosylated 16mer) and 3.1D (Tn3,Tn4-glycosylated 16mer). All peptides display reduced coupling constants for Ala5 and Ala11, a result of their placement prior to a proline (Pro6 and Pro12) in the MUC1 sequence[5]. All peptides also display a reduced coupling constant for Asp7 in position two of the putative type I β-turn, which is the same value within error (5.9 ± 0.1 Hz) across the series of 16mer peptides and glycopeptides. This value, however, does not fall within the range of 4 Hz $\leq {}^{3}J_{N\alpha} \leq$ 5 Hz predicted for the second residue of a stably folded

---

dNN(2,3) crosspeak, corresponding to a distance of 3.8 Å, and a weak dαN(2,3) crosspeak corresponding to a distance of 4.3 Å (Inai *et al.*, 2000; MacArthur & Thornton, 1991).

[5] In general, the residue proceeding a proline experiences steric clashes between its NH, Hα and Hβ protons and the Hδ protons and carbonyl carbons of the proline. This results in a displacement towards more negative φ values for the proceeding residue, and a concommitant decrease in the measured ${}^{3}J_{N\alpha}$ value (MacArthur & Thornton, 1991).

type I β-turn. Since the partially structured 16mer peptides and glycopeptides are likely to be undergoing a conformational equilibrium between folded (β-turn) and unfolded (extended) states, the measured coupling constants for Asp7 should represent a populated weighted average of the $^3J_{\alpha N}$ values associated with each interconverting state. Using a very simplistic two-state model (Campbell *et al.*, 1995; Yao *et al.*, 1994) in which Asp7 can find itself either in a turn conformation ($^3J_{N\alpha}$ = 5 Hz) or in an extended conformation ($^3J_{N\alpha}$ = 9 Hz), a measured coupling constant of $^3J_{N\alpha}$ = 5.9 ± 0.1 Hz translates into approximately 70 - 75% of Asp7 sites in a folded turn conformation for each peptide. This rough estimate suggests that the turn population within the PDTRP epitope region is unaffected by upstream glycosylation events at Thr3 and Ser4, in agreement with the NOE and chemical shift perturbation data previously discussed.

Whereas the coupling constant data suggest no long range effects of glycosylation, the dependence of the $^3J_{N\alpha}$ of Thr3 on the glycosylation state suggests significant localized effects. For example, the $^3J_{N\alpha}$ of Thr3 increases from 5.7 Hz in the unglycosylated 16mer, to 7.3 Hz in the Tn4-glycosylated 16mer, to 8.8 Hz in the Tn3-glycosylated 16mer. Using the simple but conceptually effective two-state model described above, these coupling constants translate into approximately 17%, 58% and 95% local extended conformation, respectively, for each peptide. These rough estimates suggest that glycosylation shifts the conformational equilibrium of the underlying peptide backbone toward extended strand, a finding consistent with the chemical shift data presented earlier in the chapter.

Temperature Coefficients for the Unglycosylated and Tn-Glycosylated MUC1 16mers. The temperature dependence of the amide proton chemical shift, or temperature coefficient ($-\Delta\delta/\Delta T$), is often interpreted as a measure of solvent shielding in folded

peptides and proteins. For unfolded regions of the sequence, temperature coefficients are expected to be $6 \leq -\Delta\delta/\Delta T \leq 10$ ppb/K (Rose *et al.*, 1985), indicating that the backbone is freely solvated by water and that no hydrogen bonds are present which would protect the backbone amides from solvent exchange. For folded regions of the sequence, temperature coefficients are expected to decrease to $-\Delta\delta/\Delta T < 6$ ppb/K (Rose et al., 1985), indicating either the presence of a hydrogen bond or a high degree of solvent shielding. The temperature dependence of the amide proton chemical shift can therefore be an indication of possible intramolecular hydrogen bonding.

Temperature coefficients ($-\Delta\delta/\Delta T$) were measured for all non-proline residues in the unglycosylated and Tn-glycosylated MUC1 16mer peptides, and these values are presented in Table A3 in Appendix A and Figures 3.1A (unglycosylated 16mer), 3.1B (Tn3-glycosylated 16mer), 3.1C (Tn4-glycosylated 16mer) and 3.1D (Tn3,Tn4-glycosylated 16mer). All peptides display reduced temperature coefficients of $6.0 \leq -\Delta\delta/\Delta T \leq 6.5$ ppb/K for Arg9 in position four of the putative type I β-turn. These reduced temperature coefficients suggest involvement of the Arg9 NH in a hydrogen bond that partially protects it from solvent exchange, an interpretation consistent with the presence of Pro6-CO to Arg9-NH (1,4) hydrogen bonds stabilizing the type I β-turn proposed to span Pro6-Asp7-Thr8-Arg9 within the PDTRP peptide epitope region of each peptide.

Also observed in the temperature coefficient data is an unusually strong dependence of the $-\Delta\delta/\Delta T$ of Thr3 on the glycosylation state of this residue. For example, the $-\Delta\delta/\Delta T$ of Thr3 is much more elevated in the Tn3- and Tn3,Tn4-glycosylated 16mers (12.6 and 12.0 ppb/K, respectively) than in the unglycosylated or Tn4-glycosylated 16mers (8.0 and 8.6 ppb/K, respectively). These elevated values of $-\Delta\delta/\Delta T$ correlate with the significant downfield shifts observed for Thr3 NH in the Tn3-

and Tn3,Tn4-glycosylated 16mers (8.91 and 8.90 ppm, respectively), in agreement with the strong correlation that exists between $-\Delta\delta/\Delta T$ and NH chemical shift in unstructured systems (Andersen *et al.*, 1997)[6]. One way to interpret the significant downfield shifts of Thr3 NH in the Tn3-glycosylated and Tn3,Tn4-glycosylated 16mers is to relate it to the possible existence of a hydrogen bond between the backbone NH proton of Thr3 and the carbonyl of the N-acetyl group of Tn3, as the presence of hydrogen bonds is often accompanied by marked downfield shifts in folded peptides and proteins (Andersen et al., 1997). This proposal receives some support from molecular modeling studies of a glycosylated trimer Ac-Thr(α-GalNAc)-Ala-Ala-OMe (Mimura *et al.*, 1989) in which the existence of a hydrogen bond between the peptide NH protons and the GalNAc N-acetyl carbonyl was demonstrated. Were such hydrogen bonds to exist in the Tn-glycosylated MUC1 16mers, these bonds might also play a role in shifting the conformation of the underlying peptide backbone toward more extended structure.

^{13}C NMR Relaxation Experiments for the Unglycosylated and Tn3,Tn4-Glycosylated MUC1 16mers. Natural abundance $^{13}C\alpha$ T_1 and $T_1\rho$ relaxation times, and $\{^1H\alpha\}$-$^{13}C\alpha$ heteronuclear NOE values were measured for the unglycosylated and Tn3,Tn4-glycosylated MUC1 16mer peptides in order to assess the effect of carbohydrate attachment at Thr3 and Ser4 on peptide backbone dynamics. The relaxation times and NOE values presented in Table A4 in Appendix A and Figures 3.2A ($^{13}C\alpha$ T_1 and $T_1\rho$) and 3.2B ($\{^1H\alpha\}$-$^{13}C\alpha$ NOE) show that glycosylation significantly affects the backbone dynamics of glycosylated (Thr3, Ser4) and neighboring (Val2, Ala5) residues, but has no

---

[6] It should be noted that the proposal of a hydrogen bond based on large negative values of $-\Delta\delta/\Delta T$ is consistent with the 'equilibrium between states' interpretation of temperature coefficients (Yao et al., 1994), although it does contradict the conventional 'solvent shielding' interpretation of $-\Delta\delta/\Delta T$ (MacArthur & Thornton, 1991) which assumes a correlation between small $-\Delta\delta/\Delta T$ and the presence of a hydrogen bond.

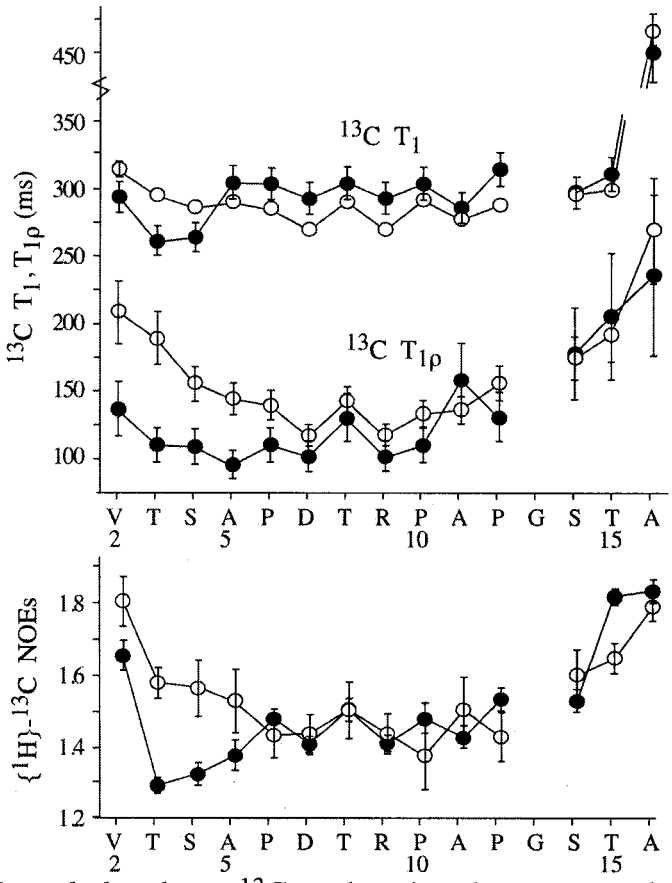

Figure 3.2: Natural abundance $^{13}C\alpha$ relaxation data measured for the unglycosylated (open circles) and Tn3,Tn4-glycosylated (black circles) MUC1 16mer peptides. Panel A plots the $^{13}C\alpha$ T_1 and $T_1\rho$ relaxation times, and panel B plots the $\{^1H\alpha\}$-$^{13}C\alpha$ heteronuclear NOE values measured for each residue. Error bars (standard deviations calculated for each relaxation parameter) are plotted only when the bars are larger than the actual size of the symbol. Experimental conditions were 10 mM peptide in 99.9% D_20 PBS buffer, pH 7.0, 5 °C.

significant effects on the backbone dynamics of more remote residues within the PDTRP core epitope region.

For example, the relaxation times and NOE values of Thr3 are T_1 = 295 ± 5 ms, $T_1\rho$ = 188 ± 19 ms, and NOE = 1.58 ± 0.04 for the unglycosylated 16mer, and T_1 = 262 ± 11 ms, $T_1\rho$ = 110 ± 13 ms, and NOE = 1.29 ± 0.02 for the Tn3,Tn4-glycosylated 16mer. These times and values are consistent with glycosylation-induced increases in the local correlation time and order of the Thr3 $^{13}C\alpha$-$^1H\alpha$ bond vector. In contrast, the relaxation

times and NOE values averaged over the central residues of the peptide (Pro6-Asp7-Thr8-Arg9-Pro10-Ala11-Pro12) are not significantly changed by upstream glycosylation at Thr3 and Ser4; i.e., $\langle T_1 \rangle_{6\text{-}12} = 281 \pm 9$ ms, $\langle T_1\rho \rangle_{6\text{-}12} = 134 \pm 21$ ms, and $\langle NOE \rangle_{6\text{-}12} = 1.44 \pm 0.05$ for the unglycosylated 16mer, and $\langle T_1 \rangle_{6\text{-}12} = 298 \pm 9$ ms, $\langle T_1\rho \rangle_{6\text{-}12} = 120 \pm 21$ ms, and $\langle NOE \rangle_{6\text{-}12} = 1.46 \pm 0.05$ for the Tn3,Tn4-glycosylated 16mer. Our findings of only localized effects of glycosylation on underlying peptide backbone dynamics are in agreement with the ^{13}C NMR relaxation studies of a sequentially deglycosylated native ovine submaxillary mucin (OSM) (Gerken *et al.*, 1989), where a 'stiffening effect' was transmitted from the site of glycosylation only to adjacent residues.

Peptide-Sugar NOE Connectivities Identified for the Tn3,Tn4-Glycosylated MUC1 16mer. The ^{13}C NMR relaxation results described above suggest that glycosylation exerts its conformational effects on the underlying mucin peptide backbone through the imposition of steric constraints on ϕ, ψ, χ^1 dihedral space. However, a second mechanism involving conformational effects through specific peptide-sugar interactions is also possible. In order to probe for the existence of specific peptide-sugar interactions that could mediate conformational effects on local peptide backbone, NOESY spectra of the Tn3,Tn4-glycosylated MUC1 16mer peptide were carefully scrutinized for peptide-sugar NOEs. These NOEs, listed in Table A5 in Appendix A and shown diagramatically in Figure 3.3, suggest that interactions between the attached sugar and the underlying peptide backbone are specific and localized.

For example, the Tn3 carbohydrate displays close contacts only to Val2, Thr3 and Ser4, whereas the Tn4 carbohydrate displays close contacts only to Ser4, Ala5 and Pro6. The absence of longer range contacts between the attached Tn carbohydrates and the peptide backbone is consistent with the absence of longer range effects on the

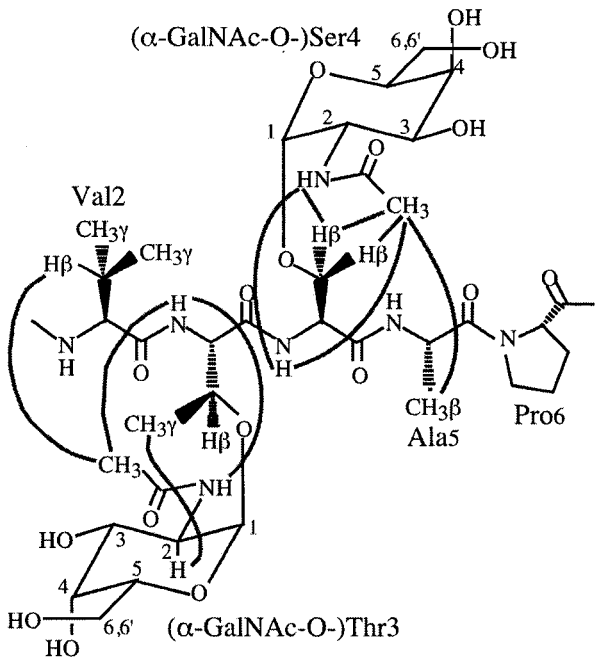

Figure 3.3: Diagrammatic representation of strong peptide-sugar NOEs observed in the NOESY spectrum of the Tn3,Tn4-glycosylated MUC1 16mer peptide acquired in 90% H_20/10% D_20 PBS buffer, pH 7.0, 5 °C. Refer to Table A5 in Appendix A for a complete list of peptide-sugar NOEs.

conformation or dynamics of the peptide PDTRP epitope region following upstream glycosylation at either Thr3 or Ser4.

Some of the strongest NOEs observed in the NOESY spectra of the Tn3,Tn4-glycosylated MUC1 16mer peptide include those between the NH protons of Thr3 and Ser4 and the methyl and NH protons of the N-acetyl groups of their directly attached Tn moieties. Similar peptide-sugar connectivities have been observed in other NMR studies of α-GalNAc O-glycosylated peptides (Kirnarsky et al., 2000; Liang *et al.*, 1995; Live *et al.*, 1999; Schuman et al., 2003). For example, Kirnarsky and co-workers observed a strong NOE between the NH proton of their glycosylated threonine residue and the N-acetyl group of GalNAc in their α-linked O-glycosylated 15-residue MUC1 peptide (Kirnarsky et al., 2000). The presence of these specific peptide-sugar NOEs between the N-acetyl group of the attached GalNAc and the backbone NH of the glycosylated residue

suggests that the N-acetyl of the GalNAc might interact directly with the peptide backbone, providing some evidence for the existence of hydrogen bonds between the NH proton of the peptide backbone and the carbonyl on the N-acetyl group of the GalNAc. The pattern of peptide-sugar NOEs does not explain why the Thr3-Tn3 pair displays a much larger temperature coefficient than does the Ser4-Tn4 pair.

^{1}H NMR-Monitored Titrations of the Unglycosylated and Tn3,Tn4-Glycosylated MUC1 16mers with Fab 27.29. Competitive ELISA binding studies on mucin solid phase have shown that Tn-glycosylation at Thr3 and Ser4 in the MUC1 synthetic peptides leads to a small but reproducible increase in the affinity of the peptide for Mab B27.29, an antibody raised against the intact tumor-associated MUC1 mucin (Liu et al., 1995). As upstream glycosylation at Thr3 and Ser4 does not affect the conformation and dynamics of the immunodominant PDTRP peptide epitope region, this increased affinity for B27.29 cannot be due to the proximal carbohydrate stabilizing the peptide epitope conformation most favored for binding (presumably the type I β-turn spanning PDTR). A more likely scenario is that the carbohydrates comprise part of the recognition domain for B27.29, whose natural MUC1 antigen remains extensively glycosylated with cryptic carbohydrate structures in the tumor-associated state.

In order to determine the contribution of defined peptide secondary structure (peptide epitope) versus specific-site glycosylation (carbohydrate epitope) in antibody recognition and binding, ^{1}H NMR-monitored titrations of the unglycosylated and Tn3,Tn4-glycosylated MUC1 16mers with the Fab fragment of Mab B27.29 were performed. Figure 3.4 shows the backbone amide region of the 500 MHz ^{1}H NMR spectra of the unglycosylated 16mer (Figure 3.4A) and Tn3,Tn4-glycosylated 16mer

(Figure 3.4B) in the absence and presence of 0.4 molar equivalents Fab B27.29. Several amide resonances are observed to diminish appreciably in the bound spectrum, due to

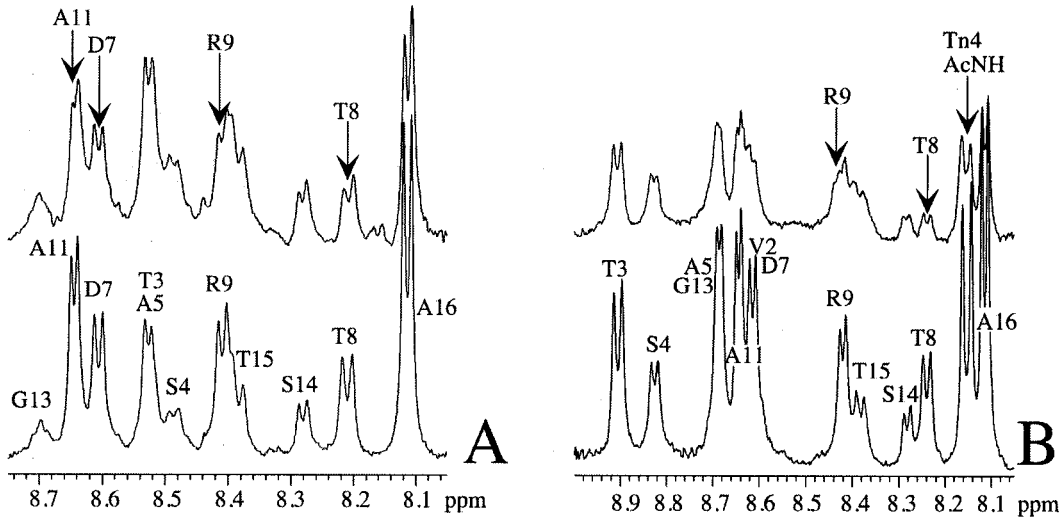

Figure 3.4: Backbone amide NH regions of ^{1}H NMR spectra showing the forward titration of the unglycosylated (panel A) and Tn3,Tn4-glycosylated (panel B) MUC1 16mer peptides with Fab B27.29. The lower traces correspond to the free peptides, whereas the upper traces correspond to the peptide in presence of 0.4 molar equivalents Fab. Resonances marked by arrows experience the greatest losses in signal intensity due to linebroadening in the presence of Fab. Experimental conditions were 1 mM peptide ± 400 μM Fab in 90% H_20/10% D_20 PBS buffer, pH 7.0, 5 °C.

exchange broadening and/or increases in local correlation time as these residues are preferentially bound and immobilized in the antibody combining site. The spectrum of the glycosylated 16mer shows greater line broadening effects than does the spectrum of the unglycosylated 16mer at the same molar equivalents of Fab. The difference in linebroadening between the 16mer peptide and glycopeptide bound to Fab B27.29 suggests a stronger interaction for the glycosylated peptide, in agreement with the competitive ELISA binding experiments (Liu et al., 1995). Regardless of these differences in overall linebroadening, the most selectively broadened amide resonances for each peptide correspond to Asp7, Thr8, Arg9 and Ala11 within or near the PDTR β-turn region. This collection of residues suggests that the turn is preferentially bound in

the antibody combining site, and constitutes the peptide portion of the B-cell epitope for both the unglycosylated 16mer and the Tn3,Tn4-glycosylated 16mer. The sugar moieties must also be involved in the binding of Fab, since the N-acetyl NH resonance(s) of Tn3 (not shown) and Tn4 are observed to substantially diminish in intensity in the bound spectra of the glycosylated 16mer.

The identification of epitope regions using differential linebroadening is best accomplished using the DQFCOSY experiment, as the antiphase nature of the crosspeaks render them uniquely sensitive to the linewidth of the detected proton (the positive and negative lobes cancel when peak linewidth is greater than the coupling constant). Thus, the DQFCOSY experiment can act as a dynamic filter of differential proton mobilities and has been used in this capacity to identify the residues comprising the determinants of several peptide antigens when these are bound to antibody (Campbell *et al.*, 1997; Cheetham *et al.*, 1991; Zvi *et al.*, 1995). Figure 3.5 shows the $d_{\alpha N}$ fingerprint regions of the 500 MHz DQFCOSY spectra of the unglycosylated and Tn3,Tn4-glycosylated 16mer peptides in the absence (Figure 3.5A) and presence (Figure 3.5B) of Fab B27.29, where several $d_{\alpha N}$ crosspeaks are observed to disappear or diminish appreciably in intensity upon the addition of antibody. Those $d_{\alpha N}$ crosspeaks correspond to Ala5, Asp7, Arg9 and Ala11 in each peptide, residues within or near the PDTR β-turn region. However, the backbone (as detected by the $d_{\alpha N}$ crosspeak) is not the only portion of the turn that is selectively immobilized upon binding to antibody. When the $d_{\alpha\beta}$ regions of the DQFCOSY experiments are plotted for each peptide in the absence and presence of Fab (see Figures 3.6A and 3.6B), the $d_{\alpha\beta}$ crosspeaks which experience the greatest linebroadening correspond to the β-protons of Asp7, Arg9 and Pro10 in each peptide, suggesting that the side-chains of these residues are also partially immobilized in the antibody combining site. Thus, the side chains as well as backbone portion of the

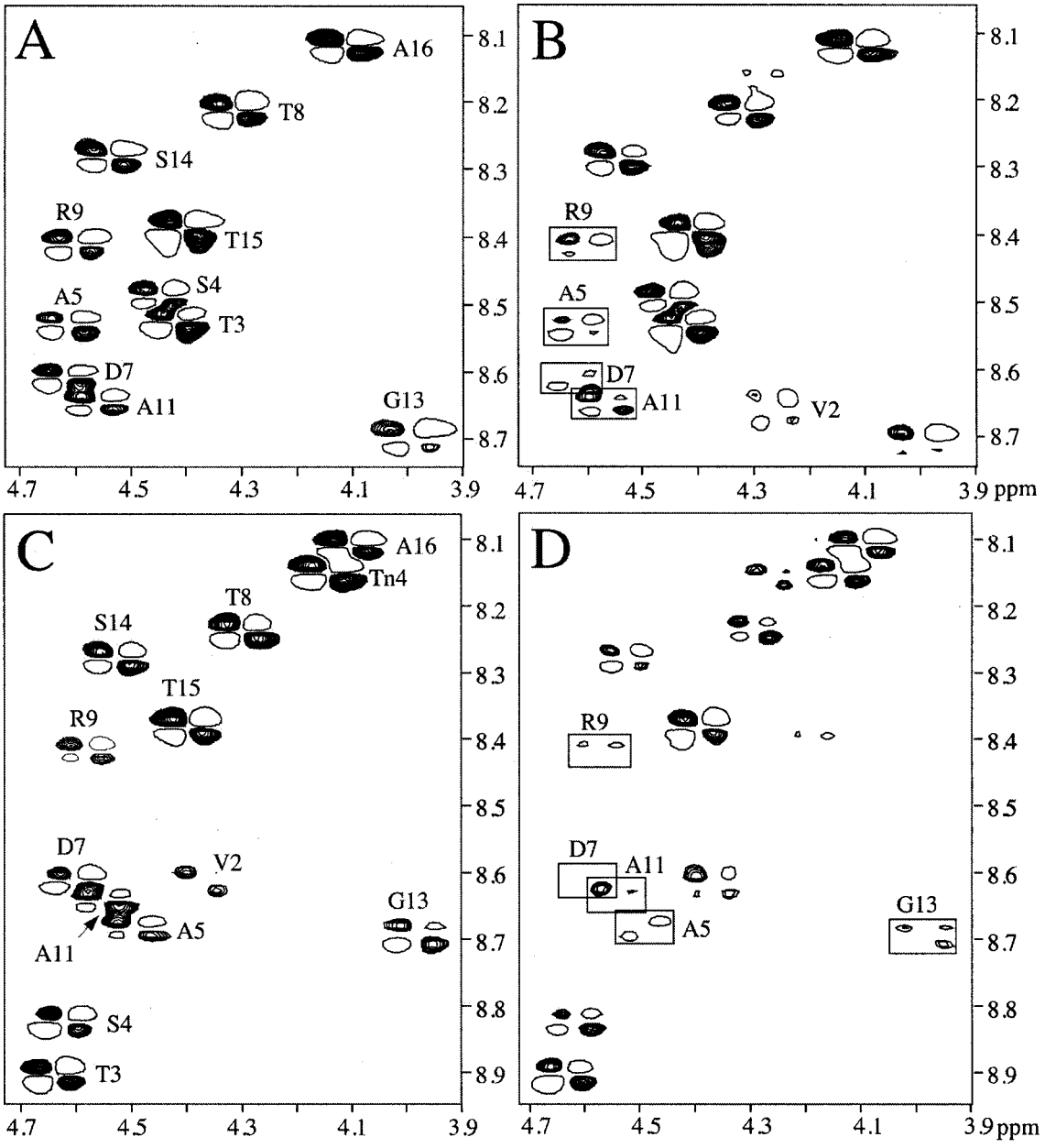

Figure 3.5: Fingerprint dαN regions of DQFCOSY spectra showing the forward titration of the unglycosylated and Tn3,Tn4-glycosylated MUC1 16mers with Fab B27.29. Panels A and B correspond to the unglycosylated 16mer in the absence (panel A) and presence (panel B) of 0.4 molar equivalents Fab, whereas panels C and D correspond to the Tn3,Tn4-glycosylated 16mer in the absence (panel C) and presence (panel D) of 0.4 molar equivalents Fab. Boxed crosspeaks experience the greatest losses in signal intensity due to linebroadening in the presence of Fab. Experimental conditions were 1 mM peptide ± 400 μM Fab in 90% H_20/10% D_20 PBS buffer, pH 7.0, 5 °C.

PDTRP peptide epitope appear to be involved in the recognition and binding of Fab B27.29.

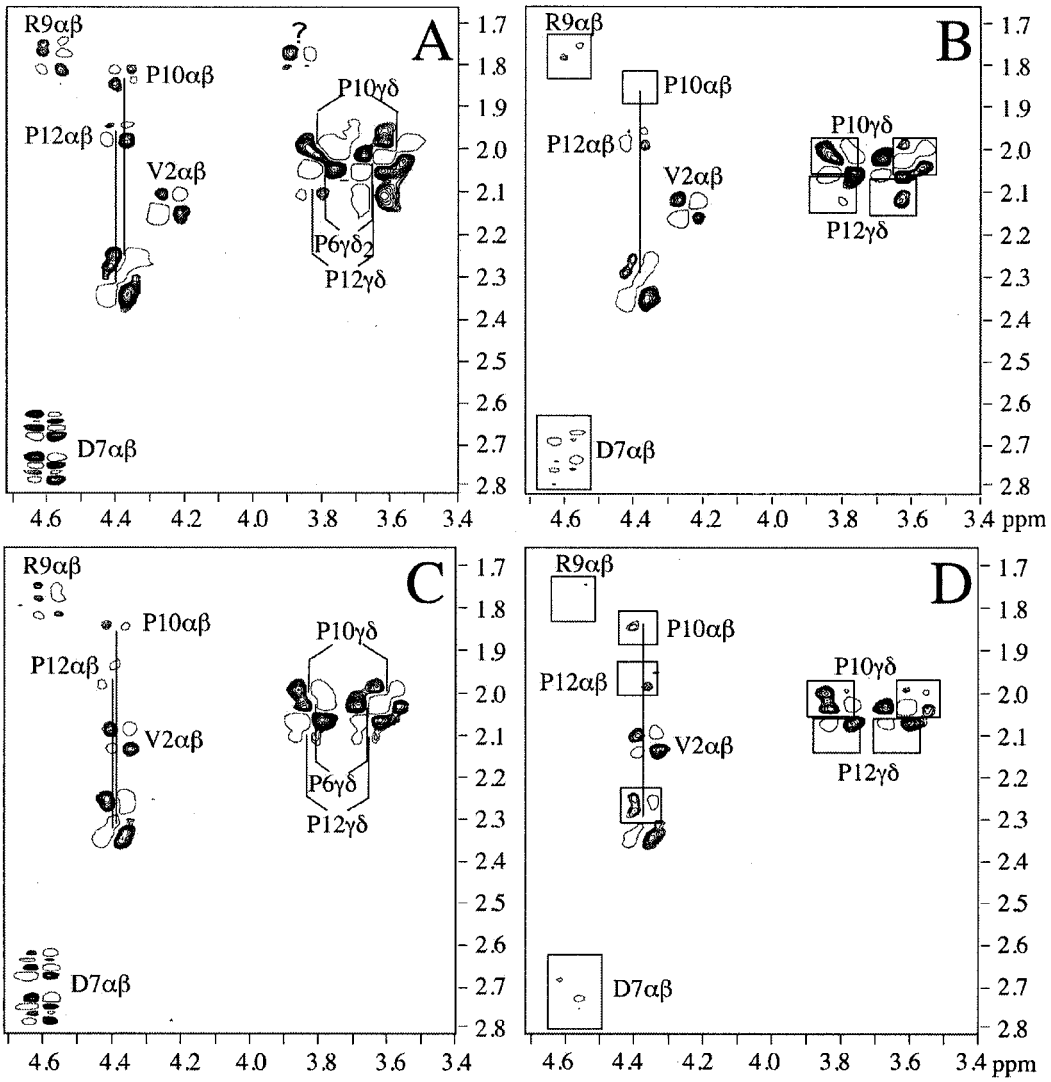

Figure 3.6: Aliphatic regions of DQFCOSY spectra showing the forward titration of the unglycosylated and Tn3,Tn4-glycosylated MUC1 16mers with Fab B27.29. Panels A and B correspond to the unglycosylated 16mer in the absence (panel A) and presence (panel B) of 0.4 molar equivalents Fab, whereas panels C and D correspond to the Tn3,Tn4-glycosylated 16mer in the absence (panel C) and presence (panel D) of 0.4 molar equivalents Fab. Boxed crosspeaks experience the greatest losses in signal intensity due to linebroadening in the presence of Fab. Experimental conditions were 1 mM peptide ± 400 μM Fab in 90% H_20/10% D_20 PBS buffer, pH 7.0, 5 °C.

TRNOESY Studies of the Binding of the Tn3,Tn4-Glycosylated MUC1 16mer to Fab 27.29. TRNOESY experiments were next performed at both 5 and 25 °C for the Tn3,Tn4-glycosylated 16mer peptide in the presence of Fab B27.29. The goals of these TRNOESY experiments were threefold: 1. to map the MUC1 B-cell epitope recognized by B27.29, 2. to identify peptide-Fab and sugar-Fab NOEs across the binding interface so as to better define the MUC1 antigen-B27.29 interaction, and 3. to determine if the PDTR type I β-turn found within the free solution state MUC1 peptide is conserved within the B27.29 combining site.

Figure 3.7 shows the dαN, dβN, dγN and dδN regions of the NOESY and TRNOESY spectra acquired at 25 °C from the reverse titration of the Tn3,Tn4-glycosylated 16mer in the absence (Figure 3.7A) and the presence (Figure 3.7B) of Fab B27.29. This figure illustrates the development of TRNOEs in the bound glycopeptide, which are more easily observed at 25 °C due to the attenuation of the free peptide NOEs at this temperature. The strongest of these TRNOEs correspond to residues within the PDTRP epitope. For example, the dβN and dγN crosspeaks of Asp7, Thr8 and Arg9 are observed only in the presence of Fab (Figure 3.7B). TRNOE effects are also observed for the Tn-glycosylated residues Thr3 and Ser4 and for the Tn carbohydrates attached to these residues. No TRNOE effects are observed for the C-terminal residues of the glycopeptide, as evidenced by the absence of dαN, dβN and dγN crosspeaks for Gly13, Ser14, Thr15 and Ala16 in the presence of Fab (Figure 3.7B). The aliphatic portion of the TRNOESY spectrum of the Tn3,Tn4-glycosylated 16mer in the presence of Fab B27.29 was also analyzed (data not shown), and showed a similar pattern of TRNOE effects - significant enhancements for the glycosylated residues, Thr3 and Ser4, and

Figure 3.7: dαN, dβN, dγN and dδN regions of NOESY spectra acquired at 25°C from the reverse titration of the Tn3,Tn4-glycosylated MUC1 16mer with Fab B27.29. This figure illustrates the development of TRNOEs in the bound peptide, which are easier to identify at 25°C due to the attenuation of the free peptide NOEs at this temperature. Peaks corresponding to sugar-peptide or sugar-protein NOEs are colored red. Panel A corresponds to 1.4 mM peptide (no Fab), whereas panel B corresponds to 200 μM Fab + 1.4 mM peptide (0.14 molar equivalents Fab/peptide). Experimental conditions were 90% H_2O/10% D_2O PBS buffer, pH 7.0, 25°C.

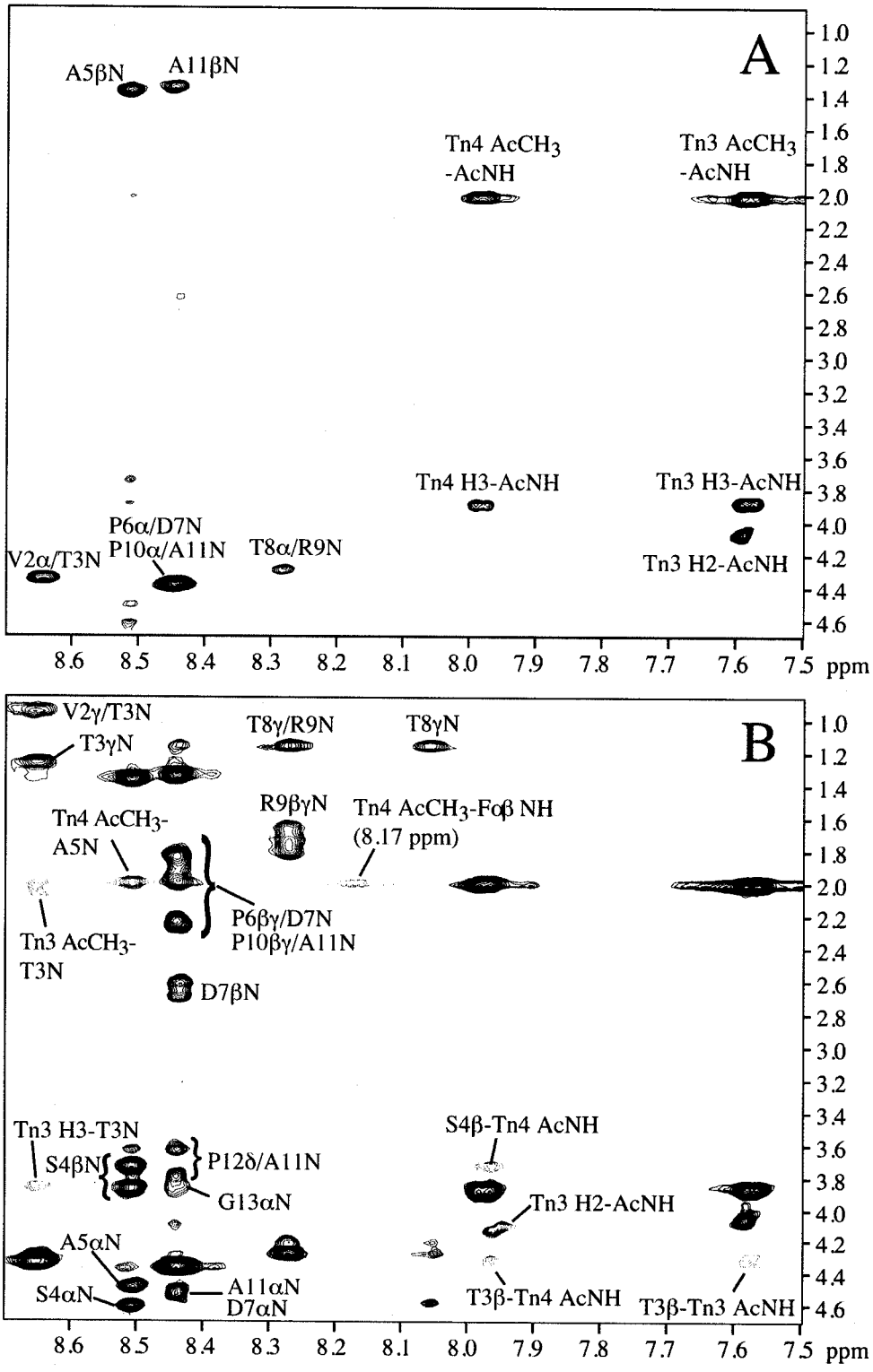
A
A5βN
A11βN
Tn4 AcCH3
-AcNH
Tn3 AcCH3
-AcNH
Tn4 H3-AcNH
Tn3 H3-AcNH
P6α/D7N
P10α/A11N
V2α/T3N
T8α/R9N
Tn3 H2-AcNH
B
V2γ/T3N
T3γN
T8γ/R9N
T8γN
R9βγN
Tn4 AcCH3-Foβ NH
(8.17 ppm)
Tn4 AcCH3-
A5N
P6βγ/D7N
P10βγ/A11N
Tn3 AcCH3-
T3N
D7βN
Tn3 H3-T3N
S4βN
P12δ/A11N
G13αN
S4β-Tn4 AcNH
Tn3 H2-AcNH
A5αN
S4αN
A11αN
D7αN
T3β-Tn4 AcNH
T3β-Tn3 AcNH
1.0
1.2
1.4
1.6
1.8
2.0
2.2
2.4
2.6
2.8
3.0
3.2
3.4
3.6
3.8
4.0
4.2
4.4
4.6
8.6
8.5
8.4
8.3
8.2
8.1
8.0
7.9
7.8
7.7
7.6
7.5
ppm

significant enhancements for residues Asp7, Thr8, Arg9 and Pro10 within the PDTRP epitope.

The pattern of TRNOE enhancements observed for the Tn3,Tn4-glycosylated 16mer in the presence of Fab closely mirrors the pattern of linebroadening observed in the ^{1}H NMR-monitored titration of this glycopeptide (selective linebroadening for PDTRP peptide epitope and Tn carbohydrate resonances). This similarity in TRNOE and linebroadening patterns suggests that both effects derive from increases in localcorrelation times (i.e., $\tau_B > \tau_F$; see Eqn. 4) as the PDTRP peptide epitope and the Tn carbohydrates are preferentially bound and immobilized in the antibody combining site. Thus, the MUC1 B-cell epitope in the Tn3,Tn4-glycosylated 16mer appears to be comprised of two separate portions, a peptide epitope spanning the PDTRP sequence, and a carbohydrate epitope consisting of Tn sugars attached at Thr3 and Ser4.

TRNOESY experiments were also performed at 5 and 25 ^{o}C for the unglycosylated 16mer peptide in the presence of Fab B27.29 (data not shown). These experiments demonstrated TRNOE enhancements for residues within the PDTRP peptide epitope, but no enhancements for residues at the C-terminus of the peptide, in agreement with the results obtained for the Tn3,Tn4-glycosylated 16mer. Significantly, no TRNOE enhancements were observed for either Thr3 or Ser4 in the unglycosylated peptide, presumably because these residues lack the attached carbohydrate that can bind directly to antibody.

Having mapped the B27.29 B-cell epitope in the glycosylated MUC1 antigen to separate peptide and carbohydrate epitopes, TRNOESY spectra were then carefully scrutinized for peptide-Fab and sugar-Fab NOEs. Figure 3.8 shows the dNN region of the NOESY/TRNOESY spectra acquired at 5 ^{o}C from the reverse titration of Tn3,Tn4-

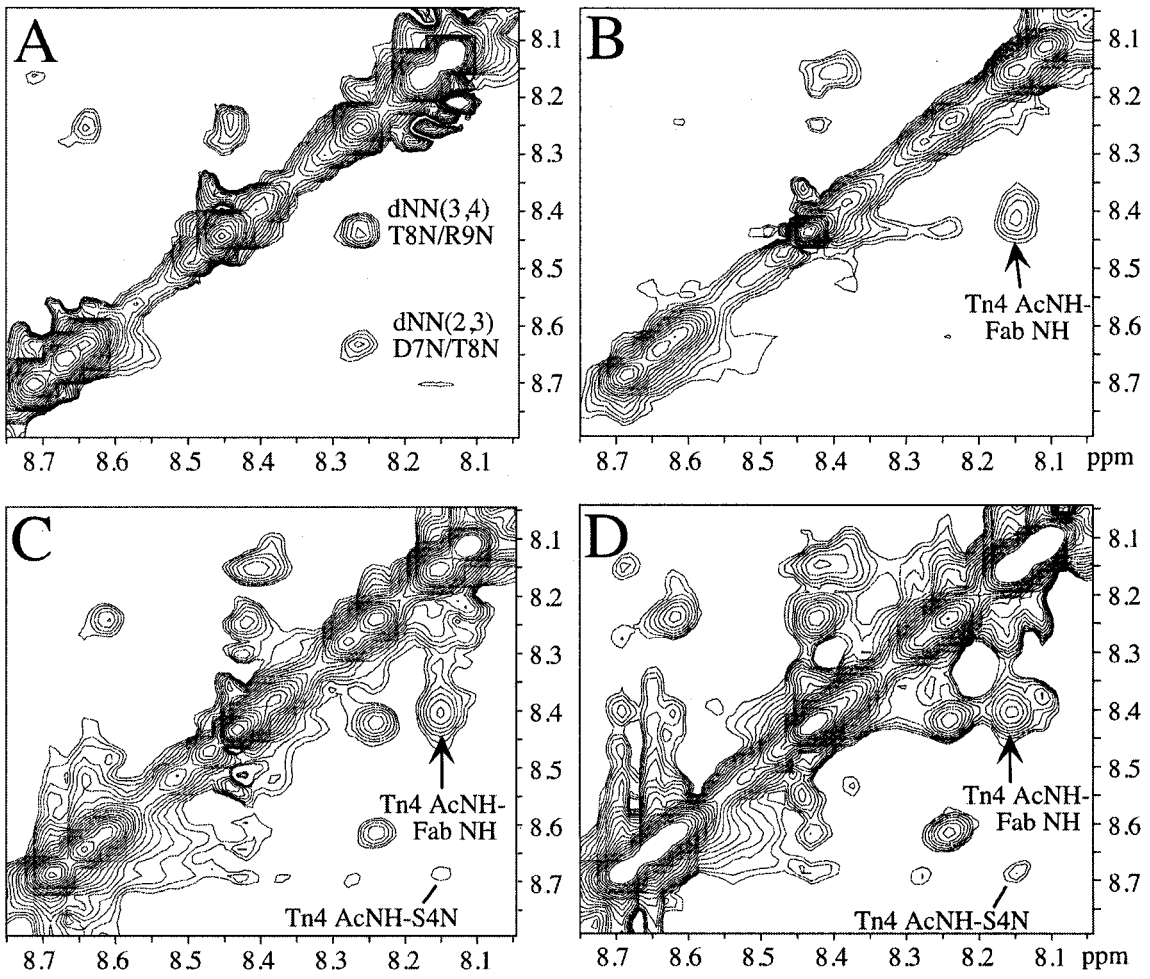

Figure 3.8: dNN regions of NOESY spectra acquired at 5 °C from the reverse titration of the Tn3,Tn4-glycosylated MUC1 16mer with Fab B27.29. Panel A corresponds to the 800 μM peptide (no Fab), panel B to 200 μM Fab + 400 μM peptide (0.5 molar equivalents Fab/peptide), panel C to 200 μM Fab + 800 μM peptide (0.25 molar equivalents Fab/peptide), and panel D to 200 μM Fab + 1.4 mM peptide (0.14 molar equivalents Fab/peptide). Experimental conditions were 90% H_20/10% D_20 PBS buffer, pH 7.0, 5 °C.

glycosylated 16mer, and at four different molar equivalents of Fab. Panel A corresponds to no Fab (only peptide), panel B to 0.5 molar equivalents Fab/peptide, panel C to 0.25 molar equivalents Fab/peptide, and panel D to 0.14 molar equivalents Fab/peptide. These four ratios of Fab/peptide were explored so as to better discriminate peptide-peptide TRNOEs from intermolecular peptide-Fab and sugar-Fab NOEs. Examination of Figure

3.8 reveals an important sugar-Fab NOE, which is labeled Tn4 AcNH-Fab NH. This NOE is absent in both the free peptide (Figure 3.8A) and the free Fab NOESY spectrum (not shown), confirming its source as sugar-Fab. The presence of such a strong and unequivocal sugar-Fab contact suggests a direct interaction of the Tn4 carbohydrate with Fab B27.29, supporting the linebroadening and TRNOE results observed for this carbohydrate resonance.

Figure 3.9 shows the dβN and dγN regions of the NOESY/TRNOESY spectra acquired at 5 °C from the same reverse titration of Tn3,Tn4-glycosylated 16mer, and using the same four molar equivalents of Fab described above. Another sugar-Fab NOE is observed in this figure, labeled Tn4 $AcCH_3$-Fab NH, which is absent in both the free peptide (Figure 3.9A) and free Fab NOESY spectrum. The Fab NH partner (@8.41 ppm) in this Tn4 $AcCH_3$-Fab NH crosspeak is the same Fab NH in the Tn4 AcNH-Fab NH crosspeak shown in Figure 3.8, an assignment confirmed by temperature titrations. Panels C and D of Figure 3.9 also show a peptide-sugar TRNOE of special interest, Tn4 $AcCH_3$-T8 NH, which is absent in both the free peptide (panel A) and the free Fab NOESY spectrum (not shown). This existence of this medium-range peptide-sugar TRNOE implies that T8 and Tn4 are both bound at the antibody combining site, and supports the notion that the MUC1 B-cell epitope is comprised of both a peptide portion and a carbohydrate portion. The simultaneous binding of T8 and Tn4 at the B27.29 combining site is supported by an analysis of all sugar-Fab and peptide-Fab NOEs observed in the reverse titration. These NOEs are listed in Table A6 in Appendix A, and show Fab contacts to Tn3, Tn4 and T8 in the peptide. Of particular interest in Table A6 in Appendix A are the strong T8 γ(CH_3)-Fab NOEs linking the γ methyl protons of Thr8 to the upfield Fab methyl group at -0.30 ppm (this peptide-Fab is observed at both 5 and 25 °C) and the strong T8 γ(CH_3)-Fab NOE linking the γ methyl protons of Thr8 to

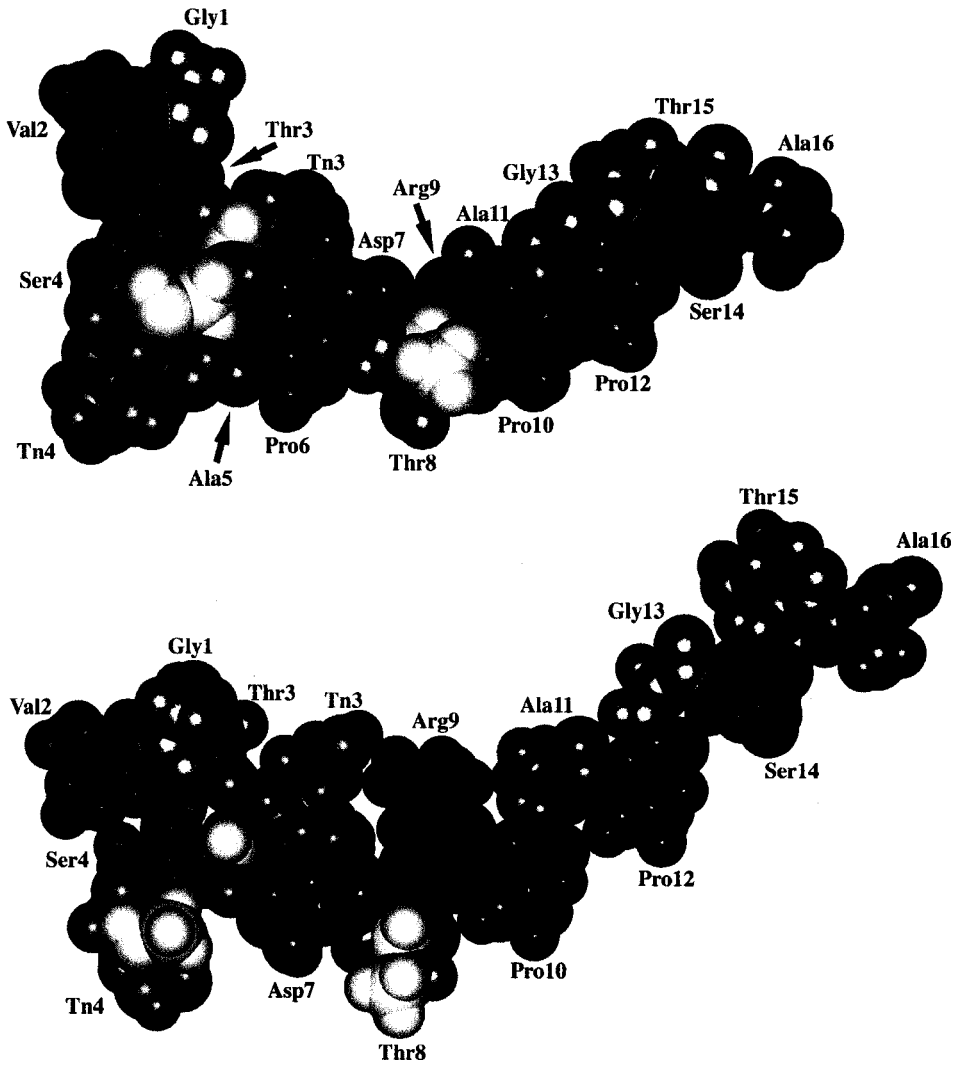

Figure 3.9: Space-filling model of the Tn3,Tn4-glycosylated MUC1 16mer peptide showing a proposed antibody binding interface, based on the peptide-Fab and sugar-Fab NOEs observed for the peptide in the presence of Fab B27.29 (see Table A6 in Appendix A). Two views of the model are shown, related by a 40° rotation around a horizontal axis. The amino acids are coded by type, and the carbohydrate moieties are shaded gray. White atoms correspond to hydrogens and their directly bonded heteroatoms for which peptide-Fab and sugar-Fab NOEs were observed. Asp7, situated in the middle of the binding pocket in the model, is significantly linebroadened in the presence of Fab, which may account for the lack of observable peptide-Fab NOEs to this residue.

aromatic Fab resonances at 6.91 ppm (observed at 25 °C). These NOEs identify Thr8 as a key Fab contact residue for the PDTRP peptide epitope.

Finally, turn defining TRNOEs were carefully analyzed in the TRNOESY spectra of the Tn3,Tn4-glycosylated 16mer in order to determine if the type I β-turn found within the PDTRP core peptide epitope of the free peptide is conserved within the B27.29 combining site. Referring back to Figure 3.8, dNN(2,3) and dNN(3,4) connectivities diagnostic of turn conformation are observed both in the presence (Figure 3.8C, 3.8D) and in the absence (Figure 3.8A) of Fab. This finding implies that the β-turn conformation is conserved in the antibody-bound peptide. In addition, a careful examination of the two panels that represent the same concentration of peptide (Figure 3.8A and 3.8C, respectively) show modest 30% TRNOE enhancements for dNN(2,3) and dNN(3,4) in the presence of Fab, although the exact contributions of the free versus the bound state to these observed TRNOEs are difficult to quantitate. However, coupling constant and temperature coefficient measurements made for the Tn3,Tn4-glycosylated 16mer in the presence of 0.4 molar equivalents Fab B27.29 (see Table A7 in Appendix A) do support a small increase in turn population in the bound state - Fab binding leads to a decrease in the $^{3}J_{N\alpha}$ coupling constant of Asp7 (5.9 Hz to 5.4 Hz) and a decrease in the $-\Delta\delta/\Delta T$ of Arg9 (6.0 to 5.2 ppb/K). Future studies by the group will involve isotope-edited and isotope-filtered experiments of labeled MUC1 peptides binding to Fab, so as to better define the involvement of the PDTR β-turn in MUC1 humoral immune recognition.

Conclusions:

The cryptic core carbohydrates that remain on the underglycosylated MUC1-

expressing tumor are believed to contribute significantly to humoral immune recognition of the tumor (Karsten *et al.*, 1998; Liu et al., 1995; Spencer *et al.*, 1999; Spencer *et al.*, 1996; von Mensdorff-Pouilly *et al.*, 2000). However, the mechanism through which this occurs is not fully understood, especially as an exact glycosylation state (if there is only one) of the MUC1-expressing tumor remains to be determined. In the absence of a clear picture of the tumor-associated glycosylation state, we advance two plausible mechanisms to explain how MUC1 carbohydrate might contribute to humoral immune recognition of the intact tumor. In the first of these mechanisms, the cryptic carbohydrates are proposed to affect MUC1 humoral immune recognition by altering the conformation of the PDTRP peptide epitope portion of the MUC1 antigen. In the second of these mechanisms, the cryptic carbohydrates are proposed to affect MUC1 humoral immune recognition by directly interacting with the B-cell receptor.

In order to explore the first of these mechanisms, that carbohydrates alter the conformation of the PDTRP core peptide epitope, NMR studies were performed probing the structural and dynamical effects of glycosylation in a series of synthetic MUC1 glycopeptides of the form (Gly1-Val2-Thr3-Ser4-Ala5-Pro6-Asp7-Thr8-Arg9-Pro10-Ala11-Pro12-Gly13-Ser14-Thr15-Ala16). The results of these studies showed that Tn3,Tn4-glycosylation at Thr3 and Ser4 produced only localized effects on the conformation and backbone dynamics of residues at or immediately adjacent to the site(s) of carbohydrate attachment. No longer range effects on the conformation and dynamics of the downstream type I β-turn that spans residues Pro6-Asp7-Thr8-Arg9 within the core peptide epitope were observed. These results suggest that the increased affinity displayed by the Tn3,Tn4-glycosylated MUC1 peptide for the anti-MUC1 antibody B27.29 (Liu et al., 1995) is not caused by the carbohydrate stabilizing a peptide epitope conformation most favored for binding (presumably the type I β-turn).

In order to explore the second mechanism, that the MUC1 carbohydrates contribute to MUC1 humoral immunogenicity by directly binding to B-cell receptor, two-dimensional ^1H TRNOESY experiments of the binding of the Tn3,Tn4-glycosylated MUC1 16mer to the Fab fragment of B27.29 were performed. The results of these studies showed that the B27.29 MUC1 B-cell epitope maps to two separate parts of the glycopeptide, the core peptide epitope spanning the PDTRP sequence, and a second carbohydrate epitope comprised of the Tn moieties attached at Thr3 and Ser4. Careful analysis of intermolecular sugar-Fab and peptide-Fab NOEs observed in the TRNOESY also showed that the Tn4 carbohydrate and the Thr8 sidechain directly contact the Fab across the combining site interface, defining separate carbohydrate and peptide 'contact points'. Finally, turn defining peptide-peptide TRNOEs observed in the TRNOESY spectra are consistent with the PDTRP peptide epitope maintaining its free solution state β-turn conformation in the B27.29 combining site. Taken together, these results point to the involvement of the PDTR β-turn and the upstream cryptic Tn carbohydrates in the humoral immune recognition of the underglycosylated MUC1 tumor *in vivo*.

Significance of Results to MUC1 Glycopeptide Vaccine Design. Several lines of evidence suggest that the key to boosting MUC1 specific immunity in adenocarcinoma patients may be the inclusion of the MUC1 tumor associated carbohydrates at select sites in the MUC1 peptide vaccine. Exposure of these tumor-associated core carbohydrate epitopes through the use of O-glycosylation inhibitors has been shown to lead to lysis of MUC1 transfected targets in a Class I MHC-restricted manner (Bohm *et al.*, 1997). In addition, immunization trials using MUC1 carbohydrate epitopes alone (no peptide) can elicit both a cytotoxic response against the MUC1-expressing tumor and a protective effect against further tumor challenge in mice (Fung *et al.*, 1990; Henningsson *et al.*,

1987). These results suggest that preferential killing of MUC1 expressing tumors may be due to the T-cell recognition of an internal carbohydrate epitope accessible only on the underglycosylated MUC1. Furthermore, natural MUC1 antibodies from breast cancer patients have been shown to react more strongly with Tn-glycosylated peptides than with the naked peptide sequence (von Mensdorff-Pouilly et al., 2000), implying that a Tn-glycosylated MUC1 peptide more closely approximates the mucin epitope as it exists on the partially glycosylated tumor cell surface. All of these results indicate that a MUC1 glycopeptide might make a better vaccine candidate than its unglycosylated counterpart.

In the present study, we have shown that the inclusion of the tumor-associated Tn carbohydrates at Thr3 and Ser4 upstream from the PDTRP core peptide epitope (GVTSAPDTRPAPGSTA) increases B27.29 binding affinity through direct carbohydrate-antibody interactions. These results demonstrate that proximal carbohydrate and peptide structural epitopes are part of the recognition domain for B27.29, whose natural tumor-associated antigen is extensively glycosylated with 'cryptic' carbohydrate structures, but also underglycosylated in the region of the PDTRP core peptide epitope. Future studies by this group will involve other MUC1 glycoforms, so as to arrive at a more detailed understanding of the conformation and glycosylation state of the MUC1 antigen as it exists on the tumor cell surface. This work should ultimately provide information relevant to the design of a more potent and immunospecific MUC1 glycopeptide vaccine.

Notes to Chapter 3

Andersen, N. H., Neidigh, J. W., Harris, S. M., Lee, G. M., Liu, Z. & Tong, H. (1997). Extracting Information from the Temperature Gradients of Polypeptide NH Chemical Shifts. 1. The Importance of Conformational Averaging. *J Am Chem Soc* **119**, 8547-8561.

Apostolopoulos, V., Pietersz, G. A. & McKenzie, I. F. (1999a). MUC1 and breast cancer. *Curr Opin Mol Ther* **1**(1), 98-103.

Apostolopoulos, V., Sandrin, M. S. & McKenzie, I. F. C. (1999b). Carbohydrate/Peptide mimics: effect on MUC1 Cancer Immunotherapy. *J Mol Med* **77**, 427-436.

Bashford, J. L., Robins, R. A. & Price, M. R. (1993). Development of an anti-idiotypic antibody reactive with an antibody defining the epitope RPAP in the MUC-1 epithelial mucin core. *Int J Cancer* **54**(5), 778-83.

Bax, A. & Davis, D. G. (1985). *J Magn Reson* **65**, 355.

Bohm, C. M., Mulder, M. C., Zennadi, R., Notter, M., Schmitt-Graff, A., Finn, O. J., Taylor-Papadimitriou, J., Stein, H., Clausen, H., Riecken, E. O. & Hanski, O. (1997). Carbohydrate Recognition on MUC-1 Expressing Targets Enhances Cytoxicity of a T Cell Subpopulation,. *Scand J Immunol* **46**, 27-34.

Brockhausen, I., Yang, J., Dickinson, N., Ogata, S. & Itzkowitz, S. H. (1998). Enzymatic basis for sialyl-Tn expression in human colon cancer cells. *Glycoconj J* **15**(6), 595-603.

Burchell, J., Taylor-Papadimitriou, J., Boshell, M., Gendler, S. & Duhig, T. (1989). *Int J Cancer* **44**, 691-696.

Campbell, A. P., McInnes, C., Hodges, R. S. & Sykes, B. D. (1995). Comparison of NMR solution structures of the receptor binding domains of Pseudomonas aeruginosa pili strains PAO, KB7, and PAK: implications for receptor binding and synthetic vaccine design. *Biochemistry* **34**(50), 16255-68.

Campbell, A. P. & Sykes, B. D. (1993). The two-dimensional transferred nuclear Overhauser effect: theory and practice. *Annu Rev Biophys Biomol Struct* **22**, 99-122.

Campbell, A. P., Wong, W. Y., Houston, M., Jr., Schweizer, F., Cachia, P. J., Irvin, R. T., Hindsgaul, O., Hodges, R. S. & Sykes, B. D. (1997). Interaction of the receptor binding domains of Pseudomonas aeruginosa pili strains PAK, PAO, KB7 and P1 to a cross-reactive antibody and receptor analog: implications for synthetic vaccine design. *J Mol Biol* **267**(2), 382-402.

Cao, Y., Karsten, U., Otto, G. & Bannasch, P. (1999). Expression of MUC1, Thomsen-Friedenreich antigen, Tn, sialosyl-Tn, and alpha2,6-linked sialic acid in hepatocellular carcinomas and preneoplastic hepatocellular lesions. *Virchows Arch* **434**(6), 503-9.

Cao, Y., Schlag, P. M. & Karsten, U. (1997). Immunodetection of epithelial mucin (MUC1, MUC3) and mucin-associated glycotopes (TF, Tn, and sialosyl-Tn) in benign and malignant lesions of colonic epithelium: apolar localization corresponds to malignant transformation. *Virchows Arch* **431**(3), 159-66.

Carlstedt, I. & Davies, J. R. (1997). Glycoconjugates facing the outside world. *Biochem Soc Trans* **25**(1), 214-9.

Chandrasekhar, K., Profy, A. T. & Dyson, H. J. (1991). Solution Conformational Preferences of Immunogenic Peptides Derived from the Principal Neutralizing Determinant of the HIV-1 Envelope Glycoprotein Gp120. *Biochemistry* **30**(38), 9187-9194.

Cheetham, J. C., Raleigh, D. P., Griest, R. E., Redfield, C., Dobson, C. M. & Rees, A. R. (1991). Antigen mobility in the combining site of an anti-peptide antibody. *Proc Natl Acad Sci U S A* **88**(18), 7968-72.

David, L., Nesland, J. M., Clausen, H., Carneiro, F. & Sobrinho-Simoes, M. (1992). Simple mucin-type carbohydrate antigens (Tn, sialosyl-Tn and T) in gastric mucosa, carcinomas and metastases. *APMIS Suppl* **27**, 162-72.

Delaglio, F., Grsesiek, S., Vuister, G. W., Zhu, G., Pfeifer, J. & Bax, A. (1995). NMRPipe: A multidimensional spectral processing system based on UNIX pipes. *J Biomol NMR* **6**, 277 - 293.

Denton, G., Sekowski, M. & Price, M. R. (1993). Induction of antibody responses to breast carcinoma associated mucins using synthetic peptide constructs as immunogens. *Cancer Lett* **70**(3), 143-50.

Fontenot, J. D. (1993). Biophysical Characterization of One, Two, and Three-Tandem Repeats of Human Mucin (MUC-1) Protein Core. *Cancer Research* **53**, 5386-5394.

Fontenot, J. D., Finn, O. J., Dales, N., Andrews, P. C. & Montelaro, R. C. (1993). Synthesis of large multideterminant peptide immunogens using a poly-proline beta-turn helix motif. *Pept Res* **6**(6), 330-6.

Fontenot, J. D., Mariappan, S. V., Catasti, P., Domenech, N., Finn, O. J. & Gupta, G. (1995). Structure of a tumor associated antigen containing a tandemly repeated immunodominant epitope. *J Biomol Struct Dyn* **13**(2), 245-60.

Fung, P. Y., Madej, M., Koganty, R. R. & Longenecker, B. M. (1990). Active specific immunotherapy of a murine mammary adenocarcinoma using a synthetic tumor-associated glycoconjugate. *Cancer Res* **50**(14), 4308-14.

Gemmecker, G. (1999). Ch.9: NMR Spectroscopy in Drug Development and Analysis. In *NMR as a Tool in Drug Research* (Holzgrabe, U., Wawer, I. & Diehl, B., eds.), pp. 140-141. John Wiley & Sons, Inc., New York.

Gerken, T. A., Butenhof, K. J. & Shogren, R. (1989). Effects of glycosylation on the conformation and dynamics of O-linked glycoproteins: carbon-13 NMR studies of ovine submaxillary mucin. *Biochemistry* **28**(13), 5536-43.

Girling, A., Bartkova, J., Burchell, J., Gendler, S., Gillett, C. & Taylor-Papadimitriou, J. (1989). A core protein epitope of the polymorphic epithelial mucin detected by the monoclonal antibody SM-3 is selectively exposed in a range of primary carcinomas. *Int J Cancer* **43**(6), 1072-6.

Grinstead, J. S., Schuman, J. T. & Campbell, A. P. (2003). Epitope Mapping of Antigenic MUC1 Peptides to Breast Cancer Antibody Fragment B27.29: a Heteronuclear NMR Study. *Biochemistry* **accepted for publication**.

Hanisch, F. G. (2001). O-glycosylation of the mucin type. *Biol Chem* **382**(2), 143-9.

Henningsson, C. M., Selvaraj, S., MacLean, G. D., Suresh, M. R., Noujaim, A. A. & Longenecker, B. M. (1987). T cell recognition of a tumor-associated glycoprotein and its synthetic carbohydrate epitopes: stimulation of anticancer T cell immunity in vivo. *Cancer Immunol Immunother* **25**(3), 231-41.

Itzkowitz, S. H., Yuan, M., Montgomery, C. K., Kjeldsen, T., Takahashi, H. K., Bigbee, W. L. & Kim, Y. S. (1989). Expression of Tn, sialosyl-Tn, and T antigens in human colon cancer. *Cancer Res* **49**(1), 197-204.

Jeener, J., Meier, B. H., Bachmann, P. & Ernst, R. R. (1979). *J Chem Phys* **71**, 4546-4553.

Karanikas, V., Patton, K., Jamieson, G., Pietersz, G. & McKenzie, I. (1998). Affinty of Antibodies to MUC1 Antigens. *Tumor Biology* **19**, 71-78.

Karsten, U., Diotel, C., Klich, G., Paulsen, H., Goletz, S., Muller, S. & Hanisch, F. G. (1998). Enhanced binding of antibodies to the DTR motif of MUC1 tandem repeat peptide is mediated by site-specific glycosylation. *Cancer Res* **58**(12), 2541-9.

Kirnarsky, L., Prakash, O., Vogen, S. M., Nomoto, M., Hollingsworth, M. A. & Sherman, S. (2000). Structural effects of O-glycosylation on a 15-residue peptide from the mucin (MUC1) core protein. *Biochemistry* **39**(39), 12076-82.

Kishikawa, T., Ghazizadeh, M., Sasaki, Y. & Springer, G. F. (1999). Specific role of T and Tn tumor-associated antigens in adhesion between a human breast carcinoma cell line and a normal human breast epithelial cell line. *Jpn J Cancer Res* **90**(3), 326-32.

Koganty, R. R., Reddish, M. A. & Longenecker, B. M. (1997). Glycopeptides in the Immunotherapy of Cancer. In *Glycopeptides and Related Compounds: Synthesis, Analysis and Application* (C.D., L. D. G. a. W., ed.), pp. 707-743. Dekker, New York.

Kotera, Y., Fontenot, J. D., Pecher, G., Metzgar, R. S. & Finn, O. J. (1994). Humoral immunity against a tandem repeat epitope of human mucin MUC-1 in sera from breast, pancreatic, and colon cancer patients. *Cancer Res* **54**(11), 2856-60.

Liang, R., Andreotti, A. H. & Kahne, D. (1995). Sensitivity of Glycopeptide Conformation to Carbohydrate Chain Length. *J Am Chem Soc* **117**, 10395-10396.

Liu, X., Sejbal, J., Kotovych, G., Koganty, R. R., Reddish, M. A., Jackson, L., Gandhi, S. S., Mendonca, A. J. & Longenecker, B. M. (1995). Structurally defined synthetic cancer vaccines: analysis of structure, glycosylation and recognition of cancer associated mucin, MUC-1 derived peptides. *Glycoconj J* **12**(5), 607-17.

Live, D. H., Williams, L. J., Kuduk, S. D., Schwarz, J. B., Glunz, P. W., Chen, X. T., Sames, D., Kumar, R. A. & Danishefsky, S. J. (1999). Probing cell-surface architecture through synthesis: an NMR-determined structural motif for tumor-associated mucins. *Proc Natl Acad Sci U S A* **96**(7), 3489-93.

MacLean, G. D., Bowen-Yacyshyn, M. B., Samuel, J., Meikle, A., Stuart, G., Nation, J., Poppema, S., Jerry, M., Koganty, R., Wong, T. & et al. (1992). Active immunization of human ovarian cancer patients against a common carcinoma (Thomsen-Friedenreich) determinant using a synthetic carbohydrate antigen. *J Immunother* **11**(4), 292-305.

Macura, S. & Ernst, R. R. (1980). *Mol Phys* **41**, 95-117.

Miles, D. W. & Taylor-Papadimitriou, J. (1999). Therapeutic aspects of polymorphic epithelial mucin in adenocarcinoma. *Pharmacol Ther* **82**(1), 97-106.

Mimura, Y., Inoue, Y., Maeji, N. J. & Chujo, R. (1989). N.m.r. study on conformation of Ac-Thr(alpha-GalNAc)-Ala-Ala-OMe as a model for mucin type glycoprotein. *Int J Pept Protein Res* **34**(5), 363-8.

Muller, S., Alving, K., Peter-Katalinic, J., Zachara, N., Gooley, A. A. & Hanisch, F. G. (1999). High density O-glycosylation on tandem repeat peptide from secretory MUC1 of T47D breast cancer cells. *J Biol Chem* **274**(26), 18165-72.

Muller, S., Goletz, S., Packer, N., Gooley, A., Lawson, A. M. & Hanisch, F. G. (1997). Localization of O-glycosylation sites on glycopeptide fragments from lactation-associated MUC1. All putative sites within the tandem repeat are glycosylation targets in vivo. *J Biol Chem* **272**(40), 24780-93.

Nice, E. C., McInerney, T. L. & Jackson, D. C. (1996). Analysis of the interaction between a synthetic peptide of influenza virus hemagglutinin and monoclonal antibodies using an optical biosensor. *Mol Immunol* **33**(7-8), 659-70.

Nishimori, I., Johnson, N. R., Sanderson, S. D., Perini, F., Mountjoy, K., Cerny, R. L., Gross, M. L. & Hollingsworth, M. A. (1994a). Influence of acceptor substrate primary amino acid sequence on the activity of human UDP-N-acetylgalactosamine:polypeptide N-acetylgalactosaminyltransferase. Studies with the MUC1 tandem repeat. *J Biol Chem* **269**(23), 16123-30.

Nishimori, I., Perini, F., Mountjoy, K. P., Sanderson, S. D., Johnson, N., Cerny, R. L., Gross, M. L., Fontenot, J. D. & Hollingsworth, M. A. (1994b). N-acetylgalactosamine glycosylation of MUC1 tandem repeat peptides by pancreatic tumor cell extracts. *Cancer Res* **54**(14), 3738-44.

Piatini, U., Sorenson, O. W. & Ernst, R. R. (1982). *J Amer Chem Soc* **104**, 6800-6801.

Rance, M., Sorensen, O. W., Bodenhausen, G., Wagner, G., Ernst, R. R. & Wuthrich, K. (1983). Improved spectral resolution in cosy 1H NMR spectra of proteins via double quantum filtering. *Biochem Biophys Res Commun* **117**(2), 479-85.

Reddish, M. A., Helbrecht, N., Almeida, A. F., Madiyalakan, R., Suresh, M. R. & Longenecker, B. M. (1992). Epitope mapping of CA27.29 within the protein core of the malignant breast carcinoma associated mucin antigen MUC-1. *J Tumor Marker Oncol* **7**, 19.

Richardson, J. S. (1981). The anatomy and taxonomy of protein structure. *Adv Protein Chem* **34**, 167-339.

Rose, G. D., Gierasch, L. M. & Smith, J. A. (1985). Turns in peptides and proteins. *Adv Protein Chem* **37**, 1-109.

Rudd, P. M. & Dwek, R. A. (1997). Glycosylation: heterogeneity and the 3D structure of proteins. *Crit Rev Biochem Mol Biol* **32**(1), 1-100.

Scanlon, M. J., Morley, S. D., Jackson, D. E., Price, M. R. & Tendler, S. J. (1992). Structural and computational investigations of the conformation of antigenic peptide fragments of human polymorphic epithelial mucin. *Biochem J* **284**(Pt 1), 137-44.

Schol, D. J., Meulenbroek, M. F., Snijdewint, F. G., von Mensdorff-Pouilly, S., Verstraeten, R. A., Murakami, F., Kenemans, P. & Hilgers, J. (1998). 'Epitope fingerprinting' using overlapping 20-mer peptides of the MUC1 tandem repeat sequence. *Tumour Biol* **19 Suppl 1**, 35-45.

Schuman, J., Campbell, A. P., Koganty, R. R. & Longenecker, B. M. (2003). Probing the conformational and dynamical effects of O-glycosylation within the immunodominant region of a MUC1 peptide tumor antigen. *J Pept Res* **61**(3), 91-108.

Spencer, D. I., Missailidis, S., Denton, G., Murray, A., Brady, K., Matteis, C. I., Searle, M. S., Tendler, S. J. & Price, M. R. (1999). Structure/activity studies of the anti-MUC1 monoclonal antibody C595 and synthetic MUC1 mucin-core-related peptides and glycopeptides. *Biospectroscopy* **5**(2), 79-91.

Spencer, D. I., Price, M. R., Tendler, S. J., De Matteis, C. I., Stadie, T. & Hanisch, F. G. (1996). Effect of glycosylation of a synthetic MUC1 mucin-core-related peptide on recognition by anti-mucin antibodies. *Cancer Lett* **100**(1-2), 11-5.

Springer, G. F. (1995). T and Tn pancarcinoma markers: autoantigenic adhesion molecules in pathogenesis, prebiopsy carcinoma-detection, and long-term breast carcinoma immunotherapy. *Crit Rev Oncog* **6**(1), 57-85.

Springer, G. F. (1997). Immunoreactive T and Tn epitopes in cancer diagnosis, prognosis, and immunotherapy. *J Mol Med* **75**(8), 594-602.

States, D. J., Haberkorn, R. A. & D.J., R. (1982). *J Magn Reson* **48**, 286-292.

Taylor-Papadimitriou, J., Burchell, J., Miles, D. W. & Dalziel, M. (1999). MUC1 and cancer. *Biochim Biophys Acta* **1455**(2-3), 301-13.

Terasawa, K., Furumoto, H., Kamada, M. & Aono, T. (1996). Expression of Tn and sialyl-Tn antigens in the neoplastic transformation of uterine cervical epithelial cells. *Cancer Res* **56**(9), 2229-32.

Van den Steen, P., Rudd, P. M., Dwek, R. A. & Opdenakker, G. (1998). Concepts and principles of O-linked glycosylation. *Crit Rev Biochem Mol Biol* **33**(3), 151-208.

von Mensdorff-Pouilly, S., Petrakou, E., Kenemans, P., van Uffelen, K., Verstraeten, A. A., Snijdewint, F. G., van Kamp, G. J., Schol, D. J., Reis, C. A., Price, M. R., Livingston, P. O. & Hilgers, J. (2000). Reactivity of natural and induced human antibodies to MUC1 mucin with MUC1 peptides and n-acetylgalactosamine (GalNAc) peptides. *Int J Cancer* **86**(5), 702-12.

Wandall, H. H., Hassan, H., Mirgorodskaya, E., Kristensen, A. K., Roepstorff, P., Bennett, E. P., Nielsen, P. A., Hollingsworth, M. A., Burchell, J., Taylor-Papadimitriou, J. & Clausen, H. (1997). Substrate specificities of three members of the human UDP-N-acetyl-alpha-D-galactosamine:Polypeptide N-acetylgalactosaminyltransferase family, GalNAc-T1, -T2, and -T3. *J Biol Chem* **272**(38), 23503-14.

Wilmot, C. M. & Thornton, J. M. (1988). Analysis and prediction of the different types of beta-turn in proteins. *J Mol Biol* **203**(1), 221-32.

Wishart, D. S., Bigam, C. G., Holm, A., Hodges, R. S. & Sykes, B. D. (1995). 1H, 13C and 15N random coil NMR chemical shifts of the common amino acids. I. Investigations of nearest-neighbor effects. *J Biomol NMR* **5**(1), 67-81.

Wishart, D. S., Sykes, B. D. & Richards, F. M. (1991). Relationship between nuclear magnetic resonance chemical shift and protein secondary structure. *J Mol Biol* **222**(2), 311-33.

Wuthrich, K. (1986). *NMR of proteins and nucleic acids / Kurt Wuthrich*, Wiley,, New York :.

Xing, P. X., Prenzoska, J. & McKenzie, I. F. (1992a). Epitope mapping of anti-breast and anti-ovarian mucin monoclonal antibodies. *Mol Immunol* **29**(5), 641-50.

Xing, P. X., Prenzoska, J., Quelch, K. & McKenzie, I. F. (1992b). Second generation anti-MUC1 peptide monoclonal antibodies. *Cancer Res* **52**(8), 2310-2317.

Yamazaki, T., Muhandiram, R. & Kay, L. E. (1994). NMR Experiments for the Measurement of Carbon Relaxation Properties inHighly Enriched, Uniformly 13C, 15N-Labeled Proteins: Application to 13C-alpha Carbons. *J Am Chem Soc* **116**(18), 8266-8278.

Yao, J., Dyson, H. J. & Wright, P. E. (1994). Three-dimensional structure of a type VI turn in a linear peptide in water solution. Evidence for stacking of aromatic rings as a major stabilizing factor. *J Mol Biol* **243**(4), 754-66.

Zvi, A., Kustanovich, I., Feigelson, D., Levy, R., Eisenstein, M., Matsushita, S., Richalet-Sécordel, P., Regenmortel, M. H. V. & Anglister, J. (1995). NMR Mapping of the Antigenic Determinant Recognized by an Anti-gp120, Human Immunodeficiency Virus Neutralizing Antibody. *Eur J Biochem* **229**(1), 178-187.

Chapter 4: Epitope Mapping and NMR Relaxation Measurements of Recombinant MUC1 Peptides Free and Bound to Breast Cancer Antibody Fragment B27.29

ABSTRACT: MUC1 mucin is a breast cancer-associated transmembrane glycoprotein, of which the extracellular domain is formed by the repeating 20 amino acid sequence, GVTSA**PDTRPAP**GSTAPPAH. In neoplastic breast tissue, the highly immunogenic sequence PDTRPAP (in bold above) is exposed. This sequence has been the target of many recent clinical vaccine trials, none of which have been successful at shrinking solid MUC1-expressing tumor. The failure of these MUC1-based immunotherapies to generate effective immune responses may stem from the use of vaccine candidates that do not best represent the structure, dynamics, peptide epitope exposure, or even glycosylation state of the tumor-associated MUC1 mucin.

Antibodies raised directly against MUC1-expressing tumors offer unique access to this tumor-associated state, as they represent immunologically relevant 'reverse-templates' of the tumor-associated mucin. In a previous study (Grinstead *et al.*, 2002), ^{1}H NMR methods were used to correlate the effects of cryptic glycosylation outside of the PDTRPAP core epitope sequence on the recognition and binding of Mab B27.29, a monoclonal antibody raised against breast tumor cells. In the present study, isotope-edited NMR methods are used to probe the recognition and binding of the PDTRPAP epitope sequence to Fab B27.29. Two peptides were studied: a one-repeat MUC1 16mer peptide of the sequence (GVTSAPDTRPAPGSTA), and a two-repeat MUC1 40mer peptide of the sequence $(VTSAPDTRPAPGSTAPPAHG)_2$. The results of this study provide direct spectroscopic evidence that the PDTRPAP epitope sequence of both peptides is bound and immobilized within the Fab B27.29 combining site, and that an

increase in repeat number from one to two has no effect on the affinity, dynamics or specificity of this interaction. The implications of these results are discussed within the context of the MUC1 breast cancer vaccine design.

Introduction:

Mucins have been implicated as targets for vaccine development in cancers of the breast, colon, pancreas, lung, and ovary because of the differences between normal and tumor-associated mucin (Apostolopoulos *et al.*, 1999a; Apostolopoulos *et al.*, 1999b; Miles & Taylor-Papadimitriou, 1999; Taylor-Papadimitriou *et al.*, 1999). Mucin 1 (MUC1) is a large transmembrane glycoprotein that is expressed on the ductal surface of epithelial cells. The extracellular region of the protein consists of a variable number of tandem repeats (VNTR) of the 20-amino acid sequence GVTSA**PDTRPAP**GSTAPPAH, extensively O-glycosylated at threonine and serine sites with large, branched sugars (Carlstedt & Davies, 1997; Koganty *et al.*, 1997; Rudd & Dwek, 1997; Van den Steen *et al.*, 1998). However, in the tumor-associated state MUC1 becomes an autoantigen as a result of incomplete glycosylation and sparse distribution of remaining carbohydrate structures (Hanisch, 2001). The reduced glycosylation is believed to result in the exposure of a highly immunogenic core peptide sequence (PDTRPAP in bold above) (Girling *et al.*, 1989), identified as the immunodominant B-cell epitope from monoclonal antibody studies in mice (Bashford *et al.*, 1993; Burchell *et al.*, 1989; Denton *et al.*, 1993; Kotera *et al.*, 1994; Xing *et al.*, 1992). This PDTRPAP core peptide sequence is also believed to be immunodominant in humans. Breast cancer patients with MUC1-expressing tumors develop limited humoral and cellular immune responses against the tumor (Finn *et al.*, 1995; Nakamura *et al.*, 1998; Petrarca *et al.*,

1999), with the elicited antibodies and T cells cross-reactive to the PDTRPAP core peptide sequence (Ding *et al.*, 1993; Jerome *et al.*, 1991; Musselli *et al.*, 2002).

Many different clinical trials have been undertaken over the past few years to assess the ability of MUC1-based vaccines to generate strong and cytotoxic anti-MUC1 immune responses against the solid MUC1-expressing tumor. Several of these trials have explored the use of MUC1 peptides coupled to different haptens, keyhole limpet hemocyanin, oxidized mannan, and glutathione S-transferase (Apostolopoulos et al., 1999a). In addition, at least two different vaccine trials have used MUC1-associated antigenic sugars (without peptide) (Mitchell, 2002). Other more recent clinical trials have utilized peptide- or DNA-pulsed dendritic cells as vaccine vectors, attempting to capitalize on the superior immune activation by these antigen presenting cells. Dendritic cells pulsed with either MUC1 peptides or cDNA have been able to generate limited $CD8^+$ T cell responses to solid breast tumors (Brossart *et al.*, 2000; Pecher *et al.*, 2002), although these responses did not result in tumor rejection. Indeed, none of the MUC1 vaccine candidates described above have been shown to be effective at tumor rejection, although the reasons for this are not clear (Denda-Nagai & Irimura, 2000; Doehn & Jocham, 2000; Foon, 2001; Morse, 2000; Morse, 2001).

The failure of MUC1-based vaccines to generate effective immune responses may stem from the use of vaccine candidates that do not represent the structure, dynamics, peptide epitope exposure, or even glycosylation state of the tumor-associated mucin. For example, vaccination with a MUC1 peptide is unlikely to generate an immune response to the heavily glycosylated region of the extracellular domain of MUC1 on the surface of healthy epithelial cells. While this situation should limit the possibility of an autoimmune response against healthy epithelial tissues, it is also unlikely to lead to a

strong tumor-specific immune response against the partially glycosylated tumor-associated MUC1 protein.

In an effort to better characterize the glycosylation state and peptide epitope exposure of the tumor-associated MUC1 protein, many *in vitro* and *in vivo* glycosylation studies have been undertaken. *In vitro* glycosylation studies using human tumor cell extracts (Nishimori *et al.*, 1994a; Nishimori *et al.*, 1994b; Wandall *et al.*, 1997) have demonstrated the presence of cryptic carbohydrate structures at only three sites in the sequence (GVTSA and GSTAP), and not at the central threonine within the PDTRPAP core peptide epitope region. However, recent *in vivo* studies have demonstrated that all five sites are glycosylation targets in the tumor cell (Muller *et al.*, 1999; Muller *et al.*, 1997). Thus, the glycosylation state of the tumor-associated MUC1 mucin remains indeterminate at present. Furthermore, while spectroscopic techniques such as NMR and CD have identified native β-turn secondary structure and polyproline type II helix, respectively, in unglycosylated MUC1 (Fontenot, 1993; Fontenot *et al.*, 1993; Fontenot *et al.*, 1995; Grinstead et al., 2002; Liu *et al.*, 1995; Schuman *et al.*, 2003a), these studies have not been extrapolated to the intact partially-glycosylated MUC1 protein as it exists *in situ* on the tumor cell surface. In the absence of a clear and definitive picture of the MUC1 mucin in its tumor-associated state, the design of a peptide or glycopeptide vaccine that mimics this 'unknown' state is a difficult undertaking.

In order to circumnavigate this difficulty, we propose an approach that does not rely on *a priori* knowledge of peptide conformation or glycosylation state for the tumor-associated MUC1 mucin. This alternative approach involves the use of an anti-MUC1 antibody, Mab B27.29, as a 'reverse-template' for MUC1 vaccine design. Mab B27.29 was raised directly against MUC1-expressing tumors, so should bind most tightly to a MUC1 peptide or glycopeptide that best approximates the structure, dynamics, and

glycosylation state of the tumor-associated mucin. As such, Mab B27.29 is an immunologically relevant reverse-template of the structure, dynamics, and chemistry of the tumor-associated MUC1 mucin. In brief, this approach identifies the immunologically relevant peptide conformation and glycosylation states of the tumor-associated MUC1 mucin by probing the structure and dynamics of MUC1 peptide - Mab B27.29 recognition and binding. Solution state NMR is used as the probe in these systems, as it allows both structure and dynamics information to be obtained for the bound state, even if that bound state is dynamic and conformationally heterogenous.

Using this NMR-based approach, we recently examined the effect of glycosylation on Fab B27.29 recognition of a series of 16-residue MUC1 glycopeptides of the sequence GVTSAPDTRPAPGSTA (Grinstead et al., 2002). The results of this study showed that the B27.29 epitope maps to two separate parts of the glycopeptide, the core peptide epitope spanning the PDTRPAP sequence, and a second (carbohydrate) epitope comprised of two cryptic carbohydrate moieties attached at Thr3 and Ser4 in the 16mer sequence. In the present study, we extend this NMR-based approach to examine the role of peptide structure and dynamics on Fab B27.29 recognition of the same 16 residue MUC1 peptide, as well as of a 40 residue MUC1 peptide, $(VTSAPDTRPAPGSTAPPAHG)_2$, that represents two repeats of the MUC1 sequence.

NMR studies probing the structure and dynamics of the 16 and 40 residue MUC1 peptides in free versus Fab-bound states are significantly facilitated by our ability to generate isotopically labeled recombinant peptides. This allows for the acquisition of isotope-edited NMR experiments of the MUC1 peptide-B27.29 antibody complex, offering a significant increase in the information content relative to our previous efforts with simple homonuclear NMR experiments. Included in this present study are two-dimensional isotope-edited NMR experiments, as well as heteronuclear NMR relaxation

measurements, monitoring the binding of the isotopically-labeled MUC1 peptides to the unlabeled Fab fragment of B27.29. These experiments allow a precise mapping of the boundary of the B27.29 epitope, based on a determination of the immobilized portion of the peptide as it is bound within the B27.29 antibody combining site. The results of these studies are discussed within the framework of developing a second-generation MUC1 peptide vaccine that better represents the peptide portion of the tumor-associated MUC1 mucin, as it is recognized *in situ* by B27.29.

Materials and Methods:

Peptide and Fab samples. Fab (~50kDa) was generated by papain and pepsin cleavage of IgG B27.29, and was a generous gift from Biomira Inc. (Edmonton, Alberta, Canada).

Cloning of 16mer and 40mer peptides. Two MUC1 sequences derived from the extracellular domain of the MUC1 protein were cloned and expressed for the purposes of this study: (1) a one-repeat 16mer MUC1 sequence (Gly1-Val2-Thr3-Ser4-Ala5-Pro6-Asp7-Thr8-Arg9-Pro10-Ala11-Pro12-Gly13-Ser14-Thr15-Ala16); and (2) a two-repeat 40mer MUC1 sequence (Val1-Thr2-Ser3-Ala4-Pro5-Asp6-Thr7-Arg8-Pro9-Ala10-Pro11-Gly12-Ser13-Thr14-Ala15-Pro16-Pro17-Ala18-His19-Gly20-Val21-Thr22-Ser23-Ala24-Pro25-Asp26-Thr27-Arg28-Pro29-Ala30-Pro31-Gly32-Ser33-Thr34-Ala35-Pro36-Pro37-Ala38-His39-Gly40). These two 16mer and 40mer MUC1 sequences were expressed as ^{15}N,^{13}C-labeled recombinant peptides in *E. coli* using a methodology previously described (Kuliopulos & Walsh, 1994). Briefly stated, genes with multiple repeats of MUC1 DNA sequences were constructed from purchased oligonucleotides, purified, and ligated into plasmid DNA vector pET-31b(+). The MUC1 16mer and

40mer DNA-containing plasmids were separately transformed into the competent *E. coli* strain BLR(DE3) for protein expression. Isotopically ^{15}N,^{13}C-labeled peptides were then expressed by growing the transformed bacteria in minimal media containing M9 salts, and with $^{15}NH_4Cl$ and $^{13}C_6$-glucose as the sole sources of nitrogen and carbon, respectively. Isotopically labeled minimal media was inoculated at OD_{600} of 0.1 from an overnight culture, and grown to an OD_{600} of 0.6 - 0.8 before induction of protein expression with 1mM IPTG. Induced cultures were grown overnight before cell harvest by centrifugation.

Harvested cell pellets were lysed by sonication, and the insoluble fraction was collected by centrifugation. The insoluble fraction was washed several times with Tris buffer (50mM, pH 8), and then solubilized using 4 M guanidine hydrochloride-containing Tris buffer. The solubilized fusion protein was purified using nickel column chromatography under denaturing conditions of 4 M guanidine. Purified fusion protein was eluted from the column with a linear gradient of 4 - 500 mM imidazole. Fractions containing protein were dialyzed against water overnight, exchanging with fresh water several times. The water-insoluble fusion protein precipitate was collected by centrifugation.

The expressed fusion protein was designed with methionine residues separating the insoluble KSI domain from the inserted MUC1 peptide sequence, between each repeat of the MUC1 peptide sequence, and before the histidine tag. The fusion was digested with an excess of CNBr in 88% formic acid under nitrogen gas overnight at room temperature to cleave at all methionine residues to leave a homoserine lactone at the C-terminus of all fragments. Formic acid was removed by rotary evaporation, and the products were stirred in distilled water. The insoluble KSI domain remained as

precipitate, and was removed by centrifugation. The soluble peptide cleavage products were lyophilized and resuspended in 90% H_2O/10% acetonitrile for HPLC purification.

MUC1 peptides were purified using reverse-phase HPLC on a prep scale radial compression C18 column (Alltech, USA). MUC1 peptides were eluted with a linear gradient of 10% - 95% acetonitrile. One major peak was observed in most cases, which eluted with the same retention time as a standard synthetic MUC1 peptide. Fractions containing purified MUC1 peptides were collected, and the volatile solvents were removed by rotary evaporation. The remaining aqueous solutions lyophilized to give pure peptide at a yield of 17 mg isotope-labeled peptide per liter of minimal media (50mg/L for unlabeled peptide in LB medium).

Fluorescence binding measurements. Fluorescence measurements were used to determine the equilibrium dissociation constants (K_D) and kinetic dissociation rate constants (k_{-1}) for the binding of the MUC1 16mer and 40mer peptides to Fab B27.29. Fab B27.29 (0.86 μM stock solution) was titrated with small aliquots of peptide to a final concentration greater than 200-fold in excess of Fab concentration. The change in Fab fluorescence intensity was monitored, and the concentration of bound ligand was calculated (percent of maximum fluorescence change). The natural log of the free ligand concentration was plotted against the concentration of the bound ligand, and the curve was fit to equation 1

$$[\text{bound}] = (\text{capacity} * [\text{free ligand}]) / (K_D + [\text{free ligand}]) \qquad (1)$$

according to Michaelis-Menton kinetics, where the capacity is the concentration of the Fab, and the K_D is the equilibrium dissociation constant.

Titration of Fab with peptides. Samples for NMR spectroscopy were dissolved in 90% H_2O, 10% D_2O PBS, 1mM DSS, 0.01% NaN_3, and adjusted to pH 7.1 (uncorrected for D_2O concentration). Titrations were performed on samples containing 200 μM Fab B27.29 (by mass), with MUC1 16mer peptide at 40, 80, 140, 200, 500, 800 and 1600 μM, and 40mer peptide at 80, 160, 240, 320, 400, 800, and 1200 μM. Peptide was added from concentrated 30 mM stock solutions to minimize dilution of the Fab sample. At the final titration point, dilution of the Fab sample was less than 5%. The concentrations of the stock peptide solutions were determined by comparing the 1D NMR integration of peptide peaks relative to an external DSS standard. The integration of the external DSS standard was calibrated against the integration of the aromatic resonances of the primary standard, potassium hydrogen phthalate. At each titration point, ^1H NMR spectra were obtained, as well as ^1H-^{15}N HSQC and ^1H-^{13}C HSQC spectra. At select titration points, ^{15}N T_1, ^{15}N T_2, {^1H}-^{15}N NOE, ^{13}C T_1, and ^{13}C $T_{1\rho}$ experiments were also collected. The {^1H}-^{13}C NOE data sets were obtained by lyophilizing the samples and resuspending in 99.9% D_2O to aid in water suppression.

NMR experiments. Most NMR experiments were performed on a Varian Inova 500 MHz spectrometer at 5°C. Triple resonance and ^{15}N-edited NOESY-HSQC experiments to identify Fab-bound peptide resonances were acquired on a Varian Inova 750 MHz spectrometer at 5°C. All NMR spectra were referenced to DSS at 0 ppm. Proton NMR resonances were assigned as previously reported (Grinstead et al., 2002). Carbon and nitrogen resonances were assigned using the known proton chemical shifts in the ^1H-^{15}N HSQC and ^1H-^{13}C HSQC spectra, as well as a 3D ^1H-^{15}N NOESY-HSQC experiment. 1D ^1H NMR spectra were acquired at 5°C, with a spectral width of 7000 Hz, using 32000

acquired points. ^{1}H-^{15}N HSQC spectra were typically acquired using a spectral width of 1114 Hz and 32 points in t_1, and 7000 Hz and 2048 points in t_2. ^{1}H-^{13}C HSQC spectra of alpha carbon-proton pairs were typically acquired using a spectral width of 3000 Hz and 48 points in t_1, and a spectral width of 7000 Hz and 2048 points in t_2. Relaxation experiments utilized similar parameters. ^{15}N T_1 experiments recorded spectra with relaxation delays of 10.3, 51.3, 102.5, 153.8, 205, 307.5, and 410 ms, with duplicate experiments recorded for the 51.3 ms data point to confirm our error estimates. ^{13}C T_1 experiments recorded spectra with relaxation delays of 10, 50, 100, 150, 200, and 300 ms, with the 100 ms data set duplicated for confirmation of error estimates. ^{15}N T_2 experiments recorded spectra with relaxation delays of 14.4, 28.8, 57.6, 86.4, 115.2, 144, and 158.4 ms, with a duplicate data set at 57.6 ms. ^{13}C $T_{1\rho}$ experiments recorded spectra with relaxation delays of 10, 20, 40, 60, 100, 150, 200, and 250 ms, with the 40 ms data set duplicated for confirmation of error estimates. Steady-state $\{^{1}H\}$-^{15}N NOE and $\{^{1}H\}$-^{13}C NOE experiments were performed with and without a 3 s presaturation period. During this presaturation period, proton frequencies were irradiated with a continuous low power pulse. In the experiment without presaturation, the low power irradiation was replaced with a delay period of 3 s. The NOE values were calculated as the ratio of peak intensities in the experiments with and without proton presaturation. Pulse sequences were utilized as reported (Farrow *et al.*, 1994; Yamazaki *et al.*, 1994).

Triple resonance experiments HNCACB (Wittekind & Mueller, 1993) and CBCA(CO)NNH (Grzesiek & Bax, 1992) were performed at 750 MHz to assign the bound peptide resonances that appear in the Fab-bound spectra. The MUC1 16mer peptide was used for these experiments due to its spectral simplicity. MUC1 16mer (250 μM final concentration) was added to Fab B27.29 (200 μM) to drive occupancy of the Fab and therefore to achieve the highest intensity for the Fab-bound resonances without

complicating the spectra with resonances from the free MUC1 16mer. 2D versions of the HNCACB and CBCA(CO)NNH experiments were employed, because under sample conditions used, and with the greater spectral dispersion of the higher magnetic field strength of 750 MHz, the amide protons of interest were resolved from all other resonances. The HNCACB experiment was acquired using 1000 transients and 1024 complex points in the acquired dimension, 120 complex points in the indirect carbon dimension, and sweep widths (750 MHz) of 15100 Hz for carbon and 10500 Hz for proton. The CBCA(CO)NNH experiment was acquired using 2048 transients and 1024 complex points in the acquired dimension, 80 complex points in the indirect carbon dimension, and sweep widths (750 MHz) of 11000 Hz for carbon and 10500 Hz for proton. In addition, a 2D ^{15}N-edited NOESY-HSQC experiment was acquired at 750 MHz on the same MUC1 16mer-Fab B27.29 sample. This experiment utilized 1216 transients and 1024 complex points in the acquired dimension, 188 points in the indirect proton dimension, and sweep widths (750 MHz) of 7500 Hz for the indirect proton and 10500 Hz for the acquired proton dimensions.

Data processing and analysis. All 2D data sets were processed on a Silicon Graphics O2 workstation using the NMRPipe System software (Delaglio *et al.*, 1995). In both dimensions, 2D data sets were multiplied by a 90°-shifted squared sine bell and zero-filled prior to Fourier transformation. T_1 and T_2 values were determined using non-linear least-squares fitting of the measured peak heights to a two-parameter exponential decay, also within the NMRPipe package. Uncertainties in the calculated T_1 and T_2 values from the least-squares fitting were determined by the signal-to-noise ratio of individual peaks in each of the T_1 and T_2 experiments (Farrow et al., 1994; Yamazaki et al., 1994). Two groups have recently shown error estimates from least-squared fitting to be unreasonably

small, and have used the value of 5% as being more realistic (Volkman *et al.*, 1998; Zhang *et al.*, 1997). Therefore, we have set the error in the calculated T_1 and T_2 to 5% of the values.

Reduced spectral density mapping. Reduced spectral density mapping is a convenient method for characterizing the motion of each N-H bond at J(0), $J(\omega_N)$, and $J(\omega_H)$ frequencies (Farrow *et al.*, 1995; Peng & Wagner, 1995). The spectral densities at these three frequencies can be obtained from relaxation rates R_1 ($1/T_1$) and R_2 ($1/T_2$) and the steady-state heteronuclear NOE using equations 2 - 4.

$$J(\omega_H) = [4/(5d^2)]\,(\gamma_N/\gamma_H)\,(NOE - 1)/T_1 \quad (2)$$

$$J(\omega_N) = [1/T_1 - (7d^2/4)\,J(\omega_H)]/\,[(3d^2/4) + c^2] \quad (3)$$

$$J(0) = [1/T_2 - (3d^2/8 + c^2/2)J(\omega_N) - (13d^2/8)\,J(\omega_H)]/[(d^2/2) + 2c^2/3] \quad (4)$$

For the above equations, $d = [\mu_0 h(\gamma_N\gamma_H)/8\pi^2]\langle 1/r^3_{NH}\rangle$ and $c = (\omega_N/(3)^{1/2})(\sigma_{\|} - \sigma_{\perp})$, and ω_N and ω_H are the Larmor frequencies of the ^{15}N and ^{1}H nuclei, respectively.

Results:

Assignment of resonances. ^{1}H, ^{15}N and ^{13}C resonance assignments for the $^{15}N/^{13}C$-labeled recombinant MUC1 16mer and 40mer peptides are shown in Table B1 in Appendix B.

Fluorescence binding measurements. The equilibrium dissociation constant (K_D) for a ligand binding to a macromolecule is equal to the ratio of the intrinsic kinetic association (k_1) and dissociation (k_{-1}) rate constants.

$$K_D = k_{-1}/k_1 \qquad (5)$$

Fluorescence binding measurements were used to determine the K_D, k_{-1}, and stoichiometry for the binding of the MUC1 16mer and 40mer peptides to Fab B27.29. These experiments yielded $K_D = 10.9 \pm 0.4$ μM for the 16mer, and $K_D = 11.1 \pm 0.5$ μM for the 40mer, with 1:1 binding stoichiometry measured in each case.

Exchange timescales of MUC1 peptide-Fab B27.29 binding. Using the K_D values measured from the fluorescence binding titrations, we have attempted to establish kinetic dissociation rates and timescales for the binding of the MUC1 16mer and 40mer peptides to Fab B27.29, a prerequisite for accurate NMR data interpretation. Surface plasmon resonance experiments in other systems indicate that a diffusion-controlled association rate ($10^8\ M^{-1}s^{-1}$) is not a valid assumption for a flexible peptide binding to solution-state Fab. Based on estimates for similar complexes (Foote & Eisen, 1995; Karlsson & Falt, 1997; Northrup & Erickson, 1992; Raman *et al.*, 1992), we therefore assume a value of 10^6 - $10^7\ M^{-1}s^{-1}$ for the kinetic association rate k_1. Combining this value with the measured equilibrium binding constant K_D, equation 5 gives a kinetic dissociation rate k_{-1} of 10 – 100 s^{-1}.

The first relevant NMR timescale to be considered is the chemical shift timescale. Intermediate exchange on the chemical shift timescale ($k_{-1} \sim \Delta\delta$[1]) is expected for the

[1] $\Delta\delta$ represents the difference between the frequencies of the exchanging free and bound peptide resonances, ($\Delta\delta = |\delta_B - \delta_F|$).

majority of peptide resonances in the MUC1-B27.29 complex, as a k_{-1} of 10 – 100 s^{-1} is within range of the typical differences between free and bound chemical shifts ($\Delta\delta$ = 100 - 1000 Hz; (Gemmecker, 1999)). In this regime, MUC1 peptide resonances are not expected to shift with varying concentration of ligand, but instead experience a loss in signal intensity due to linebroadening (Gemmecker, 1999). However, the MUC1-B27.29 system is additionally complicated due to portions of the peptide co-existing on different exchange timescales, contingent on the relative magnitudes of the $\Delta\delta$ terms (which vary across the peptide sequence). For example, peptide resonances belonging to the Fab binding epitope residues PDTRPAP, which are expected to have the largest $\Delta\delta$ terms, may experience slow exchange on the chemical shift timescale ($k_{-1} << \Delta\delta$). In this regime, distinct free and bound MUC1 peptide resonances would be expected at their respective chemical shifts. Conversely, smaller $\Delta\delta$ values for resonances at the MUC1 peptide termini could well translate into fast exchange on the chemical shift timescale ($k_{-1} >> \Delta\delta$). This third regime, if present, would be characterized by a single MUC1 peptide resonance at the population-weighted average of the free and bound chemical shifts. Thus, we anticipate a mixture of exchange regimes for MUC1 peptide resonances in an HSQC-monitored Fab B27.29 titration, marked by complex spectral behavior.

Another relevant NMR timescale to be considered is the relaxation timescale. Relaxation parameters such as the spin-lattice relaxation rate, R_1, spin-spin relaxation rate, R_2, and steady-state heteronuclear NOE are characterized by rate differences between their free and bound states that are smaller than those associated with chemical shift. For example, typical differences cited in the literature are 0.1 - 10 Hz for R_1, 1 - 50 Hz for R_2, and 0.1 - 5 Hz for NOE (Gemmecker, 1999). Thanks to these faster timescales, a k_{-1} of 10 – 100 s^{-1} puts the MUC1 peptide-Fab system in the fast exchange limit with respect to spin relaxation ($k_{-1} >> R_{1B}$, where $R_{1B} = 1/T_{1B}$, the spin-lattice

relaxation rate of the bound state). In this regime, relaxation properties of the bound state are transferred to the resonances of the free state, and the observed R_1 is a population-weighted average of the free and bound R_1 values (equation 6; (Lian *et al.*, 1994)).

$$R_{1obs} = P_B R_{1B} + P_F R_{1F} \quad (6)$$

The same principle allows implementation of the TRNOESY experiment (Campbell & Sykes, 1993). We have previously shown that the MUC1 peptide experiences a significant transferred NOESY effect upon binding to Fab B27.29 (Grinstead et al., 2002), providing further credence that the system is in fast exchange with respect to the NMR relaxation timescale.

The existence of two exchange regimes for the MUC1 system, intermediate on the chemical shift timescale, but fast on the relaxation timescale, allows dynamics information to be obtained for the bound state, regardless of whether an averaged resonance is monitored (fast exchange on the chemical shift timescale), an exchange broadened resonance is monitored (intermediate exchange on the chemical shift timescale), or separate free and bound resonances are monitored (slow exchange on the chemical shift timescale). An interesting corollary of this condition is that these separate free and bound MUC1 resonances should also manifest the same linewidth, as linewidths are largely dependent on spin-spin relaxation rates, and these rates are population-weighted averages in the limits of fast exchange with respect to relaxation.

^{15}N HSQC-monitored titrations of MUC1 peptides with Fab B27.29. Figures 4.1A and 4.1C present the ^{15}N-edited HSQC spectra acquired for the ^{15}N,^{13}C-labeled 16mer and 40mer MUC1 peptides, respectively, in the absence of Fab B27.29. A cursory

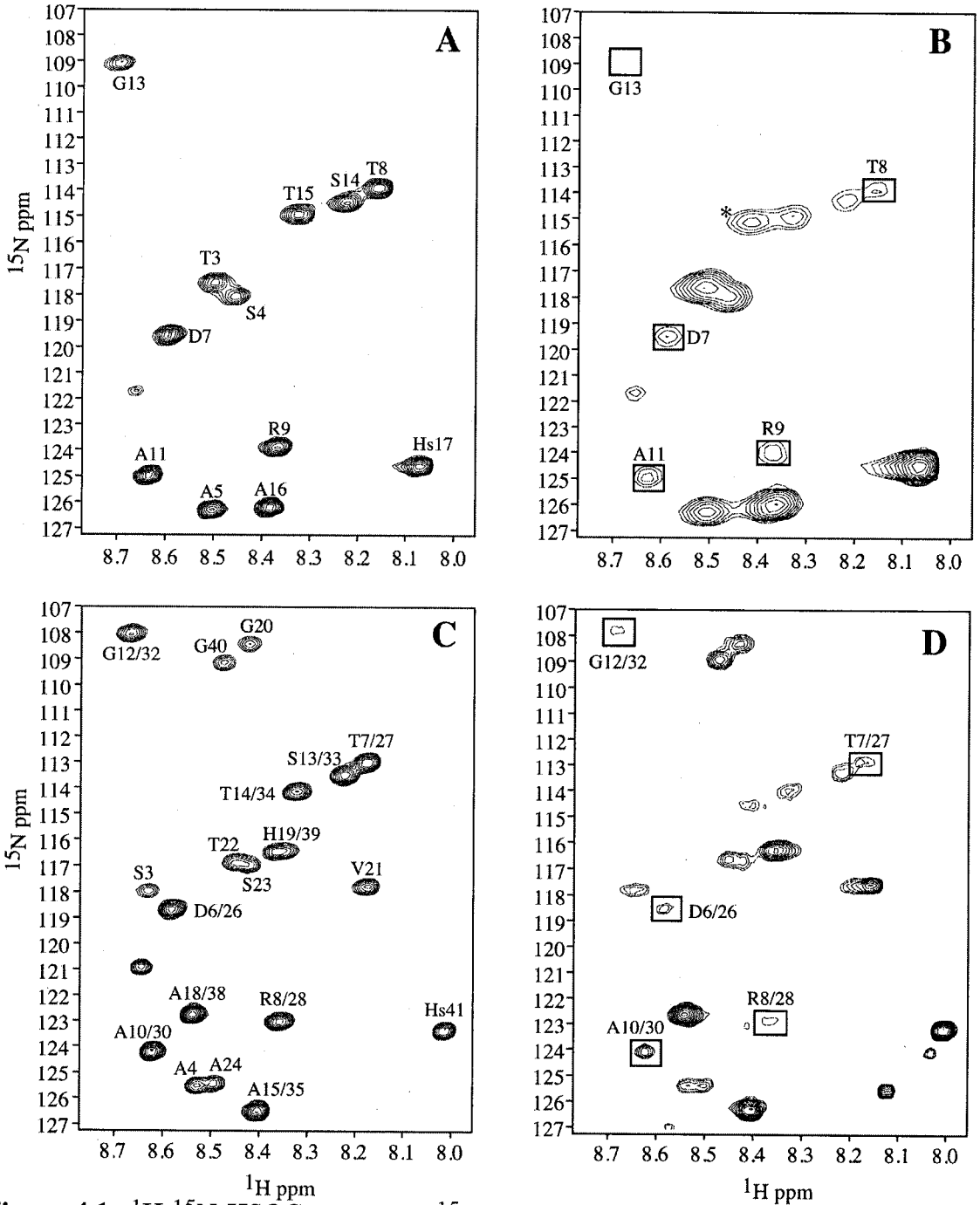

Figure 4.1: ^{1}H-^{15}N HSQC spectra of ^{15}N-labeled recombinant MUC1 peptides in the absence and presence of Fab B27.29: (A) 800 μM 16mer, (B) 500 μM 16mer + 200 μM Fab, (C) 800 μM 40mer, and (D) 320 μM 40mer + 200 μM Fab. Boxed crosspeaks experience the greatest losses in signal intensity due to exchange broadening in the presence of Fab. The peptide ± Fab spectra were recorded at 500 MHz on a Varian Inova 500 NMR spectrometer. NMR samples were in PBS buffer, pH 7.1, 90% H_2O/10% D_2O, 5.0 °C.

examination of these spectra reveals that the chemical shifts for residues APDTRPAPGSTA are almost identical for the two peptides (i.e., the peaks representing A5-A16 in the 16mer sequence are roughly superimposable with the peaks representing A4-A15 in the 40mer sequence). This suggests that the PDTRPAP epitope regions in the 16mer and 40mer explore similar, if not identical, conformational space. Further examination of just the 40mer HSQC spectrum (Figure 4.1C) reveals that the peaks corresponding to residues PDTRPAPGSTA (D6/16-A18/38) are chemical shift degenerate, indicating that the conformational space explored by the core peptide epitope is identical from one repeat to the next. A full characterization of the dependence of MUC1 structure and dynamics on the number of repeat sequences is presented elsewhere (Schuman *et al.*, 2003b). However, previous ^{1}H NMR studies published by this group have identified a significantly populated type I β-turn spanning residues PDTR within the PDTRPAP epitope region (Grinstead et al., 2002; Schuman et al., 2003a; Schuman et al., 2003b). As the β-turn is a common structural motif of in antigenic regions of proteins (Koebnik *et al.*, 2000), and is commonly found in NMR and crystal structures of antibody-antigen complexes (Derrick *et al.*, 1999; Stanfield *et al.*, 1999; Tugarinov *et al.*, 1999; Zvi *et al.*, 2000), the presence of a β-turn within the MUC1 B-cell epitope may explain the immunodominance of this region.

Figures 4.1B and 4.1D present the ^{15}N-edited HSQC spectra acquired for the $^{15}N,^{13}C$-labeled 16mer and 40mer MUC1 peptides, respectively, in the presence of Fab B27.29. These spectra correspond to the first titration point with greater than unity molar ratio of peptide to Fab ([peptide]/[Fab] > 1), a point at which resonances for the significantly exchange broadened residues within the PDTRPAP epitope region could begin to be detected. These resonances correspond to D7, T8, R9, A11 and G13 within the 16mer (boxed in Figure 4.1B), and D6/26, T7/27, R8/28, A10/30 and G12/32 within

the 40mer (boxed in Figure 4.1D), an identical collection of residues that indicates an identical mode of epitope recognition and binding in the one-repeat versus the two-repeat system.

As predicted, complex spectral behavior is observed in Figures 4.1B and 4.1D, marked by a mixture of chemical shift exchange timescales. For example, extensive linebroadening consistent with an intermediate exchange timescale ($k_{-1} \sim \Delta\delta$), renders the PDTRPAP resonances unobservable until the Fab is saturated ([peptide]/[Fab] > 1) and a significant pool of free peptide is allowed to build up. In contrast, MUC1 residues outside the PDTRPAP epitope sequence display sizeable peaks, even for [peptide]/[Fab] < 1(see Figure 4.2A, 4.2B), at which point all of the peptide would be expected to be in the Fab-bound pool. The intensities of these peaks increase with increasing concentration of peptide, and resonate at or near their free chemical shifts ($\Delta\delta \sim 0$), implying no change in chemical environment upon Fab binding and therefore little or no contact with the antibody combining site. This behavior is consistent with fast exchange on the chemical shift timescale ($k_{-1} >> \Delta\delta$), as predicted for residues at the MUC1 peptide termini.

Finally, Figure 4.1B shows one of several new peaks in the Fab-bound spectrum of the 16mer (starred in the spectrum). These peaks appear at the lowest concentrations of MUC1 peptide, and increase in intensity with peptide concentration until the Fab is saturated with peptide, and the free peptide peaks of the bound epitope sequence begin to appear in the spectrum (see Figure 4.2). In other words, these new bound peptide peaks display classic slow-exchange titration behavior. Similar bound resonances are also seen in the ^{1}H-^{15}N HSQC spectrum of the 40mer. As these new 16mer peaks are absent in the free peptide spectrum, they must correspond to a set of bound peptide resonances that experiences slow exchange on the chemical shift timescale ($k_{-1} << \Delta\delta$). Interestingly, only two new bound peptide resonances are observed with strong intensity, not four

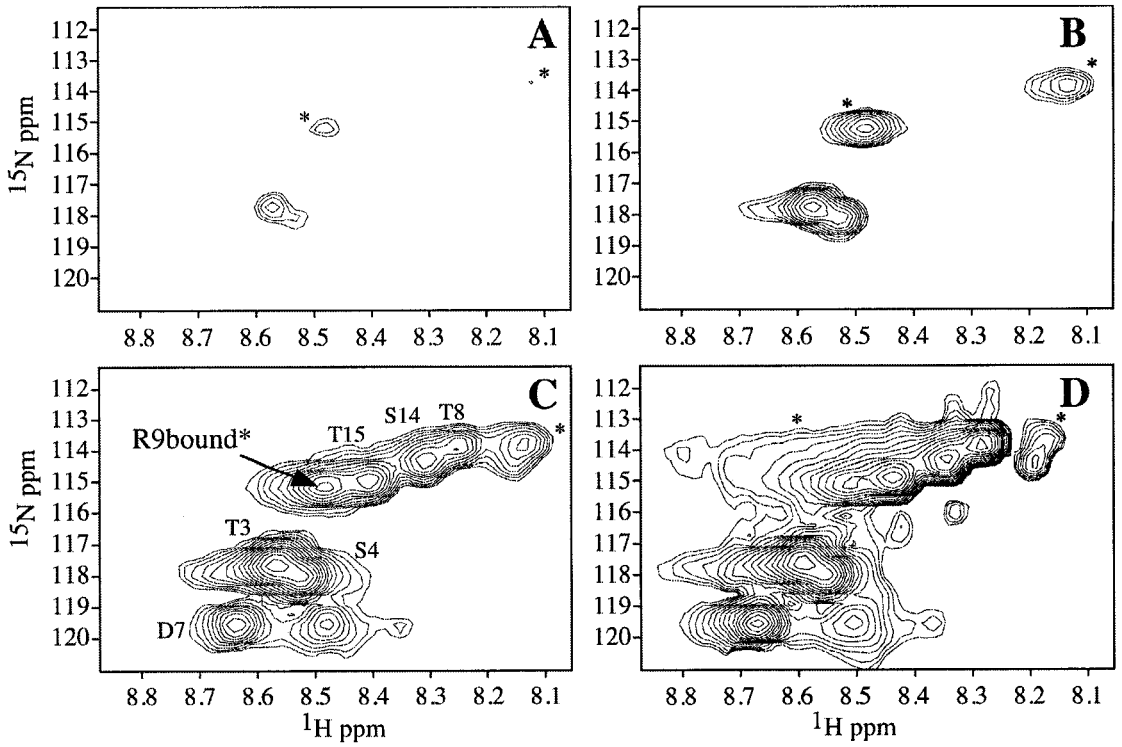

Figure 4.2: ^{1}H-^{15}N HSQC-monitored reverse titration of Fab B27.29 with ^{15}N-labeled recombinant MUC1 16mer peptide: (A) 200 μM Fab + 40 μM 16mer ([peptide]/[Fab] = 0.2) (B) 200 μM Fab + 200 μM 16mer ([peptide]/[Fab] = 1.0), (C) 200 μM Fab + 500 μM 16mer ([peptide]/[Fab] = 2.5), and (D) 200 μM Fab + 800 μM 16mer ([peptide]/[Fab] = 4.0). The Fab-bound peptide resonances are starred, and increase in intensity until [peptide]/[Fab] = 1.0. At [peptide]/[Fab] > 1.0, the 'free' resonances of the PDTRPAP epitope sequence begin to appear, whereas the bound resonances experience no further increases in intensity. This behavior is consistent with slow exchange on the chemical shift timescale. Notice that the resonances for T3 and S4 (near the termini of the MUC1 peptide and outside the epitope sequence) have strong intensity throughout the titration, even for [peptide]/[Fab] < 1.0. This behavior is consistent with fast exchange on the chemical shift timescale. The peptide ± Fab spectra were recorded at 500 MHz on a Varian Inova 500 NMR spectrometer. NMR samples were in PBS buffer, pH 7.1, 90% H_2O/10% D_2O, 5.0 °C.

bound peptide resonances as might be expected since the PDTRPAP epitope sequence contains four non-proline residues. Therefore, these two bound peptide resonances must represent a subset of residues within the peptide epitope that experience the greatest change in chemical environment upon Fab binding (the largest $\Delta\delta$ terms), and thus the most intimate contact with the antibody combining site. In order to probe further the identities of these bound peptide resonances, triple-resonance experiments were

performed. Although chemical exchange broadening of most epitope resonances within the PDTRPAP sequence prohibits complete assignment of the observed bound state resonances, the triple resonance experiments confirm that the new peak at 8.51 ppm in the ^{15}N HSQC spectrum of the 16mer (starred in Figure 4.1B and Figure 4.2) is from R9. This conclusion is supported by mutational analysis demonstrating that the presence of R9 in the MUC1 sequence is necessary for binding to other breast and ovarian cancer antibodies (Xing et al., 1992).

^{13}C HSQC-monitored titrations of MUC1 peptides with Fab B27.29. The ^{13}C-edited HSQC spectra acquired for the ^{15}N,^{13}C-labeled 16mer and 40mer MUC1 peptides in the absence (Figures 4.3A and 4.3C) and presence (Figures 4.3B and 4.3D) of Fab B27.29 is also shown. These ^{13}C-edited HSQC spectra provide chemical shift information for the many proline residues in the MUC1 sequences, as well as for select sidechain resonances. As previously noted for Figure 4.1, APDTRPAPGSTA backbone and sidechain resonances are chemical shift degenerate in the 16mer versus the 40mer spectra, and from one repeat to the next in the 40mer spectra. Consistent with the ^{15}N-edited HSQC monitored titration is the appearance of exchange broadened ^{13}C peptide resonances for molar ratios [peptide]/[Fab] > 1 (Figures 4.3B and 4.3D). These resonances correspond to P6, D7, T8, R9, P10, A11, P12 and G13 within the 16mer (boxed in Figure 4.3B), and P5/25, D6/26, T7/27, R8/28, P9/29, A10/30, P11/31 and G12/32 within the 40mer (boxed in Figure 4.3D), an identical collection of residues that indicates identical binding epitopes in the one-repeat versus two-repeat systems.

Taken together, the results of the ^{15}N-edited and ^{13}C-edited HSQC monitored titrations are consistent and complimentary. The exchange broadening observed for residues PDTRPAP demonstrates selective interactions of this region of the sequence

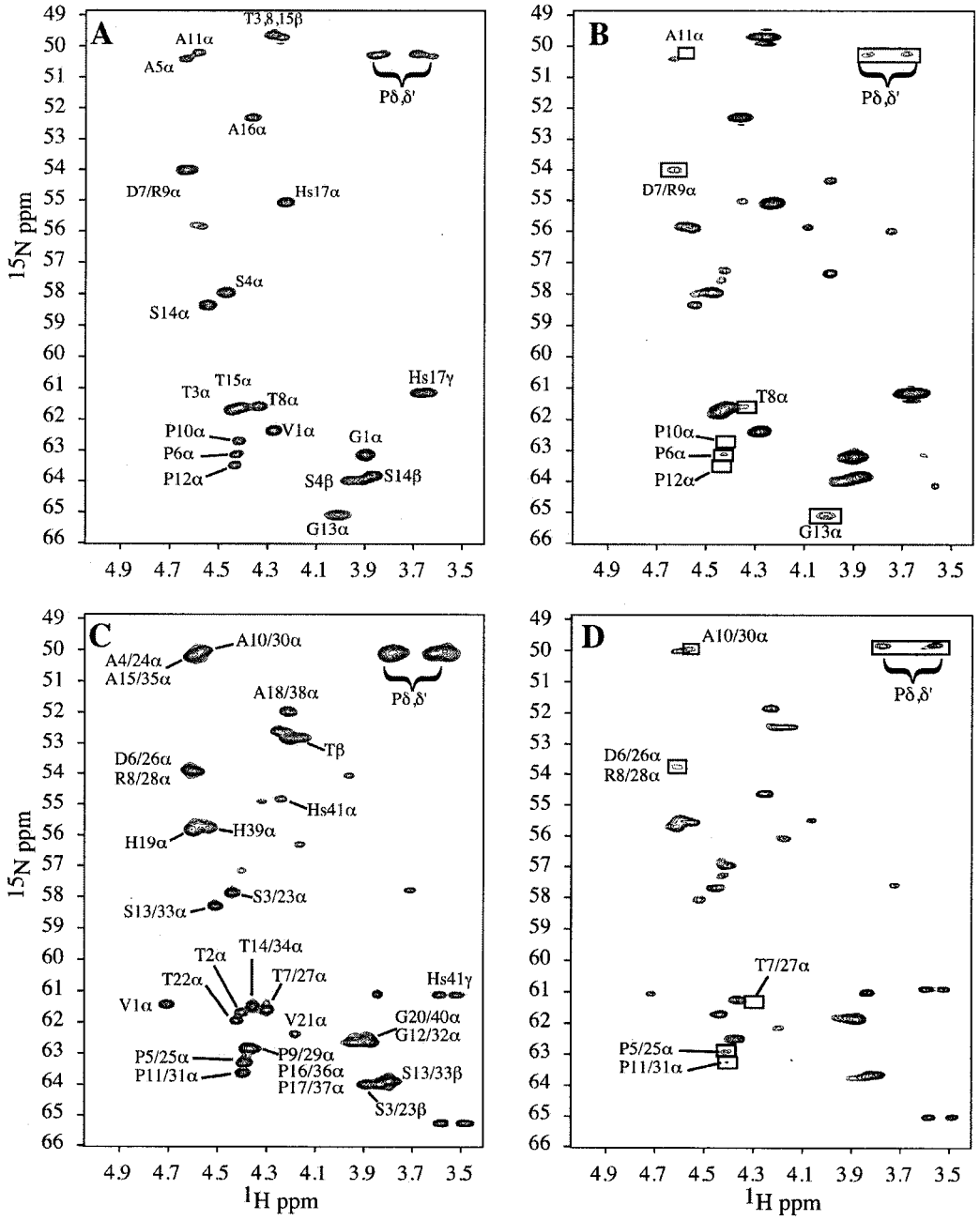

Figure 4.3: ^{1}H-^{13}C HSQC spectra of ^{13}C-labeled recombinant MUC1 peptides in the absence and presence of Fab B27.29: (A) 800 μM 16mer, (B) 500 μM 16mer + 200 μM Fab, (C) 800 μM 40mer, and (D) 320 μM 40mer + 200 μM Fab. Boxed crosspeaks experience the greatest losses in signal intensity due to exchange broadening in the presence of Fab. The spectra were recorded at 500 MHz on a Varian Inova 500 NMR spectrometer. NMR samples were in PBS buffer, pH 7.1, 90% H_2O/10% D_2O, 5.0 °C.

with Fab B27.29, in agreement with the epitope mapping of B27.29 provided by ELISA binding studies (Price *et al.*, 1998). Significantly, earlier NMR studies by this group have identified a type I β-turn spanning residues PDTR within the PDTRPAP epitope region of both the 16mer and the 40mer (Grinstead et al., 2002; Schuman et al., 2003a; Schuman et al., 2003b). These same studies also identified a second less well-defined β-turn in the 40mer, spanning residues GSTA immediately downstream of the peptide epitope region (Schuman et al., 2003b). However, our present studies demonstrate that only the glycine residue from the GSTA sequence (G13 in the 16mer, and G12/32 in the 40mer) is exchange broadened in the presence of Fab. These results point to the specificity of the antibody as recognizing uniquely the PDTRPAP sequence, and not β-turn structures in general.

^{15}N NMR relaxation measurements. Once enough peptide was added to obtain sufficient intensity for the PDTRPAP resonances, NMR relaxation experiments were performed to probe the dynamics of the system at this high percentage of bound ligand ([peptide]/[Fab] >> 1). These experiments included the measurement of ^{15}N T_1 and T_2 relaxation rates and steady-state heteronuclear $\{^1H\}$-^{15}N NOEs for the ^{15}N,^{13}C-labeled 16mer and 40mer MUC1 peptides in the absence and presence of Fab B27.29. The values of these relaxation parameters are presented in Tables B2, B3, and B4 in Appendix B. The ^{15}N T_1 relaxation data from these tables are plotted in Figures 4.4A (16mer ± Fab) and 4.4B (40mer ± Fab).

In general, the ^{15}N T_1 and T_2 values acquired for the 16mer and 40mer MUC1 peptides become shorter in the presence of Fab, consistent with an overall increase in the correlation time of the peptides as they are bound to antibody. For example, the averaged

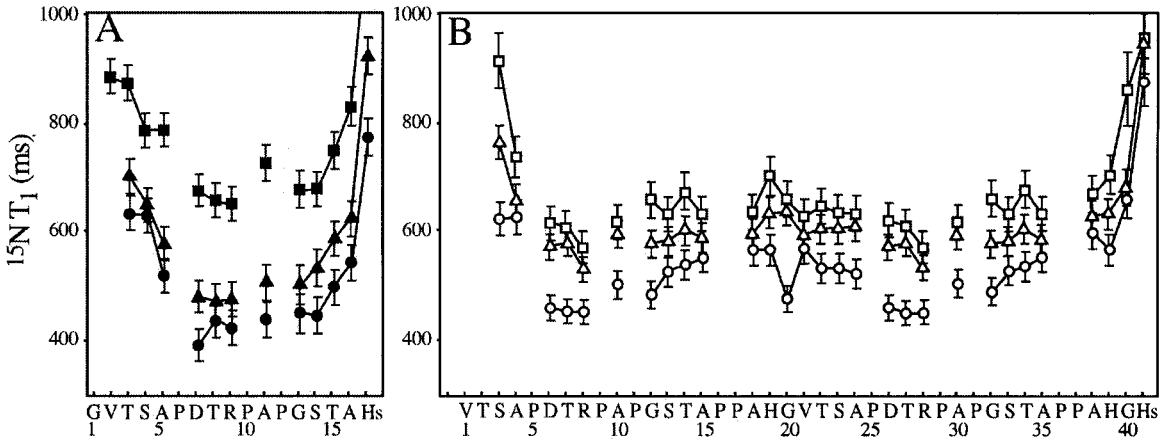

Figure 4.4: ^{15}N T_1 relaxation times measured for the ^{15}N-labeled recombinant MUC1 peptides in the absence and presence of Fab B27.29: (A) 800 μM 16mer (solid squares), 1600 μM 16mer + 200 μM Fab (solid triangles), 800 μM 16mer + 200 μM Fab (solid circles); and (B) 800 μM 40mer (open squares), 1200 μM 40mer + 200 μM Fab (open triangles), and 800 μM 40mer + 200 μM Fab (open circles). All measurements were made at 500 MHz on a Varian Inova 500 NMR spectrometer. NMR samples were in PBS buffer, pH 7.1, 90% H_2O/10% D_2O, 5.0 °C. The 5% error estimated for each measurement is plotted as an error bar.

^{15}N T_1 value of the 16mer across the entire sequence is $\langle T_1 \rangle$ = 767 ms in the absence of Fab, but $\langle T_1 \rangle$ = 508 ms in the presence of Fab (800μM 16mer + 200μM Fab B27.29, or [peptide]/[Fab] = 4). The corresponding ^{15}N T_1 values for the 40mer are $\langle T_1 \rangle$ = 669 ms and 539 ms in the absence and presence of the same relative ratios of Fab. These T_1 values show titration dependent behavior (see Figures 4.4A and 4.4B), in that an increase in the [peptide]/[Fab] ratio leads to a corresponding increase in the ^{15}N T_1 value measured for each residue in the peptide sequence. This concentration dependent behavior demonstrates that the MUC1 peptide-Fab B27.29 complex experiences fast exchange behavior on the NMR relaxation timescale, and thus the measured ^{15}N T_1 values are population-weighted averages of the free and bound states (see equation 6). Under these conditions, relaxation measurements made for exchange broadened or even 'free state' peptide resonances (i.e., exchange intermediate to slow on the chemical shift

timescale) will nevertheless yield information relevant to the dynamics of the bound state. Thus, Fab-induced changes in the measured relaxation parameters can be interpreted within the context of Fab-induced changes to the backbone dynamics of the MUC1 peptides as these peptides are bound and immobilized within the B27.29 combining site.

^{13}C NMR relaxation measurements. While the ^{15}N NMR relaxation measurements discussed above provide evidence of fast exchange on the relaxation timescale, the Fab-induced changes measured for individual relaxation parameters (T_1, T_2 and NOE) are fairly uniform across the MUC1 peptide sequence. The limited sequence-specific information provided by the ^{15}N nucleus arises from the magnetic susceptibility of the ^{15}N-^{1}H bond vector to a variety of environmental influences, including changes in solvent exposure and solvent exchange. In contrast, the magnetic susceptibility of the $^{13}C\alpha$-$^{1}H\alpha$ bond vector is uniquely sensitive to changes in local backbone conformation and chemical environment. Thus, ^{13}C NMR relaxation measurements can provide high-resolution, sequence-specific information of Fab-induced changes to the backbone dynamics of the MUC1 peptides, allowing a precise mapping of the boundaries of the peptide epitope recognized and bound by Fab B27.29. $^{13}C\alpha$ T_1 and $T_{1\rho}$ relaxation rates and steady-state heteronuclear $\{^{1}H\alpha\}$-$^{13}C\alpha$ NOEs were therefore also measured for the ^{15}N,^{13}C-labeled 16mer and 40mer MUC1 peptides in the absence and presence of Fab B27.29. The values of these relaxation parameters are presented in Tables B2, B3, and B4 in Appendix B.

Of the three parameters measured (T_1, $T_{1\rho}$ and NOE), the T_1 parameter arguably provides the best probe of local ns-ps timescale dynamics, as its contains no exchange

contributions[2], nor does it suffer from low signal-to-noise or propagated error[3]. Figure 4.5 therefore only presents the $^{13}C\alpha$ T_1 measured for the 16mer (4.5A) and 40mer (4.5B) MUC1 peptides in the absence (squared symbols) and presence (circular symbols) of Fab B27.29. In the presence of Fab, significant decreases in T_1 (> 50 ms) are observed only

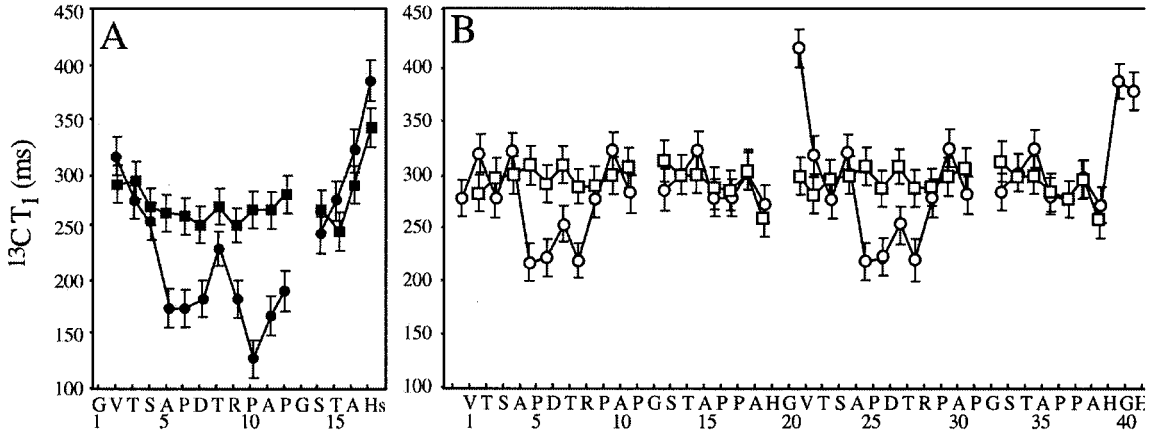

Figure 4.5: ^{13}C T_1 relaxation times measured for the ^{13}C-labeled recombinant MUC1 peptides in the absence and presence of Fab B27.29: (A) 800 μM 16mer (solid squares), 800 μM 16mer + 200 μM Fab (solid circles); and (B) 800 μM 40mer (open squares), 800 μM 40mer peptide + 200 μM Fab (open circles). All measurements were made at 500 MHz on a Varian Inova 500 NMR spectrometer. NMR samples were in PBS buffer, pH 7.1, 90% H_2O/10% D_2O, 5.0 °C. The 5% error estimated for each measurement is plotted as an error bar.

for residues A5, P6, D7, R9, P10, A11, and P12 in the 16mer, and P5/25, D6/26, T7/27, and R8/28 in the 40mer, indicating increases in the local correlation times of these PDTRPAP core epitope residues as they are bound and immobilized within the B27.29 combining site. That this collection of 'bound and immobilized residues' differs somewhat between the two peptides (PDTR for the 40mer, and APDTRPAP for the 16mer) is not a reflection of different binding modes. Rather, the disparity between the

---

[2] The paramaters that measure transverse magnetization, $T_{1\rho}$ and T_2, contain a contribution from exchange between the free and bound state, according to $R_{2obs} = P_B R_{2B} + P_F R_{2F} + P_B P_F(\tau)(2\pi\Delta\delta)^2$, where $\tau \sim 1/k_{-1}$ (compare to the analogous expression for R_{1obs} shown in equation 6).

[3] The steady-state heteronuclear NOE is calculated from difference spectra (with and without ^1H saturation), so experimental errors are summed. In addition, the spectrum acquired without ^1H saturation often suffers from low to signal-to-noise, contributing a significant error to the final calculated NOE.

epitope profiles detected in the 16mer versus the 40mer arises from the overlap of alanine and proline peaks in the 40mer T_1 spectra, which leads to averaged T_1 values measured for P9/29, P16/36 and P17/37, and for A4/24, A10/30 and A15/35 in the 40mer, and therefore artifically elevated values for P9/29 and A10/30 within the PDTRPAP core epitope. Thus, the epitope profile detected from the 16mer T_1 experiment probably best represents the true boundaries of the peptide epitope recognized and bound by Fab B27.29 (APDTRPAP), a profile which very closely matches that identified from earlier indirect ELISA based experiments (PDTRPAP) (Bashford et al., 1993; Burchell et al., 1989; Denton et al., 1993; Girling et al., 1989; Kotera et al., 1994; Xing et al., 1992).

Spectral density analysis. Raw relaxation rates are usually analyzed within the context of a relaxation formalism that can provide simplified motional models, as well as some insight into the timescales and amplitudes of internal motions. One such formalism is the model-free approach of Lipari and Szabo (Davis & Agard, 1998; Peng & Wagner, 1992), which provides a means of assessing the contributions of internal motions and conformational exchange to spin relaxation. However, there are limitations to this approach that arise from inherent assumptions. The overall molecular reorientation must be isotropic and independent from fast internal motions (which contribute negligibly to measured relaxation). These assumptions do not hold for small flexible peptides, like the MUC1 peptides, which can experience a broad range of motional timescales.

An alternative relaxation analysis approach for characterizing molecular dynamics is provided by spectral density analysis (Davis & Agard, 1998; Peng & Wagner, 1992), which has the advantage that it makes no assumptions about the separability of the timescales between the motions, and allows the possibility of sizeable contributions to relaxation from high-frequency motions. Moreover, this methodology is analytic and

independent of error estimates. In general, the spectral density at J(0) is proportional to the local correlation time of the backbone nitrogen (Peng & Wagner, 1992). Thus, it is possible to interpret Fab binding-induced chances in J(0) on the basis of changes in local correlation times. However, this interpretation is valid only in the absence of conformational exchange phenomena, which can lead to shortening of T_2 times, and therefore larger values of J(0) (Davis & Agard, 1998). Therefore, the contribution of slow exchange motions (μs-ms) to J(0) must also be considered in spectral density analysis.

Using equations 2 – 4 in Materials and Methods, the J(ω) spectral density values, J(0), $J(\omega_N)$ and $J(\omega_H)$, were calculated from the ^{15}N T_1 and T_2 relaxation rates and the steady-state heteronuclear $\{^1H\}$-^{15}N NOEs measured for the $^{15}N/^{13}C$-labeled MUC1 16mer and 40mer peptides free in solution versus bound to Fab B27.29[4] (see Tables B2, B3, and B4 in Appendix B). These values are shown in Figure 4.6, which plots the J(0) (4.6A and B) and $J(\omega_N)$ (4.6C and D) values only (see Table B5 in Appendix B for the raw values). The free peptide J(0) (squared symbols) yield average values across the entire sequence of $\langle J(0)\rangle = 0.53$ ns rad^{-1} for the 16mer and $\langle J(0)\rangle = 0.78$ ns rad^{-1} for the 40mer, consistent with the longer global correlation time of the larger two-repeat peptide. In comparison, the average J(0) value for the PDTRPAP epitope sequence is $\langle J(0)\rangle^{epitope} = 0.57$ for the 16mer, and $\langle J(0)\rangle^{epitope} = 0.79$ for the 40mer. Thus, the epitope sequences are not especially ordered relative to other parts of the sequence, at least in the free solution states of these peptides.

---

[4] The reduced spectral density mapping approach assumes that the high-frequency spectral density terms are of approximately equal magnitude, i.e. $J(\omega_H \pm \omega_N) \approx J(\omega_H)$, and may therefore be replaced by a single equivalent term, $J(\omega_H)$ (47, 48). This assumption does not hold for ^{13}C NMR relaxation, where $J(\omega_H \pm \omega_C)$ cannot be expected to equal $J(\omega_H)$. Thus, reduced spectral density terms were calculated only for the ^{15}N NMR relaxation data set.

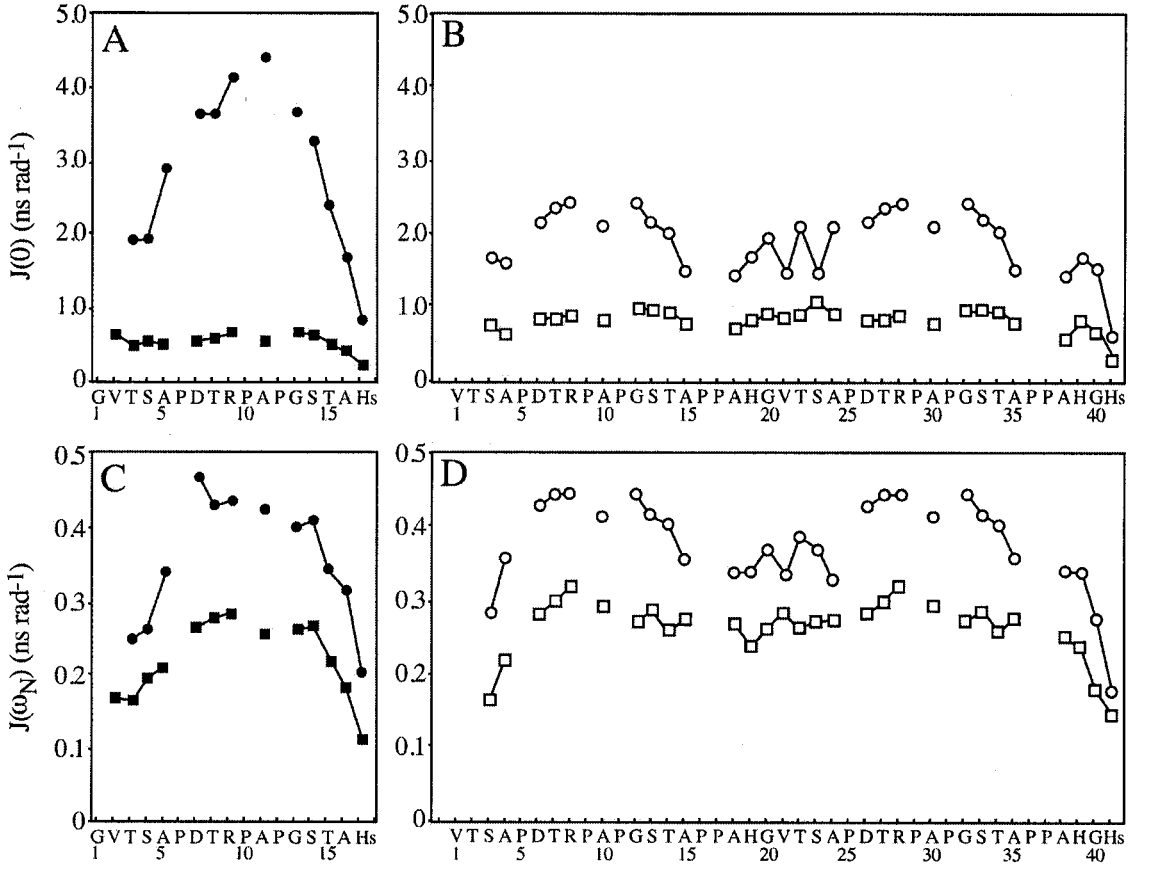

Figure 4.6: J(0) (panels A and B) and $J(\omega_N)$ (panels C and D) spectral density values calculated from ^{15}N NMR relaxation data acquired for the ^{15}N-labeled recombinant MUC1 peptides in the absence and presence of Fab B27.29: (A, C) 800 μM 16mer (solid squares), 800 μM 16mer + 200 μM Fab B27.29 (solid circles); and (B, D) 800 μM 40mer (open squares), 800 μM 40mer + 200 μM Fab B27.29 (open circles). NMR samples were in PBS buffer, pH 7.1, 90% H_2O/10% D_2O, 5.0 °C.

Addition of Fab (Figure 4.6, circular symbols) leads to significant increases in the J(0) values measured across the 16mer and 40mer sequences, commensurate with increases in the global correlation times experienced by these peptides as they are bound to antibody. These increases in J(0) are not uniform across the length of the peptides, being the most pronounced for residues within the PDTRPAP epitope region. For example, <J(0)> for the entire 16mer sequence increases from 0.53 to 2.8 ns rad^{-1} (an increase of ~ 2.3 ns rad^{-1}), whereas $\langle J(0)\rangle^{epitope}$ for just the PDTRPAP epitope within the 16mer increases from 0.57 to 3.9 ns rad^{-1} (an increase of ~ 3.3 ns rad^{-1}). Similarly,

$\langle J(0) \rangle$ for the entire 40mer sequence increases from 0.78 to 1.8 ns rad^{-1} (an increase of ~ 1.0 ns rad^{-1}), whereas $\langle J(0) \rangle^{epitope}$ increases from 0.79 to 2.2 ns rad^{-1} (an increase of ~ 1.4 ns rad^{-1})[5]. These substantially elevated $\langle J(0) \rangle^{epitope}$ values are consistent with significant increases in the local correlation times of residues that directly contact the antibody, well in excess of the uniform increases in global correlation time expected as a result of binding. Thus, the J(0) spectral density terms calculated from ^{15}N NMR relaxation experiments are sensitive indicators of specific epitope-antibody interactions across the molecular interface, even if the constituent relaxation parameters (T_1, T_2 and NOE) appear to provide a less well-resolved picture upon first analysis.

As previously alluded to, conformational exchange processes on slow timescales can artificially elevate the value of J(0) (Davis & Agard, 1998). However, these slow timescale motions have a negligible effect on the calculated values of the $J(\omega_N)$ and $J(\omega_H)$ spectral densities, as these represent only high frequency motions (Bhattacharya *et al.*, 2002; Peng & Wagner, 1992; Peng & Wagner, 1995). Figure 4.6 (panels C and D) plots the $J(\omega_N)$ values calculated from the relaxation data presented in Table B5 (see Appendix B). A comparison of the $J(\omega_N)$ and J(0) plots reveals the same pattern of increases for PDTRPAP epitope residues, supporting our interpretation of increased local correlation time for these epitope residues upon antibody binding (Bhattacharya et al., 2002; Lefevre *et al.*, 1996), and further confirming that exchange effects do not dominate the observed increases in J(0). Most importantly, the quality of the $J(\omega_N)$ and J(0) data presented for the MUC1 system illustrates the utility of spectral density analysis in epitope mapping, even in the presence of slow chemical exchange.

---

[5] The smaller increases in J(0) measured for the 40mer versus the 16mer (at the same molar ratios of Fab to peptide) may be a result of the doubled effective ligand concentration of the 40mer, which presumably leads to a J(0) value averaged between the one bound epitope and the one free epitope in the two repeat peptide.

Peptide epitope mapping. In the present study, two different classes of isotope-edited NMR experiments have been used to map the binding of Fab B27.29 to one- and two-repeat MUC1 peptides: (1) HSQC-monitored titrations that measure exchange broadening, and therefore relative magnitude of the Fab-induced chemical shift; and (2) NMR relaxation measurements that measure changes in the ps-ns timescale motions in the peptide backbone as a function of Fab-induced increases in local correlation time. A comparison of the 40mer peptide epitope profiles obtained from ^{1}H-^{15}N HSQC-monitored spectral analysis versus ^{15}N NMR relaxation analysis is presented in Figure 4.7. The top panel (4.7A) plots differences in the HSQC peak intensities (ΔI) as a consequence of Fab-induced chemical shifts, whereas the bottom two panels (4.7B and C) plot differences in the low and high frequency spectral density values ($\Delta J(0)$ and $\Delta J(\omega_N)$) as a consequence of Fab-induced increases in local correlation time. As expected, these profiles show very similar trends, indicating that changes in chemical environment track changes in local dynamics. Thus, regions of the 40mer peptide backbone that experience a marked change in chemical environment upon binding to B27.29 also show significant decreases in ps-ns timescale motions as they become immobilized within the antibody combining site. The consistency and complimentarity of the information provided by these two independent NMR observables (chemical shift and spin relaxation) illustrates the power of a direct spectroscopic approach in peptide epitope mapping, especially if it can provide additional structural and dynamical information useful in peptide vaccine design.

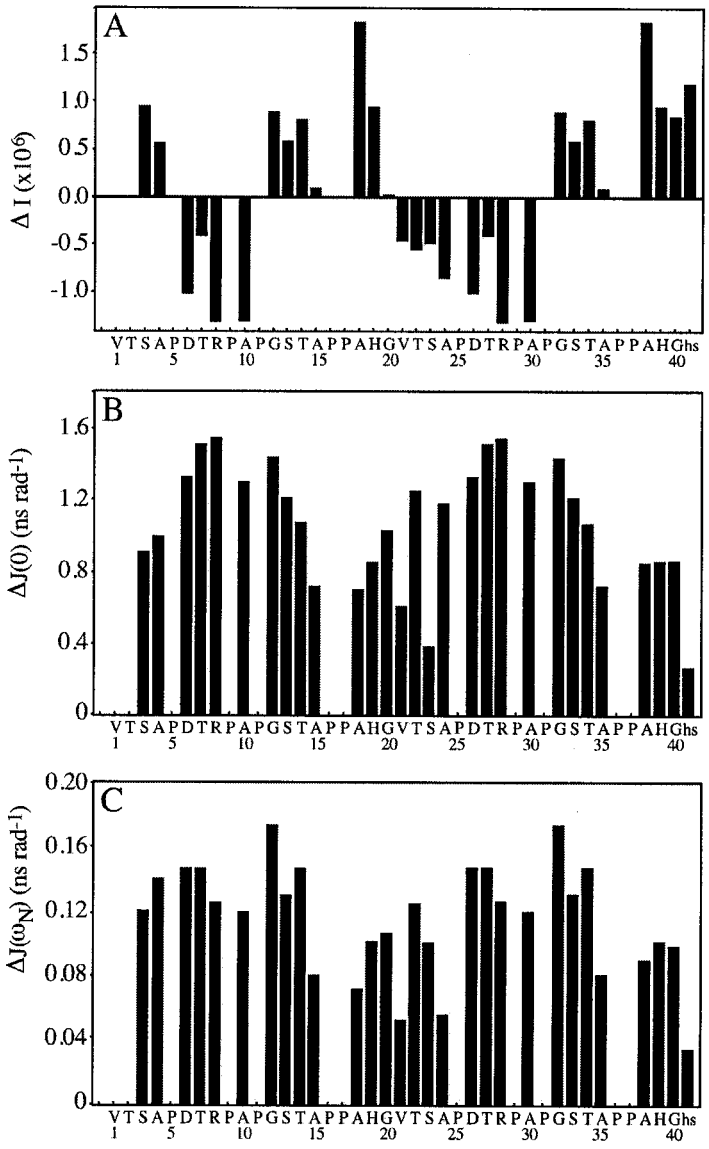

Figure 4.7: B27.29 epitope mapping of the MUC1 40mer peptide from analysis of linebroadening and relaxation data. (A) Differences in the ^{1}H-^{15}N HSQC peak intensities, ΔI, measured for the 400 μM 40mer ± 200 μM Fab B27.29 ($\Delta I = I^{+Fab} - I^{-Fab}$). Negative values of ΔI indicate significant Fab-induced linebroadening, i.e. $I^{+Fab} << I^{-Fab}$. (B) Differences in the J(0) spectral density values, $\Delta J(0)$, calculated from ^{15}N NMR relaxation data measured for the 400 μM 40mer ± 200 μM Fab B27.29 ($\Delta J(0) = J(0)^{+Fab} - J(0)^{-Fab}$). Increased values of $\Delta J(0)$ indicate significant Fab-induced increases in local correlation time, i.e. $J(0)^{+Fab} >> J(0)^{-Fab}$. (B) Differences in the $J(\omega_N)$ spectral density values, $\Delta J(\omega_N)$, calculated from ^{15}N NMR relaxation data measured for the 400 μM 40mer ± 200 μM Fab B27.29 ($\Delta J(\omega_N) = J(\omega_N)^{+Fab} - J(\omega_N)^{-Fab}$). Fab-induced increases in $J(\omega_N)$ 'track' Fab-induced increases in J(0).

Conclusions:

We have developed an approach utilizing NMR relaxation measurements and heteronuclear correlation experiments to map antibody epitopes. These NMR experiments allow a direct, sequence-specific probe of binding, and demonstrate which parts of the MUC1 peptide epitope are immobilized upon binding antibody. We apply this technique to determining the epitope of an antibody raised against tumor cells for the purposes of designing a cancer vaccine. Our method uses the antibody epitope as an indirect probe of a structural/dynamic state present on the tumor cell surface, and as a probe of the peptide state that is immunogenic. Our approach to vaccine design is of general utility for any antigen that lacks sufficient analytical characterization, as is the case with most tumor-associated antigens.

In this study, we provide direct spectroscopic evidence that the MUC1 peptide sequence PDTRPAP, portions of which were identified from earlier ELISA based experiments (Bashford et al., 1993; Burchell et al., 1989; Denton et al., 1993; Girling et al., 1989; Kotera et al., 1994; Xing et al., 1992) and our own previous ^{1}H NMR study (Grinstead et al., 2002), is bound and preferentially immobilized in the Fab B27.29 combining site. Immobilization of the entire PDTRPAP sequence implies that the B27.29 epitope is continuous and all residues in the epitope contribute to the binding energy. Furthermore, we observe for the first time the bound-state resonance of arginine within the PDTRPAP epitope sequence. The observation of a bound state resonance for arginine suggests that this residue makes intimate contact with B27.29, consistent with the mutational studies of Xing *et al.* (Xing et al., 1992). In addition, we show that the residues in the MUC1 sequence outside the boundaries of this defined epitope remain

highly flexible in the bound state, demonstrating that they do not interact with antibody and extend into solution out of the antibody combining site.

Our characterization of the B27.29 epitope can be used to increase the immunogenicity of MUC1 peptide vaccine candidates. For example, since the MUC1 sequence outside the PDTRPAP epitope retains its conformational heterogeneity in the Fab-bound state and is not important for binding, it could be engineered for increased oral bioavailability, or to act as a linker for multiple PDTRPAP epitopes or other immunogenic peptide sequences. These changes could significantly improve the efficacy of a MUC1 peptide-based vaccine, while not altering the specificity of the immune response. In addition, our results suggest that since the PDTRPAP sequence is highly ordered in the antibody binding site, preordering of the structure of the vaccine candidate could increase similarity with the immunologically relevant MUC1 structure and therefore increase immunogenicity. Future studies will continue to probe the structure of the antibody-bound MUC1 peptide sequence, with the ultimate goal of developing a second-generation MUC1 peptide vaccine that better represents the peptide portion of the tumor-associated MUC1 mucin.

Notes to Chapter 4

Apostolopoulos, V., Pietersz, G. A. & McKenzie, I. F. (1999a). MUC1 and breast cancer. *Curr Opin Mol Ther* **1**(1), 98-103.

Apostolopoulos, V., Sandrin, M. S. & McKenzie, I. F. C. (1999b). Carbohydrate/Peptide mimics: effect on MUC1 Cancer Immunotherapy. *J Mol Med* **77**, 427-436.

Bashford, J. L., Robins, R. A. & Price, M. R. (1993). Development of an anti-idiotypic antibody reactive with an antibody defining the epitope RPAP in the MUC-1 epithelial mucin core. *Int J Cancer* **54**(5), 778-83.

Bhattacharya, S., Botuyan, M. V., Hsu, F., Shan, X., Arunkumar, A. I., Arrowsmith, C. H., Edwards, A. M. & Chazin, W. J. (2002). Characterization of binding-induced changes in dynamics suggests a model for sequence-nonspecific binding of ssDNA by replication protein A. *Protein Sci* **11**(10), 2316-25.

Brossart, P., Wirths, S., Stuhler, G., Reichardt, V. L., Kanz, L. & Brugger, W. (2000). Induction of cytotoxic T-lymphocyte responses in vivo after vaccinations with peptide-pulsed dendritic cells. *Blood* **96**(9), 3102-8.

Burchell, J., Taylor-Papadimitriou, J., Boshell, M., Gendler, S. & Duhig, T. (1989). *Int J Cancer* **44**, 691-696.

Campbell, A. P. & Sykes, B. D. (1993). The two-dimensional transferred nuclear Overhauser effect: theory and practice. *Annu Rev Biophys Biomol Struct* **22**, 99-122.

Carlstedt, I. & Davies, J. R. (1997). Glycoconjugates facing the outside world. *Biochem Soc Trans* **25**(1), 214-9.

Davis, J. H. & Agard, D. A. (1998). Relationship between enzyme specificity and the backbone dynamics of free and inhibited alpha-lytic protease. *Biochemistry* **37**(21), 7696-707.

Delaglio, F., Grsesiek, S., Vuister, G. W., Zhu, G., Pfeifer, J. & Bax, A. (1995). NMRPipe: A multidimensional spectral processing system based on UNIX pipes. *J Biomol NMR* **6**, 277 - 293.

Denda-Nagai, K. & Irimura, T. (2000). MUC1 in carcinoma-host interactions. *Glycoconj J* **17**(7-9), 649-58.

Denton, G., Sekowski, M. & Price, M. R. (1993). Induction of antibody responses to breast carcinoma associated mucins using synthetic peptide constructs as immunogens. *Cancer Lett* **70**(3), 143-50.

Derrick, J. P., Maiden, M. C. & Feavers, I. M. (1999). Crystal structure of an Fab fragment in complex with a meningococcal serosubtype antigen and a protein G domain. *J Mol Biol* **293**(1), 81-91.

Ding, L., Lalani, E. N., Reddish, M., Koganty, R., Wong, T., Samuel, J., Yacyshyn, M. B., Meikle, A., Fung, P. Y. & Taylor-Papadimitriou, J. (1993). Immunogenicity of synthetic peptides related to the core peptide sequence encoded by the human MUC1 mucin gene: effect of immunization on the growth of murine mammary adenocarcinoma cells transfected with the human MUC1 gene. *Cancer Immunol Immunother* **36**(1), 9-17.

Doehn, C. & Jocham, D. (2000). Technology evaluation: TG-1031, Transgene SA. *Curr Opin Mol Ther* **2**(1), 106-11.

Farrow, N. A., Muhandiram, R., Singer, A. U., Pascal, S. M., Kay, C. M., Gish, G., Shoelson, S. E., Pawson, T., Forman-Kay, J. D. & Kay, L. E. (1994). Backbone dynamics of a free and phosphopeptide-complexed Src homology 2 domain studied by 15N NMR relaxation. *Biochemistry* **33**(19), 5984-6003.

Farrow, N. A., Zhang, O., Forman-Kay, J. D. & Kay, L. E. (1995). Comparison of the backbone dynamics of a folded and an unfolded SH3 domain existing in equilibrium in aqueous buffer. *Biochemistry* **34**(3), 868-78.

Finn, O. J., Jerome, K. R., Henderson, R. A., Pecher, G., Domenech, N., Magarian-Blander, J. & Barratt-Boyes, S. M. (1995). MUC-1 epithelial tumor mucin-based immunity and cancer vaccines. *Immunol Rev* **145**, 61-89.

Fontenot, J. D. (1993). Biophysical Characterization of One, Two, and Three-Tandem Repeats of Human Mucin (MUC-1) Protein Core. *Cancer Research* **53**, 5386-5394.

Fontenot, J. D., Finn, O. J., Dales, N., Andrews, P. C. & Montelaro, R. C. (1993). Synthesis of large multideterminant peptide immunogens using a poly-proline beta-turn helix motif. *Pept Res* **6**(6), 330-6.

Fontenot, J. D., Mariappan, S. V., Catasti, P., Domenech, N., Finn, O. J. & Gupta, G. (1995). Structure of a tumor associated antigen containing a tandemly repeated immunodominant epitope. *J Biomol Struct Dyn* **13**(2), 245-60.

Foon, K. A. (2001). Immunotherapy for colorectal cancer. *Curr Oncol Rep* **3**(2), 116-26.

Foote, J. & Eisen, H. N. (1995). Kinetic and affinity limits on antibodies produced during immune responses. *Proc Natl Acad Sci U S A* **92**(5), 1254-6.

Gemmecker, G. (1999). Ch.9: NMR Spectroscopy in Drug Development and Analysis. In *NMR as a Tool in Drug Research* (Holzgrabe, U., Wawer, I. & Diehl, B., eds.), pp. 140-141. John Wiley & Sons, Inc., New York.

Girling, A., Bartkova, J., Burchell, J., Gendler, S., Gillett, C. & Taylor-Papadimitriou, J. (1989). A core protein epitope of the polymorphic epithelial mucin detected by the monoclonal antibody SM-3 is selectively exposed in a range of primary carcinomas. *Int J Cancer* **43**(6), 1072-6.

Grinstead, J. S., Koganty, R. R., Krantz, M. J., Longenecker, B. M. & Campbell, A. P. (2002). Effect of glycosylation on MUC1 humoral immune recognition: NMR studies of MUC1 glycopeptide-antibody interactions. *Biochemistry* **41**(31), 9946-61.

Grzesiek, S. & Bax, A. (1992). *J Am Chem Soc* **114**, 6291-6293.

Hanisch, F. G. (2001). O-glycosylation of the mucin type. *Biol Chem* **382**(2), 143-9.

Jerome, K. R., Barnd, D. L., Bendt, K. M., Boyer, C. M., Taylor-Papadimitriou, J., McKenzie, I. F., Bast, R. C., Jr. & Finn, O. J. (1991). Cytotoxic T-lymphocytes derived from patients with breast adenocarcinoma recognize an epitope present on the protein core of a mucin molecule preferentially expressed by malignant cells. *Cancer Res* **51**(11), 2908-16.

Karlsson, R. & Falt, A. (1997). Experimental design for kinetic analysis of protein-protein interactions with surface plasmon resonance biosensors. *J Immunol Methods* **200**(1-2), 121-33.

Koebnik, R., Locher, K. P. & Van Gelder, P. (2000). Structure and function of bacterial outer membrane proteins: barrels in a nutshell. *Mol Microbiol* **37**(2), 239-53.

Koganty, R. R., Reddish, M. A. & Longenecker, B. M. (1997). Glycopeptides in the Immunotherapy of Cancer. In *Glycopeptides and Related Compounds: Synthesis, Analysis and Application* (C.D., L. D. G. a. W., ed.), pp. 707-743. Dekker, New York.

Kotera, Y., Fontenot, J. D., Pecher, G., Metzgar, R. S. & Finn, O. J. (1994). Humoral immunity against a tandem repeat epitope of human mucin MUC-1 in sera from breast, pancreatic, and colon cancer patients. *Cancer Res* **54**(11), 2856-60.

Kuliopulos, A. & Walsh, C. T. (1994). Production, Purification, and Cleavage of Tandem Repeats of Recombinant Peptides. *J Am Chem Soc* **116**, 4599-4607.

Lefevre, J. F., Dayie, K. T., Peng, J. W. & Wagner, G. (1996). Internal mobility in the partially folded DNA binding and dimerization domains of GAL4: NMR analysis of the N-H spectral density functions. *Biochemistry* **35**(8), 2674-86.

Lian, L. Y., Barsukov, I. L., Sutcliffe, M. J., Sze, K. H. & Roberts, G. C. (1994). Protein-ligand interactions: exchange processes and determination of ligand conformation and protein-ligand contacts. *Methods Enzymol* **239**, 657-700.

Liu, X., Sejbal, J., Kotovych, G., Koganty, R. R., Reddish, M. A., Jackson, L., Gandhi, S. S., Mendonca, A. J. & Longenecker, B. M. (1995). Structurally defined synthetic cancer vaccines: analysis of structure, glycosylation and recognition of cancer associated mucin, MUC-1 derived peptides. *Glycoconj J* **12**(5), 607-17.

Miles, D. W. & Taylor-Papadimitriou, J. (1999). Therapeutic aspects of polymorphic epithelial mucin in adenocarcinoma. *Pharmacol Ther* **82**(1), 97-106.

Mitchell, M. S. (2002). Cancer vaccines, a critical review--Part II. *Curr Opin Investig Drugs* **3**(1), 150-8.

Morse, M. A. (2000). Technology evaluation: Theratope, Biomira Inc. *Curr Opin Mol Ther* **2**(4), 453-8.

Morse, M. A. (2001). Technology evaluation: BLP-25, Biomira Inc. *Curr Opin Mol Ther* **3**(1), 102-5.

Muller, S., Alving, K., Peter-Katalinic, J., Zachara, N., Gooley, A. A. & Hanisch, F. G. (1999). High density O-glycosylation on tandem repeat peptide from secretory MUC1 of T47D breast cancer cells. *J Biol Chem* **274**(26), 18165-72.

Muller, S., Goletz, S., Packer, N., Gooley, A., Lawson, A. M. & Hanisch, F. G. (1997). Localization of O-glycosylation sites on glycopeptide fragments from lactation-associated MUC1. All putative sites within the tandem repeat are glycosylation targets in vivo. *J Biol Chem* **272**(40), 24780-93.

Musselli, C., Ragupathi, G., Gilewski, T., Panageas, K. S., Spinat, Y. & Livingston, P. O. (2002). Reevaluation of the cellular immune response in breast cancer patients vaccinated with MUC1. *Int J Cancer* **97**(5), 660-7.

Nakamura, H., Hinoda, Y., Nakagawa, N., Makiguchi, Y., Itoh, F., Endo, T. & Imai, K. (1998). Detection of circulating anti-MUC1 mucin core protein antibodies in patients with colorectal cancer. *J Gastroenterol* **33**(3), 354-61.

Nishimori, I., Johnson, N. R., Sanderson, S. D., Perini, F., Mountjoy, K., Cerny, R. L., Gross, M. L. & Hollingsworth, M. A. (1994a). Influence of acceptor substrate primary amino acid sequence on the activity of human UDP-N-acetylgalactosamine:polypeptide N-acetylgalactosaminyltransferase. Studies with the MUC1 tandem repeat. *J Biol Chem* **269**(23), 16123-30.

Nishimori, I., Perini, F., Mountjoy, K. P., Sanderson, S. D., Johnson, N., Cerny, R. L., Gross, M. L., Fontenot, J. D. & Hollingsworth, M. A. (1994b). N-acetylgalactosamine glycosylation of MUC1 tandem repeat peptides by pancreatic tumor cell extracts. *Cancer Res* **54**(14), 3738-44.

Northrup, S. H. & Erickson, H. P. (1992). Kinetics of protein-protein association explained by Brownian dynamics computer simulation. *Proc Natl Acad Sci U S A* **89**(8), 3338-42.

Pecher, G., Haring, A., Kaiser, L. & Thiel, E. (2002). Mucin gene (MUC1) transfected dendritic cells as vaccine: results of a phase I/II clinical trial. *Cancer Immunol Immunother* **51**(11-12), 669-73.

Peng, J. W. & Wagner, G. (1992). Mapping of the spectral densities of N-H bond motions in eglin c using heteronuclear relaxation experiments. *Biochemistry* **31**(36), 8571-86.

Peng, J. W. & Wagner, G. (1995). Frequency spectrum of NH bonds in eglin c from spectral density mapping at multiple fields. *Biochemistry* **34**(51), 16733-52.

Petrarca, C., Casalino, B., von Mensdorff-Pouilly, S., Rughetti, A., Rahimi, H., Scambia, G., Hilgers, J., Frati, L. & Nuti, M. (1999). Isolation of MUC1-primed B lymphocytes from tumour-draining lymph nodes by immunomagnetic beads. *Cancer Immunol Immunother* **47**(5), 272-7.

Price, M. R., Rye, P. D., Petrakou, E., Murray, A., Brady, K., Imai, S., Haga, S., Kiyozuka, Y., Schol, D., Meulenbroek, M. F., Snijdewint, F. G., von Mensdorff-Pouilly, S., Verstraeten, R. A., Kenemans, P., Blockzjil, A., Nilsson, K., Nilsson, O., Reddish, M., Suresh, M. R., Koganty, R. R., Fortier, S., Baronic, L., Berg, A., Longenecker, M. B., Hilgers, J. & et al. (1998). Summary report on the ISOBM TD-4 Workshop: analysis of 56 monoclonal antibodies against the MUC1 mucin. San Diego, Calif., November 17-23, 1996. *Tumour Biol* **19 Suppl 1**, 1-20.

Raman, C. S., Jemmerson, R., Nall, B. T. & Allen, M. J. (1992). Diffusion-limited rates for monoclonal antibody binding to cytochrome c. *Biochemistry* **31**(42), 10370-9.

Rudd, P. M. & Dwek, R. A. (1997). Glycosylation: heterogeneity and the 3D structure of proteins. *Crit Rev Biochem Mol Biol* **32**(1), 1-100.

Schuman, J., Campbell, A. P., Koganty, R. R. & Longenecker, B. M. (2003a). Probing the conformational and dynamical effects of O-glycosylation within the immunodominant region of a MUC1 peptide tumor antigen. *J Pept Res* **61**(3), 91-108.

Schuman, J., Grinstead, J. S. & Campbell, A. P. (2003b). **submitted**.

Stanfield, R., Cabezas, E., Satterthwait, A., Stura, E., Profy, A. & Wilson, I. (1999). Dual conformations for the HIV-1 gp120 V3 loop in complexes with different neutralizing fabs. *Structure Fold Des* **7**(2), 131-42.

Taylor-Papadimitriou, J., Burchell, J., Miles, D. W. & Dalziel, M. (1999). MUC1 and cancer. *Biochim Biophys Acta* **1455**(2-3), 301-13.

Tugarinov, V., Zvi, A., Levy, R. & Anglister, J. (1999). A cis proline turn linking two beta-hairpin strands in the solution structure of an antibody-bound HIV-1IIIB V3 peptide. *Nat Struct Biol* **6**(4), 331-5.

Van den Steen, P., Rudd, P. M., Dwek, R. A. & Opdenakker, G. (1998). Concepts and principles of O-linked glycosylation. *Crit Rev Biochem Mol Biol* **33**(3), 151-208.

Volkman, B. F., Alam, S. L., Satterlee, J. D. & Markley, J. L. (1998). Solution structure and backbone dynamics of component IV Glycera dibranchiata monomeric hemoglobin-CO. *Biochemistry* **37**(31), 10906-19.

Wandall, H. H., Hassan, H., Mirgorodskaya, E., Kristensen, A. K., Roepstorff, P., Bennett, E. P., Nielsen, P. A., Hollingsworth, M. A., Burchell, J., Taylor-Papadimitriou, J. & Clausen, H. (1997). Substrate specificities of three members of the human UDP-N-acetyl-alpha-D-galactosamine:Polypeptide N-acetylgalactosaminyltransferase family, GalNAc-T1, -T2, and -T3. *J Biol Chem* **272**(38), 23503-14.

Wittekind, M. & Mueller, L. (1993). *J Magn Reson Series B* **101**, 201.

Xing, P. X., Prenzoska, J. & McKenzie, I. F. (1992). Epitope mapping of anti-breast and anti-ovarian mucin monoclonal antibodies. *Mol Immunol* **29**(5), 641-50.

Yamazaki, T., Muhandiram, R. & Kay, L. E. (1994). NMR Experiments for the Measurement of Carbon Relaxation Properties inHighly Enriched, Uniformly 13C, 15N-Labeled Proteins: Application to 13C-alpha Carbons. *J Am Chem Soc* **116**(18), 8266-8278.

Zhang, P., Dayie, K. T. & Wagner, G. (1997). Unusual lack of internal mobility and fast overall tumbling in oxidized flavodoxin from Anacystis nidulans. *J Mol Biol* **272**(3), 443-55.

Zvi, A., Tugarinov, V., Faiman, G. A., Horovitz, A. & Anglister, J. (2000). A model of a gp120 V3 peptide in complex with an HIV-neutralizing antibody based on NMR and mutant cycle-derived constraints. *Eur J Biochem* **267**(3), 767-79.

Chapter 5: NMR Studies of an Isotope-labeled Antigenic Peptide in Complex with Class I MHC HLA-A*0201

ABSTRACT: T cell responses are an integral part of the human immune response to pathogenic bacteria and viruses. Recent clinical trials have attempted to use tumor-associated antigens to elicit immune responses capable of rejecting solid tumors. T cells recognize antigenic peptides when they are presented to the T cell on the surface of an antigen-presenting cell (APC). These peptides are presented on the surface of the APC in complex with Class I MHC molecules. The affinity of the peptide-MHC complexes determines their ability to stimulate T cells. Cancer-associated MUC1 mucin peptides are known to elicit T cell responses, although they bind MHC with low affinity. Increasing the affinity of these peptides for MHC without changing their specificity for the T cell receptor should lead to a more active immune response. Here, we demonstrate a methodology for generating peptide-MHC complexes and for studying these complexes using NMR spectroscopy. The methodology allows assay of changes in binding affinity for Class I MHC and characterization of the structural and dynamic properties of MUC1 peptide or glycopeptide.

Introduction:

Cytosolic proteins are routinely degraded by the proteasome into small, 8- to 10-residue peptides that are imported into the endoplasmic reticulum by the transporter associated with antigen processing (TAP). These peptides are then loaded onto newly translated Class I MHC proteins and trafficked to the cell surface, where they are

observed by circulating T cells. Cytotoxic T cells (expressing the cell surface receptor CD8) recognize and bind to surface-expressed Class I MHC-peptide complexes and determine if the presented peptide is from a self or foreign protein. In the case of a self-peptide, the T cell dissociates unactivated and continues to survey MHC-peptide complexes on the surface of other cells. In the case of a cell infected with a virus or bacterium, some of the peptides presented by Class I MHC will be of viral or bacterial origin. Binding of a T cell to these foreign peptide-MHC complexes causes T cell activation and lysis of the antigen presenting cell. Mature T cells in circulation recognize and bind only foreign peptide-MHC complexes because during the T cell maturation process in the thymus, T cells that recognize self peptide-MHC complexes are selectively destroyed.

In addition to pathogenic bacteria and viruses, cancer cells are also known to produce peptides capable of inducing an immune response, and recent clinical research has focused on generation of a cancer vaccine or immunotherapy. This seems counterintuitive, because cancer cells are self-cells, and therefore produce self-proteins. However, cancer cells also may produce a tumor-associated antigen, or a protein that is expressed differently in a tumor relative to a healthy cell. For example, mutations in protein sequence, altered glycosylation patterns, or differential protein expression can all result in a tumor-associated antigen that is capable of inducing a tumor-specific immune response. In the case of the tumor-associated MUC1 antigen, it is believed that reduced and aberrant glycosylation exposes the MUC1 protein and carbohydrate core to solution. In fact, two T cell epitopes have been identified in the MUC1 sequence: a 9-residue sequence (SAPDTRPAP) overlapping the B cell epitope (PDTRPA) (Apostolopoulos & McKenzie, 1994; Barnd *et al.*, 1989; Bashford *et al.*, 1993; Burchell *et al.*, 1989; Denton *et al.*, 1993; Ioannides *et al.*, 1993; Jerome *et al.*, 1991; Kotera *et al.*, 1994; Xing *et al.*,

1992) and a 9-residue sequence (STAPPAHGV) just downstream of this region (Apostolopoulos *et al.*, 1997a; Apostolopoulos *et al.*, 1997b; Domenech & Finn, 1995). Since MUC1 on healthy cells is normally heavily glycosylated, T cells specific for the MUC1 sequence are not deleted during thymic development, and therefore recognize the MUC1 sequence as a foreign antigen. Immune responses specific for the MUC1 sequence have been identified in breast cancer patients, and for this reason MUC1 has been the target of clinical research to develop a MUC1-based cancer vaccine.

Vaccine trials. First-generation MUC1 synthetic peptide vaccines have been designed from multiple repeats of the 20-amino acid MUC1 sequence (see Chapters 1 and 3 for a discussion of MUC1 structure). Conjugated and administered with the proper adjuvant, these peptides have generated B cell and T cell immune responses in animal models (Apostolopoulos *et al.*, 2000; Apostolopoulos *et al.*, 1996; Barratt-Boyes *et al.*, 1999; Lofthouse *et al.*, 1997; Vaughan *et al.*, 1999). Most encouraging were the immunization results with MUC1-transgenic mice where MHC Class 1 restricted CD8+ cytotoxic T-cells were produced that eradicated the MUC1 tumors and provided protection against further MUC1 tumor challenge (Apostolopoulos et al., 2000; Apostolopoulos et al., 1996; Lofthouse et al., 1997).

Unfortunately, the strong cellular immune responses observed in animals do not translate well to humans. Phase I & II clinical trials of a 5-repeat MUC1 peptide-GST fusion protein conjugated to oxidized mannan produced only weak T-cell proliferative responses in adenocarcinoma patients, demonstrating instead a high antibody titre indicative of a predominantly humoral immune response (Apostolopoulos et al., 1996; Goydos *et al.*, 1996; Karanikas *et al.*, 1997). Several other recent clinical trials have explored the use of MUC1 peptides coupled to different haptens, keyhole limpet

hemocyanin, glutathione S-transferase, and oxidized mannan (Apostolopoulos *et al.*, 1999). All of these clinical trials have demonstrated predominantly humoral immune responses, and none have been able to shrink the solid tumor. Therefore, boosting MUC1-specific cellular immunity in adenocarcinoma patients may be essential to successful development of a MUC1-based cancer vaccine, although this still represents a major hurdle in MUC1 vaccine design.

Structural studies of Class I MHC-presented tumor-associated antigens. Many groups are presently studying the structural basis for T cell recognition of antigen, with the hope of designing a vaccine capable of inducing an immune response effective at destroying solid tumor. CD8+ cytotoxic T cells (CTL) are the primary immune mechanism for killing diseased cells. These T cells recognize antigenic peptides that are bound to cell surface-expressed Class I MHC. Some of the principles for Class I-restricted CTL recognition of antigen in cellular immunity have been defined recently (Garcia *et al.*, 1999a; Garcia *et al.*, 1999b; Hennecke & Wiley, 2001). Central to these principles is an understanding of how Class I MHC binds and presents peptide to the T cell receptor. Class I MHC binds 8- to 10-residue peptides along a platform of eight antiparallel β-strands between two α-helices that make a conserved network of hydrogen bonds to the main chain of the bound peptide (depicted in Figure 5.1) (Madden, 1995). Conserved hydrogen bonding of the peptide N- and C-termini anchor the ends of the antigenic peptide in the MHC binding groove and produce the 8- to 10-residue length preference. Detailed structural studies have identified six different pockets (A-F) in the beta sheet platform of the Class I MHC molecule HLA-A*0201 (Apostolopoulos *et al.*, 2002). The two main pockets (B and F) bind the canonical sidechains of the N-terminal and C-terminal peptide residues, located at position 2 (P2) and 9 (P9) of the sequence. The

canonical P2 and P9 anchor residues are necessary, but not sufficient, for high affinity binding, because the fit of secondary anchors into the remaining four pockets has been shown to modulate affinity of the peptide-MHC complex. Table 5.1 lists the HLA-A*0201 binding pocket preferences for canonical (P2, P9) and secondary (P1, P3-P8) anchor residues.

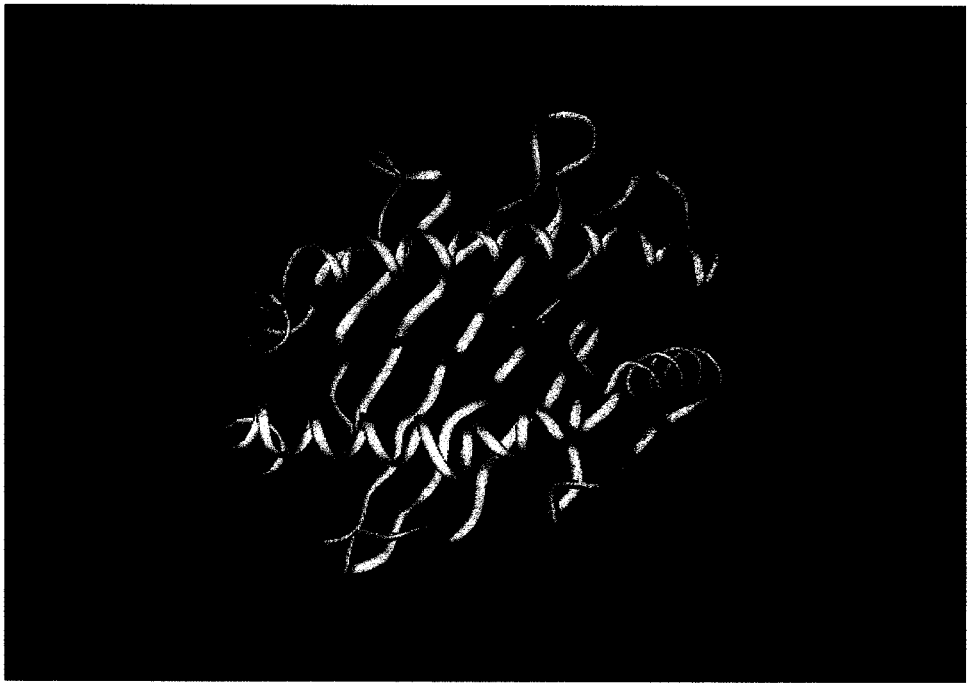

Figure 5.1: Crystal structure of human Class I MHC HLA-A*0201 (in yellow) (Madden *et al.*, 1993). The bottom of the peptide binding groove is formed by a β-sheet, with two α-helices forming the sides of the groove. A MUC1 peptide (in red) is modeled bound to the MHC.

Viral antigens that bind with high affinity to HLA-A*0201 contain a high proportion of preferred sidechains for the secondary anchor residues. In contrast, many peptide tumor antigens that bind with weak affinity to HLA-A*0201 contain the preferred sidechains for the canonical P2 and P9 anchor residues, but lack preferred sidechains for the secondary anchor residues. Furthermore, a handful of peptide tumor antigens (MUC1

included) lack one or both of the preferred sidechains for P2 and P9, as well as many of the preferred sidechains for the secondary anchor residues (see Table 5.2). Surprisingly, these non-canonical weak-binding peptides are still presented by Class I MHC to elicit a CTL response (Apostolopoulos et al., 1997b).

Table 5.1: HLA-A*0201 Binding Pocket Preferences.

Position	Pocket	Sidechain	Local Hydrophobicity
P1	A	Aromatic favored	Hydrophobic preferred
P2	B	Long favored	Hydrophobic preferred
P3	D	Aromatic favored	Hydrophobic preferred
P4		Branched disfavored	Hydrophilic preferred
P5		Branched, aromatic preferred	Hydrophilic preferred
P6	C		
P7	E	Short favored	Hydrophobic preferred
P8		Short favored	Hydrophilic preferred
P9	F	Short required	Hydrophobic preferred

Several recent crystal studies of Class I MHC-associated peptide tumor antigens have begun to reveal the structural basis for the low affinity binding exhibited by both canonical and non-canonical binders. In a study using HLA-A*0201, the weakly binding HER-2/neu epitope **I**ISAVVGI**L** (which contains the preferred P2 and P9 anchor residues in bold) was not found to make stabilizing contacts with the center of the peptide binding cleft, leading to uninterpretable electron density within the center of the peptide (Boniface *et al.*, 1999). The authors concluded that the center of the peptide does not assume one unique conformation, and may be interconverting between several

conformational states. Most relevant to the present study is a crystal structure of murine H-2k^b in complex with an 8-residue MUC1 peptide that spans the overlapping B-cell/T-cell epitope SAPDTRPA (Rudolph & Wilson, 2002). Although the MUC1 peptide contains only small nonpreferred sidechains in the anchor positions, it was still found to bind with the same overall features as high affinity peptides, i.e. the peptide was

Table 5.2: HLA-A*0201 Epitope Sequences.

High-affinity HLA-A2 Epitope Sequences (mainly viral antigens)		
Canonical Binding Peptides	**Peptide**	**Source**
	I L K E P V H G V	HTV-1 RT
	L L F G Y P V Y V	HTLV-1 Tax
	G I L G F V F T L	Influenza A matrix
	T L T S C N T S V	HIV-1 gp120
	F L P S D F F P S V	Hepatitis B
Low-affinity HLA-A2 Epitope Sequences (mainly tumor-associated antigens)		
Canonical Weak-Binding Peptides	**Peptide**	**Source**
	P L Q P E Q L Q V	HER2/neu 369
	T L E E I T G Y L	HER2/neu 402
	L L G R N S F E V	p53(264-272)
	F L W G P R A L V	MAGE-3(271-279)
	Y M D G T M S Q V	Tyrosinase(368-376)
	I M D Q V P F S V	gp100(280-288)
Non-Canonical Weak-Binding Peptides	**Peptide**	**Source**
	S A P D T R P A P	MUC1
	S T A P P A H G V	MUC1
	E A A G I G I L T V	MART-1/Melan-A(26-35)

anchored at the N- and C-termini. However, deviations from canonical binding were observed in the center of the peptide. Small secondary anchors at positions P2, P5 and P8, the absence of water-mediated hydrogen bonds, and a large cavity at the side of the C pocket (accompanied by a high B factor for the P5 sidechain) were hypothesized to account for the low affinity of the peptide for MHC. Despite the fact that a murine (H-

$2k^b$) haplotype was used in these studies, the H-$2k^b$/MUC1 structure does suggest that the weak anti-MUC1 T-cell immune responses observed in humans may similarly be linked to a poor fit of non-canonical MUC1 sidechain anchors in human Class I MHC pockets. Furthermore, the high B factors and weak electron densities observed in the HLA-A*0201/HER-2/neu and H-$2k^b$/MUC1 crystal structures suggest a correlation between poor fit and increased peptide backbone and sidechain motions. The putative flexibility of the MHC-bound MUC1 antigens has consequences for the kinetic and thermodynamic properties of T cell receptor/peptide-MHC recognition, modulation of T cell selection, T cell activation, and even alloreactivity (Oukka *et al.*, 1996; Rudolph *et al.*, 2002; Sette *et al.*, 1994; Sundberg & Mariuzza, 2000).

Structural approach to characterizing and optimizing MUC1 T cell epitope presentation. An observed correlation between immunogenicity and peptide-MHC binding affinity (Haurum *et al.*, 1994; Tourdot *et al.*, 2000; van der Burg *et al.*, 1996) has led to the proposal that once the basis for low affinity MHC binding of breast TAAs has been identified, MUC1 antigenic peptides or glycopeptides might be modified to increase Class I MHC-binding affinity, and thus the strength of the CTL response against the parent tumor (Mouritsen *et al.*, 1994). In theory, it is possible to identify the structural and dynamic features that account for the low affinity, then modify these features to increase Class I MHC binding. As an illustration of this concept, thirty-two low affinity peptides derived from tumor and viral antigens were recently converted to high affinity HLA-A*0201 binders by replacing the amino acid at P1 with tyrosine (Mouritsen et al., 1994). Our approach uses a similar concept, and is outlined in Figure 5.2. The first phase of our approach involves determining the unique structural and dynamic features of each MHC-peptide or glycopeptide complex. For example, the first phase of the

approach could involve a determination of which peptide sidechains are responsible for binding MHC versus interaction with the TCR, or a determination of how carbohydrate moieties on a MUC1 tumor-associated glycopeptide might be available to interact with TCR.

The second phase of our approach involves selective modification of both canonical and secondary sidechain anchors to enhance complex stability, while leaving unaltered the upper face of the peptide that interacts with the T cell receptor. If we

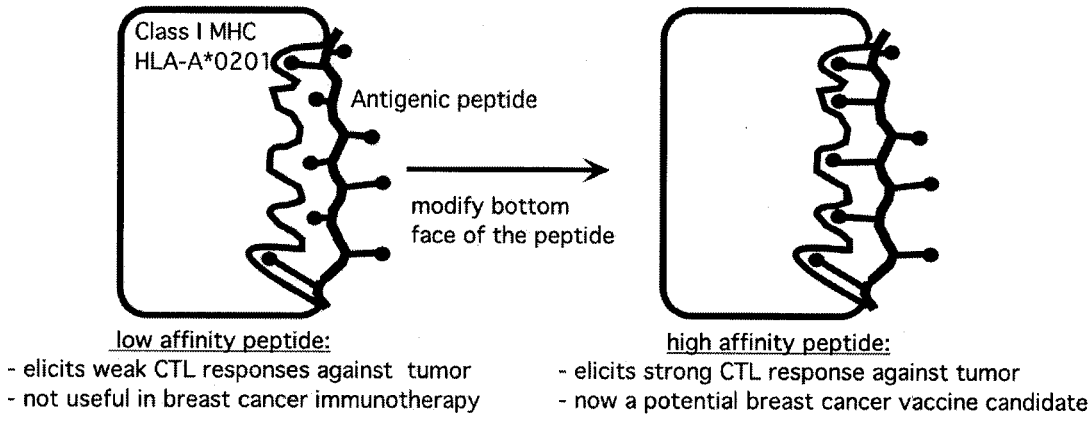

Figure 5.2: Outline of structural hypothesis for optimization of MUC1 peptide vaccines binding to Class I MHC. A breast tumor associated antigenic peptide may have poor sidechain complementarity with MHC binding pockets. Characterization of which peptide sidechains do not properly occupy the pockets, followed by rational mutation, should improve affinity of the peptide for MHC without altering the upper face of the peptide that interacts with the T cell receptor.

determine that MUC1 tumor-associated carbohydrates are responsible for anchoring MUC1 glycopeptides in the MHC binding groove, then these carbohydrate moieties might also be altered to optimize MUC1 presentation to TCR. Ultimately, our two-phase approach should allow redesign of a more immunogenic MUC1 vaccine.

NMR spectroscopy provides an excellent technique for determining the unique structural and dynamic features of each Class I MHC-associated peptide tumor antigen. In fact, NMR may provide the only viable structural technique in the case of low-affinity MHC binding, where the absence of stabilizing contacts across the peptide-MHC interface leads to conformational heterogeneity of the bound peptides. For systems like the MUC1-MHC complex, the NMR technique is arguably at its strongest, with its ability to characterize structurally interconverting states and measure timescales of interconversion. NMR spectroscopy can also identify MUC1 backbone and sidechain atoms buried in the MHC binding cleft versus pointed toward a potential interaction with the T cell receptor. We have made significant progress in generating MHC refolded with ^{15}N-/^{13}C-labeled antigenic peptides, and preliminary NMR experiments have been performed. The results of these experiments are discussed within the context of developing a system to study the structure and dynamics of HLA-A*0201-bound MUC1 peptide tumor antigens for the purpose of defining features of low-affinity MHC binding and mechanisms of T cell activation.

Materials and Methods:

Peptide synthesis. Peptides were synthesized using an ABI system synthesizer with standard FMOC chemistry. Peptides were synthesized on the 250 μmol scale, and at least a 4-fold molar excess of each unlabeled amino acid was used. An equimolar equivalent was used for the isotope-labeled amino acids.

Synthesis of ^{13}C-/^{15}N-labeled valine and alanine. Uniformly ^{13}C and ^{15}N-labeled valine and alanine were purchased from Cambridge Isotope Laboratories (Cambridge, MA).

FMOC-ethyl ester (9-fluorenyl methyl oxycarbonate-ethyl ester) was purchased from SIGMA (IL). Labeled valine and alanine were solubilized separately in a mixture of DMF:MeOH:pyridine along with FMOC-ethyl ester. Reaction progress was monitored using thin-layer chromatography. The products FMOC-valine and FMOC-alanine were purified using flash column chromatography (silica) in MeOH:Acetic acid, running a gradient from 95:5 to 50:50. Solvent was removed from the fractions by rotary evaporation to leave a gel. The gel was highly hygroscopic, yet not water-soluble. Therefore, the product was solubilized in a minimal amount of methanol, and water was added to cause a fine, suspended white precipitate to form. The methanol was removed by rotary evaporation, and the resulting suspension was lyophilized. The flocculent, white, highly hygroscopic lyophilate was stored at -20°C under nitrogen gas to prevent water absorption. Product left exposed to moisture in the air turned into a gel within 24 hours.

*Expression and purification of HLA-A*0201 subunits.* The HC and β_2m of HLA-A*0201 were expressed separately in *E. coli* and purified as previously published (Garboczi *et al.*, 1992). In brief, HLA-A*0201 HC and β_2m subunits were expressed as inclusion bodies. Bacterial cell pellets were lysed, insoluble inclusion bodies were pelleted and washed multiple times with detergent, and then with buffer. Inclusion bodies were then solubilized with 6M guanidine buffer and remaining insoluble material removed by centrifugation.

*Refolding of HLA-A*0201/peptide complexes.* HLA-A*0201 HC and β_2m inclusion bodies were refolded according to a published redox-shuffling refolding protocol (Garboczi et al., 1992), by diluting the HC into buffer with β_2m, antigenic peptide,

arginine, and the redox pair cystamine/cysteamine. Refolded complexes were dialyzed against pure water to remove arginine.

Column chromatography. Refolded, dialyzed, concentrated HLA-A*0201/peptide complex was purified using a DEAE weak anion exchange column, followed by Superdex 200 and Superdex 75 size exclusion chromatography. The DEAE column was equilibrated with 10mM Tris-HCl, pH 8. Sample was loaded on the column, washed, and then eluted with a NaCl gradient (0-500mM). The major peak was concentrated and further purified on the size exclusion columns. Size exclusion columns were run using 10mM Tris, pH 8 isocratically. Peak elution was monitored by absorbance at 280nm, and standard molecular weight proteins (BSA, ~60kDa; cyt b_5, ~11kDa) were used to calibrate the retention time of the HLA-A*0201 complex (~42kDa) and the excess β_2m (~12kDa).

*Characterization of purified HLA-A*0201 complex.* Antibody W6/32 (specific for correctly folded HLA-A family proteins) was used in an immunoprecipitation assay to identify the refolded HLA-A*0201. Purified protein was incubated for two hours at room temperature with antibody W6/32. Next, protein A covalently linked to sepharose beads was added to bind to the antibody/HLA-A*0201 complex. The sepharose beads were recovered by centrifugation and rinsed several times with buffer to remove any contaminating proteins. The original supernatant and the final precipitated product were analyzed on a 20% SDS-PAGE with purified HLA-A*0201 as a standard.

*Generation of uniformly ^{13}C-/^{15}N-labeled peptides for refolding with HLA-A*0201.* In order to generate uniformly labeled peptides for refolding with HLA-A*0201, a cloning

strategy similar to that discussed in Chapter 4 was used. However, since the N- and C-termini of the antigenic peptides are essential for native hydrogen bonding interactions with the HLA-A*0201 binding groove, the C-terminal homoserine left by the cloning process had to be removed. Therefore, a strategy for cloning a longer peptide sequence followed by proteolytic cleavage of the peptide into the desired sequence was used. Initial studies with this protocol were performed to generate a MUC1 peptide sequence predicted to bind to HLA-A*0201. The 8mer sequence SAPDTRPA is known to bind to murine H-2k^b, so the following peptide sequence was designed: SAPDTRPAKVWPAM. After CNBr cleavage from the fusion protein, the C-terminal methionine becomes a homoserine (SAPDTRPAKVWPAhs). This initial peptide sequence was then digested with 0.1 equivalents of trypsin (recrystallized Type I from bovine pancreas) to cleave C-terminal of the lysine residue into two peptide fragments (SAPDTRPAK and VWPAhs). The trypsin reaction was specific for the lysine residue and not for the arginine residue, because trypsin will not cleave at a basic residue followed by a proline. Identical results were obtained for sequencing grade trypsin, so the lower grade recrystallized trypsin was used. The N–terminal fragment was purified using HPLC (it is easily distinguishable from the C-terminal fragment because the C-terminal fragment absorbs light at 280nm due to the tryptophan residue). The N-terminal fragment was then digested using 0.01 equivalents of carboxypeptidase B to cleave the basic lysine from the C-terminus of the peptide to leave the peptide SAPDTRPA. This peptide was also purified using HPLC. Intermediate and final products were identified using MALDI MS, as well as comparison of HPLC retention times to a synthetic SAPDTRPA peptide.

In theory, the same protocol can be extrapolated to many sequences. For example, the MUC1 sequence STAPPAHGVKVWPAM (another MUC1 T cell epitope) could be used. Other MUC1 peptides related to the sequence containing the B-cell

epitope sequence APDTRPAP could also be cloned. The only requirement for using this strategy is that the peptide sequence must contain no basic residues, unless they are followed by a proline.

NMR samples. All NMR samples were exchanged into 90%H_2O/10%D_2O PBS buffer, pH 7.1, with 0.02% sodium azide. HPLC-pure peptide samples were lyophilized and resuspended in buffer. Protein samples were buffer-exchanged using a 10,000 MWCO of 30,000 MWCO centrifugal filter. All NMR experiments were performed on a Varian Inova 500 MHz spectrometer.

Results:

*Synthesis of ILKEPV*HGV labeled with ^{13}C and ^{15}N at valine 6.* ^{1}H NMR and ^{1}H-^{13}C HSQC spectra demonstrate correct synthesis of labeled ILK peptide. In addition, MALDI mass spectra gave the correct isotopic mass for the peptide, 6 mass units larger than the unlabeled peptide.

*Expression and refolding of HLA-A*0201.* The SDS-PAGE in Figure 5.3 demonstrates expression of the HLA-A*0201 HC and β_2m subunits separately in *E. coli.* In order to assess the feasibility of the refolding protocol, the tight-binding viral peptide antigen from HIV-1 RT, ILKEPVHGV (ILK), was used in initial refolding trials with the bacterially expressed HLA-A*0201 protein subunits. In addition, refolding of HLA-

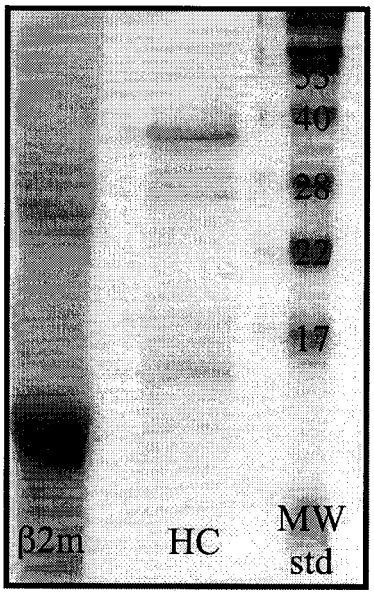

Figure 5.3: SDS-PAGE of purified inclusion bodies of Class I MHC HLA-A*0201 HC and β_2m subunits expressed in *E. coli*. The HC (~33kDa) and β_2m (~11kDa) inclusion bodies are relatively pure before subsequent refolding with peptide.

A*0201 with the ILK peptide was compared to refolding with three different MUC1 peptides: GVTSAPDTRPAPGSTA, SAPDTRPA, and STAPPAHGV. Figure 5.4 depicts size exclusion chromatography traces of HLA-A*0201 refolded with these peptides. Panel A shows the complex with the ILK peptide. The major peak eluted at the molecular weight corresponding to the correctly refolded HC/β_2m/peptide complex (~42kDa). A minor peak eluted at the molecular weight of free β_2m, and is due to excess β_2m present in the refolding mixture. Panel B shows the same refolding protocol, but using the MUC1 16-residue peptide GVTSAPDTRPAPGSTA. In this trace only the β_2m peak is present, because the peptide failed to refold any of the HC. This is not surprising, since the HLA-A*0201 molecule prefers to bind 8- to 10-residue peptides. Panel C shows refolding of the HLA-A*0201 subunits with the MUC1 peptide STAPPAHGV. This trace depicts free β_2m, some large aggregates, and also a large peak corresponding to correct refolding of the HLA-A*0201-peptide complex. Finally, Panel D depicts the

trace of the same refolding protocol performed with the MUC1 peptide SAPDTRPA. This refolding exhibits a large free β_2m peak, many species of large, soluble aggregates, and very little specific refolding into the soluble, monomeric complex. The SEC traces in Figure 5.4 demonstrate that the refolding process was highly efficient using the viral ILK peptide. Refolding efficiency was lower with the MUC1 peptides, with the STAPPAHGV peptide (containing one of the canonical sidechain anchor residues) demonstrating higher refolding efficiency relative to the other two MUC1 sequences (containing none of the canonical sidechain anchor residues). Fractions corresponding to the correctly refolded complex with ILK were further purified on a Superdex 75 size exclusion column (shown in Figure 5.5). The results of an immunoprecipitation assay with the conformationally sensitive antibody W6/32 (specific for HLA-A family proteins) positively identified the purified complex, and are shown in Figure 5.6. Identical immunoprecipitation results were obtained when refolding unlabeled or isotope-labeled ILK peptides with HLA-A*0201.

*NMR spectroscopy of HLA-A*0201 complexes.* Figure 5.7 shows the 1D ^{1}H NMR spectra of the free peptide and the HLA-A*0201 complex. No free peptide resonances are observable, although spectral overlap prevents observation of small peptide peaks. Several characteristics of the refolded complex can be ascertained from the 1D spectrum. Between 0.7 and –1 ppm, several protein methyl resonances are visible. These peaks are upfield-shifted from their normal positions near 0.9 ppm due to ring-current shifts from nearby aromatic residues in a well-packed hydrophobic core of the refolded complex. The spectrum also shows amide resonances downfield of 10 ppm, indicative of folded beta secondary structure. The 1D spectrum implies that the protein is correctly folded

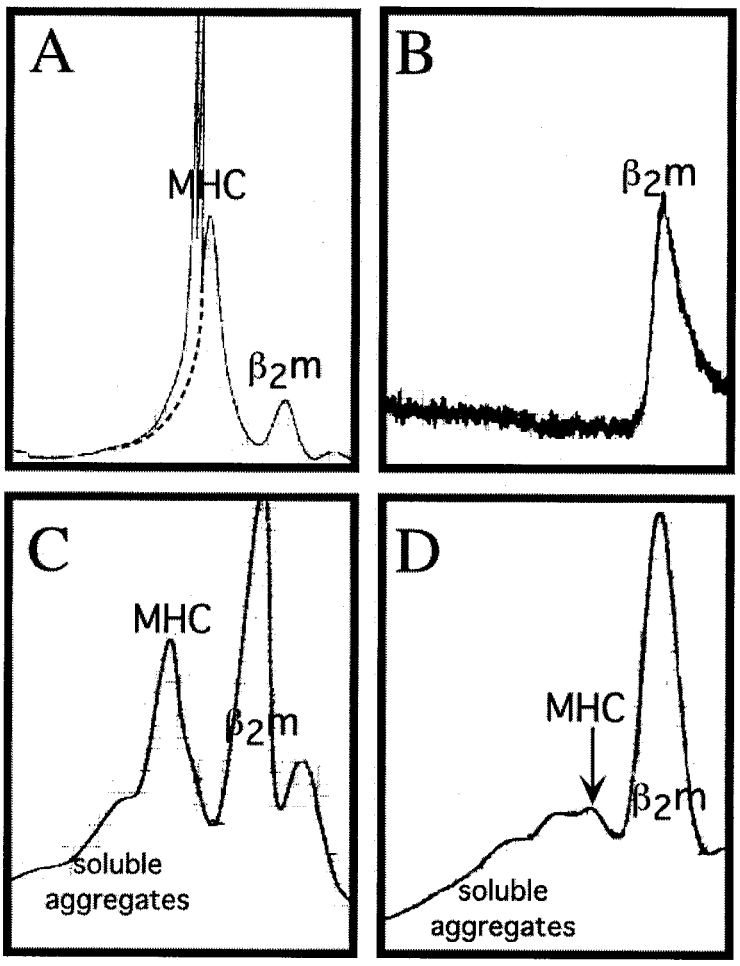

Figure 5.4: Size exclusion chromatography traces of HLA-A*0201 HC and β_2m subunits refolding with antigenic peptides. Panel A shows efficient refolding with the viral ILKEPVHGV peptide. The two peaks in the trace are correctly refolded complex and free β_2m (excess in the refolding reaction). None of the HC is observed in the traces because it is insoluble free in solution. Panel B shows the same refolding protocol, but with the MUC1 16mer peptide GVTSAPDTRPAPGSTA. None of the HC was solubilized in the refolding, because the peptide is too long to bind MHC. Panel C shows refolding with the MUC1 9mer peptide STAPPAHGV. The efficiency of refolding was not at efficient as the ILK peptide. Panel D shows refolding with the MUC1 8mer peptide SAPDTRPA. The efficiency of this refolding is much worse than the ILK peptide.

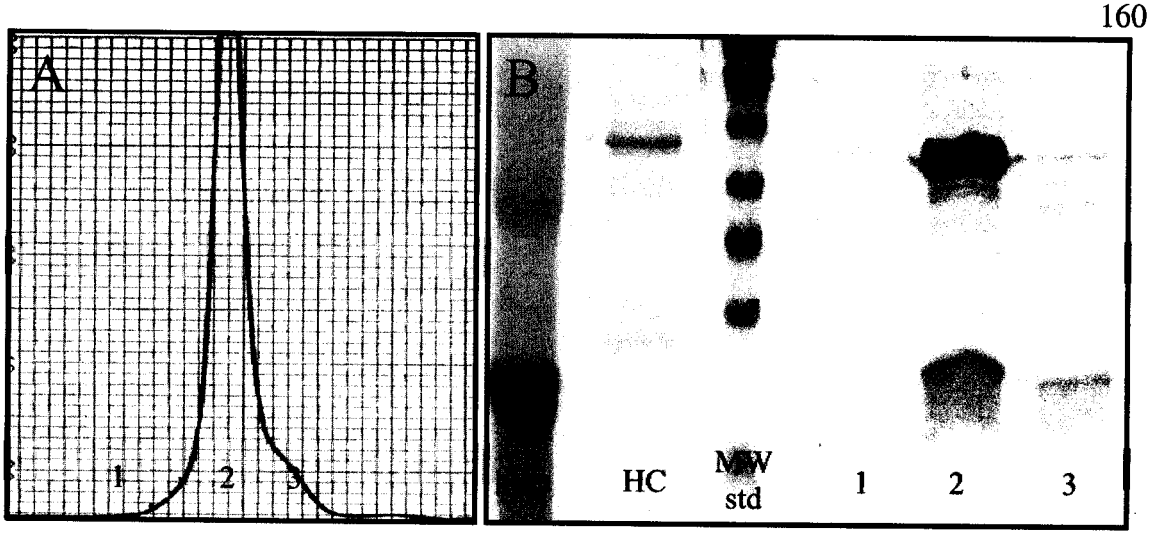

Figure 5.5: Panel A shows the SEC trace of HLA-A*0201 refolded with the ILK peptide. Panel B shows an SDS-PAGE of the fractions from the SEC. The purified complex breaks down into its HC and β_2m subunits on the SDS-PAGE.

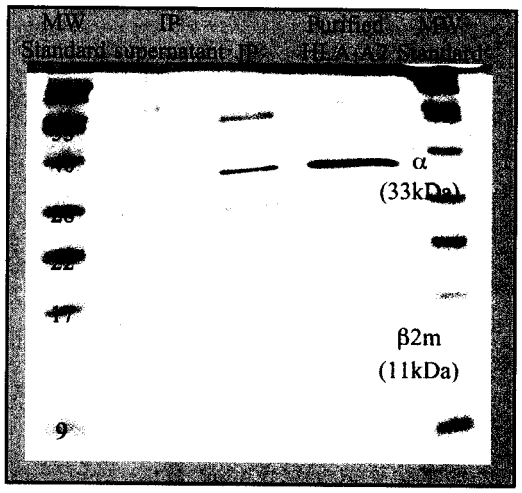

Figure 5.6: Immunoprecipitation of purified HLA-A*0201/ILK complex with antibody W6/32, which is specific for correctly folded HLA-A family proteins. The immunoprecipitation supernatant lane shows no HLA-A*0201. The immunoprecipitation lane shows both HC and β_2m subunits, as well as the antibody heavy and light chains.

and well structured. Figure 5.8 shows the 2D ^{1}H-^{13}C HSQC spectra of the unlabeled HLA-A*0201 complex refolded with unlabeled peptide in panel A. Several peaks are observed at natural abundance from the unlabeled protein. Panel B shows the 2D ^{1}H-^{13}C

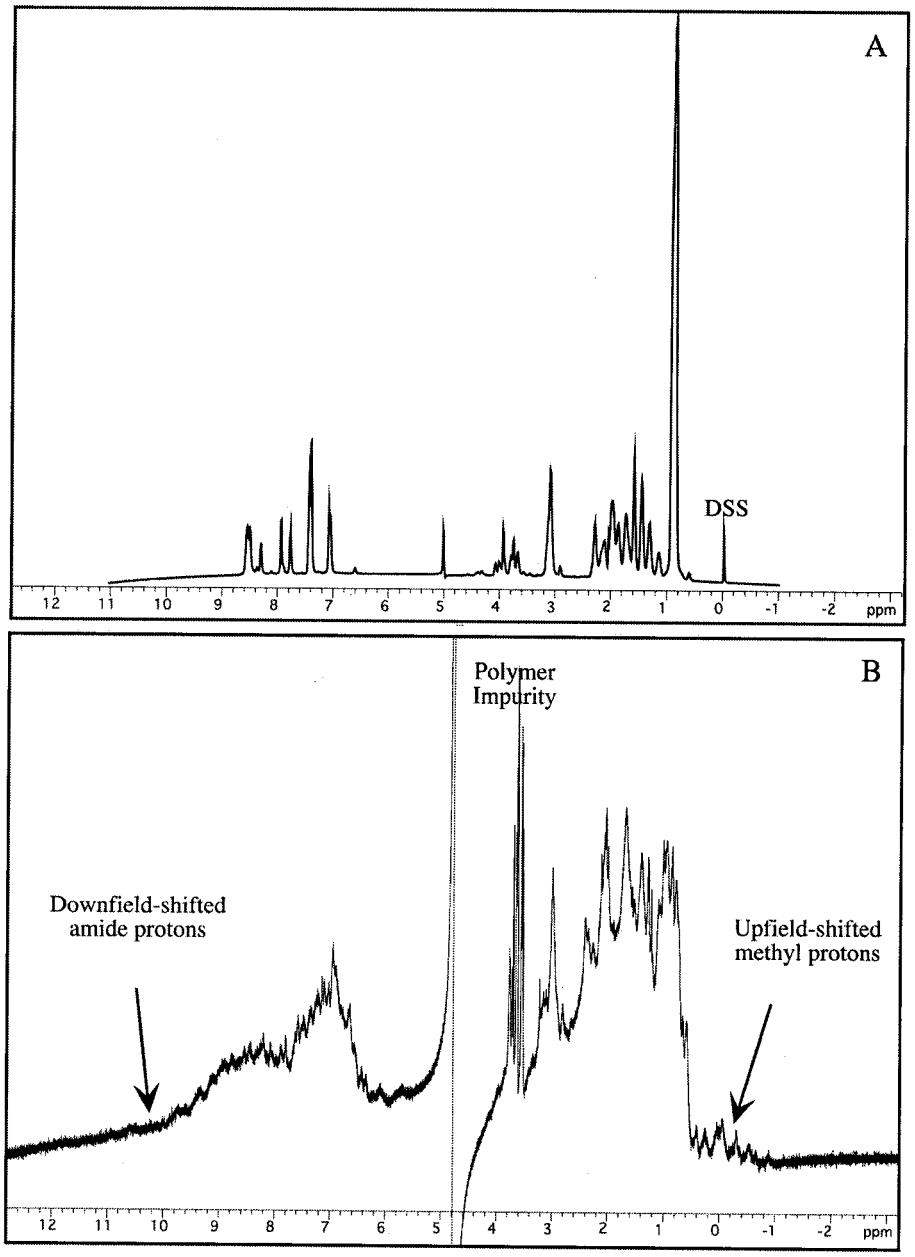

Figure 5.7: 1D ^{1}H NMR spectra of free ILK peptide (A) and the HLA-A*0201 complex (B). In the complex, upfield-shifted methyl protons indicate hydrophobic packing within the refolded complex, and downfield-shifted amide protons are characteristic of beta sheet structure.

Figure 5.8: ^{1}H-^{13}C HSQC spectra of unlabeled HLA-A*0201/ILKEPVHGV complex. The top panel shows the protein refolded with unlabeled ILK peptide. Only natural abundance peaks from the protein are observed. The bottom panel shows the protein refolded with the ILKEPVHGV peptide unniformly labeled at valine 6 with ^{15}N and ^{13}C. In this spectrum, new peptide peaks appear that are most likely from the peptide valine methyl groups. The peaks do not correspond to the free peptide peaks, which are overlaid in red.

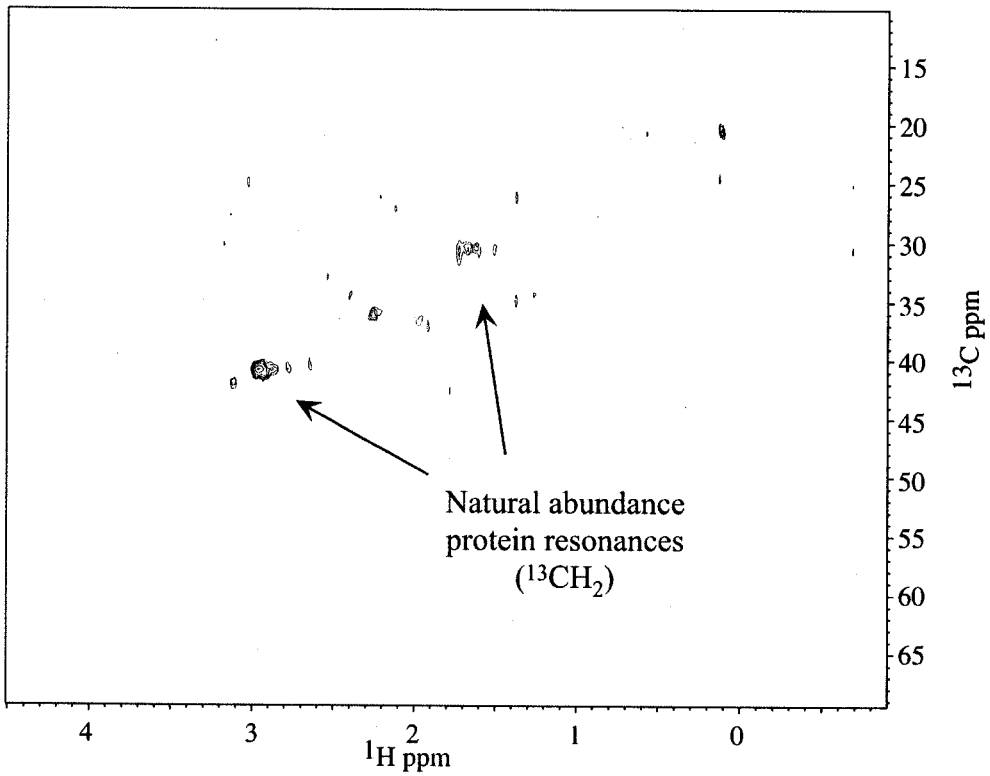
Natural abundance
protein resonances
($^{13}CH_2$)
^{13}C ppm
^{1}H ppm

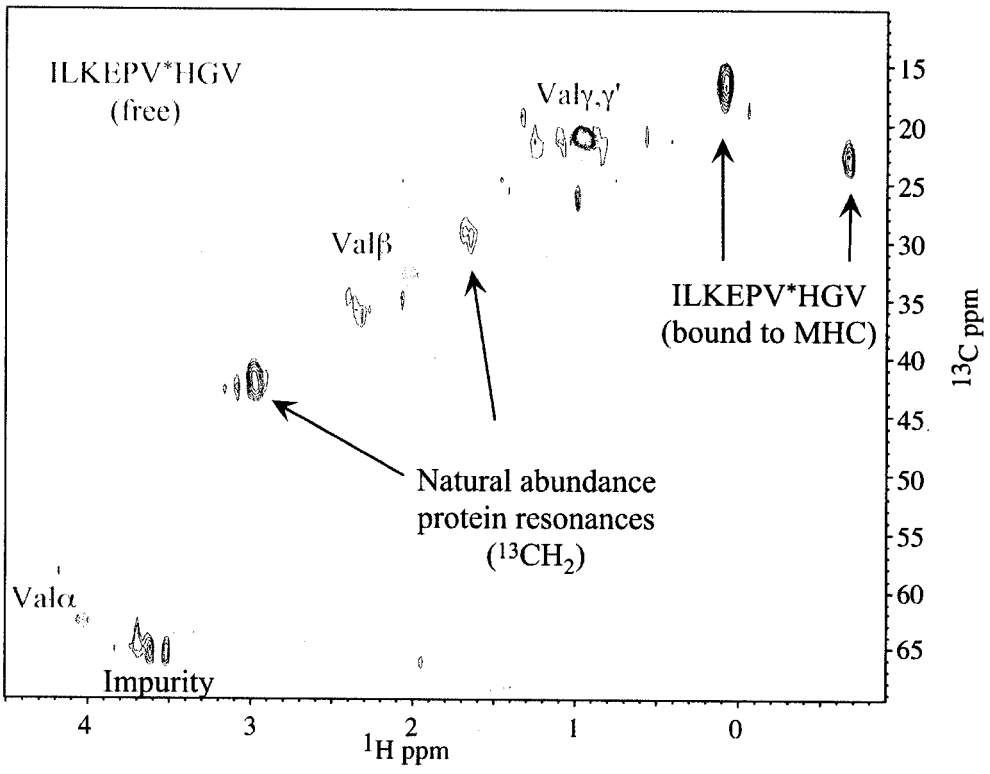
ILKEPV*HGV
(free)
Valγ,γ'
Valβ
ILKEPV*HGV
(bound to MHC)
Natural abundance
protein resonances
($^{13}CH_2$)
Valα
Impurity
^{13}C ppm
^{1}H ppm

HSQC spectrum of the same protein refolded with ILK peptide with uniformly ^{15}N-/^{13}C-labeled valine at position 6. Superimposed upon this spectrum is the 2D ^{1}H-^{13}C HSQC spectrum (in red) of the free ILK peptide with uniformly labeled valine 6. The free peaks for valine 6 do not appear in the spectrum with the HLA-A*0201/peptide complex, indicating no free peptide in solution. In the spectrum of the complex with isotope-labeled ILK peptide, two new peaks appear in the spectrum. These resonances are from valine 6 in the bound peptide, and they experience a strong upfield shift in their chemical shift relative to their position in the free state. This shift could be due to close contact with aromatic sidechains in the HLA-A*0201 binding groove. In Figure 5.9 is the 2D ^{1}H-^{15}N HSQC spectrum of the HLA-A*0201-peptide complex. One resonance is observed for the ^{1}H-^{15}N bond vector of the valine 6 amide group, highly upfield-shifted from the free peptide resonance (in red). In addition, the linewidth of the bound resonance (> 50 Hz) is much greater than that of the free peak (~20 Hz), reflecting the large size of the complex relative to the free peptide.

Initial NMR studies using the HLA-A*0201-ILK peptide complex were completed. The results imply that the sidechain of the isotope-labeled valine 6 interacts with the MHC binding pocket and has close contact with aromatic sidechains. This contact causes strong upfield shifting of the valine methyl resonances from 0.97 ppm to 0.1 ppm and –0.6 ppm. The loss of chemical shift degeneracy for these two methyl resonances also implies that the sidechain rotation is hindered so that the methyl groups do not exist in identical magnetic environments. Figure 5.10 shows the crystal structure of the ILK peptide bound to HLA-A*0201. In the figure, the valine 6 sidechain is pointed into the MHC binding groove. In addition, aromatic sidechains within 5Å of the residue are shown. Several histidine and tyrosine sidechains are shown that could be responsible for the aromatic ring current shifting of the valine methyl groups.

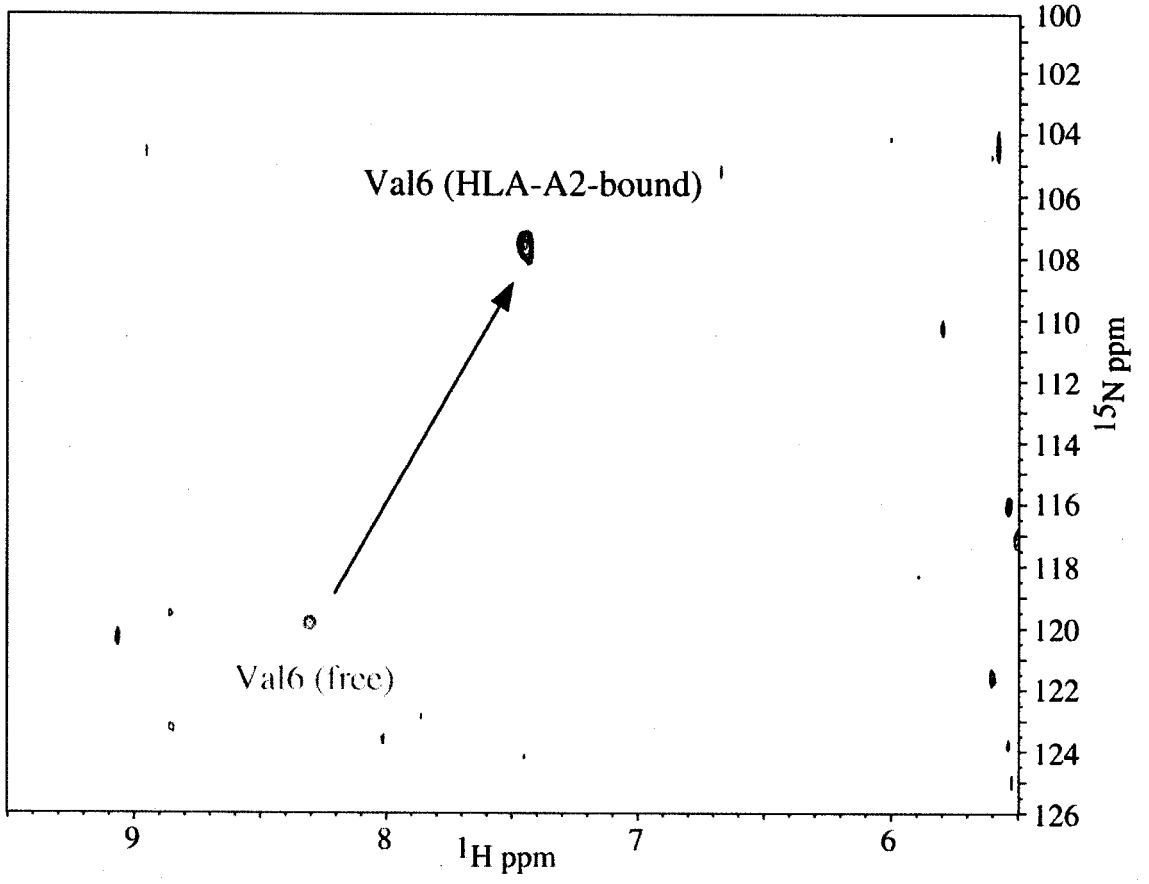

Figure 5.9: 2D ^{1}H-^{15}N HSQC spectra of the free ILK peptide in red (uniformly labeled at valine 6) superimposed on the spectrum of the same peptide in complex with HLA-A*0201. The resonance for the bound peptide exhibits a dramatic upfield shift and broadened linewidth relative to the free peptide.

Further NMR experiments. Subsequently, 3D triple resonance and NOESY-based experiments were attempted for the purpose of assigning the bound peptide peaks and gaining structural information about the orientation of the valine 6 sidechain. However, since the large size of the ternary HLA-A*0201-peptide complex results in fast transverse spin-spin relaxation, the signal-to-noise decreased dramatically for those longer 3D pulse sequences (the result of dipolar relaxation with neighboring proton nuclei prior to acquisition), and no usable data were obtained. It is difficult to obtain solution structures from larger proteins, but many systems larger than the HLA-A*0201-peptide complex

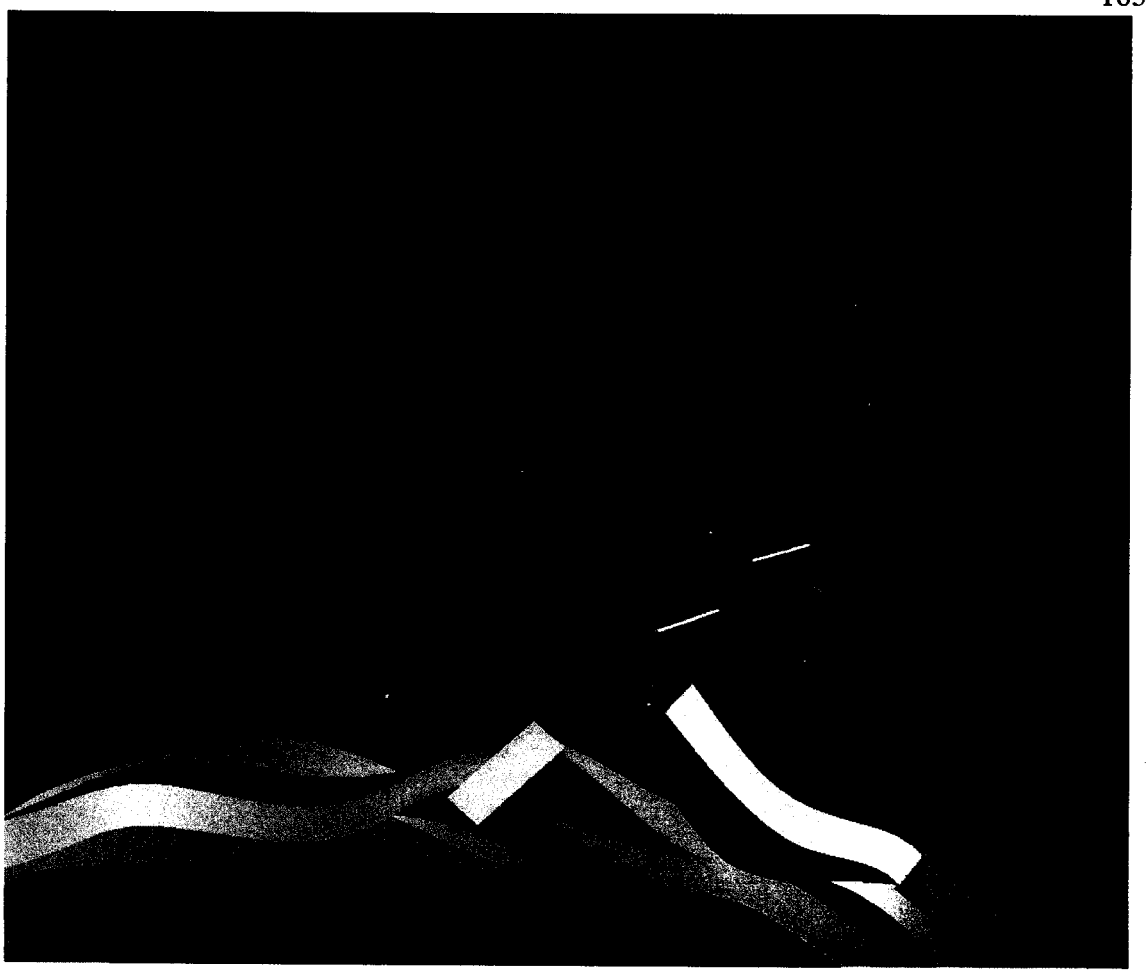

Figure 5.10: Crystal structure of ILK peptide bound to Class I MHC HLA-A*0201 (Madden et al., 1993). The α-helices flanking the binding groove have been removed in the figure for ease of view. The bound ILK peptide is colored purple, and the labeled valine is colored cyan. HLA-A*0201 sidechains within 5Å of the peptide valine sidechain are shown in yellow. Ring current shifts from these histidine and tyrosine sidechains could be responsible for upfield shifting of the peptide resonances of the complex.

have been studied using several techniques. Partial or full deuteration of recombinant proteins reduces transverse relaxation rates of the protein considerably and can be achieved by growth in deuterated minimal media (Venters *et al.*, 1995). In addition, deuteration schemes that retain protons for the methyl groups of isoleucine, leucine and valine sidechains offers a method for reducing transverse relaxation rates while also

retaining some protons for getting NOE information (Goto *et al.*, 1999). Transverse relaxation optimized spectroscopy (TROSY) has recently been developed as a way to obtain narrower linewidths for large proteins (Pervushin *et al.*, 1997). In addition, selective isotope labeling of protein domains or ligands reduces the spectral complexity of some larger systems. All of these techniques can be utilized with the study of Class I MHC-bound antigenic peptides. Therefore, to obtain structural information about the MHC-bound peptide structure and dynamics, deuteration of the MHC appears to be necessary. It should be noted that our observation of bound peptide resonances without the benefit of fractionally deuterated protein or TROSY-based pulse sequences speaks to the feasibility of 3D NOESY or triple resonance experiments on the system, provided that deuterated protein and TROSY-based pulse sequences are used. These sophisticated 3D NMR experiments should then allow the assignment of uniformly labeled peptides bound to Class I MHC HLA-A*0201, a prerequisite for the structural or dynamics studies proposed herein.

*Deuteration of HLA-A*0201.* Although growth of the HLA-A*0201 HC and β_2m subunits in deuterated minimal media was attempted, it was not successful. Protein expression in unlabeled LB media did not transfer to the deuterated cultures. The reasons for this are unknown. A new HLA-A*0201 plasmid was obtained that is a single chain version of the HC and β_2m subunits that utilizes a 15 amino acid (glycine and serine) flexible linker to connect the two domains. This construct expressed the single chain MHC (scMHC), and expression was under IPTG induction control. However, in our initial studies the protein did not express in deuterated media.

Conclusions and Future Directions:

Using a methodology that assembles Class I MHC from heavy chain (HC) and β_2m subunits expressed separately in *E. coli* (Garboczi et al., 1992), we have successfully refolded Class I MHC with several synthetic peptides. These peptides include a 9-residue viral peptide antigen from HIV-1 RT (ILKEPVHGV) containing the canonical anchor residues (P2 and P9) and a 9-residue MUC1 peptide tumor antigen (STAPPAHGV) containing only one of the canonical anchor residues (P9). We have also established a general method for determining the relative refolding efficiency of other MUC1 peptide-MHC complexes monitored by SEC chromatography. This method allows preliminary determination of the suitability of individual peptide-MHC complexes for study by NMR spectroscopy. In addition, the method also allows an initial assay of how mutations to the peptide sequence or changes in glycopeptide carbohydrate moieties might affect peptide binding to HLA-A*0201.

Further NMR experiments will utilize uniformly isotope-labeled MUC1 peptides. Our previous work has established a cloning strategy for producing recombinant, isotope-labeled MUC1 peptides (Grinstead *et al.*, 2003; Schuman *et al.*, 2003). In this study, we have expanded that protocol to produce peptides with unaltered termini. Triple resonance experiments of MHC-bound, uniformly labeled MUC1 peptides will allow assignment of resonances. Experiments such as $^{13}C/^{15}N$-edited or $^{13}C/^{15}N$-filtered NOESY should help to define the bound peptide structure, and orientation of peptide sidechains. NMR relaxation measurements should help to characterize bound peptide sidechain and backbone flexibility. These experiments all form the basis of future work on this system.

The proposed NOESY-based and triple resonance NMR experiments outlined above have been attempted with the present MHC-bound ILK peptide complex.

However, these studies have suffered from extremely poor spectral quality because the large size of the peptide-MHC complex (~42kDa) causes fast transverse relaxation of magnetization. Therefore, the most important aspect of future studies is generation of deuterated MHC. Further attempts at deuteration of both the HLA-A*0201 HC and the scMHC construct must be made. It may be necessary to use several cell lines to see if one is better suited to deuteration than another. Several strategies for production of deuterated protein have been published, so some of those would be attempted. Once deuterated protein is expressed, biophysical experiments will allow characterization of the stability of the refolded MHC-peptide complex.

Complexes with sufficient stability can be studied directly in the NMR tube as a complex. Since peptides assembled with MHC in a 1:1 complex will not be in chemical exchange, they will not benefit from the narrow 'free linewidth' contributions of the transferred experiments as was the case with the Fab studies discussed in Chapters 3 and 4. The large size of the MHC-peptide complex will result in broad linewidths of NMR resonances. However, the recently developed ^{15}N-edited TROSY experiment may prove to be of great assistance in overcoming the rapid T_2 relaxation of the amide proton, producing significantly reduced linewidths and enhanced sensitivity for this nucleus (Zhu *et al.*, 2000).

The experiments outlined in this chapter should allow determination of which MUC1 antigenic peptide sidechains are important for peptide-MHC complex stability, versus pointed away from the MHC binding groove for potential interactions with the TCR. This would be the first step in structure-based redesign of a more immunogenic MUC1 peptide vaccine.

Notes to Chapter 5

Apostolopoulos, V., Haurum, J. S. & McKenzie, I. F. (1997a). MUC1 peptide epitopes associated with five different H-2 class I molecules. *Eur J Immunol* **27**(10), 2579-87.

Apostolopoulos, V., Karanikas, V., Haurum, J. S. & Mckenzie, I. F. C. (1997b). Induction of HLA-A2-Restricted CTL's to the Mucin 1 Human Breast Cancer Antigen [1]. *J Immunol* **159**.

Apostolopoulos, V. & McKenzie, I. F. (1994). Cellular mucins: targets for immunotherapy. *Crit Rev Immunol* **14**(3-4), 293-309.

Apostolopoulos, V., McKenzie, I. F. & Pietersz, G. A. (2000). Generation of MUC1 cytotoxic T-cells in mice and epitope mapping. *Methods Mol Biol* **125**, 455-62.

Apostolopoulos, V., Pietersz, G. A. & McKenzie, I. F. (1999). MUC1 and breast cancer. *Curr Opin Mol Ther* **1**(1), 98-103.

Apostolopoulos, V., Pietersz, G. A. & McKenzie, I. F. C. (1996). Cell-Mediated Immune Response to MUC1 Fusion Protein Coupled to Mannan. *Vaccine* **14**(9), 930-938.

Apostolopoulos, V., Yu, M., Corper, A. L., Teyton, L., Pietersz, G. A., McKenzie, I. F., Wilson, I. A. & Plebanski, M. (2002). Crystal structure of a non-canonical low-affinity peptide complexed with MHC class I: a new approach for vaccine design. *J Mol Biol* **318**(5), 1293-305.

Barnd, D. L., Lan, M. S., Metzgar, R. S. & Finn, O. J. (1989). Specific, major histocompatibility complex-unrestricted recognition of tumor-associated mucins by human cytotoxic T cells. *Proc Natl Acad Sci U S A* **86**(18), 7159-63.

Barratt-Boyes, S. M., Vlad, A. & Finn, O. J. (1999). Immunization of chimpanzees with tumor antigen MUC1 mucin tandem repeat peptide elicits both helper and cytotoxic T-cell responses. *Clin Cancer Res* **5**(7), 1918-24.

Bashford, J. L., Robins, R. A. & Price, M. R. (1993). Development of an anti-idiotypic antibody reactive with an antibody defining the epitope RPAP in the MUC-1 epithelial mucin core. *Int J Cancer* **54**(5), 778-83.

Boniface, J. J., Reich, Z., Lyons, D. S. & Davis, M. M. (1999). Thermodynamics of T cell receptor binding to peptide-MHC: evidence for a general mechanism of molecular scanning. *Proc Natl Acad Sci U S A* **96**(20), 11446-51.

Burchell, J., Taylor-Papadimitriou, J., Boshell, M., Gendler, S. & Duhig, T. (1989). *Int J Cancer* **44**, 691-696.

Denton, G., Sekowski, M. & Price, M. R. (1993). Induction of antibody responses to breast carcinoma associated mucins using synthetic peptide constructs as immunogens. *Cancer Lett* **70**(3), 143-50.

Domenech, N. & Finn, O. J. (1995). In-vitro studies of MHC-restricted recognition of a peptide from the MUC1 tandem repeat domain by CTL. *FASEB J* **9**, A1023.

Garboczi, D. N., Hung, D. T. & Wiley, D. C. (1992). HLA-A2-peptide complexes: refolding and crystallization of molecules expressed in Escherichia coli and complexed with single antigenic peptides. *Proc Natl Acad Sci U S A* **89**(8), 3429-33.

Garcia, K. C., Degano, M., Speir, J. A. & Wilson, I. A. (1999a). Emerging principles for T cell receptor recognition of antigen in cellular immunity. *Rev Immunogenet* **1**(1), 75-90.

Garcia, K. C., Teyton, L. & Wilson, I. A. (1999b). Structural basis of T cell recognition. *Annu Rev Immunol* **17**, 369-97.

Goto, N. K., Gardner, K. H., Mueller, G. A., Willis, R. C. & Kay, L. E. (1999). A robust and cost-effective method for the production of Val, Leu, Ile (delta 1) methyl-protonated 15N-, 13C-, 2H-labeled proteins. *J Biomol NMR* **13**(4), 369-74.

Goydos, J. S., Elder, E., Whiteside, T. L., Finn, O. J. & Lotze, M. T. (1996). A phase I trial of a synthetic mucin peptide vaccine. Induction of specific immune reactivity in patients with adenocarcinoma. *J Surg Res* **63**(1), 298-304.

Grinstead, J. S., Schuman, J. T. & Campbell, A. P. (2003). Epitope Mapping of Antigenic MUC1 Peptides to Breast Cancer Antibody Fragment B27.29: a Heteronuclear NMR Study. *Biochemistry* **accepted for publication**.

Haurum, J. S., Arsequell, G., Lellouch, A. C., Wong, S. Y., Dwek, R. A., McMichael, A. J. & Elliott, T. (1994). Recognition of carbohydrate by major histocompatibility complex class I-restricted, glycopeptide-specific cytotoxic T lymphocytes. *J Exp Med* **180**(2), 739-44.

Hennecke, J. & Wiley, D. C. (2001). T cell receptor-MHC interactions up close. *Cell* **104**(1), 1-4.

Ioannides, C. G., Fisk, B., Jerome, K. R., Irimura, T., Wharton, J. T. & Finn, O. J. (1993). Cytotoxic T cells from ovarian malignant tumors can recognize polymorphic epithelial mucin core peptides. *J Immunol* **151**(7), 3693-703.

Jerome, K. R., Barnd, D. L., Bendt, K. M., Boyer, C. M., Taylor-Papadimitriou, J., McKenzie, I. F., Bast, R. C., Jr. & Finn, O. J. (1991). Cytotoxic T-lymphocytes derived from patients with breast adenocarcinoma recognize an epitope present on the protein core of a mucin molecule preferentially expressed by malignant cells. *Cancer Res* **51**(11), 2908-16.

Karanikas, V., Hwang, L. A., Pearson, J., Ong, C. S., Apostolopoulos, V., Vaughan, H., Xing, P. X., Jamieson, G., Pietersz, G., Tait, B., Broadbent, R., Thynne, G. & McKenzie, I. F. (1997). Antibody and T cell responses of patients with adenocarcinoma immunized with mannan-MUC1 fusion protein. *J Clin Invest* **100**(11), 2783-92.

Kotera, Y., Fontenot, J. D., Pecher, G., Metzgar, R. S. & Finn, O. J. (1994). Humoral immunity against a tandem repeat epitope of human mucin MUC-1 in sera from breast, pancreatic, and colon cancer patients. *Cancer Res* **54**(11), 2856-60.

Lofthouse, S. A., Apostolopoulos, V., Pietersz, G. A., Li, W. & McKenzie, I. F. (1997). Induction of T1 (cytotoxic lymphocyte) and/or T2 (antibody) responses to a mucin-1 tumour antigen. *Vaccine* **15**(14), 1586-93.

Madden, D. R. (1995). The three-dimensional structure of peptide-MHC complexes. *Annu Rev Immunol* **13**, 587-622.

Madden, D. R., Garboczi, D. N. & Wiley, D. C. (1993). The antigenic identity of peptide-MHC complexes: a comparison of the conformations of five viral peptides presented by HLA-A2. *Cell* **75**(4), 693-708.

Mouritsen, S., Meldal, M., Christiansen-Brams, I., Elsner, H. & Werdelin, O. (1994). Attachment of oligosaccharides to peptide antigen profoundly affects binding to major histocompatibility complex class II molecules and peptide immunogenicity. *Eur J Immunol* **24**(5), 1066-72.

Oukka, M., Manuguerra, J. C., Livaditis, N., Tourdot, S., Riche, N., Vergnon, I., Cordopatis, P. & Kosmatopoulos, K. (1996). Protection against lethal viral infection by vaccination with nonimmunodominant peptides. *J Immunol* **157**(7), 3039-45.

Pervushin, K., Riek, R., Wider, G. & Wuthrich, K. (1997). Attenuated T2 relaxation by mutual cancellation of dipole-dipole coupling and chemical shift anisotropy

indicates an avenue to NMR structures of very large biological macromolecules in solution. *Proc Natl Acad Sci U S A* **94**(23), 12366-71.
Rudolph, M. G., Luz, J. G. & Wilson, I. A. (2002). Structural and thermodynamic correlates of T cell signaling. *Annu Rev Biophys Biomol Struct* **31**, 121-49.
Rudolph, M. G. & Wilson, I. A. (2002). The specificity of TCR/pMHC interaction. *Curr Opin Immunol* **14**(1), 52-65.
Schuman, J., Grinstead, J. S. & Campbell, A. P. (2003). **submitted**.
Sette, A., Vitiello, A., Reherman, B., Fowler, P., Nayersina, R., Kast, W. M., Melief, C. J., Oseroff, C., Yuan, L., Ruppert, J. & et al. (1994). The relationship between class I binding affinity and immunogenicity of potential cytotoxic T cell epitopes. *J Immunol* **153**(12), 5586-92.
Sundberg, E. J. & Mariuzza, R. A. (2000). Luxury accommodations: the expanding role of structural plasticity in protein-protein interactions. *Structure Fold Des* **8**(7), R137-42.
Tourdot, S., Scardino, A., Saloustrou, E., Gross, D. A., Pascolo, S., Cordopatis, P., Lemonnier, F. A. & Kosmatopoulos, K. (2000). A general strategy to enhance immunogenicity of low-affinity HLA-A2. 1-associated peptides: implication in the identification of cryptic tumor epitopes. *Eur J Immunol* **30**(12), 3411-21.
van der Burg, S. H., Visseren, M. J., Brandt, R. M., Kast, W. M. & Melief, C. J. (1996). Immunogenicity of peptides bound to MHC class I molecules depends on the MHC-peptide complex stability. *J Immunol* **156**(9), 3308-14.
Vaughan, H. A., Ho, D., Karanikas, V., Ong, C.-S., Hwang, L. A., Pearson, J., McKenzie, I. F. C. & Pietersz, G. A. (1999). Induction of Humoral and Cellular Responses in Cynomolgus Monkeys Immunisied with Mannan-human MUC1 conjugates. *Vaccine* **17**, 2740-2752.
Venters, R. A., Huang, C. C., Farmer, B. T., 2nd, Trolard, R., Spicer, L. D. & Fierke, C. A. (1995). High-level 2H/13C/15N labeling of proteins for NMR studies. *J Biomol NMR* **5**(4), 339-44.
Xing, P. X., Prenzoska, J. & McKenzie, I. F. (1992). Epitope mapping of anti-breast and anti-ovarian mucin monoclonal antibodies. *Mol Immunol* **29**(5), 641-50.
Zhu, G., Xia, Y., Nicholson, L. K. & Sze, K. H. (2000). Protein dynamics measurements by TROSY-based NMR experiments. *J Magn Reson* **143**(2), 423-6.

Chapter 6: Significance of Conclusions and Future Directions

Significance of conclusions:

One major problem with developing a MUC1 cancer vaccine capable of shrinking solid breast tumor has been accurate identification of a tumor-associated MUC1 antigen. Most information regarding the immunogenicity of the MUC1 sequence has been based on studies of MUC1 peptides binding to anti-peptide antibodies. However, recent literature reports illustrate how important tumor-associated MUC1 carbohydrate moieties are to a tumor-relevant immune response. Our strategy of using a tumor-associated antibody to identify the peptide and carbohydrate moieties responsible for binding the antibody has allowed revision of the known cancer-associated peptide epitope to incorporate carbohydrate substituents. For example, our results outlined in Chapter 3 indicate that both the β-turn spanning PDTR and sugars upstream from this sequence interact with the tumor-specific antibody B27.29, while the remaining residues in the sequence remain highly flexible in the bound state and are not affected by binding to the antibody. These results imply that a smaller, more defined glycopeptide vaccine might be more effective at stimulating a strong, tumor-specific immune response.

A second major problem in the development of a tumor-specific MUC1 vaccine is stimulation of a cellular immune response. MUC1 is poorly immunogenic, not because the immune system has been tolerized against the antigen (which would leave only low-affinity T cell clones in circulation), but because MUC1 antigenic peptides are poorly presented to T cells by MHC Class I. Therefore, if the basis for low-affinity binding to MHC could be discovered and possibly improved, then the peptide-MHC complex should be better able to stimulate T cell immunity.

Future directions:

Future studies of the MUC1 system will address the role of glycosylation in MUC1 immunogenicity. In this regard, we have developed an NMR-based methodology for study of both humoral and cellular recognition of MUC1 glycopeptides. Using this methodology, we propose in the future to probe humoral recognition of MUC1 glycopeptides by studying the structure and affinity of various MUC1 glycopeptide-Fab B27.29 complexes. These studies should help refine a model of the MUC1 tumor-associated antigen. Future studies of cellular recognition of MUC1 will examine the role of glycosylation in MUC1 peptide presentation by Class I MHC HLA-A*0201. NMR studies of isotope-labeled peptides should help to define the mode of MUC1 peptide binding to MHC, and refolding assays will determine how cancer-associated carbohydrate moieties affect assembly of the MHC-peptide complexes. Ultimately, generation of an isotope-labeled glycopeptide would allow structure determination of the glycopeptide-MHC complex, which should provide a better structural understanding of how tumor-associated carbohydrate is available to interact with a T cell receptor. Ultimately, these future studies probing the role of MUC1 carbohydrate in humoral and cellular immune recognition should enable design of a next-generation MUC1 glycopeptide vaccine capable of inducing stronger humoral and cellular immunity proficient at shrinking the solid tumor.

Bibliography

Abdel-Motal, U. M., Berg, L., Rosen, A., Bengtsson, M., Thorpe, C. J., Kihlberg, J., Dahmen, J., Magnusson, G., Karlsson, K. A. & Jondal, M. (1996). Immunization with glycosylated Kb-binding peptides generates carbohydrate-specific, unrestricted cytotoxic T cells. *Eur J Immunol* **26**(3), 544-51.

Andersen, N. H., Neidigh, J. W., Harris, S. M., Lee, G. M., Liu, Z. & Tong, H. (1997). Extracting Information from the Temperature Gradients of Polypeptide NH Chemical Shifts. 1. The Importance of Conformational Averaging. *J Am Chem Soc* **119**, 8547-8561.

Apostolopoulos, V., Haurum, J. S. & McKenzie, I. F. (1997a). MUC1 peptide epitopes associated with five different H-2 class I molecules. *Eur J Immunol* **27**(10), 2579-87.

Apostolopoulos, V., Karanikas, V., Haurum, J. S. & Mckenzie, I. F. C. (1997b). Induction of HLA-A2-Restricted CTL's to the Mucin 1 Human Breast Cancer Antigen [1]. *J Immunol* **159**.

Apostolopoulos, V. & McKenzie, I. F. (1994). Cellular mucins: targets for immunotherapy. *Crit Rev Immunol* **14**(3-4), 293-309.

Apostolopoulos, V., McKenzie, I. F. & Pietersz, G. A. (2000). Generation of MUC1 cytotoxic T-cells in mice and epitope mapping. *Methods Mol Biol* **125**, 455-62.

Apostolopoulos, V., Pietersz, G. A. & McKenzie, I. F. (1999a). MUC1 and breast cancer. *Curr Opin Mol Ther* **1**(1), 98-103.

Apostolopoulos, V., Pietersz, G. A. & McKenzie, I. F. C. (1996). Cell-Mediated Immune Response to MUC1 Fusion Protein Coupled to Mannan. *Vaccine* **14**(9), 930-938.

Apostolopoulos, V., Sandrin, M. S. & McKenzie, I. F. C. (1999b). Carbohydrate/Peptide mimics: effect on MUC1 Cancer Immunotherapy. *J Mol Med* **77**, 427-436.

Apostolopoulos, V., Yu, M., Corper, A. L., Teyton, L., Pietersz, G. A., McKenzie, I. F., Wilson, I. A. & Plebanski, M. (2002). Crystal structure of a non-canonical low-affinity peptide complexed with MHC class I: a new approach for vaccine design. *J Mol Biol* **318**(5), 1293-305.

Barnd, D. L., Lan, M. S., Metzgar, R. S. & Finn, O. J. (1989). Specific, major histocompatibility complex-unrestricted recognition of tumor-associated mucins by human cytotoxic T cells. *Proc Natl Acad Sci U S A* **86**(18), 7159-63.

Barratt-Boyes, S. M., Vlad, A. & Finn, O. J. (1999). Immunization of chimpanzees with tumor antigen MUC1 mucin tandem repeat peptide elicits both helper and cytotoxic T-cell responses. *Clin Cancer Res* **5**(7), 1918-24.

Bashford, J. L., Robins, R. A. & Price, M. R. (1993). Development of an anti-idiotypic antibody reactive with an antibody defining the epitope RPAP in the MUC-1 epithelial mucin core. *Int J Cancer* **54**(5), 778-83.

Bax, A. & Davis, D. G. (1985). *J Magn Reson* **65**, 355.

Baxter, N. J. & Williamson, M. P. (1997). Temperature dependence of 1H chemical shifts in proteins. *J Biomol NMR* **9**(4), 359-69.

Berzofsky, J. A., Ahlers, J. D. & Belyakov, I. M. (2001). Strategies for designing and optimizing new generation vaccines. *Nat Rev Immunol* **1**(3), 209-19.

Bhattacharya, S., Botuyan, M. V., Hsu, F., Shan, X., Arunkumar, A. I., Arrowsmith, C. H., Edwards, A. M. & Chazin, W. J. (2002). Characterization of binding-induced changes in dynamics suggests a model for sequence-nonspecific binding of ssDNA by replication protein A. *Protein Sci* **11**(10), 2316-25.

Bhavanandan, V. P. (1991). Cancer-associated mucins and mucin-type glycoproteins. *Glycobiology* **1**(5), 493-503.

Bohm, C. M., Mulder, M. C., Zennadi, R., Notter, M., Schmitt-Graff, A., Finn, O. J., Taylor-Papadimitriou, J., Stein, H., Clausen, H., Riecken, E. O. & Hanski, O. (1997). Carbohydrate Recognition on MUC-1 Expressing Targets Enhances Cytoxicity of a T Cell Subpopulation,. *Scand J Immunol* **46**, 27-34.

Boniface, J. J., Reich, Z., Lyons, D. S. & Davis, M. M. (1999). Thermodynamics of T cell receptor binding to peptide-MHC: evidence for a general mechanism of molecular scanning. *Proc Natl Acad Sci U S A* **96**(20), 11446-51.

Brockhausen, I., Yang, J., Dickinson, N., Ogata, S. & Itzkowitz, S. H. (1998). Enzymatic basis for sialyl-Tn expression in human colon cancer cells. *Glycoconj J* **15**(6), 595-603.

Brossart, P., Wirths, S., Stuhler, G., Reichardt, V. L., Kanz, L. & Brugger, W. (2000). Induction of cytotoxic T-lymphocyte responses in vivo after vaccinations with peptide-pulsed dendritic cells. *Blood* **96**(9), 3102-8.

Burchell, J., Taylor-Papadimitriou, J., Boshell, M., Gendler, S. & Duhig, T. (1989). *Int J Cancer* **44**, 691-696.

Campbell, A. P., McInnes, C., Hodges, R. S. & Sykes, B. D. (1995). Comparison of NMR solution structures of the receptor binding domains of Pseudomonas aeruginosa pili strains PAO, KB7, and PAK: implications for receptor binding and synthetic vaccine design. *Biochemistry* **34**(50), 16255-68.

Campbell, A. P. & Sykes, B. D. (1993). The two-dimensional transferred nuclear Overhauser effect: theory and practice. *Annu Rev Biophys Biomol Struct* **22**, 99-122.

Campbell, A. P., Wong, W. Y., Houston, M., Jr., Schweizer, F., Cachia, P. J., Irvin, R. T., Hindsgaul, O., Hodges, R. S. & Sykes, B. D. (1997). Interaction of the receptor binding domains of Pseudomonas aeruginosa pili strains PAK, PAO, KB7 and P1 to a cross-reactive antibody and receptor analog: implications for synthetic vaccine design. *J Mol Biol* **267**(2), 382-402.

Cao, Y., Karsten, U., Otto, G. & Bannasch, P. (1999). Expression of MUC1, Thomsen-Friedenreich antigen, Tn, sialosyl-Tn, and alpha2,6-linked sialic acid in hepatocellular carcinomas and preneoplastic hepatocellular lesions. *Virchows Arch* **434**(6), 503-9.

Cao, Y., Schlag, P. M. & Karsten, U. (1997). Immunodetection of epithelial mucin (MUC1, MUC3) and mucin-associated glycotopes (TF, Tn, and sialosyl-Tn) in benign and malignant lesions of colonic epithelium: apolar localization corresponds to malignant transformation. *Virchows Arch* **431**(3), 159-66.

Carlstedt, I. & Davies, J. R. (1997). Glycoconjugates facing the outside world. *Biochem Soc Trans* **25**(1), 214-9.

Chandrasekhar, K., Profy, A. T. & Dyson, H. J. (1991). Solution Conformational Preferences of Immunogenic Peptides Derived from the Principal Neutralizing Determinant of the HIV-1 Envelope Glycoprotein Gp120. *Biochemistry* **30**(38), 9187-9194.

Cheetham, J. C., Raleigh, D. P., Griest, R. E., Redfield, C., Dobson, C. M. & Rees, A. R. (1991). Antigen mobility in the combining site of an anti-peptide antibody. *Proc Natl Acad Sci U S A* **88**(18), 7968-72.

Cowan, P. M. & McGavine, S. (1955). *Nature* **176**, 501-503.

Dalcol, I., Pons, M., Ludevid, M. D. & Giralt, E. (1996). Convergent Synthesis of Repeating Peptides (Val-X-Leu-Pro-Pro-Pro)(8) Adopting a Polyproline II Conformation. *J Org Chem* **61**(20), 6775-6782.

David, L., Nesland, J. M., Clausen, H., Carneiro, F. & Sobrinho-Simoes, M. (1992). Simple mucin-type carbohydrate antigens (Tn, sialosyl-Tn and T) in gastric mucosa, carcinomas and metastases. *APMIS Suppl* **27**, 162-72.

Davis, J. H. & Agard, D. A. (1998). Relationship between enzyme specificity and the backbone dynamics of free and inhibited alpha-lytic protease. *Biochemistry* **37**(21), 7696-707.

Deck, M. B., Sjolin, P., Unanue, E. R. & Kihlberg, J. (1999). MHC-restricted, glycopeptide-specific T cells show specificity for both carbohydrate and peptide residues. *J Immunol* **162**(8), 4740-4.

Delaglio, F., Grsesiek, S., Vuister, G. W., Zhu, G., Pfeifer, J. & Bax, A. (1995). NMRPipe: A multidimensional spectral processing system based on UNIX pipes. *J Biomol NMR* **6**, 277 - 293.

Denda-Nagai, K. & Irimura, T. (2000). MUC1 in carcinoma-host interactions. *Glycoconj J* **17**(7-9), 649-58.

Denton, G., Sekowski, M. & Price, M. R. (1993). Induction of antibody responses to breast carcinoma associated mucins using synthetic peptide constructs as immunogens. *Cancer Lett* **70**(3), 143-50.

Derrick, J. P., Maiden, M. C. & Feavers, I. M. (1999). Crystal structure of an Fab fragment in complex with a meningococcal serosubtype antigen and a protein G domain. *J Mol Biol* **293**(1), 81-91.

Ding, L., Lalani, E. N., Reddish, M., Koganty, R., Wong, T., Samuel, J., Yacyshyn, M. B., Meikle, A., Fung, P. Y. & Taylor-Papadimitriou, J. (1993). Immunogenicity of synthetic peptides related to the core peptide sequence encoded by the human MUC1 mucin gene: effect of immunization on the growth of murine mammary adenocarcinoma cells transfected with the human MUC1 gene. *Cancer Immunol Immunother* **36**(1), 9-17.

Doehn, C. & Jocham, D. (2000). Technology evaluation: TG-1031, Transgene SA. *Curr Opin Mol Ther* **2**(1), 106-11.

Domenech, N. & Finn, O. J. (1995). In-vitro studies of MHC-restricted recognition of a peptide from the MUC1 tandem repeat domain by CTL. *FASEB J* **9**, A1023.

Farrow, N. A., Muhandiram, R., Singer, A. U., Pascal, S. M., Kay, C. M., Gish, G., Shoelson, S. E., Pawson, T., Forman-Kay, J. D. & Kay, L. E. (1994). Backbone dynamics of a free and phosphopeptide-complexed Src homology 2 domain studied by 15N NMR relaxation. *Biochemistry* **33**(19), 5984-6003.

Farrow, N. A., Zhang, O., Forman-Kay, J. D. & Kay, L. E. (1995). Comparison of the backbone dynamics of a folded and an unfolded SH3 domain existing in equilibrium in aqueous buffer. *Biochemistry* **34**(3), 868-78.

Finn, O. J., Jerome, K. R., Henderson, R. A., Pecher, G., Domenech, N., Magarian-Blander, J. & Barratt-Boyes, S. M. (1995). MUC-1 epithelial tumor mucin-based immunity and cancer vaccines. *Immunol Rev* **145**, 61-89.

Fontenot, J. D. (1993). Biophysical Characterization of One, Two, and Three-Tandem Repeats of Human Mucin (MUC-1) Protein Core. *Cancer Research* **53**, 5386-5394.

Fontenot, J. D., Finn, O. J., Dales, N., Andrews, P. C. & Montelaro, R. C. (1993). Synthesis of large multideterminant peptide immunogens using a poly-proline beta-turn helix motif. *Pept Res* **6**(6), 330-6.

Fontenot, J. D., Mariappan, S. V., Catasti, P., Domenech, N., Finn, O. J. & Gupta, G. (1995). Structure of a tumor associated antigen containing a tandemly repeated immunodominant epitope. *J Biomol Struct Dyn* **13**(2), 245-60.

Foon, K. A. (2001). Immunotherapy for colorectal cancer. *Curr Oncol Rep* **3**(2), 116-26.

Foote, J. & Eisen, H. N. (1995). Kinetic and affinity limits on antibodies produced during immune responses. *Proc Natl Acad Sci U S A* **92**(5), 1254-6.

Fung, P. Y., Madej, M., Koganty, R. R. & Longenecker, B. M. (1990). Active specific immunotherapy of a murine mammary adenocarcinoma using a synthetic tumor-associated glycoconjugate. *Cancer Res* **50**(14), 4308-14.

Gad, M., Jensen, T., Gagne, R., Komba, S., Daugaard, S., Kroman, N., Meldal, M., Werdelin, O., Vlad, A. M., Muller, S., Cudic, M., Paulsen, H., Otvos, L., Jr., Hanisch, F. G. & Finn, O. J. (2003). MUC1-derived glycopeptide libraries with improved MHC anchors are strong antigens and prime mouse T cells for proliferative responses to lysates of human breast cancer tissue. *Eur J Immunol* **33**(6), 1624-32.

Garboczi, D. N., Hung, D. T. & Wiley, D. C. (1992). HLA-A2-peptide complexes: refolding and crystallization of molecules expressed in Escherichia coli and complexed with single antigenic peptides. *Proc Natl Acad Sci U S A* **89**(8), 3429-33.

Garcia, K. C., Degano, M., Speir, J. A. & Wilson, I. A. (1999a). Emerging principles for T cell receptor recognition of antigen in cellular immunity. *Rev Immunogenet* **1**(1), 75-90.

Garcia, K. C., Teyton, L. & Wilson, I. A. (1999b). Structural basis of T cell recognition. *Annu Rev Immunol* **17**, 369-97.

Gemmecker, G. (1999). Ch.9: NMR Spectroscopy in Drug Development and Analysis. In *NMR as a Tool in Drug Research* (Holzgrabe, U., Wawer, I. & Diehl, B., eds.), pp. 140-141. John Wiley & Sons, Inc., New York.

Gendler, S. J. & Spicer, A. P. (1995). Epithelial mucin genes. *Annu Rev Physiol* **57**, 607-34.

Gerken, T. A., Butenhof, K. J. & Shogren, R. (1989). Effects of glycosylation on the conformation and dynamics of O-linked glycoproteins: carbon-13 NMR studies of ovine submaxillary mucin. *Biochemistry* **28**(13), 5536-43.

Gion, M., Mione, R., Leon, A. E., Luftner, D., Molina, R., Possinger, K. & Robertson, J. F. (2001). CA27.29: a valuable marker for breast cancer management. A confirmatory multicentric study on 603 cases. *Eur J Cancer* **37**(3), 355-63.

Girling, A., Bartkova, J., Burchell, J., Gendler, S., Gillett, C. & Taylor-Papadimitriou, J. (1989). A core protein epitope of the polymorphic epithelial mucin detected by the monoclonal antibody SM-3 is selectively exposed in a range of primary carcinomas. *Int J Cancer* **43**(6), 1072-6.

Glithero, A., Tormo, J., Haurum, J. S., Arsequell, G., Valencia, G., Edwards, J., Springer, S., Townsend, A., Pao, Y. L., Wormald, M., Dwek, R. A., Jones, E. Y. & Elliott, T.

(1999). Crystal structures of two H-2Db/glycopeptide complexes suggest a molecular basis for CTL cross-reactivity. *Immunity* **10**(1), 63-74.

Goto, N. K., Gardner, K. H., Mueller, G. A., Willis, R. C. & Kay, L. E. (1999). A robust and cost-effective method for the production of Val, Leu, Ile (delta 1) methyl-protonated 15N-, 13C-, 2H-labeled proteins. *J Biomol NMR* **13**(4), 369-74.

Goydos, J. S., Elder, E., Whiteside, T. L., Finn, O. J. & Lotze, M. T. (1996). A phase I trial of a synthetic mucin peptide vaccine. Induction of specific immune reactivity in patients with adenocarcinoma. *J Surg Res* **63**(1), 298-304.

Grinstead, J. S., Koganty, R. R., Krantz, M. J., Longenecker, B. M. & Campbell, A. P. (2002). Effect of glycosylation on MUC1 humoral immune recognition: NMR studies of MUC1 glycopeptide-antibody interactions. *Biochemistry* **41**(31), 9946-61.

Grinstead, J. S., Schuman, J. T. & Campbell, A. P. (2003). Epitope Mapping of Antigenic MUC1 Peptides to Breast Cancer Antibody Fragment B27.29: a Heteronuclear NMR Study. *Biochemistry* **accepted for publication.**

Grzesiek, S. & Bax, A. (1992). *J Am Chem Soc* **114**, 6291-6293.

Hanisch, F. G. (2001). O-glycosylation of the mucin type. *Biol Chem* **382**(2), 143-9.

Haurum, J. S., Arsequell, G., Lellouch, A. C., Wong, S. Y., Dwek, R. A., McMichael, A. J. & Elliott, T. (1994). Recognition of carbohydrate by major histocompatibility complex class I-restricted, glycopeptide-specific cytotoxic T lymphocytes. *J Exp Med* **180**(2), 739-44.

Haurum, J. S., Hoier, I. B., Arsequell, G., Neisig, A., Valencia, G., Zeuthen, J., Neefjes, J. & Elliott, T. (1999). Presentation of cytosolic glycosylated peptides by human class I major histocompatibility complex molecules in vivo. *J Exp Med* **190**(1), 145-50.

Hennecke, J. & Wiley, D. C. (2001). T cell receptor-MHC interactions up close. *Cell* **104**(1), 1-4.

Henningsson, C. M., Selvaraj, S., MacLean, G. D., Suresh, M. R., Noujaim, A. A. & Longenecker, B. M. (1987). T cell recognition of a tumor-associated glycoprotein and its synthetic carbohydrate epitopes: stimulation of anticancer T cell immunity in vivo. *Cancer Immunol Immunother* **25**(3), 231-41.

Ioannides, C. G., Fisk, B., Jerome, K. R., Irimura, T., Wharton, J. T. & Finn, O. J. (1993). Cytotoxic T cells from ovarian malignant tumors can recognize polymorphic epithelial mucin core peptides. *J Immunol* **151**(7), 3693-703.

Itzkowitz, S. H., Yuan, M., Montgomery, C. K., Kjeldsen, T., Takahashi, H. K., Bigbee, W. L. & Kim, Y. S. (1989). Expression of Tn, sialosyl-Tn, and T antigens in human colon cancer. *Cancer Res* **49**(1), 197-204.

Jeener, J., Meier, B. H., Bachmann, P. & Ernst, R. R. (1979). *J Chem Phys* **71**, 4546-4553.

Jerome, K. R., Barnd, D. L., Bendt, K. M., Boyer, C. M., Taylor-Papadimitriou, J., McKenzie, I. F., Bast, R. C., Jr. & Finn, O. J. (1991). Cytotoxic T-lymphocytes derived from patients with breast adenocarcinoma recognize an epitope present on the protein core of a mucin molecule preferentially expressed by malignant cells. *Cancer Res* **51**(11), 2908-16.

Karanikas, V., Hwang, L. A., Pearson, J., Ong, C. S., Apostolopoulos, V., Vaughan, H., Xing, P. X., Jamieson, G., Pietersz, G., Tait, B., Broadbent, R., Thynne, G. & McKenzie, I. F. (1997). Antibody and T cell responses of patients with adenocarcinoma immunized with mannan-MUC1 fusion protein. *J Clin Invest* **100**(11), 2783-92.

Karanikas, V., Patton, K., Jamieson, G., Pietersz, G. & McKenzie, I. (1998). Affinty of Antibodies to MUC1 Antigens. *Tumor Biology* **19**, 71-78.

Karlsson, R. & Falt, A. (1997). Experimental design for kinetic analysis of protein-protein interactions with surface plasmon resonance biosensors. *J Immunol Methods* **200**(1-2), 121-33.

Karsten, U., Diotel, C., Klich, G., Paulsen, H., Goletz, S., Muller, S. & Hanisch, F. G. (1998). Enhanced binding of antibodies to the DTR motif of MUC1 tandem repeat peptide is mediated by site-specific glycosylation. *Cancer Res* **58**(12), 2541-9.

Kirnarsky, L., Prakash, O., Vogen, S. M., Nomoto, M., Hollingsworth, M. A. & Sherman, S. (2000). Structural effects of O-glycosylation on a 15-residue peptide from the mucin (MUC1) core protein. *Biochemistry* **39**(39), 12076-82.

Kishikawa, T., Ghazizadeh, M., Sasaki, Y. & Springer, G. F. (1999). Specific role of T and Tn tumor-associated antigens in adhesion between a human breast carcinoma cell line and a normal human breast epithelial cell line. *Jpn J Cancer Res* **90**(3), 326-32.

Koebnik, R., Locher, K. P. & Van Gelder, P. (2000). Structure and function of bacterial outer membrane proteins: barrels in a nutshell. *Mol Microbiol* **37**(2), 239-53.

Koganty, R. R., Reddish, M. A. & Longenecker, B. M. (1997). Glycopeptides in the Immunotherapy of Cancer. In *Glycopeptides and Related Compounds: Synthesis, Analysis and Application* (C.D., L. D. G. a. W., ed.), pp. 707-743. Dekker, New York.

Kotera, Y., Fontenot, J. D., Pecher, G., Metzgar, R. S. & Finn, O. J. (1994). Humoral immunity against a tandem repeat epitope of human mucin MUC-1 in sera from breast, pancreatic, and colon cancer patients. *Cancer Res* **54**(11), 2856-60.

Kraulis, P. J. (1989). ANSIG. *J Magn Reson* **84**, 627-633.

Kuliopulos, A. & Walsh, C. T. (1994). Production, Purification, and Cleavage of Tandem Repeats of Recombinant Peptides. *J Am Chem Soc* **116**, 4599-4607.

Lefevre, J. F., Dayie, K. T., Peng, J. W. & Wagner, G. (1996). Internal mobility in the partially folded DNA binding and dimerization domains of GAL4: NMR analysis of the N-H spectral density functions. *Biochemistry* **35**(8), 2674-86.

Lian, L. Y., Barsukov, I. L., Sutcliffe, M. J., Sze, K. H. & Roberts, G. C. (1994). Protein-ligand interactions: exchange processes and determination of ligand conformation and protein-ligand contacts. *Methods Enzymol* **239**, 657-700.

Liang, R., Andreotti, A. H. & Kahne, D. (1995). Sensitivity of Glycopeptide Conformation to Carbohydrate Chain Length. *J Am Chem Soc* **117**, 10395-10396.

Liu, X., Sejbal, J., Kotovych, G., Koganty, R. R., Reddish, M. A., Jackson, L., Gandhi, S. S., Mendonca, A. J. & Longenecker, B. M. (1995). Structurally defined synthetic cancer vaccines: analysis of structure, glycosylation and recognition of cancer associated mucin, MUC-1 derived peptides. *Glycoconj J* **12**(5), 607-17.

Live, D. H., Williams, L. J., Kuduk, S. D., Schwarz, J. B., Glunz, P. W., Chen, X. T., Sames, D., Kumar, R. A. & Danishefsky, S. J. (1999). Probing cell-surface architecture through synthesis: an NMR-determined structural motif for tumor-associated mucins. *Proc Natl Acad Sci U S A* **96**(7), 3489-93.

Lofthouse, S. A., Apostolopoulos, V., Pietersz, G. A., Li, W. & McKenzie, I. F. (1997). Induction of T1 (cytotoxic lymphocyte) and/or T2 (antibody) responses to a mucin-1 tumour antigen. *Vaccine* **15**(14), 1586-93.

Macura, S. & Ernst, R. R. (1980). *Mol Phys* **41**, 95-117.

Madden, D. R. (1995). The three-dimensional structure of peptide-MHC complexes. *Annu Rev Immunol* **13**, 587-622.

Madden, D. R., Garboczi, D. N. & Wiley, D. C. (1993). The antigenic identity of peptide-MHC complexes: a comparison of the conformations of five viral peptides presented by HLA-A2. *Cell* **75**(4), 693-708.

Miles, D. W. & Taylor-Papadimitriou, J. (1999). Therapeutic aspects of polymorphic epithelial mucin in adenocarcinoma. *Pharmacol Ther* **82**(1), 97-106.

Mimura, Y., Inoue, Y., Maeji, N. J. & Chujo, R. (1989). N.m.r. study on conformation of Ac-Thr(alpha-GalNAc)-Ala-Ala-OMe as a model for mucin type glycoprotein. *Int J Pept Protein Res* **34**(5), 363-8.

Mitchell, M. S. (2002). Cancer vaccines, a critical review--Part II. *Curr Opin Investig Drugs* **3**(1), 150-8.

Morse, M. A. (2000). Technology evaluation: Theratope, Biomira Inc. *Curr Opin Mol Ther* **2**(4), 453-8.

Morse, M. A. (2001). Technology evaluation: BLP-25, Biomira Inc. *Curr Opin Mol Ther* **3**(1), 102-5.

Mouritsen, S., Meldal, M., Christiansen-Brams, I., Elsner, H. & Werdelin, O. (1994). Attachment of oligosaccharides to peptide antigen profoundly affects binding to major histocompatibility complex class II molecules and peptide immunogenicity. *Eur J Immunol* **24**(5), 1066-72.

Muller, S., Alving, K., Peter-Katalinic, J., Zachara, N., Gooley, A. A. & Hanisch, F. G. (1999). High density O-glycosylation on tandem repeat peptide from secretory MUC1 of T47D breast cancer cells. *J Biol Chem* **274**(26), 18165-72.

Muller, S., Goletz, S., Packer, N., Gooley, A., Lawson, A. M. & Hanisch, F. G. (1997). Localization of O-glycosylation sites on glycopeptide fragments from lactation-associated MUC1. All putative sites within the tandem repeat are glycosylation targets in vivo. *J Biol Chem* **272**(40), 24780-93.

Musselli, C., Ragupathi, G., Gilewski, T., Panageas, K. S., Spinat, Y. & Livingston, P. O. (2002). Reevaluation of the cellular immune response in breast cancer patients vaccinated with MUC1. *Int J Cancer* **97**(5), 660-7.

Nakamura, H., Hinoda, Y., Nakagawa, N., Makiguchi, Y., Itoh, F., Endo, T. & Imai, K. (1998). Detection of circulating anti-MUC1 mucin core protein antibodies in patients with colorectal cancer. *J Gastroenterol* **33**(3), 354-61.

Nice, E. C., McInerney, T. L. & Jackson, D. C. (1996). Analysis of the interaction between a synthetic peptide of influenza virus hemagglutinin and monoclonal antibodies using an optical biosensor. *Mol Immunol* **33**(7-8), 659-70.

Nishimori, I., Johnson, N. R., Sanderson, S. D., Perini, F., Mountjoy, K., Cerny, R. L., Gross, M. L. & Hollingsworth, M. A. (1994a). Influence of acceptor substrate primary amino acid sequence on the activity of human UDP-N-acetylgalactosamine:polypeptide N-acetylgalactosaminyltransferase. Studies with the MUC1 tandem repeat. *J Biol Chem* **269**(23), 16123-30.

Nishimori, I., Perini, F., Mountjoy, K. P., Sanderson, S. D., Johnson, N., Cerny, R. L., Gross, M. L., Fontenot, J. D. & Hollingsworth, M. A. (1994b). N-acetylgalactosamine glycosylation of MUC1 tandem repeat peptides by pancreatic tumor cell extracts. *Cancer Res* **54**(14), 3738-44.

Northrup, S. H. & Erickson, H. P. (1992). Kinetics of protein-protein association explained by Brownian dynamics computer simulation. *Proc Natl Acad Sci U S A* **89**(8), 3338-42.

Oukka, M., Manuguerra, J. C., Livaditis, N., Tourdot, S., Riche, N., Vergnon, I., Cordopatis, P. & Kosmatopoulos, K. (1996). Protection against lethal viral infection by vaccination with nonimmunodominant peptides. *J Immunol* **157**(7), 3039-45.

Patton, S., Gendler, S. J. & Spicer, A. P. (1995). The epithelial mucin, MUC1, of milk, mammary gland and other tissues. *Biochim Biophys Acta* **1241**(3), 407-23.

Pecher, G., Haring, A., Kaiser, L. & Thiel, E. (2002). Mucin gene (MUC1) transfected dendritic cells as vaccine: results of a phase I/II clinical trial. *Cancer Immunol Immunother* **51**(11-12), 669-73.

Peng, J. W. & Wagner, G. (1992a). *J Magn Reson* **98**, 308-332.

Peng, J. W. & Wagner, G. (1992b). Mapping of the spectral densities of N-H bond motions in eglin c using heteronuclear relaxation experiments. *Biochemistry* **31**(36), 8571-86.

Peng, J. W. & Wagner, G. (1995). Frequency spectrum of NH bonds in eglin c from spectral density mapping at multiple fields. *Biochemistry* **34**(51), 16733-52.

Pervushin, K., Riek, R., Wider, G. & Wuthrich, K. (1997). Attenuated T2 relaxation by mutual cancellation of dipole-dipole coupling and chemical shift anisotropy indicates an avenue to NMR structures of very large biological macromolecules in solution. *Proc Natl Acad Sci U S A* **94**(23), 12366-71.

Petrarca, C., Casalino, B., von Mensdorff-Pouilly, S., Rughetti, A., Rahimi, H., Scambia, G., Hilgers, J., Frati, L. & Nuti, M. (1999). Isolation of MUC1-primed B lymphocytes from tumour-draining lymph nodes by immunomagnetic beads. *Cancer Immunol Immunother* **47**(5), 272-7.

Piatini, U., Sorenson, O. W. & Ernst, R. R. (1982). *J Amer Chem Soc* **104**, 6800-6801.

Price, M. R., Rye, P. D., Petrakou, E., Murray, A., Brady, K., Imai, S., Haga, S., Kiyozuka, Y., Schol, D., Meulenbroek, M. F., Snijdewint, F. G., von Mensdorff-Pouilly, S., Verstraeten, R. A., Kenemans, P., Blockzjil, A., Nilsson, K., Nilsson, O., Reddish, M., Suresh, M. R., Koganty, R. R., Fortier, S., Baronic, L., Berg, A., Longenecker, M. B., Hilgers, J. & et al. (1998). Summary report on the ISOBM TD-4 Workshop: analysis of 56 monoclonal antibodies against the MUC1 mucin. San Diego, Calif., November 17-23, 1996. *Tumour Biol* **19 Suppl 1**, 1-20.

Raman, C. S., Jemmerson, R., Nall, B. T. & Allen, M. J. (1992). Diffusion-limited rates for monoclonal antibody binding to cytochrome c. *Biochemistry* **31**(42), 10370-9.

Rance, M., Sorensen, O. W., Bodenhausen, G., Wagner, G., Ernst, R. R. & Wuthrich, K. (1983). Improved spectral resolution in cosy 1H NMR spectra of proteins via double quantum filtering. *Biochem Biophys Res Commun* **117**(2), 479-85.

Reddish, M. A., Helbrecht, N., Almeida, A. F., Madiyalakan, R., Suresh, M. R. & Longenecker, B. M. (1992). Epitope mapping of CA27.29 within the protein core of the malignant breast carcinoma associated mucin antigen MUC-1. *J Tumor Marker Oncol* **7**, 19.

Richardson, J. S. (1981). The anatomy and taxonomy of protein structure. *Adv Protein Chem* **34**, 167-339.

Rose, G. D., Gierasch, L. M. & Smith, J. A. (1985). Turns in peptides and proteins. *Adv Protein Chem* **37**, 1-109.

Rudd, P. M. & Dwek, R. A. (1997). Glycosylation: heterogeneity and the 3D structure of proteins. *Crit Rev Biochem Mol Biol* **32**(1), 1-100.

Rudd, P. M., Elliott, T., Cresswell, P., Wilson, I. A. & Dwek, R. A. (2001). Glycosylation and the immune system. *Science* **291**(5512), 2370-6.

Rudolph, M. G., Luz, J. G. & Wilson, I. A. (2002). Structural and thermodynamic correlates of T cell signaling. *Annu Rev Biophys Biomol Struct* **31**, 121-49.

Rudolph, M. G. & Wilson, I. A. (2002). The specificity of TCR/pMHC interaction. *Curr Opin Immunol* **14**(1), 52-65.

Scanlon, M. J., Morley, S. D., Jackson, D. E., Price, M. R. & Tendler, S. J. (1992). Structural and computational investigations of the conformation of antigenic peptide fragments of human polymorphic epithelial mucin. *Biochem J* **284**(Pt 1), 137-44.

Schol, D. J., Meulenbroek, M. F., Snijdewint, F. G., von Mensdorff-Pouilly, S., Verstraeten, R. A., Murakami, F., Kenemans, P. & Hilgers, J. (1998). 'Epitope fingerprinting' using overlapping 20-mer peptides of the MUC1 tandem repeat sequence. *Tumour Biol* **19 Suppl 1**, 35-45.

Schuman, J., Campbell, A. P., Koganty, R. R. & Longenecker, B. M. (2003a). Probing the conformational and dynamical effects of O-glycosylation within the immunodominant region of a MUC1 peptide tumor antigen. *J Pept Res* **61**(3), 91-108.

Schuman, J., Grinstead, J. S. & Campbell, A. P. (2003b). **submitted**.

Sette, A., Newman, M., Livingston, B., McKinney, D., Sidney, J., Ishioka, G., Tangri, S., Alexander, J., Fikes, J. & Chesnut, R. (2002). Optimizing vaccine design for cellular processing, MHC binding and TCR recognition. *Tissue Antigens* **59**(6), 443-51.

Sette, A., Vitiello, A., Reherman, B., Fowler, P., Nayersina, R., Kast, W. M., Melief, C. J., Oseroff, C., Yuan, L., Ruppert, J. & et al. (1994). The relationship between class I binding affinity and immunogenicity of potential cytotoxic T cell epitopes. *J Immunol* **153**(12), 5586-92.

Shaka, A. J., Barker, P. B. & Freeman, R. (1985). Computer-optimized decoupling scheme for wideband applications and low-level operation. *J Magn Reson* **64**, 547-552.

Shaka, A. J., Keeler, J., Frenkiel, T. & Freeman, R. (1983). *J Magn Reson* **52**, 335-338.

Spencer, D. I., Missailidis, S., Denton, G., Murray, A., Brady, K., Matteis, C. I., Searle, M. S., Tendler, S. J. & Price, M. R. (1999). Structure/activity studies of the anti-MUC1 monoclonal antibody C595 and synthetic MUC1 mucin-core-related peptides and glycopeptides. *Biospectroscopy* **5**(2), 79-91.

Spencer, D. I., Price, M. R., Tendler, S. J., De Matteis, C. I., Stadie, T. & Hanisch, F. G. (1996). Effect of glycosylation of a synthetic MUC1 mucin-core-related peptide on recognition by anti-mucin antibodies. *Cancer Lett* **100**(1-2), 11-5.

Springer, G. F. (1995). T and Tn pancarcinoma markers: autoantigenic adhesion molecules in pathogenesis, prebiopsy carcinoma-detection, and long-term breast carcinoma immunotherapy. *Crit Rev Oncog* **6**(1), 57-85.

Springer, G. F. (1997). Immunoreactive T and Tn epitopes in cancer diagnosis, prognosis, and immunotherapy. *J Mol Med* **75**(8), 594-602.

Stanfield, R., Cabezas, E., Satterthwait, A., Stura, E., Profy, A. & Wilson, I. (1999). Dual conformations for the HIV-1 gp120 V3 loop in complexes with different neutralizing fabs. *Structure Fold Des* **7**(2), 131-42.

States, D. J., Haberkorn, R. A. & D.J., R. (1982). *J Magn Reson* **48**, 286-292.

Sundberg, E. J. & Mariuzza, R. A. (2000). Luxury accommodations: the expanding role of structural plasticity in protein-protein interactions. *Structure Fold Des* **8**(7), R137-42.

Taylor-Papadimitriou, J., Burchell, J., Miles, D. W. & Dalziel, M. (1999). MUC1 and cancer. *Biochim Biophys Acta* **1455**(2-3), 301-13.

Terasawa, K., Furumoto, H., Kamada, M. & Aono, T. (1996). Expression of Tn and sialyl-Tn antigens in the neoplastic transformation of uterine cervical epithelial cells. *Cancer Res* **56**(9), 2229-32.

Tourdot, S., Scardino, A., Saloustrou, E., Gross, D. A., Pascolo, S., Cordopatis, P., Lemonnier, F. A. & Kosmatopoulos, K. (2000). A general strategy to enhance immunogenicity of low-affinity HLA-A2. 1-associated peptides: implication in the identification of cryptic tumor epitopes. *Eur J Immunol* **30**(12), 3411-21.

Tugarinov, V., Zvi, A., Levy, R. & Anglister, J. (1999). A cis proline turn linking two beta-hairpin strands in the solution structure of an antibody-bound HIV-1IIIB V3 peptide. *Nat Struct Biol* **6**(4), 331-5.

Van den Steen, P., Rudd, P. M., Dwek, R. A. & Opdenakker, G. (1998). Concepts and principles of O-linked glycosylation. *Crit Rev Biochem Mol Biol* **33**(3), 151-208.

van der Burg, S. H., Visseren, M. J., Brandt, R. M., Kast, W. M. & Melief, C. J. (1996). Immunogenicity of peptides bound to MHC class I molecules depends on the MHC-peptide complex stability. *J Immunol* **156**(9), 3308-14.

Vaughan, H. A., Ho, D., Karanikas, V., Ong, C.-S., Hwang, L. A., Pearson, J., McKenzie, I. F. C. & Pietersz, G. A. (1999). Induction of Humoral and Cellular Responses in Cynomolgus Monkeys Immunisied with Mannan-human MUC1 conjugates. *Vaccine* **17**, 2740-2752.

Venters, R. A., Huang, C. C., Farmer, B. T., 2nd, Trolard, R., Spicer, L. D. & Fierke, C. A. (1995). High-level 2H/13C/15N labeling of proteins for NMR studies. *J Biomol NMR* **5**(4), 339-44.

Vlad, A. M., Muller, S., Cudic, M., Paulsen, H., Otvos, L., Jr., Hanisch, F. G. & Finn, O. J. (2002). Complex carbohydrates are not removed during processing of glycoproteins by dendritic cells: processing of tumor antigen MUC1 glycopeptides for presentation to major histocompatibility complex class II-restricted T cells. *J Exp Med* **196**(11), 1435-46.

Volkman, B. F., Alam, S. L., Satterlee, J. D. & Markley, J. L. (1998). Solution structure and backbone dynamics of component IV Glycera dibranchiata monomeric hemoglobin-CO. *Biochemistry* **37**(31), 10906-19.

von Mensdorff-Pouilly, S., Petrakou, E., Kenemans, P., van Uffelen, K., Verstraeten, A. A., Snijdewint, F. G., van Kamp, G. J., Schol, D. J., Reis, C. A., Price, M. R., Livingston, P. O. & Hilgers, J. (2000). Reactivity of natural and induced human antibodies to MUC1 mucin with MUC1 peptides and n-acetylgalactosamine (GalNAc) peptides. *Int J Cancer* **86**(5), 702-12.

Vuister, G. W. & Bax, A. (1992). Measurement of two-bond JCOH alpha coupling constants in proteins uniformly enriched with 13C. *J Biomol NMR* **2**(4), 401-5.

Vuister, G. W. & Bax, A. (1993). *J Am Chem Soc* **115**, 7772-7777.

Wandall, H. H., Hassan, H., Mirgorodskaya, E., Kristensen, A. K., Roepstorff, P., Bennett, E. P., Nielsen, P. A., Hollingsworth, M. A., Burchell, J., Taylor-Papadimitriou, J. & Clausen, H. (1997). Substrate specificities of three members of the human UDP-N-acetyl-alpha-D-galactosamine:Polypeptide N-acetylgalactosaminyltransferase family, GalNAc-T1, -T2, and -T3. *J Biol Chem* **272**(38), 23503-14.

Wilmot, C. M. & Thornton, J. M. (1988). Analysis and prediction of the different types of beta-turn in proteins. *J Mol Biol* **203**(1), 221-32.

Wishart, D. S., Bigam, C. G., Holm, A., Hodges, R. S. & Sykes, B. D. (1995). 1H, 13C and 15N random coil NMR chemical shifts of the common amino acids. I. Investigations of nearest-neighbor effects. *J Biomol NMR* **5**(1), 67-81.

Wishart, D. S., Sykes, B. D. & Richards, F. M. (1991). Relationship between nuclear magnetic resonance chemical shift and protein secondary structure. *J Mol Biol* **222**(2), 311-33.

Wittekind, M. & Mueller, L. (1993). *J Magn Reson Series B* **101**, 201.

Wuthrich, K. (1986). *NMR of proteins and nucleic acids / Kurt Wuthrich*, Wiley,, New York :.

Xing, P. X., Prenzoska, J. & McKenzie, I. F. (1992a). Epitope mapping of anti-breast and anti-ovarian mucin monoclonal antibodies. *Mol Immunol* **29**(5), 641-50.

Xing, P. X., Prenzoska, J., Quelch, K. & McKenzie, I. F. (1992b). Second generation anti-MUC1 peptide monoclonal antibodies. *Cancer Res* **52**(8), 2310-2317.

Xing, P. X., Reynolds, K., Pietersz, G. A. & McKenzie, I. F. (1991). Effect of variations in peptide sequence on anti-human milk fat globule membrane antibody reactions. *Immunology* **72**(2), 304-11.

Xing, P. X., Tjandra, J. J., Stacker, S. A., Teh, J. G., Thompson, C. H., McLaughlin, P. J. & McKenzie, I. F. (1989). Monoclonal antibodies reactive with mucin expressed in breast cancer. *Immunol Cell Biol* **67**(Pt 3), 183-95.

Yamazaki, T., Muhandiram, R. & Kay, L. E. (1994). NMR Experiments for the Measurement of Carbon Relaxation Properties inHighly Enriched, Uniformly 13C, 15N-Labeled Proteins: Application to 13C-alpha Carbons. *J Am Chem Soc* **116**(18), 8266-8278.

Yao, J., Dyson, H. J. & Wright, P. E. (1994). Three-dimensional structure of a type VI turn in a linear peptide in water solution. Evidence for stacking of aromatic rings as a major stabilizing factor. *J Mol Biol* **243**(4), 754-66.

Zhang, O., Kay, L. E., Olivier, J. P. & Forman-Kay, J. D. (1994). Backbone 1H and 15N resonance assignments of the N-terminal SH3 domain of drk in folded and unfolded states using enhanced-sensitivity pulsed field gradient NMR techniques. *J Biomol NMR* **4**(6), 845-58.

Zhang, P., Dayie, K. T. & Wagner, G. (1997). Unusual lack of internal mobility and fast overall tumbling in oxidized flavodoxin from Anacystis nidulans. *J Mol Biol* **272**(3), 443-55.

Zhu, G., Xia, Y., Nicholson, L. K. & Sze, K. H. (2000). Protein dynamics measurements by TROSY-based NMR experiments. *J Magn Reson* **143**(2), 423-6.

Zotter, S., Hageman, P. C., Lossnitzer, A., Mooi, W. J. & Hilgers, J. (1988). *Cancer Rev* **111**, 55-101.

Zvi, A., Kustanovich, I., Feigelson, D., Levy, R., Eisenstein, M., Matsushita, S., Richalet-Sécordel, P., Regenmortel, M. H. V. & Anglister, J. (1995). NMR Mapping of the Antigenic Determinant Recognized by an Anti-gp120, Human Immunodeficiency Virus Neutralizing Antibody. *Eur J Biochem* **229**(1), 178-187.

Zvi, A., Tugarinov, V., Faiman, G. A., Horovitz, A. & Anglister, J. (2000). A model of a gp120 V3 peptide in complex with an HIV-neutralizing antibody based on NMR and mutant cycle-derived constraints. *Eur J Biochem* **267**(3), 767-79.

Appendix A: Supplementary ^{1}H NMR and natural abundance ^{13}C NMR data for MUC1 16mer peptide and glycopeptides.

Table A1: ^{1}H NMR resonance assignments of unglycosylated and Tn-glycosylated MUC1 16mer peptides (pH 7.0, 5 °C).

A. unglycosylated 16mer (GVTSAPDTRPAPGSTA)

Residue	^{1}HN	$^{1}H\alpha$	$^{1}H\beta$	$^{1}H\gamma$	$^{1}H\delta$	$^{1}H\varepsilon$
Gly1						
Val2	8.65	4.26	2.12	0.97		
Thr3	8.52	4.42	4.22	1.22		
Ser4	8.49	4.45	3.85			
Ala5	8.53	4.62	1.37			
Pro6		4.41	1.91, 2.29	2.03	3.66, 3.81	
Asp7	8.61	4.62	2.64, 2.75			
Thr8	8.21	4.32	4.26	1.18		
Arg9	8.41	4.60	1.78	1.70	1.71	3.22
Pro10		4.40	1.86, 2.26	1.99	3.60, 3.84	
Ala11	8.65	4.56	1.36			
Pro12		4.42	1.94, 2.33	2.08	3.66, 3.85	
Gly13	8.70	4.00				
Ser14	8.28	4.54	3.94			
Thr15	8.39	4.41	4.31	1.21		
Ala16	8.12	4.11	1.34			

B. Tn3-glycosylated 16mer (GVT(Tn)SAPDTRPAPGSTA)

Residue	^{1}HN	$^{1}H\alpha$	$^{1}H\beta$	$^{1}H\gamma$	$^{1}H\delta$	$^{1}H\varepsilon$
Gly1						
Val2	8.63	4.37	2.12	0.98		
Thr3	8.91	4.66	4.32	1.28		
Ser4	8.64	4.47	3.79, 3.86			
Ala5	8.65	4.48	1.39			
Pro6		4.39	1.90, 2.31	2.04	3.66, 3.83	
Asp7	8.63	4.61	2.64, 2.75			

Thr8	8.21	4.31	4.25	1.18			
Arg9	8.41	4.60	1.78	1.70	1.70	3.21	
Pro10		4.39	1.86, 2.26	2.00	3.60, 3.84		
Ala11	8.65	4.56	1.36				
Pro12		4.41	1.94, 2.32	2.09	3.67, 3.83		
Gly13	8.70	3.99					
Ser14	8.28	4.54	3.92				
Thr15	8.39	4.41	4.31	1.21			
Ala16	8.12	4.11	1.34				

	H1	H2	H3	H4	H5	H6,H6'	$AcCH_3$	AcNH
Tn3(Thr3)	4.94	4.07	3.89				2.03	7.68

C. Tn4-glycosylated 16mer (GVTS(Tn)APDTRPAPGSTA)

Residue	^{1}HN	^{1}Hα	^{1}Hβ	^{1}Hγ	^{1}Hδ	^{1}Hε
Gly1						
Val2	8.62	4.26	2.12	0.95		
Thr3	8.52	4.39	4.18	1.22		
Ser4	8.71	4.62	3.76, 3.91			
Ala5	8.65	4.62	1.38			
Pro6		4.41	1.91, 2.30	2.03	3.67, 3.80	
Asp7	8.62	4.61	2.63, 2.74			
Thr8	8.25	4.31	4.25	1.18		
Arg9	8.43	4.59	1.78	1.70	1.70	3.21
Pro10		4.39	1.86, 2.26	2.00	3.60, 3.83	
Ala11	8.65	4.56	1.36			
Pro12		4.41	1.94, 2.33	2.07	3.67, 3.84	
Gly13	8.70	3.99				
Ser14	8.28	4.54	3.93			
Thr15	8.39	4.40	4.31	1.21		
Ala16	8.12	4.11	1.33			

	H1	H2	H3	H4	H5	H6,H6'	$AcCH_3$	AcNH
Tn4(Ser4)	4.89	4.16	3.92			3.65	2.03	8.12

D. Tn3,Tn4-glycosylated 16mer (GVT(Tn)S(Tn)APDTRPAPGSTA)

Residue	^{1}HN	^{1}Hα	^{1}Hβ	^{1}Hγ	^{1}Hδ	^{1}Hε
Gly1						
Val2	8.61	4.38	2.12	0.99		

Thr3	8.90	4.65	4.34	1.29			
Ser4	8.83	4.63	3.75, 3.91				
Ala5	8.69	4.50	1.39				
Pro6		4.39	1.91, 2.31	2.03	3.65, 3.82		
Asp7	8.61	4.61	2.63, 2.75				
Thr8	8.24	4.31	4.25	1.18			
Arg9	8.42	4.59	1.78	1.70	1.70	3.22	
Pro10		4.40	1.86, 2.26	2.00	3.60, 3.84		
Ala11	8.64	4.56	1.36				
Pro12		4.41	1.94, 2.33	2.09	3.67, 3.84		
Gly13	8.70	3.99					
Ser14	8.28	4.54	3.92				
Thr15	8.38	4.41	4.30	1.21			
Ala16	8.11	4.11	1.33				

	H1	H2	H3	H4	H5	H6,H6'	$AcCH_3$	AcNH
Tn3(Thr3)	4.92	4.07	3.90				2.05	7.74
Tn4(Ser4)	4.91	4.15	3.92				2.05	8.15

Table A2: ^{13}C NMR resonance assignments of unglycosylated and Tn3,Tn4-glycosylated MUC1 16mer peptides (pH 7.0, 5 °C).

A. unglycosylated 16mer (GVTSAPDTRPAPGSTA)

Residue	$^{13}C\alpha$	$^{13}C\beta$	$^{13}C\gamma$	$^{13}C\delta$
Gly1	42.96			
Val2	62.29	32.90	20.17, 21.01	
Thr3	61.69	69.66	21.43	
Ser4	57.92	63.65		
Ala5	50.51	18.08		
Pro6	63.23	31.92	27.44	50.51
Asp7	54.14	40.86		
Thr8	61.55	69.52	21.57	
Arg9	54.14	29.82	26.60	43.24
Pro10	62.67	32.06	27.44	50.65
Ala11	50.37	17.66		
Pro12	63.51	31.92	27.44	50.51
Gly13	45.06			
Ser14	58.34	63.79		
Thr15	61.41	69.80	21.43	
Ala16	53.86	19.75		

B. Tn3,Tn4-glycosylated 16mer (GVT(Tn)S(Tn)APDTRPAPGSTA)

Residue	$^{13}C\alpha$	$^{13}C\beta$	$^{13}C\gamma$	$^{13}C\delta$
Gly1	43.19			
Val2	62.10	33.00	20.33,21.07	
Thr3	59.84	81.69	21.07	
Ser4	55.69	64.32		
Ala5	50.41	17.84		
Pro6	62.83	32.01	27.54	50.40
Asp7	54.17	41.21		
Thr8	61.59	71.75	21.57	
Arg9	54.17	29.77	26.54	43.19
Pro10	62.72	32.01	27.54	50.65
Ala11	50.45	17.59		
Pro12	62.49	32.01	27.54	50.40
Gly13	45.18			
Ser14	58.49	64.07		
Thr15	61.55	72.02	21.32	
Ala16	54.02	19.83		

	C1	C2	C3	C4	C5	C6	Ac
Tn3(Thr3)		52.39					24.80
Tn4(Ser4)		52.39					24.80

Table A3: Comparison of temperature coefficients ($-\Delta\delta/\Delta T$), coupling constants ($^3J_{N\alpha}$) and alpha proton chemical shift index ($\Delta\delta_\alpha$) measured for the unglycosylated and Tn-glycosylated MUC1 16mer peptides (pH 7.0, 5 °C)[1].

	A. unglycosylated 16mer				B. Tn3-glycosylated 16mer		
Residue	$-\Delta\delta/\Delta T$ (ppb/K)	$^3J_{N\alpha}$ (Hz)	$\Delta\delta_{H\alpha}$ (ppm)	$\Delta\delta_{C\alpha}$ (ppm)	$-\Delta\delta/\Delta T$ (ppb/K)	$^3J_{N\alpha}$ (Hz)	$\Delta\delta_{H\alpha}$ (ppm)
Gly1				-2.1			

[1] Uncertainty in the measured temperature coefficient values is ± 0.2 ppb/K. Uncertainty in the measured coupling constants is ± 0.2 Hz. The chemical shift index for the Hα proton is calculated as the difference between the observed chemical shift and the random coil chemical shift ($\Delta\delta_\alpha = \delta_\alpha$obs - $\delta_\alpha$coil) where the random coil shift of a given residue is taken from Wishart *et al.* (Wishart et al., 1995).

Val2			0.14	0.1			0.25
Thr3	8.0	5.7	0.07	-0.1	12.6	8.8	0.31
Ser4	7.0	7.2	-0.02	-0.4	8.1	6.7	0.00
Ala5	8.0	5.7	0.00	0.0	8.1		-0.14
Pro6			-0.01	-0.1			-0.03
Asp7	8.4	5.9	-0.02	-0.1	8.7	5.9	-0.03
Thr8	7.6	7.8	-0.03	-0.3	8.0	7.9	-0.04
Arg9	6.5	6.8	-0.05	0.1	6.4	7.0	-0.05
Pro10			-0.02	-0.6			-0.03
Ala11	9.0	5.3	-0.06	-0.1	8.7	5.3	-0.06
Pro12			0.00	0.2			-0.01
Gly13	8.0		0.04	0.0	8.0		0.03
Ser14	5.0	6.6	0.07	0.0	5.6	6.9	0.07
Thr15	8.4	9.0	0.06	-0.4	8.6	9.1	0.06
Ala16	6.0	6.4	-0.21	1.4	6.4	6.5	-0.21

	C. Tn4-glycosylated 16mer			D. Tn3,Tn4-glycosylated 16mer			
Residue	$-\Delta\delta/\Delta T$ (ppb/K)	$^3J_{N\alpha}$ (Hz)	$\Delta\delta_{H\alpha}$ (ppm)	$-\Delta\delta/\Delta T$ (ppb/K)	$^3J_{N\alpha}$ (Hz)	$\Delta\delta_{H\alpha}$ (ppm)	$\Delta\delta_{C\alpha}$ (ppm)
Gly1							-1.9
Val2			0.14			0.26	-0.1
Thr3	8.6	7.3	0.04	12.0	8.7	0.30	-2.0
Ser4			0.15	7.6	7.1	0.16	-2.6
Ala5	9.4	5.6	0.00	8.0	5.3	-0.12	-0.1
Pro6			-0.01			-0.03	-0.5
Asp7	9.0	5.8	-0.03	8.0	5.9	-0.03	0.0
Thr8	8.0	8.2	-0.04	9.0	7.9	-0.04	-0.2
Arg9	6.4	7.0	-0.06	6.0	6.3	-0.06	0.2
Pro10			-0.03			-0.02	-0.6
Ala11	9.4	5.6	-0.06	8.2	5.5	-0.06	0.1
Pro12			-0.01			-0.01	-0.8
Gly13	8.6		0.03	8.0		0.03	0.1
Ser14	5.4	7.0	0.07	6.2	6.8	0.07	0.2
Thr15	8.8	9.5	0.05	8.0	9.5	0.06	-0.3
Ala16	6.8	6.6	-0.21	6.4	6.5	-0.21	1.5

Table A4: Natural abundance ^{13}C T_1 and $T_1\rho$ relaxation times, and $\{^1H\}$-^{13}C NOEs measured for the unglycosylated and Tn3,Tn4-glycosylated MUC1 16mer peptides (pH 7.0, 5 °C).

A. unglycosylated 16mer

Residue	T_1 (ms)	$T_1\rho$ (ms)	$\{^1H\}$-^{13}C NOE
Val2	313 ± 6	208 ± 23	1.80 ± 0.07
Thr3	295 ± 5	188 ± 19	1.58 ± 0.04
Ser4	286 ± 5	155 ± 13	1.56 ± 0.08
Ala5	290 ± 5	144 ± 12	1.52 ± 0.09
Pro6	285 ± 5	139 ± 11	1.43 ± 0.07
Asp7	269 ± 4	117 ± 8	1.43 ± 0.06
Thr8	290 ± 5	142 ± 11	1.50 ± 0.08
Arg9	269 ± 4	117 ± 8	1.43 ± 0.06
Pro10	291 ± 5	133 ± 10	1.37 ± 0.10
Ala11	277 ± 5	136 ± 10	1.50 ± 0.09
Pro12	288 ± 5	156 ± 13	1.43 ± 0.07
Ser14	296 ± 5	175 ± 16	1.60 ± 0.07
Thr15	298 ± 5	191 ± 19	1.65 ± 0.04
Ala16	460 ± 11	269 ± 39	1.80 ± 0.04

B. Tn3,Tn4-glycosylated 16mer

Residue	T_1 (ms)	$T_1\rho$ (ms)	$\{^1H\}$-^{13}C NOE
Val2	294 ± 12	137 ± 20	1.65 ± 0.04
Thr3	262 ± 11	110 ± 13	1.29 ± 0.02
Ser4	262 ± 11	109 ± 13	1.32 ± 0.03
Ala5	304 ± 12	96 ± 10	1.37 ± 0.04
Pro6	303 ± 12	110 ± 13	1.48 ± 0.02
Asp7	292 ± 12	101 ± 11	1.41 ± 0.02
Thr8	302 ± 12	131 ± 18	1.50 ± 0.03
Arg9	293 ± 12	101 ± 11	1.41 ± 0.02
Pro10	303 ± 12	110 ± 13	1.48 ± 0.04
Ala11	283 ± 11	159 ± 27	1.42 ± 0.03
Pro12	312 ± 13	131 ± 18	1.53 ± 0.03
Ser14	297 ± 12	178 ± 35	1.53 ± 0.03
Thr15	310 ± 13	206 ± 47	1.82 ± 0.02
Ala16	449 ± 19	236 ± 60	1.83 ± 0.03

Table A5: Peptide-sugar NOEs observed for the Tn3,Tn4-glycosylated 16mer peptide (pH 7.0, 5 °C).

Peptide resonance	Tn resonance	intensity (s, m, w), # contours[2]
Val2 αH	Tn3 AcNH	m, 4
Val2 βH	Tn3 $AcCH_3$	s, 18
Val2 $\gamma(CH_3)_2$	Tn3 AcNH	m, 4
Thr3 NH	Tn3 AcNH	s, 9
Thr3 NH	Tn3 $AcCH_3$	s, 7
Thr3 NH	Tn3 H2	m, 4
Thr3 NH	Tn3 H3	m, 5
Thr3 αH	Tn3 AcNH	m, 4
Thr3 βH	Tn3 AcNH	m, 5
Thr3 $\gamma(CH_3)$	Tn3 AcNH	m, 4
Thr3 $\gamma(CH_3)$	Tn3 H2	s, 14
Ser4 NH	Tn4 AcNH	s, 6
Ser4 NH	Tn4 $AcCH_3$	s, 6
Ser4 NH	Tn3 H2	w, 2
Ser4 NH	Tn4 H3	m, 5
Ser4 αH	Tn4 AcNH	m, 5
Ser4 βH (3.83 ppm)	Tn4 AcNH	s, 6
Ser4 β'H (3.70 ppm)	Tn4 AcNH	m, 4
Ser4 βH (3.83 ppm)	Tn4 $AcCH_3$	s, 12
Ser4 β'H (3.70 ppm)	Tn4 $AcCH_3$	s, 10
Ala5 $\beta(CH_3)$	Tn3 AcNH	w, 2
Ala5 $\beta(CH_3)$	Tn4 AcNH	w, 2
Ala5 $\beta(CH_3)$	Tn4 $AcCH_3$	s, 15
Pro6 αH	Tn4 AcNH	m, 4

Table A6: Peptide-Fab NOEs observed at 5 °C and 25 °C (pH 7.0) for the Tn3,Tn4-glycosylated MUC1 16mer peptide in the presence of 0.14 molar equivalents Fab. Peptide was 1.4 mM and Fab was 200 μM.

Peptide/Sugar resonance	Fab resonance	intensity(s,m,w), # contours
Tn3 AcNH	arom. (6.91 ppm, 25 °C)	m, 5 (25 °C)

[2] Intensity of the peptide-sugar NOE is categorized as strong (s) for # contours ≥ 6; medium (m) for 4 ≤ # contours < 6; and weak (w) for 1 ≤ # contours < 4.

Tn4 AcNH	NH (8.41 ppm, 5 °C)	s, 6 (5 °C)
Tn4 AcNH	NH (8.21 ppm, 25 °C)	s, 9 (25 °C)
Tn4 $AcCH_3$	NH (8.41 ppm, 5 °C)	s, 6 (5 °C)
Tn4 $AcCH_3$	NH (8.21 ppm, 25 °C)	m, 3 (25 °C)
T8 αH	arom. (6.91 ppm, 25 °C)	m, 3 (25 °C)
T8 γ(CH_3)	CH_3 (-0.30 ppm, 5 °C)	s, 7 (5 °C)
T8 γ(CH_3)	CH_3 (-0.30 ppm, 25 °C)	s, 12 (25 °C)
T8 γ(CH_3)	arom. (6.91 ppm, 25 °C)	s, 6 (25 °C)

Table A7: Temperature coefficients ($-\Delta\delta/\Delta T$) and coupling constants ($^3J_{N\alpha}$) measured for the unglycosylated and Tn3,Tn4-glycosylated MUC1 16mer peptides in the presence 0.4 molar equivalents Fab. Peptide was 1 mM and Fab was 400 μM (pH 7.0, 5 °C).

	A. unglycosylated 16mer + Fab		B. Tn3,Tn4-glycosylated 16mer + Fab	
Residue	$-\Delta\delta/\Delta T$ (ppb/K)	$^3J_{N\alpha}$ (Hz)	$-\Delta\delta/\Delta T$ (ppb/K)	$^3J_{N\alpha}$ (Hz)
Thr3	7.8	6.6	12.0	8.6
Ser4	8.0	7.0	7.7	7.5
Ala5	7.8	6.6	7.7	5.9
Asp7	8.4	5.6	8.6	5.4
Thr8	8.0	7.5	8.4	7.9
Arg9	6.6	7.0	5.2	
Ala11	9.4	5.4	9.3	5.2
Gly13	7.4			
Ser14	5.4	6.5	5.8	6.9
Thr15	8.8	9.6	8.6	
Ala16	6.4	6.3	6.9	6.6

Appendix B: Supplementary ^{1}H, ^{13}C, and ^{15}N NMR data for recombinant, $^{13}C/^{15}N$-labeled MUC1 16mer and 40mer.

Table B1: ^{1}H, ^{13}C, and ^{15}N NMR resonance assignments of the recombinant MUC1 16mer (A) and 40mer (B) peptides (pH 7.1, 5°C).

A. 16mer GVTSAPDTRPAPGSTA(Hs)

Residue	^{1}HN	$^{1}H\alpha$	$^{1}H\beta$	$^{1}H\gamma$	$^{1}H\delta$	$^{1}H\varepsilon$
Gly1		3.91				
Val2	8.65	4.28	2.15	0.98		
Thr3	8.57	4.44	4.25	1.22		
Ser4	8.53	4.47	3.96, 3.91			
Ala5	8.57	4.65	1.40			
Pro6		4.43	1.93, 2.31	2.04	3.69, 3.83	
Asp7	8.65	4.63	2.67, 2.76			
Thr8	8.26	4.35	4.28	1.18		
Arg9	8.45	4.63	1.83	1.72	3.24	
Pro10		4.41	1.89, 2.30	2.04	3.62, 3.85	
Ala11	8.69	4.59	1.39			
Pro12		4.44	1.97, 2.35	2.10	3.69, 3.83	
Gly13	8.75	4.02				
Ser14	8.32	4.55	3.87			
Thr15	8.41	4.41	4.28	1.21		
Ala16	8.46	4.36	1.42			
Hs 17	8.19	4.24	1.88	3.66		

Residue	^{15}N	$^{13}C\alpha$	$^{13}C\beta$	$^{13}C\gamma$	$^{13}C\delta$	$^{13}C\varepsilon$
Gly1		63.07				
Val2	119.6	62.29	32.74	20.08, 21.02		
Thr3	117.5	61.67	69.86	21.48		
Ser4	118.0	58.02	63.92			
Ala5	126.4	50.56	18.06			
Pro6		63.07	31.88	27.22	50.41	
Asp7	119.6	54.14	60.66			
Thr8	113.9	61.51	69.79	21.48		
Arg9	124.0	54.14	29.79	26.45	43.15	
Pro10		62.68	31.88	27.22	50.49	
Ala11	125.1	50.41	17.60			
Pro12		63.46	31.81	27.22	50.41	
Gly13	109.1	65.09				
Ser14	114.6	58.41	63.77			
Thr15	114.9	61.59	69.79	21.48		

Ala16	126.3	52.43	19.07		
Hs 17	123.2	55.15	56.47	61.13	

B. 40mer (VTSAPDTRPAPGSTAPPAHG)$_2$(Hs)

Residue	^{1}HN	^{1}Hα	^{1}Hβ	^{1}Hγ	^{1}Hδ	^{1}Hε
Val1		4.72	2.12	1.03, 1.05		
Thr2		4.43	4.27	1.26		
Ser3	8.62	4.46	3.89, 3.93			
Ala4	8.53	4.58	1.38			
Pro5/25		4.42	1.90, 2.31	2.04	3.62, 3.83	
Asp6/26	8.58	4.62	2.66, 2.76			
Thr7/27	8.19	4.33	4.24	1.22		
Arg8/28	8.37	4.62	1.83	1.72	3.22	
Pro9/29		4.40	1.90, 2.31	2.04	3.62, 3.83	
Ala10//30	8.62	4.61	1.38			
Pro11/31		4.42	1.90, 2.31	2.04	3.62, 3.83	
Gly12/32	8.66	3.99				
Ser13/33	8.24	4.54	3.87			
Thr14/34	8.33	4.39	4.18	1.22		
Ala15/35	8.41	4.61	1.38			
Pro16/36		4.40	1.90, 2.31	2.04	3.62, 3.83	
Pro17/37		4.40	1.90, 2.31	2.04	3.62, 3.83	
Ala18/38	8.54	4.25	1.35			
His19	8.36	4.56	3.13			
Gly20	8.42	3.94				
Val21	8.19	4.23	2.12	0.95, 0.96		
Thr22	8.45	4.45	4.27	1.26		
Ser23	8.43	4.46	3.89, 3.93			
Ala24	8.49	4.58	1.38			
His39	8.36	4.62	3.13			
Gly40	8.47	3.94				
Hs 41	8.04	4.27	1.88	3.59, 3.66		

Residue	^{15}N	^{13}Cα	^{13}Cβ	^{13}Cγ	^{13}Cδ
Val1		61.38	32.84	19.44, 20.50	
Thr2		61.49	69.42	21.54	
Ser3	118.86	57.88	63.92		
Ala4	126.43	50.31	17.93		
Pro5/25		63.24	32.04	27.48	50.32
Asp6/26	119.59	54.04	40.89		
Thr7/27	113.95	61.49	69.65	21.54	
Arg8/28	123.93	54.04	29.79	26.45	43.33
Pro9/29		62.66	32.04	27.48	50.32
Ala10/30	125.10	50.43	17.93		
Pro11/31		63.24	32.04	27.48	50.32
Gly12/32	108.97	45.18			
Ser13/33	114.44	58.35	63.79		
Thr14/34	115.06	61.38	69.65	21.54	

Ala15/35	127.41	50.43	17.93		
Pro16/36		62.66	32.04	27.48	50.32
Pro17/37		62.66	32.04	27.48	50.32
Ala18/38	123.63	52.18	19.10		
His19	117.45	55.90	27.17		
Gly20	109.37	45.18			
Val21	118.70	62.31	32.84	20.50, 21.19	
Thr22	117.78	61.73	69.42	21.54	
Ser23	117.88	57.88	63.92		
Ala24	126.35	50.31	17.93	61.13	
His39	117.45	55.90	27.17		
Gly40	110.11	45.18			
Hs 41	124.25	54.97	30.45	61.02	

Table B2: ^{15}N T_1 and ^{13}C T_1 relaxation times measured for the ^{15}N,^{13}C-labeled recombinant MUC1 peptides in the absence and presence of Fab B27.29. All measurements were made at 500 MHz on a Varian Inova 500 NMR spectrometer. NMR samples were in PBS buffer, pH 7.1, 90% H_2O/10% D_2O, 5.0 °C.

A. ^{15}N T_1 relaxation times measured for the ^{15}N-labeled 16mer ± Fab B27.29

Residue	800 μM 16mer	800 μM 16mer + 200 μM Fab	1600 μM 16mer + 200 μM Fab	2600 μM + 200 μM Fab
Gly1				
Val2	866 ± 6[3] ms			
Thr3	855 ± 2	625 ± 23	669 ± 11	693 ± 11
Ser4	772 ± 2	622 ± 30	586 ± 13	639 ± 9
Ala5	773 ± 2	512 ± 20	547 ± 10	568 ± 7
Pro6				
Asp7	663 ± 2	384 ± 27	427 ± 11	471 ± 5
Thr8	647 ± 2	429 ± 39	410 ± 14	462 ± 5
Arg9	641 ± 3	416 ± 34	483 ± 12	467 ± 5
Pro10				
Ala11	714 ± 2	430 ± 29	481 ± 10	498 ± 6
Pro12				
Gly13	664 ± 2	446 ± 72	449 ± 21	494 ± 6
Ser14	665 ± 2	438 ± 33	499 ± 14	523 ± 6
Thr15	732 ± 2	492 ± 32	533 ± 15	579 ± 7
Ala16	814 ± 2	537 ± 15	595 ± 8	615 ± 8
Hs 17	1160 ± 10	768 ± 9	867 ± 6	910 ± 18

B. ^{15}N T_1 relaxation times measured for the ^{15}N-labeled 40mer ± Fab B27.29

Residue	800 μM 16mer	400 μM 40mer + 200 μM Fab	800 μM 40mer + 200 μM Fab	1200 μM + 200 μM Fab

[3] Standard deviations calculated for each parameter are given as ± error. These standard deviations are significantly smaller than the 5% errors estimated as the more accurate reflection of uncertainty in each measurement.

Thr1				
Val2				
Ser3	916 ± 6 ms	555 ± 11	619 ± 24	767 ± 33
Ala4	737 ± 5	465 ± 8	625 ± 23	658 ± 27
Pro5				
Asp6/26	620 ± 4	413 ± 6	459 ± 18	573 ± 21
Thr7/27	609 ± 4	405 ± 5	450 ± 18	577 ± 22
Arg8/28	568 ± 4	403 ± 5	451 ± 18	534 ± 22
Pro19				
Ala10/30	617 ± 4	439 ± 6	500 ± 20	595 ± 23
Pro11				
Gly12/32	659 ± 5	406 ± 5	485 ± 20	578 ± 22
Ser13/33	633 ± 4	439 ± 6	523 ± 20	585 ± 22
Thr14/34	673 ± 4	439 ± 6	536 ± 20	602 ± 23
Ala15/35	631 ± 4	490 ± 8	550 ± 20	589 ± 22
Pro16/36				
Pro17/37				
Ala18/38	638 ± 4	515 ± 9	566 ± 21	596 ± 23
His19/39	700 ± 5	503 ± 9	566 ± 22	633 ± 25
Gly20	661 ± 5	473 ± 7	478 ± 19	640 ± 26
Val21	627 ± 4	534 ± 9	569 ± 21	594 ± 23
Thr22	649 ± 4	452 ± 6	533 ± 20	606 ± 23
Ser23	635 ± 4	473 ± 8	533 ± 20	606 ± 23
Ala24	632 ± 4	528 ± 9	523 ± 20	613 ± 24
Gly40	859 ± 6	566 ± 11	660 ± 22	687 ± 29
Hs 41	955 ± 6	804 ± 20	878 ± 34	948 ± 41

C. ^{13}C T_1 relaxation times measured for the ^{13}C-labeled 16mer ± Fab B27.29

Residue	800 μM 16mer	800 μM 16mer + 200 μM Fab
Gly1		
Val2	291 ± 10 ms	318 ± 2
Thr3	296 ± 8	279 ± 3
Ser4	270 ± 8	257 ± 4
Ala5	263 ± 7	176 ± 8
Pro6	262 ± 8	175 ± 6
Asp7	253 ± 8	186 ± 6
Thr8	269 ± 8	231 ± 17
Arg9	253 ± 8	186 ± 6
Pro10	266 ± 6	130 ± 9
Ala11	266 ± 7	170 ± 16
Pro12	284 ± 9	191 ± 9
Gly13		
Ser14	268 ± 8	244 ± 6
Thr15	247 ± 8	279 ± 3
Ala16	291 ± 11	323 ± 4

Hs 17	347 ± 22	386 ± 3

D. ^{13}C T_1 relaxation times measured for the ^{13}C-labeled 40mer ± Fab B27.29

Residue	800 μM 40mer	800 μM 40mer + 200 μM Fab
Val1		277 ± 12
Thr2	278 ± 15 ms	317 ± 14
Ser3	296 ± 12	277 ± 10
Ala4	300 ± 15	319 ± 13
Pro5	306 ± 9	216 ± 14
Asp6/26	289 ± 10	218 ± 11
Thr7/27	306 ± 11	251 ± 15
Arg8/28	289 ± 10	218 ± 11
Pro9/19	284 ± 12	217 ± 9
Ala10/30	300 ± 15	319 ± 13
Pro11/31	306 ± 12	281 ± 22
Gly12/32		
Ser13/33	311 ± 13	284 ± 12
Thr14/34	299 ± 14	299 ± 11
Ala15/35	300 ± 15	319 ± 13
Pro16/36	284 ± 12	277 ± 9
Pro17/37	284 ± 12	277 ± 9
Ala18/38	300 ± 13	295 ± 16
His19/39	255 ± 11	268 ± 10
Gly20		
Val21	296 ± 23	417 ± 48
Thr22	278 ± 15	317 ± 14
Ser23	296 ± 12	277 ± 10
Ala24	300 ± 15	319 ± 13
Gly40		
Hs 41		378 ± 25

Table B3: ^{15}N T_2 and ^{13}C $T_{1\rho}$ relaxation times measured for the ^{15}N,^{13}C-labeled recombinant MUC1 peptides in the absence and presence of Fab B27.29. All measurements were made at 500 MHz on a Varian Inova 500 NMR spectrometer. NMR samples were in PBS buffer, pH 7.1, 90% H_2O/10% D_2O, 5.0 °C.

A. ^{15}N T_2 relaxation times measured for the ^{15}N-labeled 16mer ± Fab B27.29

Residue	800 μM 16mer	500 μM 16mer + 200 μM Fab	800 μM 16mer + 200 μM Fab
Gly1			
Val2	363 ± 8 ms		
Thr3	439 ± 1	149 ± 2	142 ± 2
Ser4	395 ± 1	132 ± 5	142 ± 3
Ala5	425 ± 1	88 ± 4	98 ± 2

Pro6			
Asp7	383 ± 1	87 ± 15	77 ± 3
Thr8	372 ± 1	63 ± 14	78 ± 4
Arg9	344 ± 1	82 ± 16	69 ± 3
Pro10			
Ala11	409 ± 1	44 ± 8	66 ± 2
Pro12			
Gly13	340 ± 1	76 ± 26	78 ± 6
Ser14	358 ± 1	85 ± 10	86 ± 3
Thr15	402 ± 1	95 ± 7	115 ± 4
Ala16	491 ± 1	142 ± 3	156 ± 2
Hs 17	766 ± 7	274 ± 3	299 ± 3

B. ^{15}N T_2 relaxation times measured for the ^{15}N-labeled 40mer ± Fab B27.29

Residue	800 μM 40mer	800 μM 40mer + 200 μM Fab
Thr1		
Val2		
Ser3	336 ± 2 ms	159 ± 3
Ala4	385 ± 3	161 ± 3
Pro5		
Asp6/26	294 ± 2	124 ± 2
Thr7/27	291 ± 2	115 ± 2
Arg8/28	276 ± 1	112 ± 2
Pro19		
Ala10/30	300 ± 2	128 ± 2
Pro11		
Gly12/32	260 ± 1	112 ± 2
Ser13/33	265 ± 1	125 ± 2
Thr14/34	272 ± 1	133 ± 2
Ala15/3	312 ± 2	174 ± 4
Pro16/36		
Pro17/37		
Ala18/38	325 ± 2	182 ± 4
His19/39	302 ± 2	158 ± 3
Gly20	275 ± 2	138 ± 3
Val21	287 ± 2	180 ± 4
Thr22	286 ± 2	128 ± 2
Ser23	239 ± 1	176 ± 4
Ala24	272 ± 1	132 ± 2
Gly40	377 ± 2	174 ± 4
Hs 41	663 ± 7	406 ± 18

C. ^{13}C $T_{1\rho}$ relaxation times measured for the ^{13}C-labeled 16mer ± Fab B27.29

Residue	800 μM 16mer	800 μM 16mer + 200 μM Fab	500 μM 16mer + 200 μM Fab
Gly1			

Val2	202 ± 9 ms	133 ± 2	115 ± 6
Thr3	180 ± 8	106 ± 2	92 ± 7
Ser4	134 ± 5	83 ± 2	41 ± 8
Ala5	130 ± 4	37 ± 1	
Pro6	139 ± 4	54 ± 2	
Asp7	112 ± 3	51 ± 1	
Thr8	127 ± 3	84 ± 5	
Arg9	112 ± 3	51 ± 1	
Pro10	122 ± 5	62 ± 3	
Ala11	121 ± 3	37 ± 4	
Pro12	135 ± 5	52 ± 3	
Gly13			
Ser14	133 ± 4	65 ± 1	
Thr15	174 ± 7	105 ± 2	92 ± 8
Ala16	196 ± 10	105 ± 2	69 ± 3
Hs 17	137 ± 13	125 ± 2	109 ± 2

D. ^{13}C $T_{1\rho}$ relaxation times measured for the ^{13}C-labeled 40mer ± Fab B27.29

Residue	800 μM 40mer	800 μM 40mer + 200 μM Fab
Val1		99 ± 7
Thr2	155 ± 8 ms	197 ± 10
Ser3	117 ± 5	136 ± 6
Ala4	117 ± 5	102 ± 4
Pro5	107 ± 4	97 ± 6
Asp6/26	94 ± 3	100 ± 5
Thr7/27	96 ± 4	114 ± 5
Arg8/28	94 ± 3	100 ± 5
Pro19	101 ± 4	145 ± 8
Ala10/30	117 ± 5	102 ± 4
Pro11	107 ± 4	83 ± 4
Gly12/32		
Ser13/33	108 ± 4	96 ± 5
Thr14/34	114 ± 4	125 ±6
Ala15/35	117 ± 5	102 ± 4
Pro16/36	101 ± 4	145 ± 8
Pro17/37	101 ± 4	145 ± 8
Ala18/38	116 ± 5	126 ± 6
His19/39	100 ± 4	143 ± 7
Gly20		
Val21	115 ± 4	175 ± 8
Thr22	155 ± 8	197 ± 10
Ser23	117 ± 5	136 ± 6
Ala24	117 ± 5	102 ± 4
Gly40		
Hs 41	221 ± 16	343 ± 37

Table B4: $\{^1H\}$-^{15}N NOE and $\{^1H\alpha\}$-$^{13}C\alpha$ NOE measured for the ^{15}N,^{13}C-labeled recombinant MUC1 peptides in the absence and presence of Fab B27.29. All measurements were made at 500 MHz on a Varian Inova 500 NMR spectrometer. NMR samples were in PBS buffer, pH 7.1, 90% H_2O/10% D_2O, 5.0 °C for the $\{^1H\}$-^{15}N NOE experiments, and in 99.9% D_2O for the $\{^1H\alpha\}$-$^{13}C\alpha$ NOE experiments.

A. $\{^1H\}$-^{15}N NOE measured for the ^{15}N-labeled 16mer ± Fab B27.29

Residue	800 μM 40mer	800 μM 40mer + 200 μM Fab
Gly1		
Val2	-1.235 ± .042	
Thr3	-1.394 ± .004	-1.000 ± .130
Ser4	-1.073 ± .003	-0.686 ± .040
Ala5	-0.743 ± .002	-0.323 ± .024
Pro6		
Asp7	-0.267 ± .002	-0.097 ± .031
Thr8	-0.112 ± .002	-0.050 ± .033
Arg9	-0.086 ± .003	-0.039 ± .035
Pro10		
Ala11	-0.082 ± .002	-0.039 ± .028
Pro12		
Gly13	-0.301 ± .002	-0.135 ± .050
Ser14	-0.219 ± .002	-0.111 ± .038
Thr15	-0.779 ± .002	-0.459 ± .044
Ala16	-1.100 ± .003	-0.496 ± .020
Hs 17	-1.802 ± .004	-0.912 ± .018

B. $\{^1H\}$-^{15}N NOE measured for the ^{15}N-labeled 40mer ± Fab B27.29

Residue	800 μM 40mer	800 μM 40mer + 200 μM Fab
Thr1		
Val2		
Ser3	-1.03 ± .016	-0.77 ± .059
Ala4	-0.66 ± .005	-0.47 ± .029
Pro5		
Asp6/26	-0.17 ± .001	-0.10 ± .011
Thr7/27	0.04 ± .001	-0.01 ± .015
Arg8/28	0.05 ± .002	-0.03 ± .017
Pro19		
Ala10/30	0.05 ± .001	0.04 ± .009
Pro11		
Gly12/32	-0.04 ± .002	0.01 ± .020

Ser13/33	0.05 ± .002	0.10 ± .012
Thr14/34	-0.21 ± .002	-0.08 ± .016
Ala15/35	-0.20 ± .001	-0.20 ± .010
Pro16/36		
Pro17/37		
Ala18/38	-0.32 ± .001	-0.19 ± .008
His19/39	-0.47 ± .005	-0.34 ± .024
Gly20	-0.18 ± .005	-0.17 ± .040
Val21	-0.08 ± .002	-0.03 ± .032
Thr22	-0.34 ± .004	-0.19 ± .027
Ser23	-0.25 ± .004	-0.15 ± .032
Ala24	-0.25 ± .003	-0.23 ± .037
Gly40	-0.91 ± .011	-0.81 ± .058
Hs 41	-1.46 ± .011	-1.29 ± .059

C. {^{1}Hα}-^{13}Cα NOE measured for the ^{13}C-labeled 16mer ± Fab B27.29

Residue	800 μM 16mer	2600 μM 16mer + 200 μM Fab
Gly1		
Val2	1.63 ± .126	1.716 ± .127
Thr3	1.44 ± .069	1.761 ± .072
Ser4	1.61 ± .019	1.592 ± .022
Ala5	1.51 ± .032	1.490 ± .037
Pro6	1.49 ± .118	1.486 ± .133
Asp7	1.46 ± .057	1.404 ± .063
Thr8	1.39 ± .061	1.517 ± .077
Arg9	1.46 ± .057	1.404 ± .063
Pro10	1.42 ± .097	1.373 ± .115
Ala11	1.40 ± .033	1.447 ± .039
Pro12	1.52 ± .207	1.842 ± .389
Gly13		
Ser14	1.58 ± .019	1.511 ± .023
Thr15	1.66 ± .046	1.708 ± .049
Ala16	1.8 ± .201	2.000 ± .228
Hs 17	1.91 ± .073	1.903 ± .034

D. {^{1}Hα}-^{13}Cα NOE measured for the ^{13}C-labeled 40mer ± Fab B27.29

Residue	800 μM 40mer	800 μM 40mer + 200 μM Fab
Val1	1.56 ± .031	1.49 ± .077
Thr2	1.67 ± .033	1.74 ± .070
Ser3	1.65 ± .032	1.60 ± .072
Ala4	1.47 ± .029	1.54 ± .031
Pro5/25	1.53 ± .030	1.25 ± .280
Asp6/26	1.41 ± .028	1.30 ± .105
Thr7/27	1.52 ± .030	1.49 ± .064
Arg8/28	1.41 ± .028	1.30 ± .105

Pro9/29	1.52 ± .031	1.26 ± .164
Ala10/30	1.47 ± .029	1.54 ± .031
Pro11/31	1.53 ± .051	1.39 ± .406
Gly12/32		
Ser13/33	1.55 ± .031	1.44 ± .038
Thr14/34	1.59 ± .033	1.47 ± .033
Ala15/35	1.47 ± .029	1.54 ± .031
Pro16/36	1.52 ± .031	1.26 ± .164
Pro17/37	1.52 ± .033	1.26 ± .164
Ala18/38	1.38 ± .025	1.73 ± .225
His19/39	1.50 ± .036	1.58 ± .052
Gly20		
Val21	1.55 ± .034	1.42 ± .130
Thr22	1.67 ± .037	1.74 ± .070
Ser23	1.65 ± .033	1.60 ± .072
Ala24	1.47 ± .027	1.54 ± .031
Gly40		
Hs 41	2.02 ± .041	2.31 ± .132

Table B5: Spectral density values (J(0), $J(\omega_N)$ and $J(\omega_H)$) calculated from ^{15}N NMR relaxation data acquired for the ^{15}N-labeled recombinant MUC1 peptides in the absence and presence of Fab B27.29.

A. J(0), $J(\omega_N)$ and $J(\omega_H)$ calculated for the ^{15}N-labeled 16mer ± Fab B27.29

Residue	800 μM 16mer			800 μM 16mer + 200 μM Fab		
	J(0)	$J(\omega_N)$	$J(\omega_H)$	J(0)	$J(\omega_N)$	$J(\omega_H)$
Gly1						
Val2	0.636	0.166	0.040			
Thr3	0.480	0.162	0.044	1.906	0.241	0.050
Ser4	0.543	0.192	0.042	1.914	0.257	0.042
Ala5	0.494	0.205	0.035	2.845	0.333	0.040
Pro6						
Asp7	0.548	0.260	0.030	3.622	0.462	0.045
Thr8	0.572	0.273	0.027	3.610	0.424	0.035
Arg9	0.639	0.277	0.026	4.127	0.431	0.039
Pro10						
Ala11	0.522	0.249	0.024	4.377	0.417	0.038
Pro12						
Gly13	0.652	0.258	0.031	3.664	0.395	0.040
Ser14	0.607	0.261	0.029	3.239	0.404	0.040
Thr15	0.522	0.215	0.038	2.373	0.339	0.046
Ala16	0.398	0.181	0.040	1.675	0.308	0.043
Hs 17	0.230	0.109	0.038	0.803	0.199	0.039
Bound1	XXX	XXX	XXX	4.060	0.394	0.057
Arg9bound	XXX	XXX	XXX	2.360	0.332	0.041

B. J(0), $J(\omega_N)$ and $J(\omega_H)$ calculated for the ^{15}N-labeled 40mer ± Fab B27.29

Residue	800 μM 40mer			800 μM 40mer + 200 μM Fab		
	J(0)	$J(\omega_N)$	$J(\omega_H)$	J(0)	$J(\omega_N)$	$J(\omega_H)$
Val1						
Thr2						
Ser3	0.725	0.163	0.035	1.637	0.283	0.050
Ala4	0.562	0.218	0.035	1.558	0.358	0.049
Pro5/25						
Asp6/26	0.782	0.283	0.029	2.109	0.430	0.041
Thr7/27	0.795	0.298	0.025	2.303	0.444	0.039
Arg8/28	0.832	0.320	0.026	2.374	0.445	0.040
Pro9/29						
Ala10/30	0.765	0.295	0.024	2.061	0.414	0.034
Pro11/31						
Gly12/32	0.945	0.272	0.025	2.379	0.445	0.038
Ser13/33	0.913	0.287	0.023	2.123	0.417	0.032
Thr14/34	0.891	0.259	0.028	1.963	0.405	0.038
Ala15/35	0.724	0.276	0.030	1.443	0.356	0.038
Pro16/36						
Pro17/37						
Ala18/38	0.684	0.268	0.032	1.381	0.339	0.036
His19/39	0.779	0.238	0.033	1.630	0.338	0.042
Gly20	0.873	0.265	0.028	1.903	0.371	0.039
Val21	0.814	0.284	0.027	1.419	0.336	0.030
Thr22	0.821	0.262	0.032	2.063	0.386	0.041
Ser23	1.033	0.272	0.031	1.411	0.372	0.038
Ala24	0.873	0.273	0.031	2.044	0.328	0.036
Gly40	0.611	0.178	0.035	1.471	0.276	0.050
Hs 41	0.261	0.143	0.040	0.526	0.176	0.044

Vita

Jeffrey Scott Grinstead was born in Kansas City, Kansas in 1975. He grew up in Casper, Wyoming, where he graduated from Kelly Walsh High School in 1993. He earned his Bachelor of Science degree in Chemistry from the University of Puget Sound in Tacoma, Washington in 1997. In 2003 he earned a Doctor of Philosophy at the University of Washington in Medicinal Chemistry through the Biomolecular Structure and Design Program. For his doctoral research, he characterized the interactions of tumor-associated MUC1 antigenic peptides and glycopeptides with cancer-associated antibody and Class I MHC.